frontiers | Research Topics

Ferroptosis in stroke, neurotrauma and neurodegeneration, volume II

Edited by
Anwen Shao, Zhen-Ni Guo and Weilin Xu

Published in
Frontiers in Cellular Neuroscience
Frontiers in Neuroscience

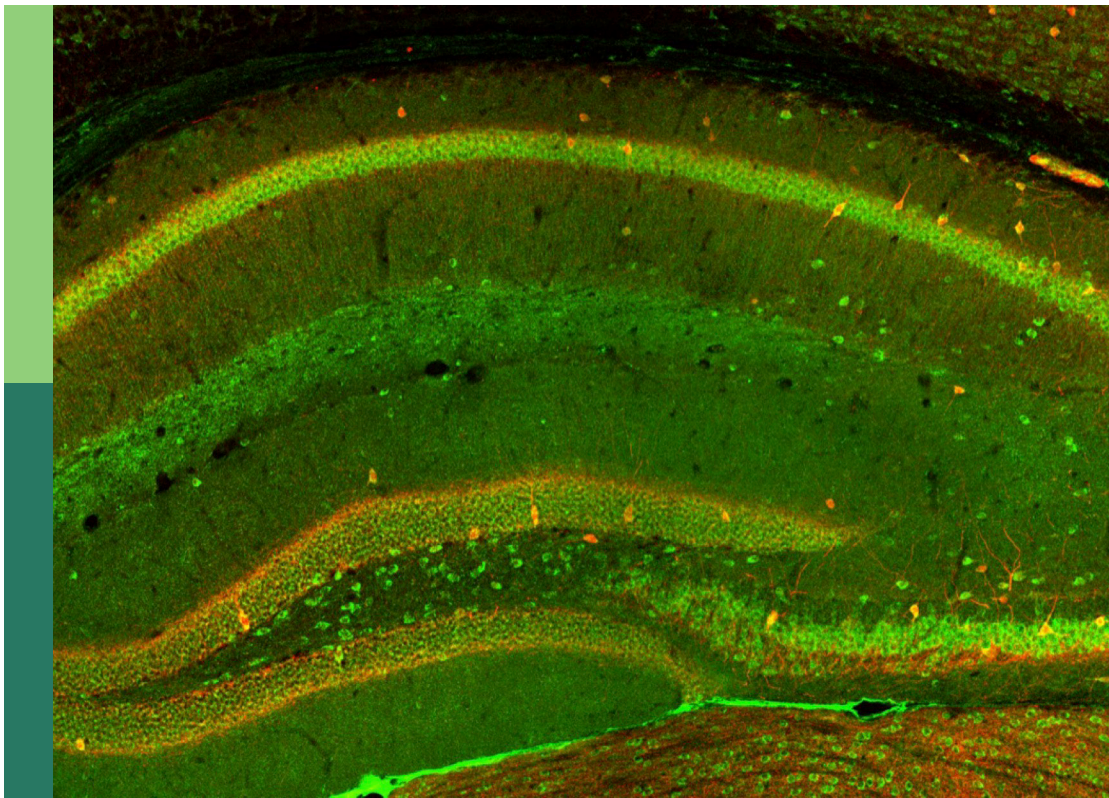

ISSN 1664-8714
ISBN 978-2-8325-3039-9
DOI 10.3389/978-2-8325-3039-9

About Frontiers

Frontiers is more than just an open access publisher of scholarly articles: it is a pioneering approach to the world of academia, radically improving the way scholarly research is managed. The grand vision of Frontiers is a world where all people have an equal opportunity to seek, share and generate knowledge. Frontiers provides immediate and permanent online open access to all its publications, but this alone is not enough to realize our grand goals.

Frontiers journal series

The Frontiers journal series is a multi-tier and interdisciplinary set of open-access, online journals, promising a paradigm shift from the current review, selection and dissemination processes in academic publishing. All Frontiers journals are driven by researchers for researchers; therefore, they constitute a service to the scholarly community. At the same time, the *Frontiers journal series* operates on a revolutionary invention, the tiered publishing system, initially addressing specific communities of scholars, and gradually climbing up to broader public understanding, thus serving the interests of the lay society, too.

Dedication to quality

Each Frontiers article is a landmark of the highest quality, thanks to genuinely collaborative interactions between authors and review editors, who include some of the world's best academicians. Research must be certified by peers before entering a stream of knowledge that may eventually reach the public - and shape society; therefore, Frontiers only applies the most rigorous and unbiased reviews. Frontiers revolutionizes research publishing by freely delivering the most outstanding research, evaluated with no bias from both the academic and social point of view. By applying the most advanced information technologies, Frontiers is catapulting scholarly publishing into a new generation.

What are Frontiers Research Topics?

Frontiers Research Topics are very popular trademarks of the *Frontiers journals series*: they are collections of at least ten articles, all centered on a particular subject. With their unique mix of varied contributions from Original Research to Review Articles, Frontiers Research Topics unify the most influential researchers, the latest key findings and historical advances in a hot research area.

Find out more on how to host your own Frontiers Research Topic or contribute to one as an author by contacting the Frontiers editorial office: frontiersin.org/about/contact

Ferroptosis in stroke, neurotrauma and neurodegeneration, volume II

Topic editors

Anwen Shao — Zhejiang University, China

Zhen-Ni Guo — First Affiliated Hospital of Jilin University, China

Weilin Xu — Zhejiang University, China

Citation

Shao, A., Guo, Z.-N., Xu, W., eds. (2023). *Ferroptosis in stroke, neurotrauma and neurodegeneration, volume II*. Lausanne: Frontiers Media SA.

doi: 10.3389/978-2-8325-3039-9

Table of contents

frontiers | Frontiers in Cellular Neuroscience

TYPE Editorial
PUBLISHED 05 July 2023
DOI 10.3389/fncel.2023.1238425

OPEN ACCESS

EDITED AND REVIEWED BY
Dirk M. Hermann,
University of Duisburg-Essen, Germany

*CORRESPONDENCE
Weilin Xu
✉ 11618330@zju.edu.cn
Anwen Shao
✉ anwenshao@sina.com

RECEIVED 11 June 2023
ACCEPTED 20 June 2023
PUBLISHED 05 July 2023

CITATION
Xu W, Guo Z-N and Shao A (2023) Editorial: Ferroptosis in stroke, neurotrauma and neurodegeneration, volume II.
Front. Cell. Neurosci. 17:1238425.
doi: 10.3389/fncel.2023.1238425

Editorial: Ferroptosis in stroke, neurotrauma and neurodegeneration, volume II

Weilin Xu[1,2]*, Zhen-Ni Guo[3] and Anwen Shao[1,2]*

[1]Department of Neurosurgery, The Second Affiliated Hospital, Zhejiang University School of Medicine, Hangzhou, Zhejiang, China, [2]Key Laboratory of Precise Treatment and Clinical Translational Research of Neurological Diseases, Hangzhou, Zhejiang, China, [3]Department of Neurology, The First Hospital of Jilin University, Changchun, China

KEYWORDS

ferroptosis, stroke, neurotrauma, neurodegeneration, cell death

Editorial on the Research Topic
Ferroptosis in stroke, neurotrauma and neurodegeneration, volume II

Ferroptosis, a new form of cell death, is characterized by the accumulation of intracellular iron and lipid reactive oxygen species (ROS) (Deng et al., 2023). The primary morphologic manifestations of ferroptosis include cell volume shrinkage and increased mitochondrial membrane density. This process of ferroptosis differs from other apoptotic types of cell death such as necroptosis and pyroptosis (Costa et al., 2023). Growing evidence indicates that ferroptosis plays key roles in neurological diseases such as stroke, traumatic brain injury (TBI), and neurodegenerative diseases [Alzheimer's disease (AD), Parkinson's disease (PD), amyotrophic lateral sclerosis (ALS), vascular dementia (VD), Huntington's disease (HD)] (Costa et al., 2023; Du et al., 2023). Ferroptosis inhibition has been shown to protect neurons and ameliorate cognitive impairment in various disease animal models (Li et al., 2022; Zhang et al., 2023). However, to date, the underlying mechanisms that how ferroptosis causes neurological injuries are still unclear. This Research Topic finally published nine studies, which extensively explored the relationships between ferroptosis and neurological diseases (stroke, TBI, and neurodegenerative diseases), including underlying mechanisms of ferroptosis, potential targeting, and the relationship between ferroptosis and other kinds of cell death (necroptosis and pyroptosis).

Ferroptosis and stroke

Zhu et al. adopted the method of bioinformatics analysis to explore the ferroptosis-related ceRNA regulation network in intracranial aneurysm. They analyzed data from the Gene Expression Omnibus (GEO) datasets and tried to identify differentially expressed genes (DEGs), differentially expressed miRNAs (DEMs), and differentially expressed lncRNAs (DELs) in intracranial aneurysm. In all, 30 ferroptosis DEGs, five key DEMs, and 17 key DELs were screened and they found that CeRNA (PVT1-hsa-miR-4644-SLC39A14 and DUXAP8-hsa-miR-378e/378f-SLC2A3) overexpression networks were associated with ferroptosis in intracranial aneurysm. Pan et al. extensively elucidated the underlying mechanisms of ferroptosis in hemorrhagic stroke. They reported that ferroptosis plays important roles in the hemorrhagic stroke. The mechanisms include ion overloaded, lipid

peroxidation, and dysfunctional antioxidant system. Moreover, they also discussed the crosstalk between ferroptosis and other types of neuronal death or autophagy. Finally, they pointed out that ferroptosis marker detection, diversity of ferroptotic cell, and the uncertainty about the magnitude and duration of ferroptotic action are mainly the research dilemma and will be the research prospects of ferroptosis. The third study by Cao et al. also introduced the underlying mechanism and crosstalk of ferroptosis with other modes of neuronal death after intracerebral hemorrhage. Except for the overlaping content showed by Pan et al., Cao et al. discussed several therapeutic targets of inhibitors of ferroptosis in ICH, including selenium supplementation, iron chelators (DFX, VK-28, deferiprone), lipoxygenase inhibitors, and DMT1 inhibitor (Ebselen). The study by Chen et al. extensively introduced different patterns of neuronal death and their molecular mechanisms after subarachnoid hemorrhage (SAH), including necrosis, apoptosis, pyroptosis, autophagy, necroptosis, and ferroptosis. In ferroptosis, they emphatically introduced three primary anti-ferroptosis systems, GPX4–GSH–cysteine system, FSP1–CoQ10–NAD (P)H system and GCH1-BH4-DHFR system. These studies extensively demonstrated the underlying mechanisms of ferroptosis in stroke and its potential therapeutic targets, which provides key information for future study of ferroptosis in stroke.

Ferroptosis and neurodegenerative diseases

Among the rest, three studies emphasized the important roles of ferroptosis in neurodegenerative diseases. Wang et al. applied bioinformatic analysis to explore ferroptosis-related biomarkers for AD. They also analyzed the data from GEO datasets and performed enrichment analyses of protein–protein interaction (PPI), the Gene Ontology (GO), and Kyoto Encyclopedia of Genes and Genomes (KEGG) pathway. Twenty-four ferroptosis-related genes were identified as target genes. Finally, ASNS and SENS2 are screened as potential diagnostic biomarkers for AD and provide additional evidence regarding the essential role of ferroptosis in AD. In another study, Fu et al. focused on investigating the expression pattern of ferroptosis and iron metabolism-related genes (FIRGs) in amyotrophic lateral sclerosis (ALS). They performed a conjoint analysis of bulk-RNA sequence and single-nucleus RNA sequence data using the datasets from GEO. Fifteen FIRGs was identified as target genes. Final analysis of bulk single-nucleus RNA-seq data showed that CHMP5 was expressed significantly higher in ALS than pathologically normal (PN), specifically in excitatory neuron populations. The third study comprehensively reviewed the relationship of ferroptosis and neurodegenerative diseases. Firstly, they introduced the mechanisms of ferroptosis, including transport and storage of iron in the brain, the glutamate/cysteine antiporter in ferroptosis and lipid peroxidation in ferroptosis. In the second part, they reviewed the roles of ferroptosis in each neurodegenerative disease, such as AD, vascular dementia (VD), PD, HD, ALS, and TBI. These three studies interestingly showed the molecular patterns and underlying mechanisms of ferroptosis in neurodegenerative diseases.

Ferroptosis and other neurological diseases

The remaining two studies provided another view of neuronal death in neurological diseases. Li et al. used bioinformatic analysis to identify cuproptosis-related genes (CRGs) on disease progression and the immune microenvironment in acute spinal cord injury (ASCI) patients. Their results showed that dihydrolipoamide dehydrogenase (DLD) affects the ASCI immune microenvironment by promoting copper toxicity, leading to increased peripheral M2 macrophage polarization and systemic immunosuppression. In the second study, Shi et al. demonstrated the underlying mechanisms of deep brain stimulation (DBS) for treatment of refractory obsessive-compulsive disorder (OCD).

In conclusion, ferroptosis plays important roles in various neurological diseases and its pathological mechanism is complicated. Ferroptosis differs from other apoptotic types of cell death (necrosis, apoptosis, pyroptosis, autophagy, necroptosis, and ferroptosis), however, it also connects with many physiological processes (apoptosis, autophagy, oxidative stress, inflammation). This Research Topic comprehensively discussed the underlying mechanisms and potential targets of ferroptosis in each neurological disease, which provides key insights for further study of ferroptosis in the central nervous system.

Author contributions

All authors listed have made a substantial, direct, and intellectual contribution to the work and approved it for publication.

Funding

This work was funded by National Natural Science Foundation of China (82001231), Zhejiang Provincial Natural Science Foundation of China (LQ21H090009), and Huadong Medicine Joint Funds of the Zhejiang Provincial Natural Science Foundation of China under Grant (LHDMZ22H300014).

Acknowledgments

We thank all authors for their contributions for this topic.

Conflict of interest

The authors declare that the research was conducted in the absence of any commercial or financial relationships that could be construed as a potential conflict of interest.

Publisher's note

References

Costa, I., Barbosa, D. J., Benfeito, S., Silva, V., Chavarria, D., Borges, F., et al. (2023). Molecular mechanisms of ferroptosis and their involvement in brain diseases. *Pharmacol. Ther.* 244, 108373. doi: 10.1016/j.pharmthera.2023.108373

Deng, X., Wu, Y., Hu, Z., Wang, S., Zhou, S., Zhou, C., et al. (2023). The mechanism of ferroptosis in early brain injury after subarachnoid hemorrhage. *Front. Immunol.* 14, 1191826. doi: 10.3389/fimmu.2023.1191826

Du, L., Wu, Y., Fan, Z., Li, Y., Guo, X., Fang, Z., et al. (2023). The role of ferroptosis in nervous system disorders. *J. Integr. Neurosci.* 22, 19. doi: 10.31083/j.jin2201019

Li, Y., Xiao, D., and Wang, X. (2022). The emerging roles of ferroptosis in cells of the central nervous system. *Front Neurosci.* 16, 1032140. doi: 10.3389/fnins.2022.1032140

Zhang, R. F., Zeng, M., Lv, N., Wang, L. M., Yang, Q. Y., Gan, J. L., et al. (2023). Ferroptosis in neurodegenerative diseases: inhibitors as promising candidate mitigators. *Eur. Rev. Med Pharmacol. Sci.* 27, 46–65. doi: 10.26355/eurrev_202301_30852

frontiers | Frontiers in Cellular Neuroscience

TYPE Original Research
PUBLISHED 13 October 2022
DOI 10.3389/fncel.2022.1016682

OPEN ACCESS

EDITED BY
Anwen Shao,
Zhejiang University, China

REVIEWED BY
Salam Pradeep Singh,
Suchee Bioinformatics Institute, India
Quanhui Chen,
Bethune International Peace Hospital, China

*CORRESPONDENCE
Yeyu Zhao
zyp19850922@126.com
Meihua Li
limeihua2000@sina.com

SPECIALTY SECTION
This article was submitted to Cellular Neuropathology, a section of the journal Frontiers in Cellular Neuroscience

RECEIVED 11 August 2022
ACCEPTED 29 September 2022
PUBLISHED 13 October 2022

CITATION
Zhu H, Tan J, Wang Z, Wu Z, Zhou W, Zhang Z, Li M and Zhao Y (2022) Bioinformatics analysis constructs potential ferroptosis-related ceRNA network involved in the formation of intracranial aneurysm. *Front. Cell. Neurosci.* 16:1016682. doi: 10.3389/fncel.2022.1016682

Bioinformatics analysis constructs potential ferroptosis-related ceRNA network involved in the formation of intracranial aneurysm

Huaxin Zhu, Jiacong Tan, Zhihua Wang, Zhiwu Wu, Wu Zhou, Zhixiong Zhang, Meihua Li* and Yeyu Zhao*

Department of Neurosurgery, The First Affiliated Hospital of Nanchang University, Nanchang, Jiangxi, China

Background: Intracranial aneurysm (IA) causes more than 80% of nontraumatic subarachnoid hemorrhages (SAHs). The mechanism of ferroptosis involved in IA formation remains unclear. The roles played by competitive endogenous RNA (ceRNA) regulation networks in many diseases are becoming clearer. The goal of this study was to understand more fully the ferroptosis-related ceRNA regulation network in IA.

Materials and methods: To identify differentially expressed genes (DEGs), differentially expressed miRNAs (DEMs), and differentially expressed lncRNAs (DELs) across IA and control samples, the GEO datasets GSE122897 and GSE66239 were downloaded and analyzed with the aid of R. Ferroptosis DEGs were discovered by exploring the DEGs of ferroptosis-related genes of the ferroptosis database. Potentially interacting miRNAs and lncRNAs were predicted using miRWalk and StarBase. Enrichment analysis was also performed. We utilized the STRING database and Cytoscape software to identify protein-protein interactions and networks. DAB-enhanced Prussian blue staining was used to detect iron in IA tissues.

Results: Iron deposition was evident in IA tissue. In all, 30 ferroptosis DEGs, 5 key DEMs, and 17 key DELs were screened out for constructing a triple regulatory network. According to expression regulation of DELs, DEMs, and DEGs, a hub triple regulatory network was built. As the functions of lncRNAs are determined by their cellular location,

PVT1-hsa-miR-4644-SLC39A14 ceRNA and DUXAP8-hsa-miR-378e/378f-SLC2A3 ceRNA networks were constructed.

Conclusion: CeRNA (PVT1-hsa-miR-4644-SLC39A14 and DUXAP8-hsa-miR-378e/378f-SLC2A3) overexpression networks associated with ferroptosis in IA were established.

KEYWORDS

intracranial aneurysm, ferroptosis, ceRNA network, gene expression omnibus, bioinformatics (genome and proteome) databases

Introduction

Intracranial aneurysm (IA) is a common cerebrovascular disease, with an incidence of about 1–2%, and saccular aneurysm is its most common type (Brown and Broderick, 2014; Etminan and Rinkel, 2016). In the Chinese population aged 35–75 years, the prevalence of IA is as high as 7% (Chen et al., 2018). More than 80% of nontraumatic subarachnoid hemorrhages (SAHs) are caused by IA rupture (Kassell et al., 1990; Koo et al., 2022). Aneurysmal SAHs have high mortality and disability rates, and are associated with devastating complications, such as delayed cerebral ischemia, seizures, and cerebral vasospasm (CVS), which can lead to poor prognosis and a heavy burden on society (Chalouhi et al., 2013; Chaudhry et al., 2021). IA is currently thought to be related to many factors, including age, hypertension, a genetic predisposition, hemodynamic changes, and environmental factors (Kwon, 2019). Despite decades of research on IA, the pathophysiological mechanisms underlying aneurysm formation, progression, and rupture remain unknown (Chalouhi et al., 2016; Pascale et al., 2020).

Stockwell was the first to propose the concept of ferroptosis, a type of cell death that differs from apoptosis, necroptosis, and autophagy (Dixon et al., 2012). Its occurrence has specific characteristics and regulatory genes or proteins. Morphologically, mitochondrial volume is reduced and mitochondrial cristae are reduced or absent (Jang et al., 2021). The inability to metabolize lipid peroxides reflects glutathione depletion and diminished glutathione peroxidase-4 (GPX4) activity, promoting ferroptosis (Imai et al., 2017). Immune cells release pro-inflammatory mediators including high mobility group protein B1 (HMGB1) when proteins with damage-associated molecular patterns (DAMPs) are released (Wu et al., 2021). The pathophysiology of cardiovascular disorders such as cardiomyopathy, atherosclerosis, and abdominal aortic aneurysms (AAAs) is complicated by ferroptosis (Sawada et al., 2015; Chen et al., 2019; Fang et al., 2019; Ouyang et al., 2021). HMGB1 is highly expressed in IA walls, particularly in ruptured IA tissue, and in patients with intracranial aneurysmal SAHs; increased HMGB1 levels are positively correlated with poor prognosis and cerebral vasospasm (Zhang et al., 2016; Chaudhry et al., 2018). However, the relationship between IA formation and ferroptosis remains unclear, and more research is needed to confirm the mechanism.

Non-coding RNAs, such as long non-coding RNAs (lncRNAs), short microRNAs (miRNAs), and circular RNAs (circRNAs), account for 95% of all eukaryotic RNAs (Hombach and Kretz, 2016). MiRNAs are small RNA molecules of about 22 nucleotides that regulate gene expression by degrading or inhibiting the transcription of target messenger RNA (mRNA). The functions affected include cell proliferation, differentiation, apoptosis, and disease onset and progression (Bartel, 2004; Zhang et al., 2019; Wittstatt et al., 2020). MiRNA-29a controls the mitochondrial apoptotic pathway, while miRNA-513b-5p targets the COL1A1 and COL1A2 proteins involved in IA formation and rupture (Zhao et al., 2018; Zheng et al., 2021). The lncRNAs are more than 200 nucleotides in length but do not have protein-coding capacity (Wilusz, 2016). The aberrant expression of lncRNAs in IA suggests a possible role in its pathogenesis, and various studies have reported the importance of lncRNAs in IA (Li et al., 2020; Pan W. et al., 2021; Pan Y. B. et al., 2021). Both miRNAs and lncRNAs also play critical roles in ferroptosis regulation. The lncRNAs are longer than 200 nucleotides but do not encode proteins. The lncRNA ZFAS1 promotes lung fibroblast-to-myofibroblast transition and ferroptosis through the miR-150-5p/SLC38A1 axis, whereas the lncRNA PVT1 controls ferroptosis through miR-214-mediated TFR1 and p53 (Lu et al., 2020; Yang et al., 2020). However, ferroptosis regulation by the lncRNA-miRNA-mRNA axis has rarely been investigated in IA.

Thus, we used staining to confirm iron deposition in IA and concluded that ferroptosis may be involved in IA onset and progression. We compared IA and normal tissues; we performed data mining and analysis to detect differentially expressed genes (DEGs), differentially expressed miRNAs (DEMs), and differentially expressed lncRNAs (DELs). An important lncRNA-miRNA-mRNA axis was discovered by constructing a ceRNA network using key DEGs, DEMs, and

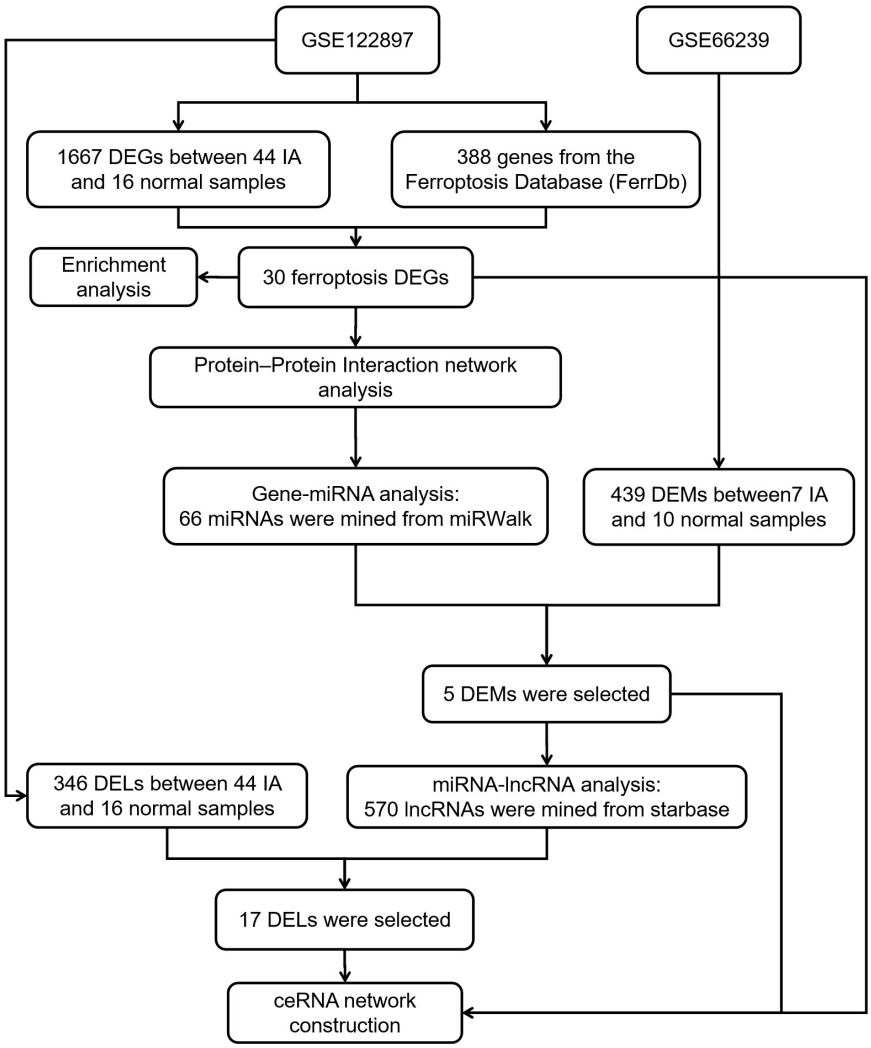

FIGURE 1
A flowchart showing how the lncRNA–miRNA–mRNA regulatory network of an intracranial aneurysm (IA) was constructed.

DELs. To better understand further the molecular causes of IA, we built a possible ferroptosis lncRNA-miRNA-mRNA regulation network.

Materials and methods

Superficial temporal artery and intracranial aneurysm tissues

Intracranial aneurysm tissue was obtained from patients undergoing surgical IA clipping, and STA tissue was obtained from patients with brain trauma who underwent removal of intracranial hematomas. All tissues were immediately fixed with 4% (v/v) paraformaldehyde and embedded in paraffin. All patients gave written informed consent prior to surgery. The First Affiliated Hospital of Nanchang University Ethics Committee approved the work.

Diaminobenzidine-enhanced Prussian blue staining

The Prussian Blue Iron Stain Kit, enhanced with diaminobenzidine (DAB), was obtained from Beijing Solarbio Science and Technology Co., Ltd. (Beijing, China). Paraffin tissues were dewaxed and hydrated with xylene and ethanol. The tissues were first exposed to Prussian blue for 30 min at 37°C, and then to the DAB chromogenic solution for 15 min at 37°C; they were counterstained for 5 min in hematoxylin staining solution, rendered transparent using xylene, dehydrated through graded ethanol baths, and mounted with neutral gum.

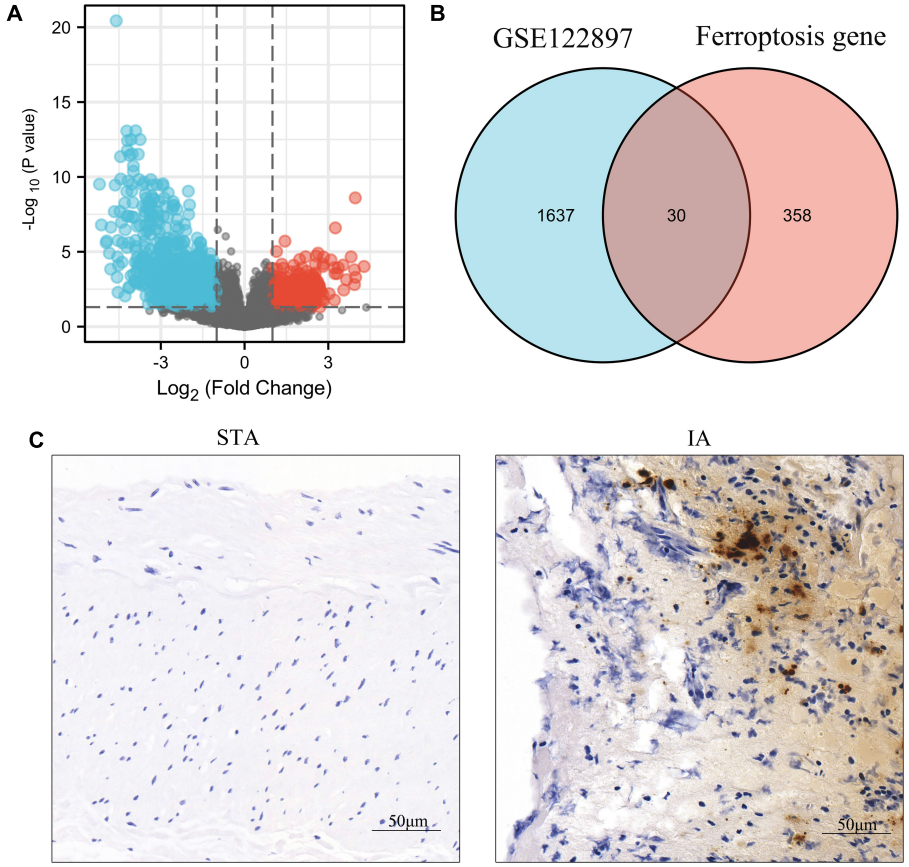

FIGURE 2
Identification of ferroptosis-related differentially expressed genes (DEGs) in GSE122897 and detection of iron in tissues. **(A)** Volcano plot of DEGs. **(B)** Venn diagram of ferroptosis DEGs. **(C)** Iron staining within superficial temporal artery (STA) and intracranial aneurysm (IA) tissues.

Data collection and preprocessing

Transcriptome information on IA patients was gathered from the Gene Expression Omnibus (GEO database at https://www.ncbi.nlm.nih.gov/geo/). IA-related datasets, GSE122897 and GSE66239, were downloaded from the GEO database and included in the analysis. The GSE122897 dataset, which contained 44 IA and 16 control samples, was used for expression profiling. GSE66239 is a microRNA dataset that contained 7 IA and 10 control samples. The workflow is depicted in **Figure 1**.

Differentially expressed gene, miRNA, and long non-coding RNA analysis

R package DESeq2 (1.26.0: The R foundation, Vienna, Austria) was used to analyze IA and control samples for obtaining DEGs, DEMs, and DELs. DEGs and DELs were obtained from GSE122897, while DEMs were obtained from GSE66239. Log2(FC) $>$ 1.0 and *P*-value $<$ 0.05 were considered the thresholds for DEGs, DEMs, and DELs. The results were displayed using volcano plots. We also used a dataset from the Ferroptosis database (FerrDb)[1] to find ferroptosis DEGs by intersecting ferroptosis genes with DEGs.

Functional and pathway enrichment analyses

For the GO and KEGG enrichment analyses, the R package clusterProfiler (3.14.3) was utilized. The findings were downloaded using the R packages dplyr (version 1.0.7) and ggplot2 (version 3.3.5). We uploaded the ferroptosis DEGs to Metascape, an online tool for gene function annotation analysis (Li et al., 2014).[2]

1 http://www.zhounan.org/ferrdb/
2 https://metascape.org/

TABLE 1 Ferroptosis differentially expressed genes (DEGs) of intracranial aneurysm (IA).

Gene symbol	Fold change	*P*-value	Gene title
Upregulated genes			
ABCC1	1.14	<0.001	ATP binding cassette subfamily C member 1
AQP3	1.03	0.013	Aquaporin 3
CDKN2A	1.40	0.031	Cyclin dependent kinase inhibitor 2A
CP	1.34	0.012	Ceruloplasmin
CXCL2	1.30	0.011	C–X–C motif chemokine ligand 2
DDIT4	1.11	0.016	DNA damage inducible transcript 4
HIF1A	1.02	0.017	Hypoxia inducible factor 1 subunit alpha
IL6	1.94	0.005	Interleukin 6
NNMT	1.38	0.013	Nicotinamide *N*-methyltransferase
NOX4	1.12	0.035	NADPH oxidase 4
PLIN2	1.72	0.003	Perilipin 2
PTGS2	1.20	0.011	Prostaglandin-endoperoxide synthase 2
RGS4	1.22	0.011	Regulator of G protein signaling 4
SAT1	1.04	0.033	Spermidine/spermine N1-acetyltransferase 1
SLC2A3	1.01	0.012	Solute carrier family 2 member 3
SLC39A14	1.32	0.007	Solute carrier family 39 member 14
TNFAIP3	1.49	0.004	TNF alpha induced protein 3
VDR	1.53	0.028	Vitamin D receptor
VEGFA	1.31	0.019	Vascular endothelial growth factor A
ZFP69B	1.01	0.003	ZFP69 zinc finger protein B
Downregulated genes			
AQP5	−1.98	0.022	Aquaporin 5
ATP6V1G2	−2.53	0.000	ATPase H+ transporting V1 subunit G2
FNDC5	−1.05	0.031	Fibronectin type III domain containing 5
GLS2	−1.06	0.010	Glutaminase 2
GPT2	−1.39	0.003	Glutamic–pyruvic transaminase 2
MT3	−3.61	<0.001	Metallothionein 3
PRKCA	−1.00	0.003	Protein kinase C alpha
PSAT1	−1.93	0.001	Phosphoserine aminotransferase 1
SLC2A12	−2.34	<0.001	Solute carrier family 2 member 12
SLC7A11	−1.35	0.013	Solute carrier family 7 member 11

TABLE 2 The ferroptosis differentially expressed genes (DEGs) were divided into ferroptosis driver, suppressor, and marker.

Driver	Suppressor	Marker
NOX4, ABCC1, SLC39A14, TNFAIP3, SAT1, GLS2, CDKN2A, PRKCA, AQP5, AQP3, and HIF1A IL6	CP, VDR, PLIN2, FNDC5, HIF1A, and SLC7A11	SLC2A3, PTGS2, CXCL2, MT3, VEGFA, RGS4, PSAT1, SLC2A12, GPT2, NNMT, DDIT4, ZFP69B, ATP6V1G2, IL6, and SLC7A11

Protein–protein interaction network analysis

Using String (version 11.5)[3], a PPI network for ferroptosis DEGs was created. PPI networks and modules playing essential roles in ferroptosis were further examined using Cytoscape (version 3.8.2).

Gene-miRNA interaction networks

To determine the crucial miRNAs and to develop DEG-miRNA interaction networks, we utilized miRWalk (version 3).[4] To ensure the correctness of the results, we combined the TargetScan and miRWalk results. Targeted miRNAs were intersected with DEMs from GSE66240 to identify key miRNAs. The DEG-miRNA network was visualized using Cytoscape.

miRNA–lncRNA interaction networks

Upstream lncRNAs for key miRNAs were identified using StarBase (Li et al., 2014).[5] Potential lncRNAs were intersected with DELs from GSE122897 to identify key lncRNAs. The key DEGs, DEMs, and DELs worked together to construct the triple regulatory network, and identified key ceRNAs through their expression regulation. Target sites were predicted using StarBase. DEL sequences were retrieved from LNCipedia[6]; the lncLocator database[7] was used to determine DEL cellular localizations. The networks were visualized using Cytoscape.

Immunohistochemistry

Paraffin tissues were dewaxed and rehydrated, immersed in EDTA solution (1 mM, pH 8.0), heated at 95°C for 1 h,

3 https://string-db.org

4 http://mirwalk.umm.uni-heidelberg.de/

5 https://starbase.sysu.edu.cn/

6 https://lncipedia.org

7 http://www.csbio.sjtu.edu.cn/bioinf/lncLocator/

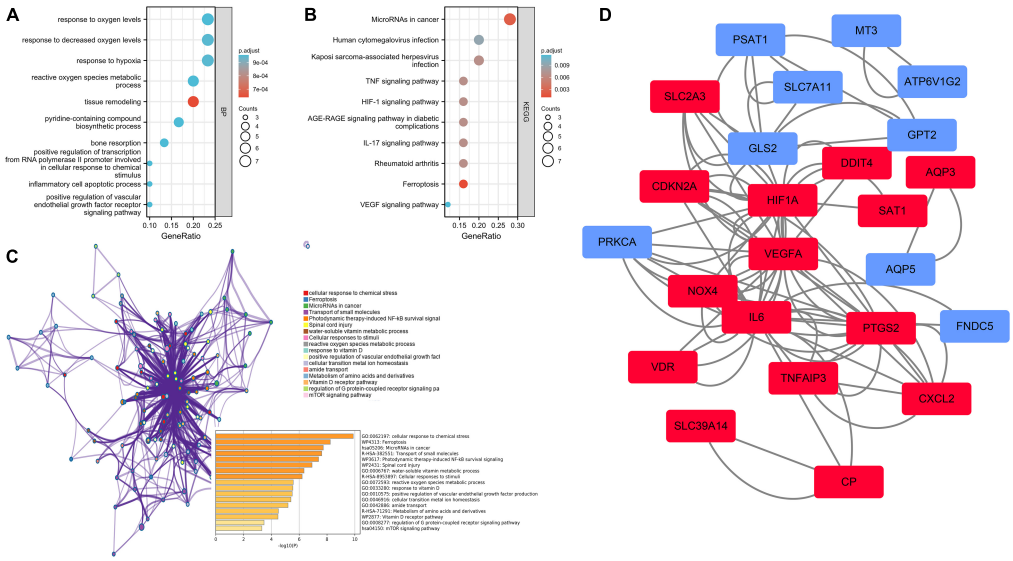

FIGURE 3
Enrichment analysis and the protein–protein interaction (PPI) network of the ferroptosis DEGs. **(A)** Gene set enrichment analysis of Gene Ontology biological process (GO-BP). **(B)** Gene set enrichment analysis of Kyoto Encyclopedia of Genes and Genomes (KEGG). **(C)** Network and bar chart of the enrichment results drawn by Metascape. **(D)** Construction of the PPI network. Navy-blue signifies downregulation and red upregulation.

treated with 3% hydrogen peroxide, incubated with 10% goat serum, and incubated overnight at 4°C using anti-SLC39A14 (Proteintech, Chicago, IL, USA) and anti-SLC2A3 (Affinity Biosciences, Nanjing, China), respectively. After incubation, slides were treated with biotinylated IgG and horseradish peroxidase-labeled streptomycin, respectively. Finally, the slides were stained with 3,3′-diaminobenzidine (DAB) and restained with hematoxylin. Images were taken under a microscope (ZEISS, Oberkochen, Germany).

Statistical analysis

R (version 4.1.0; the R foundation) was used for data preprocessing; DEG, DEM, and DEL screening; and enrichment analysis. Metascape was employed for functional annotation analysis. String was used to identify PPI networks. Potential miRNA and lncRNA interactions were mined using miRWalk and StarBase, respectively. The networks were visualized using Cytoscape. $P < 0.05$ was taken to indicate statistical significance.

Results

Ferroptosis differentially expressed genes and iron in tissues

We recovered 1,667 DEGs of the GSE122897 dataset based on a p-values 0.05 and $|\log2FC| > 1$. Of these, 483 evidenced upregulation and 1,184 downregulation (Figure 2A and Supplementary Table 1). The ferroptosis database (FerrDb) yielded 388 ferroptosis-related genes, which were overlapped with GSE122897 genes to locate ferroptosis DEGs (Figure 2B); 20 upregulated and 10 downregulated genes were identified (Table 1). Using the online FerrDb tool, the ferroptosis DEGs were further classified as ferroptosis drivers, suppressors, and markers (Table 2). DAB-enhanced Prussian blue staining revealed greater iron deposition in IA tissues compared to STA tissues (Figure 2C).

Enrichment analysis and protein–protein interaction network analysis of ferroptosis differentially expressed genes

The biological functions of ferroptosis DEGs were investigated using enrichment analysis employing the GO-BP (Figure 3A) and KEGG (Figure 3B) gene sets (Supplementary Table 2). Tissue remodeling, response to hypoxia, positive regulation of the vascular endothelial growth factor receptor signaling pathway, the response to decreased oxygen levels, the response to oxygen levels, inflammatory cell apoptotic processes, and reactive oxygen species metabolic processes were all significantly activated on GO-BP enrichment analysis. Ferroptosis and microRNAs may be involved in the IA process, as revealed by KEGG pathway enrichment analysis. Enrichment results drawn by Metascape were similar (Figure 3C). To create

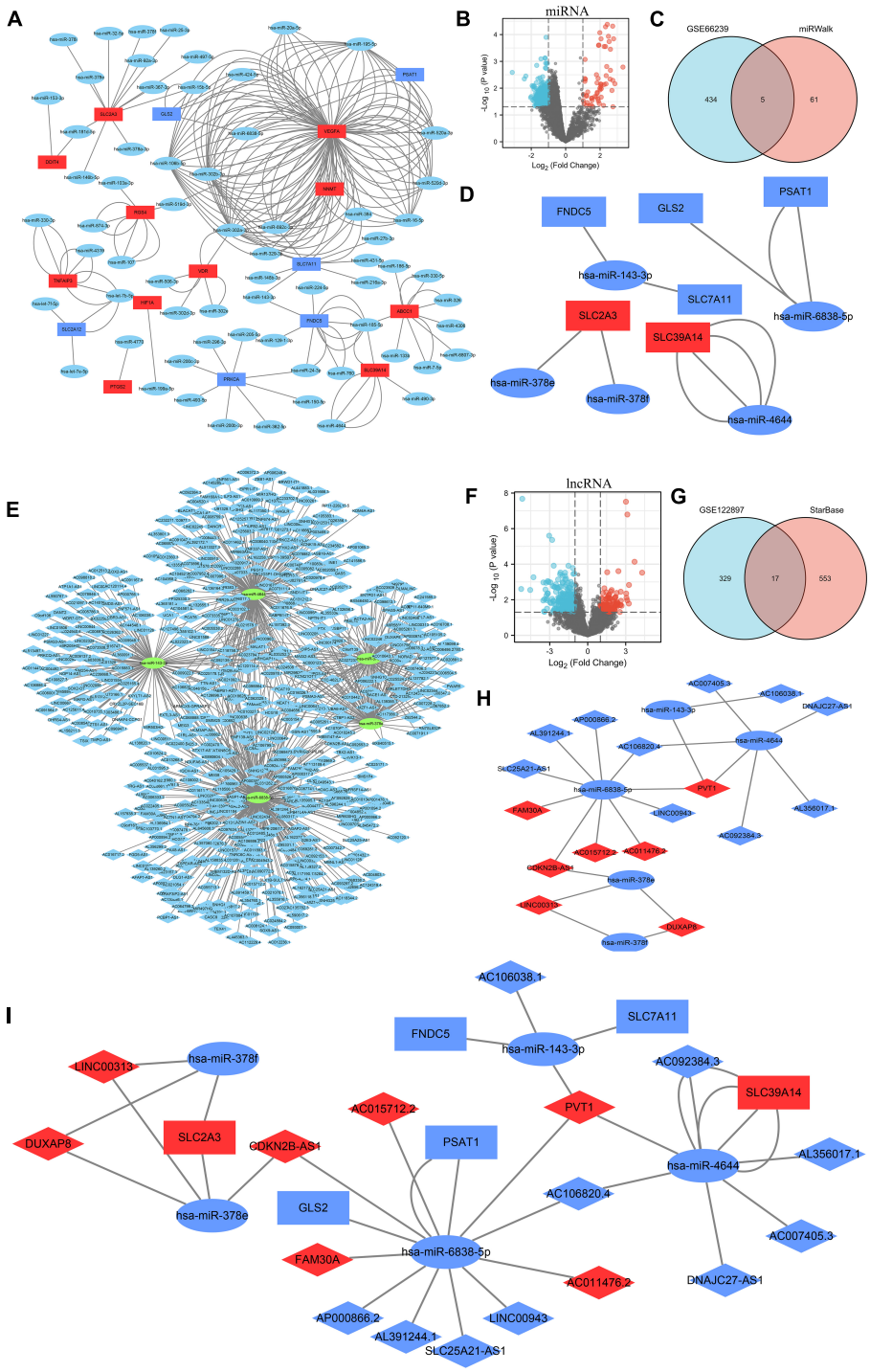

FIGURE 4
Construction of the triple regulatory network of differentially expressed lncRNAs (DELs), differentially expressed miRNAs (DEMs), and ferroptosis DEGs. **(A)** The interaction network between ferroptosis DEGs and the targeted miRNAs. **(B)** Volcano plot of DEMs in GSE66240. **(C)** Venn diagram of DEMs and potentially targeted miRNAs encoding ferroptosis DEGs. **(D)** Interaction network between the overlapped DEMs and the ferroptosis DEGs. **(E)** Interaction network between the overlapped DEMs and the targeted lncRNAs. **(F)** Volcano plot for DELs of GSE122897. **(G)** Venn diagram of DELs and the potentially targeted lncRNAs of the overlapped DELs. **(H)** Interaction network of the overlapped DELs and DEMs. **(I)** Triple regulatory network of the overlapped DELs, overlapped DEMs, and ferroptosis DEGs. MiRNAs are represented by ellipses, mRNAs by rectangles, and lncRNAs by diamonds. Navy-blue signifies downregulation and red upregulation.

TABLE 3 Overlapped DEMs.

miRNA ID	Fold change	*P*-value
hsa-miR-143-3p	−1.53	0.040
hsa-miR-143-5p	−3.10	0.003
hsa-miR-378e	−1.44	0.035
hsa-miR-378f	−1.09	0.021
hsa-miR-4644	−1.95	0.008

DELs, differentially expressed miRNAs.

TABLE 4 Overlapped DELs.

lncRNA ID	Fold change	*P*-value
LINC00313	1.14	0.044
LINC00943	−1.73	0.037
DUXAP8	3.02	<0.001
DNAJC27-AS1	−1.38	0.002
AL391244.1	−1.86	0.026
FAM30A	2.01	0.028
AC007405.3	−1.98	0.001
CDKN2B-AS1	1.17	0.028
AC106038.1	−1.12	0.050
PVT1	1.31	0.002
AP000866.2	−1.02	0.033
SLC25A21-AS1	−1.59	0.003
AL356017.1	−1.15	0.008
AC015712.2	1.22	0.018
AC106820.4	−2.33	0.007
AC092384.3	−1.39	0.050
AC011476.2	1.69	0.039

DELs, differentially expressed lncRNAs.

PPI networks, all ferroptosis DEGs were entered into the String database. The results were downloaded and visualized using Cytoscape (Figure 3D).

Further miRNA interactions and mining

Using miRWalk 2.0 software, we screened 30 ferroptosis DEGs and performed DEG-miRNA analysis. To assure the correctness of the results, crosslinked miRNAs were chosen from the miRWalk and TargetScan databases. Seventeen DEGs and 66 potential miRNA were mined and the network was constructed (Figure 4A and Supplementary Table 3). Based on a p-value < 0.05 and $|\log_2 FC| > 1$, 439 DEMs were screened from the GSE66240 dataset, including 55 upregulated and 384 downregulated DEMs (Figure 4B and Supplementary Table 4). Sixty-six mining miRNAs were intersected with DEMs from GSE66240 to identify key miRNAs (Figure 4C). Five overlapped miRNAs were selected (Table 3), and the network was constructed with ferroptosis DEGs (Figure 4D).

Further long non-coding RNA interactions and mining

Potential lncRNAs interacting with five key DEMs were screened using Starbase. A network of 570 lncRNAs interacted with five key DEMs (Figure 4E and Supplementary Table 5). Based on a p-value < 0.05 and $|\log_2 FC| > 1$, 346 DELs were screened from the GSE122897 dataset, including 109 that were upregulated and 237 that were downregulated (Figure 4F and Supplementary Table 6). A total of 254 mining lncRNAs were intersected with DELs from GSE122897 (Figure 4G). Seventeen overlapped lncRNAs were selected (Table 4), and the network was constructed using key DEMs (Figure 4H).

Construction of the competitive endogenous RNA network

In all, 17 overlapped DELs, three overlapped DEMs, and six DEGs were screened to construct a triple regulatory network (Figure 4I). According to expression regulation of DELs, DEMs, and DEGs, a hub triple regulatory network was built using four DELs, three DEMs, and two DEGs (Figure 5G). The areas under the curves (AUCs) for three DELs (PVT1, DUXAP8, and CDKN2B-AS1), three DEMs (hsa-miR-4644, hsa-miR-378e, and hsa-miR-378f), and two DEGs (SLC39A14 and SLC2A3) surpassed 0.7 for all included genes (Figures 5A–C). The expression levels of DELs, DEMs, and DEGs from the triple regulatory network are shown in Figures 5D–F.

The subcellular localization of the four DELs was investigated using lncLocator because the cellular localizations of lncRNAs determine their functions. The remaining two lncRNAs (LINC00313 and CDKN2B-AS1) were present principally in the nucleus, whereas PVT1 and DUXAP8 were largely confined to the cytoplasm (Figure 6A). These findings suggest that PVT1 and DUXAP8 may serve as ceRNAs that improve SLC39A14 and SLC2A3 expression, respectively. Thus, PVT1-hsa-miR-4644-SLC39A14 ceRNA (Figure 6B) and DUXAP8-hsa-miR-378e/378f-SLC2A3 ceRNA (Figure 6D) networks were constructed. The target sites in the PVT1 and SLC39A14 were predicted to pair with hsa-miR-4644 using StarBase (Figure 6C). Base pairing between hsa-miR-378e/378f, PVT1, and SLC39A14 were also predicted using StarBase (Figure 6E). Immunohistochemistry showed that SLC39A14 (Figure 6F) and SLC2A3 (Figure 6G) were significantly increased in IA tissue.

Discussion

On the one hand, bioinformatic analyses revealed abnormal expression of ferroptosis-related genes in IA; on the other hand, we found obvious iron deposition in IA tissue samples. This is

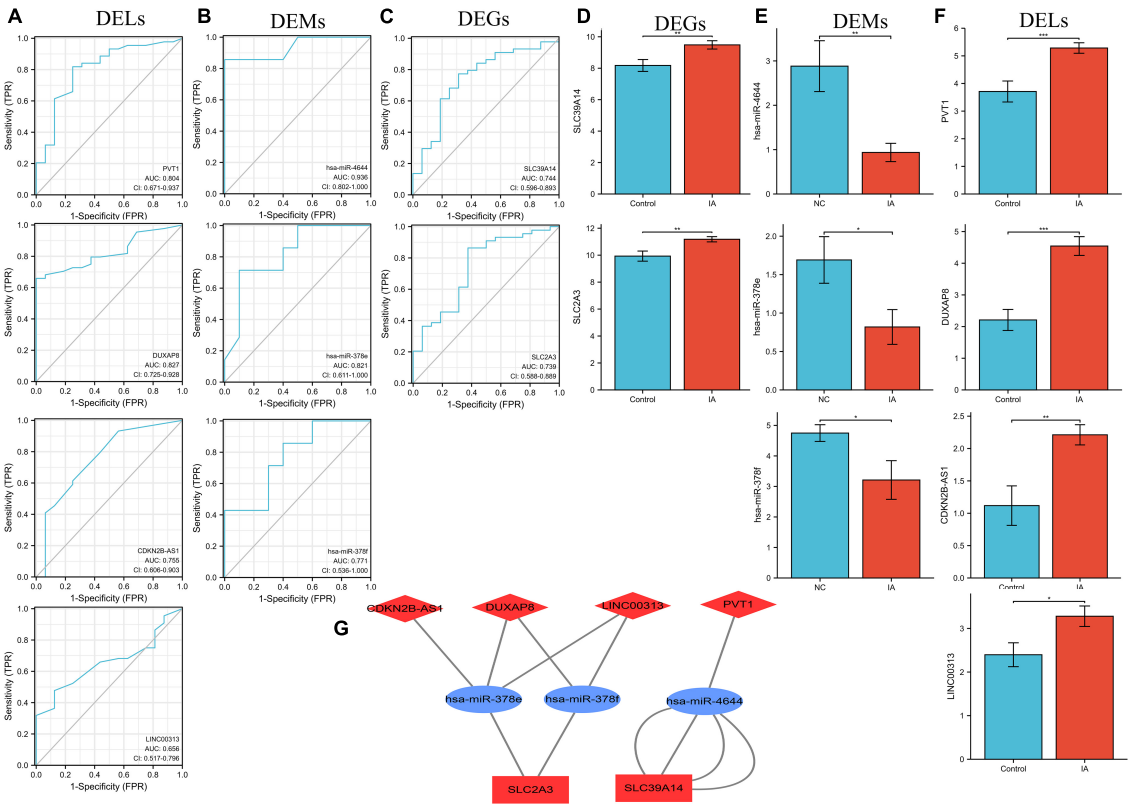

FIGURE 5
Construction of the key triple regulatory network. ROC analysis of DELs **(A)**, DEMs **(B)**, and DEGs **(C)**. The expression levels of DEGs **(D)**, DEMs **(E)**, and DELs **(F)**. **(G)** The key triple regulatory network components identified by regulation of their expression. MiRNAs are represented by ellipses, mRNAs by rectangles, and lncRNAs by diamonds. Navy-blue signifies downregulation and red upregulation.

the first time that IA has been associated with ferroptosis by combined analysis of bioinformatics and pathological samples. We then constructed potential ceRNA regulatory networks using various approaches, providing a possible molecular basis for regulation by ferroptosis of IA formation.

Worldwide, cardiovascular illnesses continue to be the major cause of death. Among them, aneurysms are considered silent killers, and the gravity of their consequences should not be underestimated (Chung et al., 2021). IA is the most common cause of SAH; the multiple pathophysiological alterations that develop after SAH frequently cause irreparable brain damage, complications, and death (Brouwers et al., 1993; Macdonald and Schweizer, 2017; Petridis et al., 2017). Although different treatment options for IA patients have been implemented, most focus on IA development or rupture; they do seek to prevent IA (Arena et al., 2017). A focus on IA formation, progression, and prevention (rather than the molecular mechanisms underlying pathogenesis) may be more beneficial for patients. Many cardiovascular disorders, including atherosclerosis, abdominal aortic aneurysms, and hypertension, are linked to the ceRNA regulatory network (Cai et al., 2020; Yu X. H. et al., 2020; Zhang et al., 2020). Few studies, however, have sought a whole-ceRNA regulation network for IA. As a result, the goal of this study was to create a ferroptosis-related ceRNA triple network for IA. Although there is growing evidence that ferroptosis functions as a regulator in several cardiovascular disorders, any involvement in IA remains unknown.

In this study, IA-related DEGs, DEMs, and DELs were first analyzed from the GEO database using bioinformatic techniques, and 30 ferroptosis-related DEGs were extracted by intersecting DEGs with ferroptosis genes. The PPI network evidenced correlations among ferroptosis-related DEGs. DAB-enhanced Prussian blue staining revealed iron deposition in IA tissues, confirming that ferroptosis may play an important role in IA. Then, the screened ferroptosis-related DEGs, key DEMs, and key DELs were constructed into triple networks, and four DELs, three DEMs, and two DEGs built the hub regulatory networks based on the expression regulation. Finally, this hub regulatory network was subjected to ROC and expression analyses. As the linkages of the ceRNA network are active only in the cytoplasm, we performed subcellular localization analyses of the three lncRNAs in the network. In conclusion, the IA ferroptosis ceRNA networks PVT1-hsa-miR-4644-SLC39A14 and DUXAP8-hsa-miR-378e/378f-SLC2A3 were discovered.

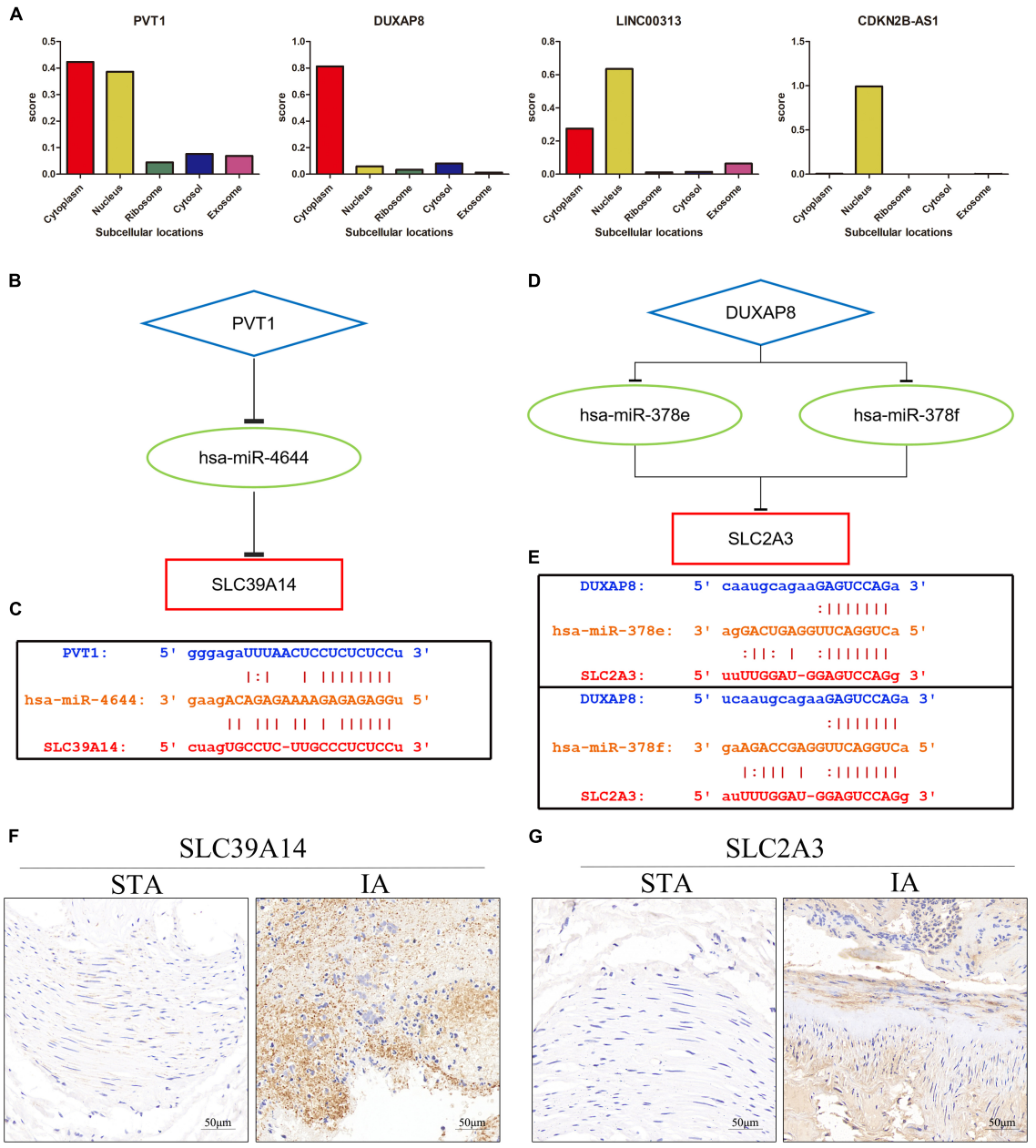

FIGURE 6
Construction of the ceRNA network. **(A)** The cellular localizations of four DELs (PVT1, DUXAP8, LINC00313, and CDKN2B-AS1). **(B)** A schematic of ceRNA (PVT1-hsa-miR-4644-SLC39A14). **(C)** Base pairing between hsa-miR-4644, PVT1, and SLC39A14 as predicted by StarBase. **(D)** A schematic of ceRNA (DUXAP8-hsa-miR-378e/378f-SLC2A13). **(E)** Base pairing between hsa-miR-378e/378f, PVT1, and SLC39A14 as predicted by StarBase. **(F)** Expression of SLC39A14 in STA and IA tissue. **(G)** Expression of SLC2A3 in STA and IA tissue.

During ferroptosis, oxygen molecules are added to lipids, usually to the polyunsaturated fatty acyl tails of phospholipids, leading to cell death (Hirschhorn and Stockwell, 2019). A variety of diseases have been linked to lipid peroxidation, which, commonly damages the unsaturated lipid moieties of cell membranes and lipoproteins (Romero et al., 1998; Barrera et al., 2008). The reactive oxygen species metabolic pathway played a key role in our function enrichment study. The first stage in IA development is endothelial dysfunction, followed by VSMC phenotypic alteration, extracellular matrix remodeling, and cell death, in turn triggering vascular degeneration, dilatation, and rupture (Starke et al., 2013). Numerous studies have linked inflammation to IA emergence, growth, and rupture (Chalouhi et al., 2012; Hasan et al., 2012). Oxidative stress, attributable to increased free radical formation and/or decreased free radical scavenging, triggers endothelial dysfunction, immune cell

infiltration, and VSMC proliferation and migration (Griendling and FitzGerald, 2003; Canes et al., 2021). After pyuvate kinase muscle isozyme 2 activation and lipid peroxidation, T lymphocyte-derived extracellular vesicles exacerbate abdominal aortic aneurysms (Dang et al., 2022). Numerous studies have found that smoking is an independent risk factor for IA, and cigarette extract specifically-triggered ferroptosis of VSMC raises the possibility that ferroptosis may contribute to the pathogenesis of aneurysms (Meschia et al., 2014; Bakker et al., 2020; Sampilvanjil et al., 2020). Few previous studies have investigated the role of ferroptosis in IA. We used bioinformatic analyses and tissue staining to discover abnormal expression of ferroptosis-related genes and iron deposition in IA tissues; ferroptosis seems to play an important role in IA.

We identified two ceRNA networks, PVT1-hsa-miR-4644-SLC39A14 and DUXAP8-hsa-miR-378e/378f-SLC2A3, which may be implicated in the IA disease process. And we verified the expression of SLC39A14 and SLC2A3 in IA by IHC, which further ensured the reliability and accuracy of the results.

SLC39A14, also known as ZIP4, is an important metal transporter that plays an important role in the regulation of metal ions such as manganese (Winslow et al., 2020). Increased levels of SLC39A14 protein on the cell membrane contribute to unstable iron accumulation in skeletal muscles, which in turn lead to the activation of ferroptosis (Ding et al., 2021). Decreased SLC39A14 expression in liver significantly reduces iron accumulation, thereby reducing liver fibrosis mediated by ferroptosis (Yu Y. et al., 2020). These results imply that SLC39A14 may also be crucial in terms of iron control. Although plasmacytoma variant translocation 1 (PVT1) is recognized as an oncogene involved in carcinogenesis, the gene also plays a role in ferroptosis control (Bohosova et al., 2021; He Y. et al., 2021). PVT1 controls ferroptosis associated with cerebral ischemia/reperfusion (I/R) via miR-214-mediated regulation of TFR1 and TP53 expression, while ketamine regulates ferroptosis in hepatoma cells via lncRNA PVT1 (Lu et al., 2020; He G. N. et al., 2021). Hsa-miR-4644 acts as a potential interacting miRNA for SLC39A14 and PVT1; the PVT1-hsa-miR-4644-SLC39A14 ceRNA network may serve as a potential regulatory axis for ferroptosis.

Glucose transmembrane transport are performed by SLC2A3, a membrane transporter that belongs to the solute carrier family (Gao et al., 2021). Lymphoid-specific helicase can inhibit ferroptosis in lung cancer cells, and LSH knockout decreases SLC2A3 and induces ferroptosis, which implies that SLC2A3 may be involved in inhibiting ferroptosis (Jiang et al., 2017). Double homeobox A pseudogene 8 (DUXAP8), as a novel, long noncoding RNA, is associated with a number of cancers, including liver, colorectal, bladder, oral, ovarian, lung, and pancreatic tumors (Xue et al., 2021). However, it is rarely studied in ferroptosis and, whether the DUXAP8-hsa-miR-378e/378f-SLC2A3 ceRNA network we constructed is involved in the regulation of ferroptosis, remains to be verified.

Although the ceRNA-based PVT1/SLC39A14 and DUXAP8/SLC2A3 axes appear to be potential ferroptosis-regulating axes in IA, our work had certain limitations. First, experimental data on the binding affinities of lncRNAs, miRNAs, and mRNAs identified in the databases are required. Second, further research is required to confirm the functions and modes of action of the PVT1/SLC39A14 and DUXAP8/SLC2A3 axes in IA.

Conclusion

In summary, we constructed two ceRNA pathways (PVT1-hsa-miR-4644-SLC39A14 and DUXAP8-hsa-miR-378e/378f-SLC2A3) using IA information; both are potentially linked to ferroptosis. We hope that our findings will aid future in-depth research.

Data availability statement

The original contributions presented in this study are included in the article/**Supplementary material**, further inquiries can be directed to the corresponding authors.

Ethics statement

Human IA and STA tissue samples were obtained from the First Affiliated Hospital of Nanchang University. The First Affiliated Hospital of Nanchang University's Ethics Committee gave its approval for this study.

Author contributions

HZ and YZ: conceptualization. HZ and WZ: methodology. JT: software. ZWa, ZWu, and ZZ: validation. YZ: formal analysis and supervision. HZ: investigation, data curation, and writing—original draft preparation. ZWa: resources. ML: writing—review and editing and project administration. JT and WZ: visualization. YZ and ML: funding acquisition. All authors read and agreed to the published version of the manuscript.

Funding

This research was funded by the National Natural Science Foundation of China (NSFC) (Nos. 81860225 and 82260248), the Key Research and Development Plan of Jiangxi Province (No. 20203BBG73060), Natural Science Foundation of Jiangxi Province (No. 20212BAB206029), and Young Talents Research and Cultivation Foundation of the First Affiliated Hospital of Nanchang University (No. YFYPY202038).

Conflict of interest

The authors declare that the research was conducted in the absence of any commercial or financial relationships that could be construed as a potential conflict of interest.

Publisher's note

All claims expressed in this article are solely those of the authors and do not necessarily represent those of their affiliated organizations, or those of the publisher, the editors and the reviewers. Any product that may be evaluated in this article, or claim that may be made by its manufacturer, is not guaranteed or endorsed by the publisher.

Supplementary material

The Supplementary Material for this article can be found online at: https://www.frontiersin.org/articles/10.3389/fncel.2022.1016682/full#supplementary-material

References

Arena, J. E., Hawkes, M. A., Farez, M. F., Pertierra, L., Kohler, A. A., Marrodan, M., et al. (2017). Headache and treatment of unruptured intracranial aneurysms. *J. Stroke Cerebrovasc. Dis.* 26, 1098–1103.

Bakker, M. K., van der Spek, R., van Rheenen, W., Morel, S., Bourcier, R., Hostettler, I. C., et al. (2020). Genome-wide association study of intracranial aneurysms identifies 17 risk loci and genetic overlap with clinical risk factors. *Nat. Genet.* 52, 1303–1313. doi: 10.1038/s41588-020-00725-7

Barrera, G., Pizzimenti, S., and Dianzani, M. U. (2008). Lipid peroxidation: control of cell proliferation, cell differentiation and cell death. *Mol. Aspects Med.* 29, 1–8. doi: 10.1016/j.mam.2007.09.012

Bartel, D. P. (2004). Micrornas: genomics, biogenesis, mechanism, and function. *Cell* 116, 281–297.

Bohosova, J., Kubickova, A., and Slaby, O. (2021). Lncrna pvt1 in the pathogenesis and clinical management of renal cell carcinoma. *Biomolecules* 11:664. doi: 10.3390/biom11050664

Brouwers, P. J., Dippel, D. W., Vermeulen, M., Lindsay, K. W., Hasan, D., and van Gijn, J. (1993). Amount of blood on computed tomography as an independent predictor after aneurysm rupture. *Stroke* 24, 809–814. doi: 10.1161/01.str.24.6.809

Brown, R. J., and Broderick, J. P. (2014). Unruptured intracranial aneurysms: epidemiology, natural history, management options, and familial screening. *Lancet Neurol.* 13, 393–404. doi: 10.1016/S1474-4422(14)70015-8

Cai, B., Yang, B., Huang, D., Wang, D., Tian, J., Chen, F., et al. (2020). Stat3-induced up-regulation of lncrna neat1 as a cerna facilitates abdominal aortic aneurysm formation by elevating tulp3. *Biosci. Rep.* 40:BSR20193299. doi: 10.1042/BSR20193299

Canes, L., Alonso, J., Ballester-Servera, C., Varona, S., Escudero, J. R., Andres, V., et al. (2021). Targeting tyrosine hydroxylase for abdominal aortic aneurysm: impact on inflammation, oxidative stress, and vascular remodeling. *Hypertension* 78, 681–692. doi: 10.1161/HYPERTENSIONAHA.121.17517

Chalouhi, N., Ali, M. S., Jabbour, P. M., Tjoumakaris, S. I., Gonzalez, L. F., Rosenwasser, R. H., et al. (2012). Biology of intracranial aneurysms: role of inflammation. *J. Cereb. Blood Flow Metab.* 32, 1659–1676. doi: 10.1038/jcbfm.2012.84

Chalouhi, N., Hoh, B. L., and Hasan, D. (2013). Review of cerebral aneurysm formation, growth, and rupture. *Stroke* 44, 3613–3622. doi: 10.1161/STROKEAHA.113.002390

Chalouhi, N., Starke, R. M., Correa, T., Jabbour, P. M., Zanaty, M., Brown, R. J., et al. (2016). Differential sex response to aspirin in decreasing aneurysm rupture in humans and mice. *Hypertension* 68, 411–417. doi: 10.1161/HYPERTENSIONAHA.116.07515

Chaudhry, S. R., Guresir, A., Stoffel-Wagner, B., Fimmers, R., Kinfe, T. M., Dietrich, D., et al. (2018). Systemic high-mobility group box-1: a novel predictive biomarker for cerebral vasospasm in aneurysmal subarachnoid hemorrhage. *Crit. Care Med.* 46, e1023–e1028. doi: 10.1097/CCM.0000000000003319

Chaudhry, S. R., Kahlert, U. D., Kinfe, T. M., Endl, E., Dolf, A., Niemela, M., et al. (2021). Differential polarization and activation dynamics of systemic t helper cell subsets after aneurysmal subarachnoid hemorrhage (sah) and during post-sah complications. *Sci. Rep.* 11:14226. doi: 10.1038/s41598-021-92873-x

Chen, J., Liu, J., Zhang, Y., Tian, Z., Wang, K., Zhang, Y., et al. (2018). China intracranial aneurysm project (ciap): protocol for a registry study on a multidimensional prediction model for rupture risk of unruptured intracranial aneurysms. *J. Transl. Med.* 16:263. doi: 10.1186/s12967-018-1641-1

Chen, X., Xu, S., Zhao, C., and Liu, B. (2019). Role of tlr4/nadph oxidase 4 pathway in promoting cell death through autophagy and ferroptosis during heart failure. *Biochem. Biophys. Res. Commun.* 516, 37–43. doi: 10.1016/j.bbrc.2019.06.015

Chung, D. Y., Abdalkader, M., and Nguyen, T. N. (2021). Aneurysmal subarachnoid hemorrhage. *Neurol. Clin.* 39, 419–442. doi: 10.1016/j.ncl.2021.02.006

Dang, G., Li, T., Yang, D., Yang, G., Du, X., Yang, J., et al. (2022). T lymphocyte-derived extracellular vesicles aggravate abdominal aortic aneurysm by promoting macrophage lipid peroxidation and migration via pyruvate kinase muscle isozyme 2. *Redox Biol.* 50:102257. doi: 10.1016/j.redox.2022.102257

Ding, H., Chen, S., Pan, X., Dai, X., Pan, G., Li, Z., et al. (2021). Transferrin receptor 1 ablation in satellite cells impedes skeletal muscle regeneration through activation of ferroptosis. *J. Cachexia Sarcopenia Muscle* 12, 746–768. doi: 10.1002/jcsm.12700

Dixon, S. J., Lemberg, K. M., Lamprecht, M. R., Skouta, R., Zaitsev, E. M., Gleason, C. E., et al. (2012). Ferroptosis: an iron-dependent form of nonapoptotic cell death. *Cell* 149, 1060–1072. doi: 10.1016/j.cell.2012.03.042

Etminan, N., and Rinkel, G. J. (2016). Unruptured intracranial aneurysms: development, rupture and preventive management. *Nat. Rev. Neurol.* 12, 699–713. doi: 10.1038/nrneurol.2016.150

Fang, X., Wang, H., Han, D., Xie, E., Yang, X., Wei, J., et al. (2019). Ferroptosis as a target for protection against cardiomyopathy. *Proc. Natl. Acad. Sci. U S A.* 116, 2672–2680. doi: 10.1073/pnas.1821022116

Gao, H., Liang, J., Duan, J., Chen, L., Li, H., Zhen, T., et al. (2021). A prognosis marker slc2a3 correlates with emt and immune signature in colorectal cancer. *Front. Oncol.* 11:638099. doi: 10.3389/fonc.2021.638099

Griendling, K. K., and FitzGerald, G. A. (2003). Oxidative stress and cardiovascular injury: part i: basic mechanisms and in vivo monitoring of ros. *Circulation* 108, 1912–1916. doi: 10.1161/01.CIR.0000093660.86242.BB

Hasan, D., Chalouhi, N., Jabbour, P., Dumont, A. S., Kung, D. K., Magnotta, V. A., et al. (2012). Early change in ferumoxytol-enhanced magnetic resonance imaging signal suggests unstable human cerebral aneurysm: a pilot study. *Stroke* 43, 3258–3265. doi: 10.1161/STROKEAHA.112.673400

He, G. N., Bao, N. R., Wang, S., Xi, M., Zhang, T. H., and Chen, F. S. (2021). Ketamine induces ferroptosis of liver cancer cells by targeting lncrna pvt1/mir-214-3p/gpx4. *Drug Des. Devel. Ther.* 15, 3965–3978. doi: 10.2147/DDDT.S332847

He, Y., Ye, Y., Tian, W., and Qiu, H. (2021). A novel lncrna panel related to ferroptosis, tumor progression, and microenvironment is a robust prognostic indicator for glioma patients. *Front. Cell Dev. Biol.* 9:788451. doi: 10.3389/fcell.2021.788451

Hirschhorn, T., and Stockwell, B. R. (2019). The development of the concept of ferroptosis. *Free Radic Biol. Med.* 133, 130–143. doi: 10.1016/j.freeradbiomed.2018.09.043

Hombach, S., and Kretz, M. (2016). Non-coding rnas: classification, biology and functioning. *Adv. Exp. Med. Biol.* 937, 3–17. doi: 10.1007/978-3-319-42059-2_1

Imai, H., Matsuoka, M., Kumagai, T., Sakamoto, T., and Koumura, T. (2017). Lipid peroxidation-dependent cell death regulated by gpx4 and ferroptosis. *Curr. Top. Microbiol. Immunol.* 403, 143–170. doi: 10.1007/82_2016_508

Jang, S., Chapa-Dubocq, X. R., Tyurina, Y. Y., St, C. C., Kapralov, A. A., Tyurin, V. A., et al. (2021). Elucidating the contribution of mitochondrial glutathione to ferroptosis in cardiomyocytes. *Redox Biol.* 45:102021.

Jiang, Y., Mao, C., Yang, R., Yan, B., Shi, Y., Liu, X., et al. (2017). Egln1/c-myc induced lymphoid-specific helicase inhibits ferroptosis through lipid metabolic gene expression changes. *Theranostics* 7, 3293–3305. doi: 10.7150/thno.19988

Kassell, N. F., Torner, J. C., Jane, J. A., Haley, E. J., and Adams, H. P. (1990). The international cooperative study on the timing of aneurysm surgery. Part 2: surgical results. *J. Neurosurg.* 73, 37–47. doi: 10.3171/jns.1990.73.1.0037

Koo, A. B., Elsamadicy, A. A., Renedo, D., Sarkozy, M., Sherman, J., Reeves, B. C., et al. (2022). Higher hospital frailty risk score is associated with increased complications and healthcare resource utilization after endovascular treatment of ruptured intracranial aneurysms. *J, Neurointerv. Surg.* Online ahead of print. doi: 10.1136/neurintsurg-2021-018484

Kwon, O. K. (2019). Headache and aneurysm. *Neuroimaging Clin. N. Am.* 29, 255–260. doi: 10.1016/j.nic.2019.01.004

Li, J. H., Liu, S., Zhou, H., Qu, L. H., and Yang, J. H. (2014). Starbase v2.0: decoding mirna-cerna, mirna-ncrna and protein-rna interaction networks from large-scale clip-seq data. *Nucleic Acids Res.* 42, D92–D97. doi: 10.1093/nar/gkt1248

Li, X., Zhao, H., Liu, J., and Tong, J. (2020). Long non-coding rna miat knockdown prevents the formation of intracranial aneurysm by downregulating enc1 via myc. *Front. Physiol.* 11:572605. doi: 10.3389/fphys.2020.572605

Lu, J., Xu, F., and Lu, H. (2020). Lncrna pvt1 regulates ferroptosis through mir-214-mediated tfr1 and p53. *Life Sci.* 260:118305. doi: 10.1016/j.lfs.2020.118305

Macdonald, R. L., and Schweizer, T. A. (2017). Spontaneous subarachnoid haemorrhage. *Lancet* 389, 655–666. doi: 10.1016/S0140-6736(16)30668-7

Meschia, J. F., Bushnell, C., Boden-Albala, B., Braun, L. T., Bravata, D. M., Chaturvedi, S., et al. (2014). Guidelines for the primary prevention of stroke: a statement for healthcare professionals from the american heart association/american stroke association. *Stroke* 45, 3754–3832. doi: 10.1161/STR.0000000000000046

Ouyang, S., You, J., Zhi, C., Li, P., Lin, X., Tan, X., et al. (2021). Ferroptosis: the potential value target in atherosclerosis. *Cell Death Dis.* 12:782. doi: 10.1038/s41419-021-04054-3

Pan, W., Gao, Y., Wan, W., Xiao, W., and You, C. (2021). Lncrna sammson overexpression suppresses vascular smooth muscle cell proliferation via inhibiting mir-130a maturation to participate in intracranial aneurysm. *Neuropsychiatr. Dis. Treat.* 17, 1793–1799. doi: 10.2147/NDT.S311499

Pan, Y. B., Lu, J., Yang, B., Lenahan, C., Zhang, J., and Shao, A. (2021). Construction of competitive endogenous rna network reveals regulatory role of long non-coding rnas in intracranial aneurysm. *BMC Neurosci.* 22:15. doi: 10.1186/s12868-021-00622-7

Pascale, C. L., Martinez, A. N., Carr, C., Sawyer, D. M., Ribeiro-Alves, M., Chen, M., et al. (2020). Treatment with dimethyl fumarate reduces the formation and rupture of intracranial aneurysms: role of nrf2 activation. *J. Cereb. Blood Flow Metab.* 40, 1077–1089. doi: 10.1177/0271678X19858888

Petridis, A. K., Kamp, M. A., Cornelius, J. F., Beez, T., Beseoglu, K., Turowski, B., et al. (2017). Aneurysmal subarachnoid hemorrhage. *Dtsch Arztebl Int.* 114, 226–236. doi: 10.3238/arztebl.2017.0226

Romero, F. J., Bosch-Morell, F., Romero, M. J., Jareno, E. J., Romero, B., Marin, N., et al. (1998). Lipid peroxidation products and antioxidants in human disease. *Environ. Health Perspect.* 106(Suppl. 5), 1229–1234. doi: 10.1289/ehp.98106s51229

Sampilvanjil, A., Karasawa, T., Yamada, N., Komada, T., Higashi, T., Baatarjav, C., et al. (2020). Cigarette smoke extract induces ferroptosis in vascular smooth muscle cells. *Am. J. Physiol. Heart Circ. Physiol.* 318, H508–H518. doi: 10.1152/ajpheart.00559.2019

Sawada, H., Hao, H., Naito, Y., Oboshi, M., Hirotani, S., Mitsuno, M., et al. (2015). Aortic iron overload with oxidative stress and inflammation in human and murine abdominal aortic aneurysm. *Arterioscler. Thromb. Vasc. Biol.* 35, 1507–1514. doi: 10.1161/ATVBAHA.115.305586

Starke, R. M., Chalouhi, N., Ali, M. S., Jabbour, P. M., Tjoumakaris, S. I., Gonzalez, L. F., et al. (2013). The role of oxidative stress in cerebral aneurysm formation and rupture. *Curr. Neurovasc. Res.* 10, 247–255. doi: 10.2174/15672026113109990003

Wilusz, J. E. (2016). Long noncoding rnas: re-writing dogmas of rna processing and stability. *Biochim. Biophys. Acta* 1859, 128–138. doi: 10.1016/j.bbagrm.2015.06.003

Winslow, J., Limesand, K. H., and Zhao, N. (2020). The functions of zip8, zip14, and znt10 in the regulation of systemic manganese homeostasis. *Int. J. Mol. Sci.* 21:3304. doi: 10.3390/ijms21093304

Wittstatt, J., Weider, M., Wegner, M., and Reiprich, S. (2020). Microrna mir-204 regulates proliferation and differentiation of oligodendroglia in culture. *Glia* 68, 2015–2027. doi: 10.1002/glia.23821

Wu, Y., Zhao, Y., Yang, H. Z., Wang, Y. J., and Chen, Y. (2021). Hmgb1 regulates ferroptosis through nrf2 pathway in mesangial cells in response to high glucose. *Biosci. Rep.* 41:BSR20202924. doi: 10.1042/BSR20202924

Xue, C., Cai, X., and Jia, J. (2021). Long non-coding rna double homeobox a pseudogene 8: a novel oncogenic propellant in human cancer. *Front. Cell Dev. Biol.* 9:709069. doi: 10.3389/fcell.2021.709069

Yang, Y., Tai, W., Lu, N., Li, T., Liu, Y., Wu, W., et al. (2020). Lncrna zfas1 promotes lung fibroblast-to-myofibroblast transition and ferroptosis via functioning as a cerna through mir-150-5p/slc38a1 axis. *Aging (Albany NY)* 12, 9085–9102. doi: 10.18632/aging.103176

Yu, X. H., Deng, W. Y., Chen, J. J., Xu, X. D., Liu, X. X., Chen, L., et al. (2020). Lncrna kcnq1ot1 promotes lipid accumulation and accelerates atherosclerosis via functioning as a cerna through the mir-452-3p/hdac3/abca1 axis. *Cell Death Dis.* 11:1043. doi: 10.1038/s41419-020-03263-6

Yu, Y., Jiang, L., Wang, H., Shen, Z., Cheng, Q., Zhang, P., et al. (2020). Hepatic transferrin plays a role in systemic iron homeostasis and liver ferroptosis. *Blood* 136, 726–739. doi: 10.1182/blood.2019002907

Zhang, D., Wu, W., Yan, H., Jiang, T., Liu, M., Yu, Z., et al. (2016). Upregulation of hmgb1 in wall of ruptured and unruptured human cerebral aneurysms: preliminary results. *Neurol. Sci.* 37, 219–226. doi: 10.1007/s10072-015-2391-y

Zhang, L., Qi, H., Liu, Z., Peng, W. J., Cao, H., Guo, C. Y., et al. (2020). Construction of a cerna coregulatory network and screening of hub biomarkers for salt-sensitive hypertension. *J. Cell Mol. Med.* 24, 7254–7265. doi: 10.1111/jcmm.15285

Zhang, N., Hu, G., Myers, T. G., and Williamson, P. R. (2019). Protocols for the analysis of microrna expression, biogenesis, and function in immune cells. *Curr. Protoc. Immunol.* 126:e78. doi: 10.1002/cpim.78

Zhao, W., Zhang, H., and Su, J. Y. (2018). Microrna29a contributes to intracranial aneurysm by regulating the mitochondrial apoptotic pathway. *Mol. Med. Rep.* 18, 2945–2954. doi: 10.3892/mmr.2018.9257

Zheng, Z., Chen, Y., Wang, Y., Li, Y., and Cheng, Q. (2021). Microrna-513b-5p targets col1a1 and col1a2 associated with the formation and rupture of intracranial aneurysm. *Sci. Rep.* 11:14897. doi: 10.1038/s41598-021-94116-5

frontiers | Frontiers in Cellular Neuroscience

TYPE Review
PUBLISHED 27 October 2022
DOI 10.3389/fncel.2022.1005182

OPEN ACCESS

EDITED BY
Zhen-Ni Guo,
First Affiliated Hospital of Jilin University, China

REVIEWED BY
Jiao Qian,
Qingdao University, China
Han Zhu,
Queen's University Belfast, United Kingdom

*CORRESPONDENCE
Haohao Zhu
zhuhaohao233@163.com
Zhenhe Zhou
zhouzh@njmu.edu.cn
Ying Jiang
jiangying911010@163.com

†These authors have contributed equally to this work

SPECIALTY SECTION
This article was submitted to Cellular Neuropathology, a section of the journal Frontiers in Cellular Neuroscience

RECEIVED 28 July 2022
ACCEPTED 14 October 2022
PUBLISHED 27 October 2022

CITATION
Ji Y, Zheng K, Li S, Ren C, Shen Y, Tian L, Zhu H, Zhou Z and Jiang Y (2022) Insight into the potential role of ferroptosis in neurodegenerative diseases.
Front. Cell. Neurosci. 16:1005182.
doi: 10.3389/fncel.2022.1005182

Insight into the potential role of ferroptosis in neurodegenerative diseases

Yingying Ji[1†], Kai Zheng[1†], Shiming Li[1†], Caili Ren[1], Ying Shen[2], Lin Tian[1], Haohao Zhu[1*], Zhenhe Zhou[1*] and Ying Jiang[1*]

[1]The Affiliated Wuxi Mental Health Center of Jiangnan University, Wuxi Central Rehabilitation Hospital, Wuxi, China, [2]Rehabilitation Medicine Center, The First Affiliated Hospital of Nanjing Medical University, Nanjing, China

Ferroptosis is a newly discovered way of programmed cell death, mainly caused by the accumulation of iron-dependent lipid peroxides in cells, which is morphologically, biochemically and genetically different from the previously reported apoptosis, necrosis and autophagy. Studies have found that ferroptosis plays a key role in the occurrence and development of neurodegenerative diseases, such as Alzheimer's disease, Parkinson's disease and vascular dementia, which suggest that ferroptosis may be involved in regulating the progression of neurodegenerative diseases. At present, on the underlying mechanism of ferroptosis in neurodegenerative diseases is still unclear, and relevant research is urgently needed to clarify the regulatory mechanism and provide the possibility for the development of agents targeting ferroptosis. This review focused on the regulatory mechanism of ferroptosis and its various effects in neurodegenerative diseases, in order to provide reference for the research on ferroptosis in neurodegenerative diseases.

KEYWORDS

ferroptosis, iron, Alzheimer's disease, neurodegenerative diseases, treatment

Introduction

Iron is involved in oxygen transport and cellular respiration, DNA synthesis and cell division, cellular metabolism and neurotransmission, which are essential for maintaining the body's function and daily metabolism. The ability of iron to circulate in an oxidative state in the body is fundamental to its biological function, and excess iron can lead to oxidative stress damage to biomolecules, as well as cellular dysfunction. However, with the increase of age, the accumulated iron in the brain will increase the risks of neurodegenerative diseases (Belaidi and Bush, 2016; Eid et al., 2017).

Ferroptosis is an iron-dependent, novel cell death mode, which is significantly different from apoptosis, cell necrosis and autophagy. The main mechanism is that under the action of ferrous iron or lipoxygenase, iron catalyzes liposomal peroxidation of highly expressed unsaturated fatty acids on cell membranes, thereby inducing cell death (Dixon et al., 2012; Nikseresht et al., 2019). The morphological features of ferroptosis are mitochondrial atrophy, increased bilayer membrane density, and loss of mitochondrial inner membrane cristae, with the intact cell membrane remaining and the normal size

of the nucleus, as well as no chromatin condensation (Alborzinia et al., 2018; Ou et al., 2022). Numerous studies have shown that ferroptosis is also related to a reduction in the expression of glutathione and glutathione peroxidase 4 (GPX4) in the antioxidant system of cells (Zhan et al., 2022; Zhao et al., 2022; Zhu et al., 2022). Lipid peroxides cannot be metabolized by the reduction reaction catalyzed by GPX4, and lipids are oxidized by ferrous iron in Fenton reaction to generate a large amount of reactive oxygen species to promote ferroptosis (Alborzinia et al., 2018; Torii, 2018; He et al., 2020). Therefore, the essence of ferroptosis is the metabolic disorder of intracellular lipid oxides, which are then abnormally metabolized under the catalysis of iron ions to produce a large amount of lipids to destroy the intracellular redox balance and attack biological macromolecules, triggering programmed cell death (Figure 1).

In recent years, studies have found that ferroptosis plays an extremely important role in neurodegenerative diseases with a common regulatory mechanism. This review will focus on ferroptosis and neurodegenerative diseases, such as Alzheimer's disease (AD), vascular dementia (VD), Parkinson's disease (PD), Huntington's disease (HD), amyotrophic lateral sclerosis (ALS) and traumatic brain injury (TBI), as well as the potential therapeutic effects of targeting ferroptosis (Table 1).

Mechanisms of ferroptosis

Transport and storage of iron in the brain

The neuronal iron metabolism related protein, TfR1 (transferrin receptor protein 1), is highly expressed on the surface of neurons (Giometto et al., 1990). Similar to BMECs, iron enters neurons through clathrin-mediated phagocytosis of holo-Tf/TfR1, and exits endosomes in the form of reduced Fe2+ through DMT1 (Burdo et al., 2001). NTBI (Non-transferrin-bound iron) can also enter neurons independently of Tf in a DMT1 (Divalent metal transporter 1)-dependent manner.

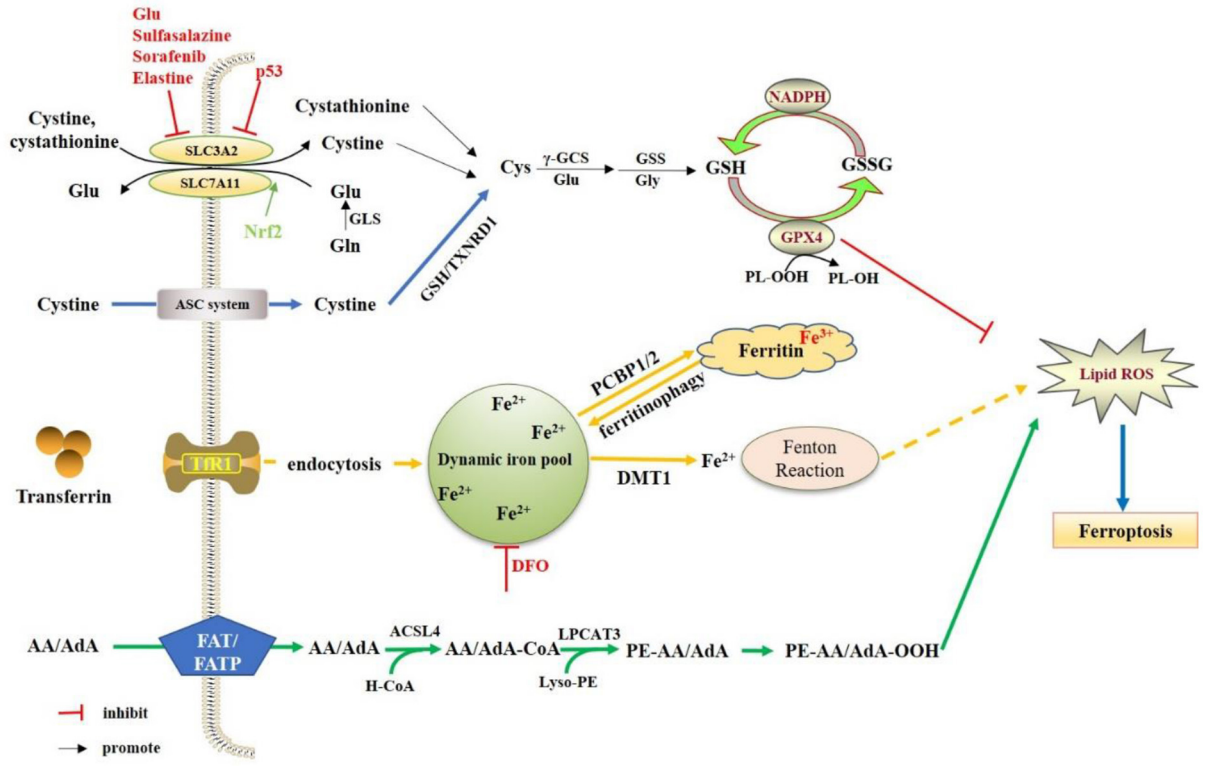

FIGURE 1
Regulation mechanisms of ferroptosis. The System Xc- is a heterodimeric amino acid transporter composed of two subunits (SLC7A11and SLC3A2). Under oxidative conditions, System Xc-extracellular uptake of cystine to release glutamate. The cellular cystine will be reduced to cysteine. Cysteine is gradually produced by γ-GCS and GSS. The GSH molecules of GPX4 act as electron donor to reduce phospholipid hydrogen peroxide (PL-OOH) to the corresponding alcohol. NADPH can also reduce GSSG (oxidized GSH) to GSH by glutathione reductase. The extracellular iron will be mediated by transferrin and TfR1 into the cell. Then Fe3+ is reduced to Fe2+, and Fe2+ will be transported to the dynamics iron pool, as well as stored in ferritin. In the presence of Fe2+, hydrogen peroxide can generate hydroxyl radicals (OH−) through the fenton reaction, thereby promoting the oxidation of AA/AdA on the cell membrane. ACSL4 incorporates AA/AdA into the membrane as AA/AdA-CoA, and LPCAT3 inserts the acyl group into the lysophospholipid as PE-AA/AdA, of which will lead to the accumulation of PE-AA/AdA-OOH.

TABLE 1 Targeting ferroptosis for the potential treatment of neurodegenerative diseases.

Diseases	Types	Name	Potential mechanism
AD	Iron chelators	DFO	Improve the excretion of iron, reduce the content of iron in the body and its pathological deposition in various organs
		DFP	
	Quinoline derivatives	Clioquinol	Downregulate the expression of ß and y secretases and APP in the brain, degrade oligomeric tau and reduce tau tangles
	Antioxidants	Vitamin E	Reduce lipid peroxidation and attenuate iron morphology
		a-LA	Block iron overload, lipid peroxidation and inflammation
		Se-containing compounds	Upregulate GPX4 to inhibit iron toxicity
		Fer-1	Inhibit ROS levels and downregulate Nrf2 and GPX4
	Hepcidin	Hepcidin	Inhibit FPN1, TfR1 and DMT1 to reduce neuronal iron uptake and release
	GBH	GBH	Inhibit lipid peroxidation and restore the expression of ferritin GPX4, HO-1, COX-2 altered by RSL3
VD	Antioxidants	Fer-1	Inhibit ROS levels and downregulate Nrf2 and GPX4
	Thiazolidinedione	ROSI	Inhibits ACSL4 activity, reduce lipid peroxidation and oxidative stress
PD	Iron chelator	DFP	Reduce oxidative stress and increase dopamine activity
	Quinoline derivatives	Clioquinol	Chelate iron and antioxidant
HD	Iron chelator	DFO	Improve the excretion of iron, reduce the content of iron in the body and its pathological deposition in various organs
	Antioxidant	Fer-1	Inhibit oxidative lipid damage
TBI	Iron chelators	DFO	Reduce the iron overload, and relieve acute oxidative brain injury
		HBED	
	Ferroptosis inhibitor	Liproxstatin-1	Reduce cerebral edema and blood-brain barrier permeability

Prion protein (PrPC), as the ferroreductase partner of DMT1, mediates the uptake of PrPc/DMT1 in the plasma membrane in the form of a complex of iron ions (Shih et al., 2003; Tripathi et al., 2015). Brain iron deficiency and increased holo-Tf uptake can be found in PrPC knockout mice (Singh, 2014). In the brain, divalent iron ions are normally metabolized in the neuronal cytoplasm, and stored in ferritin in the form of trivalent iron ions. When neurons are iron deficient, ferritin can be degraded by lysosomes, releasing stored iron to meet the normal physiological needs of neurons (Connor et al., 1992; Mancias et al., 2014; Raha et al., 2022). Studies have shown that ferritin in the brain increases with age (Belaidi et al., 2018), which is positively correlated with cognitive dysfunction. The etiology of cognitive dysfunction in the elderly is closely related to the iron overload. Iron homeostasis can also be regulated at the translation level. Iron regulatory protein 2 (IRP2), an RNA binding protein, controls the translation of a group of mRNAs involved in iron homeostasis. In the untranslated regions (UTRs) of genes encoding a variety of iron regulatory molecules (including DMT1 and TFR1), the IRP1 and IRP2 bind to the iron response elements (IREs). In an iron-deficient state, the combination of IRP2 and IREs can maximize intracellular iron levels. When the iron content increases, the extracellular iron regulatory pathway (IRE/IRP system) will be activated to weaken the iron overload state (Rouault, 2006; Sanchez et al., 2007; Hentze et al., 2010). In addition, nuclear receptor coactivator 4 (NCOA4) can degrade ferritin to mediate iron autophagy, and release free iron in the process, which can also lead to an increase in intracellular Fe2+ and ferroptosis (Li W. Y. et al., 2021). Iron-responsive element-binding protein 2 (IREB2) is a regulator of iron metabolism, which can up-regulate the expression of ferritin light chain and ferritin heavy chain in the cytoplasm during iron metabolism, and alleviate erastin-induced ferroptosis (Mishima, 2022). Nuclear factor E2-related factor 2 (Nrf2) can reduce the expression of TfR1, regulate iron metabolism, maintain the balance of intracellular iron homeostasis, and limit the production of reactive oxygen species (ROS), thereby reducing ferroptosis (Li S. W. et al., 2021).

The role of the glutamate/cysteine antiporter in ferroptosis

Cystine uptake by the glutamate/cysteine antiporter (System Xc-), including a 12-pass transmembrane protein transporter solute carrier family 7 member 11 (SLC7A11) and a single-channel transmembrane regulatory protein solute carrier family 3 member 2 (SLC3A2), is inhibited in ferroptosis (Dixon et al., 2012). Thus, inhibition of the System Xc- results in the depletion of intracellular cysteine (Ma et al., 2021).

Cysteine plays an important role in the biosynthesis of glutathione (GSH). GSH, as a substrate of GPX4, is required for its lipid repair function. GSH depletion through cysteine starvation results in the loss of GPX4 activity, as well as the accumulation of unrepaired lipid peroxides and iron toxicity (Angeli et al., 2014). GPX4 converts reduced glutathione to oxidized glutathione (GSSG) to reduce lipid hydrogen peroxide to the corresponding alcohol or free hydrogen peroxide to water (Gaschler et al., 2018). Selenium (Se) is a key regulator of GPX4 activity. Wild-type GPX4 containing Se can effectively reduce peroxides to the corresponding alcohols, thereby preventing ferroptosis (Ingold et al., 2018). GSH is also a natural ligand for Fe2+ in the labile iron pool (LIP), which is an exchange pool for loosely ligated iron in neurons (Hider and Kong, 2011), and glutathione binds Fe2+ in LIP to prevent iron oxidation, which not onlymaintains Fe2+ solubility but also prevents Fe2+ from acting as a catalyst to generate a potent oxidant, hydroxyl radical, from physiologically available hydrogen. Therefore, direct inhibition of GSH synthesis triggers ferroptosis.

The role of lipid peroxidation in ferroptosis

Lipid metabolism is also closely related to ferroptosis. Nitrogen oxides (NOXs) provide a source of accumulation of ROS in erastin-induced iron sickness, and it has been reported to modulate the sensitivity of tumor cells to erastin (Dixon et al., 2012). On the other hand, the production of membrane lipid peroxidation is also a source of ROS, which drives iron toxicity. The abundance and location of polyunsaturated fatty acids (PUFAs) determine the degree of lipid peroxidation that occurs in cells, and lead to ferroptosis. The most susceptible lipids are phospholipids containing polyunsaturated fatty acids (PUFA-PLs), which can lead to subsequent cell death (Doll et al., 2017). Free PUFAs need to be esterified to form membrane phospholipids and oxidized to iron ion signals to synthesize lipid signals, especially phospholipids containing phosphatidylethanolamine (PE) and arachidonic acid or epinephrine moieties (Kagan et al., 2017). In the membrane lipid environment, PUFAs are specifically peroxidized in iron toxicity (Doll et al., 2017; Kagan et al., 2017). There are three main classes of lipid oxidases: cyclooxygenases (cox), cytochrome p450s (CYPs), and lipid oxidases (LOXs), of which LOX enzymes have been found to be most important for ferroptosis. LOXs are a class of non-heme iron-containing enzymes that catalyze the deoxygenation of PUFAs (Shintoku et al., 2017).

Relationship between ferroptosis and neurodegenerative diseases

AD

In addition to β-amylase deposition and accumulation of intracellular neurofibrillary tangles (NFTs) composed of tau proteins, abnormal deposition of iron in the brain is a common feature of AD. The effects of iron on AD have been attributed to its interaction with AD pathological central proteins (amyloid precursor protein and tau protein) and/or through iron-mediated generation of prooxidative molecules such as hydroxyl radicals. However, the source of iron accumulation in brain pathologically relevant regions and its contribution to AD remain unclear. The potential reason for iron accumulation is that senescent cells within tissues increase with age, and these cells trigger inflammation and contribute to various pathologies associated with aging. The accumulation of iron makes aging tissues susceptible to oxidative stress, leading to cellular dysfunction and ferroptosis. In addition, elevated brain iron levels are associated with AD progression and cognitive decline. Elevated brain iron levels, a hallmark of AD, can be pharmacologically modulated to mitigate the effects of age-related dysregulation of iron balance and improve disease outcomes (Masaldan et al., 2019a).

A meta-analysis involving 300 AD cases in 19 studies reported that iron levels were significantly elevated in multiple regions of the cerebral cortex, although iron levels varied across regions and studies (Tao et al., 2014). Iron accumulation may be detrimental, as elevation of iron itself may lead to neurodegeneration (Schneider et al., 2012), possibly by inducing oxidative stress and ferroptosis (Stockwell et al., 2017). High brain iron levels, cerebrospinal fluid ferritin (Ayton et al., 2015, 2017a), and quantitative susceptibility maps have been found to have the potential to predict AD clinical severity and cognitive decline (Ayton et al., 2017b). The relationship between postmortem brain iron levels and AD clinical and pathological diagnosis, severity, and rate of cognitive decline in the 12 years preceding death was also investigated in 209 AD patients. It was found that the iron content in the brains of AD patients was significantly increased, and it was significantly related to cognitive function. Therefore, cortical iron may contribute to the deterioration of cognitive function in AD underlying proteinopathies by inducing oxidative stress or ferroptosis, or by being associated with inflammatory responses (Ayton et al., 2020). Another study found that iron deposition in the frontal lobe, parietal lobe, temporal lobe, caudate nucleus, putamen, globus pallidus, cingulate cortex, amygdala, and hippocampus of AD patients was higher than that of healthy controls (Tao et al., 2014), and histological differences in the intensity of iron accumulation in the frontal cortex of AD subtypes can be used

not only to distinguish sporadic (late-onset) from familial (early-onset) (Bulk et al., 2018a), but also to correlate with disease severity (van Duijn et al., 2017; Bulk et al., 2018b).

The accumulation of iron has been proven to accelerate the deposition of senile plaques and the generation of neurofibrillary tangles (Becerril-Ortega et al., 2014; Kim et al., 2018). Autopsy evidence and MRI analysis provide evidence that there was substantial iron deposition not only in senile plaques (James et al., 2017), but also at sites of cortical tau protein accumulation (Spotorno et al., 2020), suggesting a potential interaction of iron with senile plaques and neurofibrillary tangles. Perturbation of iron homeostasis is one of the key factors in Aβ deposition. High intracellular iron concentration enhances the IRP/IRE interaction and induces upregulation of APP. The enzymes that cleave APP are called α- and β-secretases, which are tightly balanced and regulated by furin (Silvestri and Camaschella, 2008; Guillemot et al., 2013). In the presence of iron excess, more β-secretase is activated when α-secretase is inhibited by furin injury (Silvestri and Camaschella, 2008). Up-regulated APP is cleaved by more β-secretase Aβ40/42, accelerating Aβ deposition. At the same time, the application can no longer assist FPN1, resulting in impaired iron efflux and aggravated iron deposition (Ward et al., 2014). It was suggested that in the absence of redox metals, Aß is nontoxic, and the aggregation of Aß requires the participation of metals (Li et al., 2013; Belaidi and Bush, 2016). Soluble Aß binds to Fe3+ when extracellular iron increases, removing excess iron, but it is difficult to separate after interaction. Aß can promote the reduction of Fe3+ to Fe2+, and ROS released in the process make Aß easily and rapidly to deposit and form more senile plaques (Ha et al., 2007). The interaction of iron with APP and Aß greatly increased the rate and extent of senile plaque formation (Rottkamp et al., 2001). Therefore, iron deposition could be included in the "Aβ cascade hypothesis" of AD (Peters et al., 2018). Iron can also interact with tau protein. Decreased soluble tau protein in the brains of AD patients increases cerebral iron deposition by inhibiting FPN1 activity (Lei et al., 2012). Conversely, high-iron diet led to cognitive decline in mice, abnormally increased neuronal tau phosphorylation, and abnormal expression of insulin pathway-related proteins. Insulin supplementation reduces iron-induced tau phosphorylation (Wan et al., 2019), suggesting that iron deposition may lead to tau hyperphosphorylation by interfering with insulin signaling. *In vivo* studies have found that iron can participate in tau hyperphosphorylation by activating the cyclin-dependent kinase 5 (CDK5)/P25 complex and glycogen synthase kinase 3β (GSK-3β) (Guo et al., 2013). Excessive intracellular Fe2+-induced generation of oxygen free radicals can also promote tau hyperphosphorylation by activating extracellular signal-regulated kinase 1/2 (Erk1/2) or mitogen-activated protein kinase (MAPK) signaling pathways (Chan and Shea, 2006; Munoz et al., 2006).

Glial activation and neuroinflammation have been shown to be prominent features of AD pathology (Newcombe et al., 2018; Leng and Edison, 2021). Microglia are highly responsive cells that respond to increased iron levels in the brain. When iron levels are elevated in the brain, microglia are activated (Meng et al., 2017) with increased volume and decreased length (Rathnasamy et al., 2013; Donley et al., 2021). Iron may activate microglia *via* nuclear factor-kb (NF-KB)-mediated pro-inflammatory cytokines (Meng et al., 2017). Upon activation, more ferritin will be expressed to remove extracellular iron (Streit et al., 2022), leading to intracellular iron retention (Kenkhuis et al., 2021), increased TNFα expression (Holland et al., 2018), and eventual infiltration as a ß-plaque (Peters et al., 2018; Kenkhuis et al., 2021). It can also interact with APP to promote the formation of Aβ (Tsatsanis et al., 2021). Conversely, in an environment with elevated iron levels, Aß formation leads to increased IL-1ß expression in microglia, exacerbating pro-inflammatory effects (Nnah et al., 2020). Astrocytes are highly resistant to metal-induced toxicity in the brain (Kress et al., 2002), serving as a key cell type for maintaining the homeostasis of the extracellular environment and supporting normal neuronal function (Abbott et al., 2006). Under the high-iron environment, the levels of glutathione, catalase, and manganese superoxide dismutase are significantly elevated in astrocytes to counteract oxidative stress (Iwata-Ichikawa et al., 1999; Shih et al., 2003). However, astrocytes were found to be activated by increased glial fibrillary acidic protein (GFAP) (Kress et al., 2002). Activated astrocytes release inflammatory mediators, induce oxidative stress, and promote the formation of Aß and tau tangles, hindering Aß clearance (Dolotov et al., 2022).

Abnormal expression of GPX4 mRNA and its protein levels was found in AD patients and mouse brains (Yoo et al., 2012; da Rocha et al., 2018). In glial cells, mild hypoxia can reduce the level of GSH, which is used for GPX4 biosynthesis (Makarov et al., 2006). In a mouse model of AD, GSH expression was reduced in the cortex and positively correlated with cognitive decline (Karelson et al., 2001). GSH levels in the frontal lobe and hippocampus may serve as biomarkers for predicting AD and mild cognitive impairment (Karelson et al., 2001; Ayton et al., 2020). xCT activity determines GSH availability, and subsequent GPX4 activity in the brain (Ashraf et al., 2020). Furthermore, studies have found that most of the proteins involved in ferroptosis can be regulated by Nrf2 (Habib et al., 2015; Lane et al., 2021). The genes of interest included FPN1, GSH and SLC7A11 encoding xCT. The level of Nrf2 in the brain decreases with age, as well as in AD patients (Osama et al., 2020), so the brain of AD patients is more prone to ferroptosis (Habib et al., 2015). GPX4 expression has been reported to be reduced in both AD mouse models and AD patient brains (Ansari and Scheff, 2010; Yoo et al., 2010). GPX4 knockout mice were shown to have significant hippocampal neuronal loss and cognitive impairment (Yoo et al., 2010;

Hambright et al., 2017). A diet deficient in vitamin E, an antioxidant with anti-ferroptosis activity, simultaneously results in hippocampal neurodegeneration and worsens behavioral dysfunction; the ferroptosis inhibitor liproxstatin 1 improves cognitive function and neurodegeneration in mice (Hambright et al., 2017). In addition to animal models, autopsy results of AD patients showed down-regulation of GPX4, up-regulation of arachidonic acid 12/15 lipoxygenase (ALOX15), and enhanced lipid peroxidation, and 4-hydroxynonenal (4-HNE) in AD patient brains was elevated (Yoo et al., 2010). 4-HNE has the potential to modify proteins involved in antioxidant and energy metabolism, promoting Aβ deposition and fibrogenesis (Seibt et al., 2019). These results indicate that ferroptosis plays a key role in AD, which can cause neuronal loss and cognitive decline. Therefore, modulating brain iron metabolism and reducing neuronal ferroptosis may be a promising approach for the treatment of AD.

Deferoxamine (DFO) and deferiprone (DFP) are commonly used clinical iron chelators. The clinical efficacy of DFO in the treatment of AD is as high as 50%. However, the side effects, such as weight loss and loss of appetite (Mclachlan et al., 1991), limit its clinical application. Besides, DFO is difficult to pass through the blood-brain barrier (BBB) (Ward et al., 1995; Ben Shachar et al., 2004), which could be solved by intranasal administration of DFO nanoparticles (Rassu et al., 2015). Compared to DFO, DFP could cross the BBB and is safer (Gallie and Olivieri, 2019). In a randomized controlled trial, DFP improved neurological scores and iron-related neurological symptoms (Abbruzzese et al., 2011; Klopstock et al., 2019).

Quinoline and its derivatives, which could chelate with iron, zinc, and copper, have the potential to improve cognition, reduce Aβ deposition, and promote Aβ degradation in AD animal models (Grossi et al., 2009; Crouch et al., 2011). Clioquinol could downregulate ß and y secretase and APP expression in the brain (Wang et al., 2012), as well as degrade oligomeric tau protein and reduce tau tangles (Lin et al., 2021). Besides, clioquinol has been proven to slow down cognitive decline in patients with severe AD and reduce Aß42 in cerebrospinal fluid (Ritchie et al., 2003). Studies have also found that vitamin E (an antioxidant) can reduce lipid peroxidation in the brain, reduce iron morphology on neurons, and improve cognitive function in GPX4 knockout mice. However, in a randomized clinical trial, vitamin E showed no benefit in patients with AD or mild cognitive impairment (Farina et al., 2017), while it could accelerate cognitive decline (Lloret et al., 2009). Therefore, the application of vitamin E in AD remains questionable, and more clinical trials are needed to determine its effect. Alpha-lipoic acid (a-LA) was also proven to improve cognitive impairment, slow cognitive decline (Fava et al., 2013), block iron overload, lipid peroxidation, and inflammatory responses in AD patients (Zhang et al., 2018). Se is present in various proteins in the body, such as GPX4, and has antioxidant activity. Se-containing compounds may inhibit iron toxicity by upregulating GPX4 and improve cognitive function in AD patients (Gwon et al., 2010; Cardoso et al., 2019). Ferrostatin-1 (Fer-1) is a common ferritin inhibitor and a free radical scavenger, which is much more effective than phenolic antioxidants (Miotto et al., 2020). Fer-1 could alleviate angiotensin II-induced astroglial inflammation and iron degeneration by inhibiting ROS levels and downregulating Nrf2 and GPX4 (Li S. J. et al., 2021). In the treatment of AD, Fer-1 was shown to ameliorate neuronal death and memory impairment *in vitro* and *in vivo* (Bao et al., 2021).

Hepcidin can reduce iron transport across the BBB and prevent iron overload in the brain. In cultured microvascular endothelial cells, hepcidin significantly inhibits the expression of FPN1, TfR1 and DMT1, and reduce iron uptake and release by neurons (Du et al., 2015). Hepcidin can reduce the iron level of mouse astrocortex and hippocampal neuron glial cells, reduce the formation of Aß plaques, and improve mouse cognitive function (Xu et al., 2020). The recombinant adenoviruses carrying the hepcidin gene could also reduce iron deposition and oxidative stress levels in the brain (Gong et al., 2016). Insamgobonhwan (GBH) can inhibit the impairment of ß-amyloid on cognitive function *in vivo*, and also inhibit cell death and lipid peroxidation *in vitro* cells. In addition, GBH restores ferritin GPX4, HO-1. The expression of COX-2 can improve cognitive dysfunction in mice, and it also has certain potential in AD treatment (Yang et al., 2022).

VD

The main cause of VD is chronic cerebral hypoperfusion (CCH) caused by chronic cerebral blood flow (CBF) and a variety of vascular pathologies. These include atherosclerosis, arteriosclerosis, infarcts, white matter (WM) changes, and microbleeds (Calabrese et al., 2016; Kalaria, 2018). Researchers have demonstrated that amino acid metabolism is related to ferroptosis and that CCH can cause neuronal depolarization to release excess glutamate during the pathogenesis of VD, resulting in excitotoxicity, and high levels of glutamate inhibit the function of System Xc-. Glutamate excitotoxicity is also a pathological mechanism of iron toxicity, and iron chelation prevents excitotoxic cell death (Krzyzanowska et al., 2014; Liu et al., 2016; Frank et al., 2021). Nuclear factor erythroid 2 related factor 2 (Nrf2) is a fundamental regulator of cellular antioxidant defense systems, which regulates the expression of multiple antioxidant response element-dependent genes, including NADPH-quinone oxidoreductase 1 (NQO1), heme oxidoreductase 1 (HMOX1), ferritin heavy chain 1 (FTH1), FPN1, GSH, and GPX4 (Kerins and Ooi, 2018; Milkovic et al., 2019; Sarutipaiboon et al., 2020). Studies have shown that the expression level of Nrf2 is directly related to the susceptibility to iron poisoning. Increased expression of Nrf2 inhibits ferroptosis, and decreased expression promotes ferroptosis (Sun Y. R. et al., 2020; Fan et al., 2021; Nishizawa et al., 2022). Studies have

shown that, on the one hand, Nrf2 promotes the expression of glutathione and GPX4 strengthens the function of the antioxidant system, and on the other hand, Nrf2 can also reduce intracellular iron accumulation by promoting the expression of ferritin and the simultaneous release of FPN1 storage and export. iron, thereby preventing iron poisoning (Yang et al., 2017; Kasai et al., 2019). The Nrf2 regulatory network plays a fundamental role in different mouse models of cerebral ischemia. Although the expression of Nrf2 is controversial in different studies, the neuroprotective effect of enhanced Nrf2/ARE activation has been demonstrated in different studies (Park et al., 2018; Liu et al., 2019, 2020). At the same time, NRF2 overexpression can improve cognitive dysfunction (Yang et al., 2014; Qi et al., 2018; Mao et al., 2019), suggesting that it may be related to the inhibition of iron poisoning, and the GSH metabolic network is a bridge connecting iron poisoning and VD.

CCH can also lead to massive iron deposition. Bilateral common carotid artery occlusion is the most commonly used experimental model for VD. In the study, it was found that CCH leads to iron deposition in the rat brain, and a large amount of iron deposition leads to neuronal death caused by oxidative stress. Among them, the CA1 area has the most iron deposition and neuronal death (Li et al., 2012; Du et al., 2018). Abnormal brain iron and iron ion deposition are closely related to cognitive dysfunction, and iron ion deposition has been confirmed in AD, PD, HD and other neurodegenerative diseases. It plays an important role in sexually transmitted diseases (Chen L. et al., 2019; Thomas et al., 2020; Xu et al., 2020). It has also been shown that a wide range of abnormal iron deposits in the cortex of patients with subcortical ischemic VD, especially in the lateral caudate nucleus, putamen, globus pallidus, and frontal cortex, correlate closely with the severity of cognitive impairment (Liu et al., 2015; Sun C. Y. et al., 2020). Model of cerebral ischemia-reperfusion injury confirmed that iron accumulation in the ischemic precursor is a novel mechanism of stroke injury, leading to neuronal death. Iron chelators attenuate ischemia-reperfusion injury in animal models (Tuo et al., 2017), indicating that iron-induced ferroptosis may be the underlying mechanism of VD neuron loss.

The oxidative stress produced by CCH has been proven to be one of the main pathogenic mechanisms leading to VD (Du et al., 2017; Lee et al., 2021), and studies have shown that blood lipid levels in VD patients are significantly higher than those in AD patients, suggesting lipid peroxidation. Having an important impact on the pathophysiology of VD, MDA levels may be a hallmark of VD (Gustaw-Rothenberg et al., 2010). Lipid peroxidation and ROS accumulation are key processes that induce iron toxicity (Dixon and Stockwell, 2014). LOX causes lipid peroxidation by catalyzing polyunsaturated fatty acids in phospholipid membranes, and inhibition of LOX inhibits ferroptosis (Kagan et al., 2017; Doll et al., 2019). During cerebral ischemia, the extensive increase in 12/15-LOX in brain tissue is an important cause of neuronal cell death and neurological damage. Inhibition of 12/15-LOX can reduce neuronal cell death and brain edema, and improve neurological prognosis (Piao et al., 2008; Pallast et al., 2010; Yigitkanli et al., 2017). In addition, NOX also plays an important role in lipid peroxidation. NOX1 expression was increased in hippocampal neurons during CCH, leading to lipid peroxidation and oxidative stress. It is an important cause of hippocampal neuronal degeneration and cognitive impairment (Choi et al., 2014). Lipid peroxidation caused by NOX is also one of the links of ferroptosis. NOX1 inhibitors have different effects on erastin-induced ferroptosis in Calu-1 cells and HT-1080 cells, and have a partial effect on HT-1080 cells (Dixon et al., 2012; Wang et al., 2021).

Thiazolidinediones such as rosiglitazone (ROSI), a drug for the treatment of diabetes, can selectively inhibit ACSL4 activity and thereby inhibit ferroptosis (Angeli et al., 2017; Doll et al., 2017). ACSL4 is widely expressed in brain tissue, especially in the hippocampal CA1 region, and the expression of ACSL4 is gradually increased during cerebral ischemia (Kassan et al., 2013; Peng et al., 2021). Rosiglitazone (ROSI) has been shown to reduce lipid peroxidation and oxidative stress injury in hippocampal neurons during CCH, protecting brain function (Sayan-Ozacmak et al., 2012). Multiple studies have shown that long-term use of pioglitazone in patients with insulin-dependent diabetes reduces the risk of dementia in nonpsychiatric patients (Heneka et al., 2015; Lu et al., 2018).

PD

PD is the second most common neurodegenerative disease. It is common in middle-aged and elderly people with neurodegenerative diseases. Some PD patients also have cognitive dysfunction. In the late stage of PD, patients often have severe cognitive dysfunction such as dementia. Abnormal intracranial iron deposition is thought to be one of the pathogenic mechanisms of PD (Langkammer et al., 2016; An et al., 2018; Chen Q. et al., 2019), and iron induces the formation of Lewy bodies through oxidative stress pathway, which aggregates α-synuclein (Takahashi et al., 2007). Li et al. (2018) found that the iron content of the substantia nigra pars compacta in PD patients may gradually increase during the progression of PD and manifest as more significant iron deposition in the middle and late stages of the disease. Relatedly, observation of changes in its iron deposition may serve as a potential marker for monitoring disease progression. Substantia nigra iron deposition is also related to the cognitive function of patients (Liu et al., 2017). The QSM CP value of the left substantia nigra on MRI was negatively correlated with the ADL score. The CP value of the left frontal white matter was negatively correlated with the HAMD score, CP value of left

substantia nigra and CP value of left frontal lobe were positively correlated with MOCA score, and CP value of left frontal lobe white matter was positively correlated with MMSE score. SWI reflects abnormal iron deposition in the brain through CP value, which can be used for the diagnosis of PD, but has little significance for disease staging, and can be used to study the mechanism of PD cognitive dysfunction and depression (Xiong et al., 2020). Quantitative analysis of susceptibility-weighted imaging (SWI) found that PD patients with mild cognitive impairment had increased iron concentrations in the globus pallidus and head of the caudate nucleus (Kim et al., 2021). Iron is also widely deposited in the premotor cortex, prefrontal lobe, insula, cerebellum, pons and other parts of PD patients (Acosta-Cabronero et al., 2017; Chen L. et al., 2019), which are all related to apathy and rapid eye movement sleep behavior disorder (RBD) and other non-motor symptoms. Tere was a metabolic disorder of iron in the cerebrospinal fluid of patients with PD combined with apathy and PD combined with RBD (Hu et al., 2015; Wang et al., 2016). Serum iron has also been found to be associated with anxiety in PD patients (Xu et al., 2018). In addition, Masaldan et al. (2019b) found that the abnormal accumulation of iron in PD may be closely related to the changes of iron regulatory proteins.

Alpha-synuclein (a-syn), as a key player in tyrosine hydroxylase-dependent dopamine synthesis and other dopamine metabolic processes (Do Van et al., 2016; Belarbi et al., 2017), may play a role in iron regulation (Duce et al., 2010; Zhou and Tan, 2017). In the presence of a copper catalyst, a-syn has ferroreductase potential, which, when combined with Fe3+ and converted to Fe2+, binds to the C-terminus of a-syn (Davies et al., 2011). Iron also increases the formation of non-normal fibers, a major event in PD (Abeyawardhane et al., 2018). Furthermore, GSH was found to be decreased in a mouse model of MPTP (Feng et al., 2014), while GSH depletion enhanced MPP+ toxicity in substantia nigra dopaminergic neurons (Wullner et al., 1996).

DFP has also been found to be neuroprotective in patients with early PD (Do Van et al., 2016). The MPP+-induced SH-SY5Y (a commonly used PD model) cell line is not programmed cell death and shares some similarities with iron toxicity: both involve lipid peroxidation and can be inhibited by DIM and Fer−1 suppressed. Results showed that iron chelators not only inhibited iron toxicity, but also protected dopamine neurons from cell death (Abeyawardhane et al., 2018). In a transgenic mouse model of PD, clioquinol was able to prevent the loss of substantia nigra cells due to the ability of clioquinol to chelate iron (Billings et al., 2016). Zeng et al. (2021) found that GPX4 in PD cells significantly decreased and ROS increased significantly after administration of ferric ammonium citrate, which in turn induced ferroptosis and led to neuronal death, while administration of iron chelators could inhibit ferroptosis and protect neurons.

HD

HD is a progressive neurodegenerative disease characterized by rapid involuntary movements and cognitive impairment, ultimately leading to death, due to expansion of CAG repeats in the Huntingtin (HTT). The pathological hallmark of HD is iron accumulation and abnormal levels of glutamate and glutathione (Skouta et al., 2014; Agrawal et al., 2018). It has also been reported that plasma samples from HD patients have lower levels of GSH (Klepac et al., 2007) and lower GPX activity in erythrocytes, so the pathogenesis of HD may be related to ferroptosis. In a mouse model of HD, nitropropionic acid-treated mice also exhibited reduced global (cytoplasmic and mitochondrial) GSH reduction, suppressed hippocampal and cortical glutathione s-transferase (GST) function, and exhibited an HD phenotype (Klivenyi et al., 2000). Although the underlying mechanism by which mutant huntingtin causes neurodegeneration is unclear, the ability of huntingtin to induce oxidative damage has been demonstrated. A study found that Fer-1 treatment at 10 nM, 100 nM, and 1 μM protected neurons labeled with yellow fluorescent protein (YFP) and expressed by biotransfection with a pathogenic repeat (73Q) The huntingtin exon 1 fragment (mN90Q73) induces cell death. The number of medium spiny neurons (msnn) was significantly increased compared to controls (Skouta et al., 2014). The iron chelator DFO was protective and improved cognition in R6/2 mice, a mouse model of HD (Yang et al., 2016). Fer-1 can inhibit oxidative lipid damage and cell death in a cellular model of HD (Skouta et al., 2014).

ALS

ALS is a neurodegenerative disease affecting motor neurons in the cortex, spinal cord, and brainstem, and clinically manifests as progressive muscle atrophy and weakness in the extremities and trunk. The pathogenesis of ALS is unknown, and neither is the treatment of the disease. The most common type of dementia associated with ALS is frontotemporal dementia (FTD), a progressive non-AD dementia syndrome characterized by localized frontal and temporal lobe degeneration (Ringbolz and Greene, 2006; Heidler-Gary and Hillis, 2007; Bede et al., 2018; Iridoy et al., 2019). Iron deposition was observed in the spinal cord of a mouse model of ALS (Golko-Perez et al., 2017). Abnormal iron deposits are found in ALS patients, and iron deposits were found in the motor cortex of the patient's brain at autopsy (Kwan et al., 2012). The lipid peroxidation of erythrocytes in ALS patients is significantly increased, while the content of GSH is decreased (Babu et al., 2008). The concentration of glutamate is higher, and the accumulation of glutamate can cause neuronal cell toxicity, which indicates that ferroptosis is directly involved in the

pathogenesis of ALS mechanism. At the same time, motor neurons in ALS mice are very sensitive to GPX4 knockout-induced cell death (Conrad et al., 2018). At present, the only approved treatment for ALS in the United States and the European Union is the anti-excitatory amino acid toxicity drug Riluzole, which is a glutamate antagonist, which can inhibit the release of presynaptic glutamate and inhibit nerve endings. It can inhibit the neurotoxicity of excitatory amino acids by inhibiting the neurotoxicity of excitatory amino acids. It has a certain effect on ALS patients with bulbar palsy or limb paralysis as the first symptom, can delay the progression of ALS, and can clearly prolong the survival time and postponement of tracheostomy (Gurney et al., 1998).

TBI

TBI is recognized as a disease with high mortality and complex survival, which is the main environmental risk factors for the development of neurodegenerative diseases. Complications of TBI are mainly motor function, cognitive function, and social dysfunction, which cause a serious burden on patients, family members and society, and age is an important factor affecting the prognosis of TBI (Griesbach et al., 2018; Fraser et al., 2019; Ritzel et al., 2019). Iron is considered to be an important agent of secondary injury after traumatic brain injury and can induce peroxidation and inflammation (Ayton and Lei, 2014). Studies have shown that after experimental brain trauma in rats, the production of lipid peroxidation products is significantly enhanced, the consumption of GSH and ascorbic acid is significantly increased (Bayir et al., 2002), and the activity of GPX is decreased (Xu et al., 2014). Elevated levels of 15-HpETE-PE after traumatic brain injury led to ferroptosis in the cerebral cortex and hippocampus, accompanied by increased expression of 15LO2 (a catalyst for the formation of protoferroporphyrin 15-oh-eicosapentaenoic acid) and depletion of GPX4, leading to cognitive impairment, effectively suggesting the possibility of ferroptosis (Wenzel et al., 2017).

Iron chelators such as DFO may improve cognitive function after traumatic brain injury (Khalaf et al., 2019). N,N'-bis(2-hydroxybenzyl)ethylenediamine-N,N'-diacetic acid hydrochloride (HBED) is a unique iron chelator that not only crosses the BBB, but also reduces the improvement and recovery of motor impairment and cognitive function after TBI in rats (Khalaf et al., 2019). The ferroptosis inhibitor Liproxstatin 1 can reduce brain edema and BBB permeability caused by TBI, improve motor and learning and memory impairment caused by TBI in rats, and significantly improve anxiety and cognitive function caused by TBI (Xie et al., 2019).

Discussion

Ferroptosis is a newly discovered form of cell death manifested by iron overload, accumulation of lipid peroxidation, and ROS. The current research preliminarily showed that ferroptosis plays an important role in neurodegenerative diseases. Clinically, ferroptosis can be induced by the following methods and exert a neuroprotective effect: exogenous lipid supplementation promotes lipid peroxidation in cells; inhibition of GPX4 and expression of GSH; construction of nano-drug delivery system to supplement hydrogen peroxide and iron ions to promote Fenton reaction of tumor cells, etc. Therefore, ferroptosis is a potential target for the treatment of neurodegenerative diseases. However, the exploration of ferroptosis still faces many problems to be solved. First, the study of ferroptosis in cognitive dysfunction-related diseases is still in its infancy, and its underlying molecular mechanisms remain unclear. Although iron overload and lipid peroxidation can cause ferroptosis, their involvement in ferroptosis-related regulatory targets such as DMT1, FPN1, or iron uptake proteins needs to be further investigated. Second, there is no specific ferroptosis marker to comprehensively and extensively study its process, and which are the key executive molecules of ferroptosis remain unclear. Finally, it is known that abnormal iron metabolism can cause ferroptosis, and whether other metal elements induce ferroptosis remains to be explored.

In addition, ferroptosis is different from other forms of cell death, but these different forms of cell death are not independent of each other. The various forms of cell death are likely to be interconnected and form a network to participate in the regulation of cell death. Studies have found (Sun et al., 2018; Chen et al., 2021) that ferroptosis is closely related to apoptosis, and ferroptosis, autophagy and apoptosis can synergistically promote cancer cell death. Therefore, further studies on the relationship and mechanism between ferroptosis and other known cell death pathways are still needed in the future, which may be helpful for the treatment of cognitive dysfunction-related diseases. In addition, ferroptosis inhibitors contain some traditional ROS scavengers, but compared with traditional ROS scavengers, ferroptosis inhibitors can block iron-catalyzed ROS generation, activate oxidative stress, and induce cell death. It can only clear the accumulated ROS in cells and has a weak inhibitory effect on ferroptosis, and cannot completely block the occurrence of ferroptosis in cells. Various types of ferroptosis inducers and inhibitors have been found, but ferroptosis regulators generally suffer from low bioavailability and adverse reactions. Therefore, screening of ferroptosis-related drugs and traditional Chinese medicines with few adverse effects on normal tissues and high target specificity is crucial for the development of ferroptosis.

In conclusion, with the gradual deepening of ferroptosis research, the research on targeted drugs and new drug targets

for ferroptosis is of great significance for the prevention and treatment of diseases in the future. At the same time, more and more experimental studies have confirmed the role of ferroptosis in neurodegenerative diseases, which provides more possibilities for the discovery of potential therapeutic drugs and therapeutic targets for neurodegenerative diseases, and also provides help to further explain the pathogenesis of neurodegenerative diseases. However, the research on ferroptosis in neurodegenerative diseases is still in its initial stage, and there are many unexplained problems, and more experiments are needed to deepen its understanding.

Author contributions

YJi and ZZ conceived the study. KZ, SL, CR, YS, LT, and YJia performed literature searching and summary. YJi, HZ, and YJia wrote the manuscript. YJia and ZZ edited the manuscript. All authors contributed to the article and approved the submitted version.

Funding

The work was supported by the National Natural Science Foundation of China (No. 82104244), Wuxi Municipal Health Commission (Nos. Q202050, Q202101, Q202167, M202167, and ZH202110), Wuxi Taihu Talent Project (Nos. WXTTP2020008 and WXTTP2021), Wuxi Medical Development Discipline Project (No. FZXK2021012), and Jiangsu Research Hospital Association for Precision Medication (JY202105).

Conflict of interest

The authors declare that the research was conducted in the absence of any commercial or financial relationships that could be construed as a potential conflict of interest.

Publisher's note

References

Abbott, N. J., Ronnback, L., and Hansson, E. (2006). Astrocyte-endothelial interactions at the blood-brain barrier. *Nat. Rev. Neurosci.* 7, 41–53. doi: 10.1038/nrn1824

Abbruzzese, G., Cossu, G., Balocco, M., Marchese, R., Murgia, D., Melis, M., et al. (2011). A pilot trial of deferiprone for neurodegeneration with brain iron accumulation. *Haematol-Hematol J.* 96, 1708–1711. doi: 10.3324/haematol.2011.043018

Abeyawardhane, D. L., Fernandez, R. D., Murgas, C. J., Heitger, D. R., Forney, A. K., Crozier, M. K., et al. (2018). Iron redox chemistry promotes antiparallel oligomerization of alpha-synuclein. *J. Am. Chem. Soc.* 140, 5028–5032. doi: 10.1021/jacs.8b02013

Acosta-Cabronero, J., Cardenas-Blanco, A., Betts, M. J., Butryn, M., Valdes-Herrera, J. P., Galazky, I., et al. (2017). The whole-brain pattern of magnetic susceptibility perturbations in Parkinson's disease. *Brain.* 140, 118–131. doi: 10.1093/brain/aww278

Agrawal, S., Fox, J., Thyagarajan, B., and Fox, J. H. (2018). Brain mitochondrial iron accumulates in Huntington's disease, mediates mitochondrial dysfunction, and can be removed pharmacologically. *Free Radical Bio Med.* 120, 317–329. doi: 10.1016/j.freeradbiomed.2018.04.002

Alborzinia, N., Ignashkova, T. I., Dejure, F. R., Gendarme, M., Theobald, J., Wolfi, S., et al. (2018). Golgi stress mediates redox imbalance and ferroptosis in human cells. *Commun. Biol.* 1, 210. doi: 10.1038/s42003-018-0212-6

An, H. D., Zeng, X. Y., Niu, T. F., Li, G. Y., Yang, J., Zheng, L. L., et al. (2018). Quantifying iron deposition within the substantia nigra of Parkinson's disease by quantitative susceptibility mapping. *J. Neurol. Sci.* 386, 46–52. doi: 10.1016/j.jns.2018.01.008

Angeli, J. P. F., Schneider, M., Proneth, B., Tyurina, Y. Y., Tyurin, V. A., Hammond, V. J., et al. (2014). Inactivation of the ferroptosis regulator Gpx4 triggers acute renal failure in mice. *Nat. Cell Biol.* 16, 1180–U120. doi: 10.1038/ncb3064

Angeli, J. P. F., Shah, R., Pratt, D. A., and Conrad, M. (2017). Ferroptosis Inhibition: Mechanisms and Opportunities. *Trends Pharmacol. Sci.* 38, 489–498. doi: 10.1016/j.tips.2017.02.005

Ansari, M. A., and Scheff, S. W. (2010). Oxidative stress in the progression of Alzheimer disease in the frontal cortex. *J. Neuropathol. Exp. Neurol.* 69, 155–167. doi: 10.1097/NEN.0b013e3181cb5af4

Ashraf, A., Jeandriens, J., Parkes, H. G., and So, P. W. (2020). Iron dyshomeostasis, lipid peroxidation and perturbed expression of cystine/glutamate antiporter in Alzheimer?s disease: Evidence of ferroptosis. *Redox Biol.* 32:101494. doi: 10.1016/j.redox.2020.101494

Ayton, S., Faux, N. G., and Bush, A. I. (2017a). Association of cerebrospinal fluid ferritin level with preclinical cognitive decline in APOE-epsilon 4 carriers. *JAMA Neurol.* 74, 122–125. doi: 10.1001/jamaneurol.2016.4406

Ayton, S., Faux, N. G., Bush, A. I., and Initia, A. D. N. (2015). Ferritin levels in the cerebrospinal fluid predict Alzheimer's disease outcomes and are regulated by APOE. Nat Commun. 6, 6760. doi: 10.1038/ncomms7760

Ayton, S., Fazlollahi, A., Bourgeat, P., Raniga, P., Ng, A., Lim, Y. Y., et al. (2017b). Cerebral quantitative susceptibility mapping predicts amyloid-beta-related cognitive decline. *Brain.* 140, 2112–2119. doi: 10.1093/brain/awx137

Ayton, S., and Lei, P. (2014). Nigral iron elevation is an invariable feature of parkinson's disease and is a sufficient cause of neurodegeneration. *Biomed Res. Int.* 2014, 581256. doi: 10.1155/2014/581256

Ayton, S., Wang, Y. M., Diouf, I., Schneider, J. A., Brockman, J., Morris, M. C., et al. (2020). Brain iron is associated with accelerated cognitive decline in people with Alzheimer pathology. *Mol Psychiatr.* 25, 2932–2941. doi: 10.1038/s41380-019-0375-7

Babu, G. N., Kumar, A., Chandra, R., Puri, S. K., Singh, R. L., Kalita, J., et al. (2008). Oxidant-antioxidant imbalance in the erythrocytes of sporadic amyotrophic lateral sclerosis patients correlates with the progression of disease. *Neurochem. Int.* 52, 1284–1289. doi: 10.1016/j.neuint.2008.01.009

Bao, W. D., Pang, P., Zhou, X. T., Hu, F., Xiong, W., Chen, K., et al. (2021). Loss of ferroportin induces memory impairment by promoting ferroptosis in Alzheimer's disease. *Cell Death Differ.* 28, 1548–1562. doi: 10.1038/s41418-020-00685-9

Bayir, H., Kagan, V. E., Tyurina, Y. Y., Tyurin, V., Ruppel, R. A., Adelson, P. D., et al. (2002). Assessment of antioxidant reserves and oxidative stress in cerebrospinal fluid after severe traumatic brain injury in infants and children. *Pediatr. Res*. 51, 571–578. doi: 10.1203/00006450-200205000-00005

Becerril-Ortega, J., Bordji, K., Freret, T., Rush, T., and Buisson, A. (2014). Iron overload accelerates neuronal amyloid-beta production and cognitive impairment in transgenic mice model of Alzheimer's disease. *Neurobiol. Aging*. 35, 2288–2301. doi: 10.1016/j.neurobiolaging.2014.04.019

Bede, P., Omer, T., Finegan, E., Chipika, R. H., Iyer, P. M., Doherty, M. A., et al. (2018). Connectivity-based characterisation of subcortical grey matter pathology in frontotemporal dementia and ALS: a multimodal neuroimaging study. *Brain Imaging Behav*. 12, 1696–1707. doi: 10.1007/s11682-018-9837-9

Belaidi, A. A., and Bush, A. I. (2016). Iron neurochemistry in Alzheimer's disease and Parkinson's disease: targets for therapeutics. *J. Neurochem*. 139, 179–197. doi: 10.1111/jnc.13425

Belaidi, A. A., Gunn, A. P., Wong, B. X., Ayton, S., Appukuttan, A. T., Roberts, B. R., et al. (2018). Marked age-related changes in brain iron homeostasis in amyloid protein precursor knockout mice. *Neurotherapeutics*. 15, 1055–1062. doi: 10.1007/s13311-018-0656-x

Belarbi, K., Cuvelier, E., Destee, A., Gressier, B., and Chartier-Harlin, M. C. (2017). NADPH oxidases in Parkinson's disease: a systematic review. *Mol. Neurodegener*. 12. doi: 10.1186/s13024-017-0225-5

Ben Shachar, D., Kahana, N., Kampel, V., Warshawsky, A., and Youdim, M. B. H. (2004). Neuroprotection by a novel brain permeable iron chelator, VK-28, against 6-hydroxydopamine lession in rats. *Neuropharmacology*. 46, 254–263. doi: 10.1016/j.neuropharm.2003.09.005

Billings, J. L., Hare, D. J., Nurjono, M., Volitakis, I., Cherny, R. A., Bush, A. I., et al. (2016). Effects of neonatal iron feeding and chronic clioquinol administration on the Parkinsonian human A53T transgenic mouse. *ACS Chem. Neurosci*. 7, 360–366. doi: 10.1021/acschemneuro.5b00305

Bulk, M., Abdelmoula, W. M., Nabuurs, R. J. A., van der Graaf, L. M., Mulders, C. W. H., Mulder, A. A., et al. (2018a). Postmortem MRI and histology demonstrate differential iron accumulation and cortical myelin organization in early- and late-onset Alzheimer's disease. *Neurobiol. Aging*. 62, 231–242. doi: 10.1016/j.neurobiolaging.2017.10.017

Bulk, M., Kenkhuis, B., van der Graaf, L. M., Goeman, J. J., Natte, R., van der Weerd, L., et al. (2018b). Postmortem T-2* - weighted MRI imaging of cortical iron reflects severity of Alzheimer's disease. *J. Alzheimers. Dis*. 65, 1125–1137. doi: 10.3233/JAD-180317

Burdo, J. R., Menzies, S. L., Simpson, I. A., Garrick, L. M., Garrick, M. D., Dolan, K. G., et al. (2001). Distribution of divalent metal transporter 1 and metal transport protein 1 in the normal and Belgrade rat. *J. Neurosci. Res*. 66, 1198–1207. doi: 10.1002/jnr.1256

Calabrese, V., Giordano, J., Signorile, A., Ontario, M. L., Castorina, S., Pasquale, D., et al. (2016). Major pathogenic mechanisms in vascular dementia: roles of cellular stress response and hormesis in neuroprotection. *J. Neurosci. Res*. 94, 1588–1603. doi: 10.1002/jnr.23925

Cardoso, B. R., Roberts, B. R., Malpas, C. B., Vivash, L., Genc, S., Saling, M. M., et al. (2019). Supranutritional sodium selenate supplementation delivers selenium to the central nervous system: results from a randomized controlled pilot trial in Alzheimer's disease. *Neurotherapeutics*. 16, 192–202. doi: 10.1007/s13311-018-0662-z

Chan, A., and Shea, T. B. (2006). Dietary and genetically-induced oxidative stress alter tau phosphorylation: Influence of folate and apolipoprotein E deficiency. *J. Alzheimers. Dis*. 9, 399–405. doi: 10.3233/JAD-2006-9405

Chen, L., Hua, J., Ross, C. A., Cai, S., van Zijl, P. C. M., Altered, L., et al. (2019). brain iron content and deposition rate in Huntington's disease as indicated by quantitative susceptibility MRI. *J. Neurosci. Res*. 97, 467–479. doi: 10.1002/jnr.24358

Chen, Q., Chen, Y., Zhang, Y., Wang, F., Yu, H., Zhang, C., et al. (2019). Iron deposition in Parkinson's disease by quantitative susceptibility mapping. *BMC Neurosci*. 20:23. doi: 10.1186/s12868-019-0505-9

Chen, S. W., Bu, D. F., Zhu, J., Yue, T. H., Guo, S. A., Wang, X., et al. (2021). Endogenous hydrogen sulfide regulates xCT stability through persulfidation of OTUB1 at cysteine 91 in colon cancer cells. *Neoplasia*. 23, 461–472. doi: 10.1016/j.neo.2021.03.009

Choi, D. H., Kim, J. H., Seo, J. H., Lee, J., Choi, W. S., Kim, Y. S., et al. (2014). Matrix metalloproteinase-3 causes dopaminergic neuronal death through nox1-regenerated oxidative stress. *PLoS ONE*. 9:e115954. doi: 10.1371/journal.pone.0115954

Connor, J. R., Menzies, S. L., Stmartin, S. M., and Mufson, E. J. A. (1992). Histochemical-study of iron, transferrin, and ferritin in Alzheimers diseased brains. *J. Neurosci. Res*. 31, 75–83. doi: 10.1002/jnr.490310111

Conrad, M., Kagan, V. E., Bayir, H., Pagnussat, G. C., Head, B., Traber, M. G., et al. (2018). Regulation of lipid peroxidation and ferroptosis in diverse species. *Gene Dev*. 32, 602–619. doi: 10.1101/gad.314674.118

Crouch, P. J., Savva, M. S., Hung, L. W., Donnelly, P. S., Mot, A. I., Parker, S. J., et al. (2011). The Alzheimer's therapeutic PBT2 promotes amyloid-beta degradation and GSK3 phosphorylation via a metal chaperone activity. *J. Neurochem*. 119, 220–230. doi: 10.1111/j.1471-4159.2011.07402.x

da Rocha, T. J., Alves, M. S., Guisso, C. C., de Andrade, F. M., and Camozzato, A., Oliveira, A., et al. (2018). Association of GPX1 and GPX4 polymorphisms with episodic memory and Alzheimer's disease. *Neurosci. Lett*. 666, 32–37. doi: 10.1016/j.neulet.2017.12.026

Davies, P., Moualla, D., and Brown, D. R. (2011). Alpha-synuclein is a cellular ferrireductase. *PLoS ONE*. 6, e15814. doi: 10.1371/journal.pone.0015814

Dixon, S. J., Lemberg, K. M., Lamprecht, M. R., Skouta, R., Zaitsev, E. M., Gleason, C. E., et al. (2012). Ferroptosis: an iron-dependent form of nonapoptotic cell death. *Cell*. 149, 1060–1072. doi: 10.1016/j.cell.2012.03.042

Dixon, S. J., and Stockwell, B. R. (2014). The role of iron and reactive oxygen species in cell death. *Nat. Chem. Biol*. 10, 9–17. doi: 10.1038/nchembio.1416

Do Van, B., Gouel, F., Jonneaux, A., Timmerman, K., Gele, P., Petrault, M., et al. (2016). Ferroptosis, a newly characterized form of cell death in Parkinson's disease that is regulated by PKC. *Neurobiol. Dis*. 94, 169–178. doi: 10.1016/j.nbd.2016.05.011

Doll, S., Freitas, F. P., Shah, R., Aldrovandi, M., da Silva, M. C., Ingold, I., et al. (2019). FSP1 is a glutathione-independent ferroptosis suppressor. Nature. 575, 693. doi: 10.1038/s41586-019-1707-0

Doll, S., Proneth, B., Tyurina, Y. Y., Panzilius, E., and Kobayashi, S. (2017). IngoId I, et al. ACSL4 dictates ferroptosis sensitivity by shaping cellular lipid composition. *Nat. Chem. Biol*. 13, 91–98. doi: 10.1038/nchembio.2239

Dolotov, O. V., Inozemtseva, L. S., Myasoedov, N. F., and Grivennikov, I. A. (2022). Stress-induced depression and Alzheimer's disease: focus on astrocytes. *Int. J. Mol. Sci*. 23:4999. doi: 10.3390/ijms23094999

Donley, D. W., Realing, M., Gigley, J. P., and Fox, J. H. (2021). Iron activates microglia and directly stimulates indoleamine-2,3-dioxygenase activity in the N171-82Q mouse model of Huntington's disease. *PLoS ONE*. 16:e0250606. doi: 10.1371/journal.pone.0250606

Du, F., Qian, Z. M., Luo, Q. Q., Yung, W. H., and Ke, Y. (2015). Hepcidin suppresses brain iron accumulation by downregulating iron transport proteins in iron-overloaded rats. *Mol. Neurobiol*. 52, 101–114. doi: 10.1007/s12035-014-8847-x

Du, L., Zhao, Z. F., Cui, A. L., Zhu, Y. J., Zhang, L., Liu, J., et al. (2018). Increased iron deposition on brain quantitative susceptibility mapping correlates with decreased cognitive function in Alzheimer's disease. *ACS Chem. Neurosci*. 9, 1849–1857. doi: 10.1021/acschemneuro.8b00194

Du, S. Q., Wang, X. R., Xiao, L. Y., Tu, J. F., Zhu, W., He, T., et al. (2017). Molecular mechanisms of vascular dementia: what can be learned from animal models of chronic cerebral hypoperfusion? *Mol. Neurobiol*. 54, 3670–3682. doi: 10.1007/s12035-016-9915-1

Duce, J. A., Tsatsanis, A., Cater, M. A., James, S. A., Robb, E., Wikhe, K., et al. (2010). Iron-Export Ferroxidase Activity of beta-Amyloid Precursor Protein Is Inhibited by Zinc in Alzheimer's Disease. *Cell*. 142, 857–867. doi: 10.1016/j.cell.2010.08.014

Eid, R., Arab, N. T. T., and Greenwood, M. T. (2017). Iron mediated toxicity and programmed cell death: a review and a re-examination of existing paradigms. *Bba-Mol. Cell Res*. 1864, 399–430. doi: 10.1016/j.bbamcr.2016.12.002

Fan, G. H., Zhu, T. Y., Min, X. P., and Juan, X. (2021). Melatonin protects against PM2.5-induced lung injury by inhibiting ferroptosis of lung epithelial cells in a Nrf2-dependent manner. *Ecotox Environ Safe*. 223, 112588. doi: 10.1016/j.ecoenv.2021.112588

Farina, N., Llewellyn, D., Isaac, M. G. E. N., and Tabet, N. (2017). Vitamin E for Alzheimer's dementia and mild cognitive impairment. *Cochrane Db Syst Rev*. 1:CD002845. doi: 10.1002/14651858.CD002854.pub4

Fava, A., Pirritano, D., Plastino, M., Cristiano, D., Puccio, G., Colica, C., et al. (2013). The effect of lipoic acid therapy on cognitive functioning in patients with Alzheimer's disease. *J Neurodegener Dis*. 2013, 454253. doi: 10.1155/2013/454253

Feng, G. S., Zhang, Z. J., Bao, Q. Q., Zhang, Z. J., Zhou, L. B., Jiang, J., et al. (2014). Protective effect of chinonin in MPTP-induced C57BL/6 mouse model of Parkinson's disease. *Biol. Pharm. Bull*. 37, 1301–1307. doi: 10.1248/bpb.b14-00128

Frank, C., Hoffmann, T., Zelder, O., Felle, M. F., and Bremer, E. (2021). Enhanced Glutamate Synthesis and Export by the Thermotolerant Emerging Industrial Workhorse Bacillus methanolicus in Response to High Osmolarity. *Front. Microbiol*. 12:640980. doi: 10.3389/fmicb.2021.640980

Fraser, E. E., Downing, M. G., Biernacki, K., McKenzie, D. P., and Ponsford, J. L. (2019). Cognitive reserve and age predict cognitive recovery after mild to

severe traumatic brain injury. *J Neurotraum*. 36, 2753–2761. doi: 10.1089/neu.2019.6430

Gallie, B. L., and Olivieri, N. F. (2019). The role of deferiprone in iron chelation. *New Engl. J. Med*. 380, 891–93. doi: 10.1056/NEJMc1817335

Gaschler, M. M., Andia, A. A., Liu, H. R., Csuka, J. M., Hurlocker, B., Vaiana, C. A., et al. (2018). FINO2 initiates ferroptosis through GPX4 inactivation and iron oxidation. Nat Chem Biol. 14, 507–15. doi: 10.1038/s41589-018-0031-6

Giometto, B., Bozza, F., Argentiero, V., Gallo, P., Pagni, S., Piccinno, M. G., et al. (1990). Transferrin receptors in rat central-nervous-system - an immunocytochemical study. *J. Neurol. Sci*. 98, 81–90. doi: 10.1016/0022-510X(90)90183-N

Golko-Perez, S., Amit, T., Bar-Am, O., Youdim, M. B. H., and Weinreb, O. A. (2017). Novel iron chelator-radical scavenger ameliorates motor dysfunction and improves life span and mitochondrial biogenesis in SOD1(G93A) ALS mice. *Neurotox. Res*. 31, 230–244. doi: 10.1007/s12640-016-9677-6

Gong, J., Du, F., Qian, Z. M., Luo, Q. Q., Sheng, Y., Yung, W. H., et al. (2016). Pre-treatment of rats with ad-hepcidin prevents iron-induced oxidative stress in the brain. *Free Radical Bio Med*. 90, 126–132. doi: 10.1016/j.freeradbiomed.2015.11.016

Griesbach, G. S., Masel, B. E., Helvie, R. E., and Ashley, M. J. (2018). The impact of traumatic brain injury on later life: effects on normal aging and neurodegenerative diseases. *J Neurotraum*. 35, 17–24. doi: 10.1089/neu.2017.5103

Grossi, C., Francese, S., Casini, A., Rosi, M. C., Luccarini, I., Fiorentini, A., et al. (2009). Clioquinol decreases amyloid-beta burden and reduces working memory impairment in a transgenic mouse model of Alzheimer's disease. *J. Alzheimers. Dis*. 17, 423–440. doi: 10.3233/JAD-2009-1063

Guillemot, J., Canuel, M., Essalmani, R., Prat, A., and Seidah, N. G. (2013). Implication of the proprotein convertases in iron homeostasis: proprotein convertase 7 sheds human transferrin receptor 1 and furin activates hepcidin. *Hepatology*. 57, 2514–2524. doi: 10.1002/hep.26297

Guo, C., Wang, T., Zheng, W., Shan, Z. Y., Teng, W. P., Wang, Z. Y., et al. (2013). Intranasal deferoxamine reverses iron-induced memory deficits and inhibits amyloidogenic APP processing in a transgenic mouse model of Alzheimer's disease. *Neurobiol. Aging*. 34, 562–575. doi: 10.1016/j.neurobiolaging.2012.05.009

Gurney, M. E., Fleck, T. J., Himes, C. S., and Hall, E. D. (1998). Riluzole preserves motor function in a transgenic model of familial amyotrophic lateral sclerosis. *Neurology*. 50, 62–66. doi: 10.1212/WNL.50.1.62

Gustaw-Rothenberg, K., Kowalczuk, K., and Stryjecka-Zimmer, M. (2010). Lipids' peroxidation markers in Alzheimer's disease and vascular dementia. *Geriatr. Gerontol. Int*. 10, 161–166. doi: 10.1111/j.1447-0594.2009.00571.x

Gwon, A. R., Park, J. S., Park, J. H., Baik, S. H., Jeong, H. Y., Hyun, D. H., et al. (2010). Selenium attenuates A beta production and A beta-induced neuronal death. *Neurosci. Lett*. 469, 391–395. doi: 10.1016/j.neulet.2009.12.035

Ha, C., Ryu, J., and Park, C. B. (2007). Metal ions differentially influence the aggregation and deposition of Alzheimer's beta-amyloid on a solid template. *Biochemistry-Us*. 46, 6118–6125. doi: 10.1021/bi7000032

Habib, E., Linher-Melville, K., Lin, H. X., and Singh, G. (2015). Expression of xCT and activity of system xc(-) are regulated by NRF2 in human breast cancer cells in response to oxidative stress. *Redox Biol*. 5, 33–42. doi: 10.1016/j.redox.2015.03.003

Hambright, W. S., Fonseca, R. S., Chen, L. J., Na, R., and Ran, Q. T. (2017). Ablation of ferroptosis regulator glutathione peroxidase 4 in forebrain neurons promotes cognitive impairment and neurodegeneration. *Redox Biol*. 12, 8–17. doi: 10.1016/j.redox.2017.01.021

He, Y. J., Liu, X. Y., Xing, L., Wan, X., Chang, X., Jiang, H. L., et al. (2020). Fenton reaction-independent ferroptosis therapy via glutathione and iron redox couple sequentially triggered lipid peroxide generator. *Biomaterials*. 241, 119911. doi: 10.1016/j.biomaterials.2020.119911

Heidler-Gary, J., and Hillis, A. E. (2007). Distinctions between the dementia in amyotrophic lateral sclerosis with frontotemporal dementia and the dementia of Alzheimer's disease. *Amyotroph Lateral Sc*. 8, 276–282. doi: 10.1080/17482960701381911

Heneka, M. T., Fink, A., and Doblhammer, G. (2015). Effect of pioglitazone medication on the incidence of dementia. *Ann. Neurol*. 78, 284–294. doi: 10.1002/ana.24439

Hentze, M. W., Muckenthaler, M. U., Galy, B., and Camaschella, C. (2010). Two to tango: regulation of mammalian iron metabolism. *Cell*. 142, 24–38. doi: 10.1016/j.cell.2010.06.028

Hider, R. C., and Kong, X. L. (2011). Glutathione: a key component of the cytoplasmic labile iron pool. *Biometals*. 24, 1179–1187. doi: 10.1007/s10534-011-9476-8

Holland, R., McIntosh, A. L., Finucane, O. M., Mela, V., Rubio-Araiz, A., Timmons, G., et al. (2018). Inflammatory microglia are glycolytic and iron retentive and typify the microglia in APP/PS1 mice. *Brain Behav. Immun*. 68, 183–196. doi: 10.1016/j.bbi.2017.10.017

Hu, Y., Yu, S. Y., Zuo, L. J., Piao, Y. S., Cao, C. J., Wang, F., et al. (2015). Investigation on Abnormal Iron Metabolism and Related Inflammation in Parkinson Disease Patients with Probable RBD. *PLoS ONE*. 10, e0138997. doi: 10.1371/journal.pone.0138997

Ingold, I., Berndt, C., Schmitt, S., Doll, S., Poschmann, G., Buday, K., et al. (2018). Selenium Utilization by GPX4 Is required to prevent hydroperoxide-induced ferroptosis. *Cell*. 172, 409–22.e21. doi: 10.1016/j.cell.2017.11.048

Iridoy, M. O., Zubiri, I., Zelaya, M. V., Martinez, L., Ausin, K., Lachen-Montes, M., et al. (2019). Neuroanatomical quantitative proteomics reveals common pathogenic biological routes between amyotrophic lateral sclerosis (ALS) and frontotemporal dementia (FTD). *Int. J. Mol. Sci*. 20, 4. doi: 10.3390/ijms20010004

Iwata-Ichikawa, E., Kondo, Y., Miyazaki, I., Asanuma, M., and Ogawa, N. (1999). Glial cells protect neurons against oxidative stress via transcriptional up-regulation of the glutathione synthesis. *J. Neurochem*. 72, 2334–2344. doi: 10.1046/j.1471-4159.1999.0722334.x

James, S. A., Churches, Q. I., de Jonge, M. D., Birchall, I. E., Streltsov, V., McColl, G., et al. (2017). Iron, copper, and zinc concentration in A beta plaques in the APP/PS1 mouse model of Alzheimer's disease correlates with metal levels in the surrounding neuropil. *ACS Chem. Neurosci*. 8, 629–637. doi: 10.1021/acschemneuro.6b00362

Kagan, V. E., Mao, G. W., Qu, F., Angeli, J. P. F., Doll, S., St Croix, C., et al. (2017). Oxidized arachidonic and adrenic PEs navigate cells to ferroptosis. *Nat. Chem. Biol*. 13, 81–90. doi: 10.1038/nchembio.2238

Kalaria, R. N. (2018). The pathology and pathophysiology of vascular dementia. *Neuropharmacology*. 134, 226–239. doi: 10.1016/j.neuropharm.2017.12.030

Karelson, E., Bogdanovic, N., Garlind, A., Winblad, B., Zilmer, K., Kullisaar, T., et al. (2001). The cerebrocortical areas in normal brain aging and in Alzheimer's disease: NOTICEABLE differences in the lipid peroxidation level and in antioxidant defense. *Neurochem. Res*. 26, 353–361. doi: 10.1023/A:1010942929678

Kasai, S., Yamazaki, H., Tanji, K., Engler, M. J., Matsumiya, T., Itoh, K., et al. (2019). Role of the ISR-ATF4 pathway and its cross talk with Nrf2 in mitochondrial quality control. *J. Clin. Biochem. Nutr*. 64, 1–12. doi: 10.3164/jcbn.18-37

Kassan, A., Herms, A., Fernandez-Vidal, A., Bosch, M., Schieber, N. L., Reddy, B. J. N., et al. (2013). Acyl-CoA synthetase 3 promotes lipid droplet biogenesis in ER microdomains. *J. Cell Biol*. 203, 985–1001. doi: 10.1083/jcb.201305142

Kenkhuis, B., Somarakis, A., de Haan, L., Dzyubachyk, O., IJsselsteijn, M. E., de Miranda, NFCC, et al. (2021). Iron loading is a prominent feature of activated microglia in Alzheimer's disease patients. *Acta Neuropathol Com*. 9:27. doi: 10.1186/s40478-021-01126-5

Kerins, M. J., and Ooi, A. (2018). The roles of NRF2 in modulating cellular iron homeostasis. *Antioxid Redox Sign*. 29, 1756–1773. doi: 10.1089/ars.2017.7176

Khalaf, S., Ahmad, A. S., Chamara, K. V. D. R., and Dore, S. (2019). Unique properties associated with the brain penetrant iron chelator HBED reveal remarkable beneficial effects after brain trauma. *J. Neurotraum*. 36, 43–53. doi: 10.1089/neu.2017.5617

Kim, A. C., Lim, S., and Kim, Y. K. (2018). Metal ion effects on A and Tau aggregation. *Int. J. Mol. Sci*. 19:128. doi: 10.3390/ijms19010128

Kim, M., Yoo, S., Kim, D., Cho, J. W., Kim, J. S., Ahn, J. H., et al. (2021). Extra-basal ganglia iron content and non-motor symptoms in drug-naive, early Parkinson's disease. *Neurol. Sci*. 42, 5297–5304. doi: 10.1007/s10072-021-05223-0

Klepac, N., Relja, M., Klepac, R., Hecimovic, S., Babic, T., Trkulja, V., et al. (2007). Oxidative stress parameters in plasma of Huntington's disease patients, asymptomatic Huntington's disease gene carriers and healthy subjects. *J. Neurol*. 254, 1676–1683. doi: 10.1007/s00415-007-0611-y

Klivenyi, P., Andreassen, O. A., Ferrante, R. J., Dedeoglu, A., Mueller, G., Lancelot, E., et al. (2000). Mice deficient in cellular glutathione peroxidase show increased vulnerability to malonate, 3-nitropropionic acid, and 1-methyl-4-phenyl-1,2,5,6-tetrahydropyridine. *J. Neurosci*. 20, 1–7. doi: 10.1523/JNEUROSCI.20-01-00001.2000

Klopstock, T., Tricta, F., Neumayr, L., Karin, I., Zorzi, G., Fradette, C., et al. (2019). Safety and efficacy of deferiprone for pantothenate kinase-associated neurodegeneration: a randomised, double-blind, controlled trial and an open-label extension study. *Lancet Neurol*. 18, 631–642. doi: 10.1016/S1474-4422(19)30142-5

Kress, G. J., Dineley, K. E., and Reynolds, I. J. (2002). The relationship between intracellular free iron and cell injury in cultured neurons, astrocytes, and oligodendrocytes. *J. Neurosci*. 22, 5848–5855. doi: 10.1523/JNEUROSCI.22-14-05848.2002

Krzyzanowska, W., Pomierny, B., Filip, M., and Pera, J. (2014). Glutamate transporters in brain ischemia: to modulate or not? *Acta Pharmacol. Sin*. 35, 444–462. doi: 10.1038/aps.2014.1

Kwan, J. Y., Jeong, S. Y., Van Gelderen, P., Deng, H. X., Quezado, M. M., Danielian, L. E., et al. (2012). Iron Accumulation in deep cortical layers accounts for MRI signal abnormalities in ALS: correlating 7 Tesla MRI and pathology. *PLoS ONE*. 7, e35241. doi: 10.1371/journal.pone.0035241

Lane, D. J. R., Metselaar, B., Greenough, M., Bush, A. I., and Ayton, S. J. (2021). Ferroptosis and NRF2: an emerging battlefield in the neurodegeneration of Alzheimer's disease. *Essays Biochem*. 65, 925–940. doi: 10.1042/EBC20210017

Langkammer, C., Pirpamer, L., Seiler, S., Deistung, A., Schweser, F., Franthal, S., et al. (2016). Quantitative susceptibility mapping in Parkinson's disease. *PLoS ONE*. 11:e0162460. doi: 10.1371/journal.pone.0162460

Lee, J. M., Lee, J. H., Song, M. K., and Kim, Y. J. (2021). NXP031 improves cognitive impairment in a chronic cerebral hypoperfusion-induced vascular dementia rat model through Nrf2 signaling. *Int. J. Mol. Sci*. 22:6285. doi: 10.3390/ijms22126285

Lei, P., Ayton, S., Finkelstein, D. I., Spoerri, L., Ciccotosto, G. D., Wright, D. K., et al. (2012). Tau deficiency induces parkinsonism with dementia by impairing APP-mediated iron export. *Nat. Med*. 18, 291–295. doi: 10.1038/nm.2613

Leng, F. D., and Edison, P. (2021). Neuroinflammation and microglial activation in Alzheimer disease: where do we go from here? *Nat. Rev. Neurol*. 17, 157–172. doi: 10.1038/s41582-020-00435-y

Li, D. T. H., Hui, E. S., Chan, Q., Yao, N., Chua, S. E., McAlonan, G. M., et al. (2018). Quantitative susceptibility mapping as an indicator of subcortical and limbic iron abnormality in Parkinson's disease with dementia. *Neuroimage-Clin*. 20, 365–373. doi: 10.1016/j.nicl.2018.07.028

Li, J., Li, O. W., Jiang, Z. G., and Ghanbari, H. A. (2013). Oxidative stress and neurodegenerative disorders. *Int. J. Mol. Sci*. 14, 24438–24475. doi: 10.3390/ijms141224438

Li, S. J., Zhou, C. G., Zhu, Y. H., Chao, Z. W., Sheng, Z. Y., Zhang, Y. X., et al. (2021). Ferrostatin-1 alleviates angiotensin II (Ang II)- induced inflammation and ferroptosis in astrocytes. *Int. Immunopharmacol*. 90, 107179. doi: 10.1016/j.intimp.2020.107179

Li, S. W., Zheng, L. S., Zhang, J., Liu, X. J., and Wu, Z. M. (2021). Inhibition of ferroptosis by up-regulating Nrf2 delayed the progression of diabetic nephropathy. *Free Radical. Bio. Med*. 162, 435–449. doi: 10.1016/j.freeradbiomed.2020.10.323

Li, W. Y., Li, W., Wang, Y., Leng, Y., and Xia, Z. Y. (2021). Inhibition of DNMT-1 alleviates ferroptosis through NCOA4 mediated ferritinophagy during diabetes myocardial ischemia/reperfusion injury. *Cell Death Discov*. 7, 267. doi: 10.1038/s41420-021-00656-0

Li, Y. X., He, Y. S., Guan, Q., Liu, W. C., Han, H. J., Nie, Z. Y., et al. (2012). Disrupted iron metabolism and ensuing oxidative stress may mediate cognitive dysfunction induced by chronic cerebral hypoperfusion. *Biol. Trace Elem. Res*. 150, 242–248. doi: 10.1007/s12011-012-9455-0

Lin, G. P., Zhu, F. Y., Kanaan, N. M., Asano, R., Shirafuji, N., Sasaki, H., et al. (2021). clioquinol decreases levels of phosphorylated, truncated, and oligomerized Tau protein. *Int. J. Mol. Sci*. 22:12063. doi: 10.3390/ijms222112063

Liu, J. M., Sun, J., Wang, F. Y., Yu, X. C., Ling, Z. X., Li, H. X., et al. (2015). Neuroprotective effects of clostridium butyricum against vascular dementia in mice via metabolic butyrate. *Biomed Res. Int*. 2015:412946. doi: 10.1155/2015/412946

Liu, L., Vollmer, M. K., Ahmad, A. S., Fernandez, V. M., Kim, H., Dore, S., et al. (2019). Pretreatment with Korean red ginseng or dimethyl fumarate attenuates reactive gliosis and confers sustained neuroprotection against cerebral hypoxic-ischemic damage by an Nrf2-dependent mechanism. *Free Radical Bio Med*. 131, 98–114. doi: 10.1016/j.freeradbiomed.2018.11.017

Liu, L., Vollmer, M. K., Kelly, M. G., Fernandez, V. M., Fernandez, T. G., Kim, H., et al. (2020). Reactive gliosis contributes to Nrf2-dependent neuroprotection by pretreatment with dimethyl fumarate or korean red ginseng against hypoxic-ischemia: focus on hippocampal injury. *Mol. Neurobiol*. 57, 105–117. doi: 10.1007/s12035-019-01760-0

Liu, W. X., Wang, J., Xie, Z. M., Xu, N., Zhang, G. F., Jia, M., et al. (2016). Regulation of glutamate transporter 1 via BDNF-TrkB signaling plays a role in the anti-apoptotic and antidepressant effects of ketamine in chronic unpredictable stress model of depression. *Psychopharmacology*. 233, 405–415. doi: 10.1007/s00213-015-4128-2

Liu, Z., Shen, H. C., Lian, T. H., Mao, L., Tang, S. X., Sun, L., et al. (2017). Iron deposition in substantia nigra: abnormal iron metabolism, neuroinflammatory mechanism and clinical relevance. *Sci Rep-Uk*. 7:14973. doi: 10.1038/s41598-017-14721-1

Lloret, A., Badia, M. C., Mora, N. J., Pallardo, F. V., Alonso, M. D., Vina, J., et al. (2009). Vitamin E paradox in Alzheimer's disease: it does not prevent loss of cognition and may even be detrimental. *J. Alzheimers. Dis*. 17, 143–149. doi: 10.3233/JAD-2009-1033

Lu, C. H., Yang, C. Y., Li, C. Y., Hsieh, C. Y., and Ou, H. T. (2018). Lower risk of dementia with pioglitazone, compared with other second-line treatments, in metformin-based dual therapy: a population-based longitudinal study. *Diabetologia*. 61, 562–573. doi: 10.1007/s00125-017-4499-5

Ma, L. F., Zhang, X., Yu, K. K., Xu, X., Chen, T. X., Shi, Y., et al. (2021). Targeting SLC3A2 subunit of system X-C(-) is essential for m(6)A reader YTHDC2 to be an endogenous ferroptosis inducer in lung adenocarcinoma. *Free Radical Bio Med*. 168, 25–43. doi: 10.1016/j.freeradbiomed.2021.03.023

Makarov, P., Kropf, S., Wiswedel, I., Augustin, W., and Schild, L. (2006). Consumption of redox energy by glutathione metabolism contributes to hypoxia/reoxygenation-induced injury in astrocytes. *Mol. Cell. Biochem*. 286, 95–101. doi: 10.1007/s11010-005-9098-y

Mancias, J. D., Wang, X. X., Gygi, S. P., Harper, J. W., and Kimmelman, A. C. (2014). Quantitative proteomics identifies NCOA4 as the cargo receptor mediating ferritinophagy. Nature. 509, 105. doi: 10.1038/nature13148

Mao, L., Yang, T., and Li, X. (2019). Protective effects of sulforaphane in experimental vascular cognitive impairment: contribution of the Nrf2 pathway. *J. Cerebr Blood F Met*. 39, 371. doi: 10.1177/0271678X18764083

Masaldan, S., Belaidi, A. A., Ayton, S., and Bush, A. I. (2019a). Cellular senescence and iron dyshomeostasis in Alzheimer's Disease. *Pharmaceuticals-Base*. 12:93. doi: 10.3390/ph12020093

Masaldan, S., Bush, A. I., Devos, D., Rolland, A. S., and Moreau, C. (2019b). Striking while the iron is hot: Iron metabolism and ferroptosis in neurodegeneration. *Free Radical Bio Med*. 133, 221–233. doi: 10.1016/j.freeradbiomed.2018.09.033

Mclachlan, D. R. C., Dalton, A. J., Kruck, T. P. A., Bell, M. Y., Smith, W. L., Kalow, W., et al. (1991). Intramuscular desferrioxamine in patients with Alzheimers-disease. *Lancet*. 337, 1304–1308. doi: 10.1016/0140-6736(91)92978-B

Meng, F. X., Hou, J. M., and Sun, T. S. (2017). *In vivo* evaluation of microglia activation by intracranial iron overload in central pain after spinal cord injury. *J. Orthop. Surg. Res*. 12:75. doi: 10.1186/s13018-017-0578-z

Milkovic, L., Tomljanovic, M., Gasparovic, A. C., Kujundzic, R. N., Simunic, D., Konjevoda, P., et al. (2019). Nutritional stress in head and neck cancer originating cell lines: the sensitivity of the NRF2-NQO1 axis. *Cells-Basel*. 8:1001. doi: 10.3390/cells8091001

Miotto, G., Rossetto, M., Di Paolo, M. L., Orian, L., Venerando, R., Roveri, A., et al. (2020). Insight into the mechanism of ferroptosis inhibition by ferrostatin-1. *Redox Biol*. 28, 101328. doi: 10.1016/j.redox.2019.101328

Mishima, E. (2022). The E2F1-IREB2 axis regulates neuronal ferroptosis in cerebral ischemia. *Hypertens. Res*. 45, 1085–1086. doi: 10.1038/s41440-021-00837-5

Munoz, P., Zavala, G., Castillo, K., Aguirre, P., Hidalgo, C., Nunez, M. T., et al. (2006). Effect of iron on the activation of the MAPK/ERK pathway in PC12 neuroblastoma cells. *Biol. Res*. 39, 189–190. doi: 10.4067/S0716-97602006000100021

Newcombe, E. A., Camats-Perna, J., Silva, M. L., Valmas, N., Huat, T. J., Medeiros, R., et al. (2018). Inflammation: the link between comorbidities, genetics, and Alzheimer's disease. *J Neuroinflamm*. 15:276. doi: 10.1186/s12974-018-1313-3

Nikseresht, S., Bush, A. I., and Ayton, S. (2019). Treating Alzheimer's disease by targeting iron. *Brit. J Pharmacol*. 176, 3622–3635. doi: 10.1111/bph.14567

Nishizawa, H., Yamanaka, M., and Igarashi, K. (2022). Ferroptosis: regulation by competition between NRF2 and BACH1 and propagation of the death signal. *Febs J*. doi: 10.1111/febs.16382. [Epub ahead of print].

Nnah, I. C., Lee, C. H., and Wessling-Resnick, M. (2020). Iron potentiates microglial interleukin-1 beta secretion induced by amyloid-beta. *J. Neurochem*. 154, 177–189. doi: 10.1111/jnc.14906

Osama, A., Zhang, J., Yao, J., Yao, X., and Fang, J. (2020). Nrf2: a dark horse in Alzheimer's disease treatment. *Ageing Res. Rev*. 64, 101206. doi: 10.1016/j.arr.2020.101206

Ou, M., Jiang, Y., Ji, Y., Zhou, Q., Du, Z., Zhu, H., et al. (2022). Role and mechanism of ferroptosis in neurological diseases. *Mol Metab*. 61, 101502. doi: 10.1016/j.molmet.2022.101502

Pallast, S., Arai, K., Pekcec, A., Yigitkanli, K., Yu, Z. Y., Wang, X. Y., et al. (2010). Increased nuclear apoptosis-inducing factor after transient focal ischemia: a 12/15-lipoxygenase-dependent organelle damage pathway. *J Cerebr Blood F Met*. 30, 1157–1167. doi: 10.1038/jcbfm.2009.281

Park, S. Y., Choi, Y. W., and Park, G. (2018). Nrf2-mediated neuroprotection against oxygen-glucose deprivation/reperfusion injury by emodin via AMPK-dependent inhibition of GSK-3 beta. *J. Pharm. Pharmacol.* 70, 525–535. doi: 10.1111/jphp.12885

Peng, C. L., Jiang, N., Zhao, J. F., Liu, K., Jiang, W., Cao, P. G., et al. (2021). Metformin relieves H/R-induced cardiomyocyte injury through miR-19a/ACSL axis - possible therapeutic target for myocardial I/R injury. *Toxicol Appl Pharm.* 414:115408. doi: 10.1016/j.taap.2021.115408

Peters, D. G., Pollack, A. N., Cheng, K. C., Sun, D. X., Saido, T., Haaf, M. P., et al. (2018). Dietary lipophilic iron alters amyloidogenesis and microglial morphology in Alzheimer's disease knock-in APP mice. *Metallomics*. 10, 426–443. doi: 10.1039/C8MT00004B

Piao, Y. S., Du, Y. C., Oshima, H., Jin, J. C., Nomura, M., Yoshimoto, T., et al. (2008). Platelet-type 12-lipoxygenase accelerates tumor promotion of mouse epidermal cells through enhancement of cloning efficiency. *Carcinogenesis*. 29, 440–447. doi: 10.1093/carcin/bgm274

Qi, Q. Q., Xu, J., Lv, P. Y., Dong, Y. H., Liu, Z. J., Hu, M., et al. (2018). DL-3-n-butylphthalide alleviates vascular cognitive impairment induced by chronic cerebral hypoperfusion by activating the Akt/Nrf2 signaling pathway in the hippocampus of rats. *Neurosci. Lett.* 672, 59–64. doi: 10.1016/j.neulet.2017.11.051

Raha, A. A., Biswas, A., Henderson, J., Chakraborty, S., Holland, A., Friedland, R. P., et al. (2022). Interplay of ferritin accumulation and ferroportin loss in ageing brain: implication for protein aggregation in down syndrome dementia, Alzheimer's, and Parkinson's diseases. *Int. J. Mol. Sci.* 23:1060. doi: 10.3390/ijms23031060

Rassu, G., Soddu, E., Cossu, M., Brundu, A., Cerri, G., Marchetti, N., et al. (2015). Solid microparticles based on chitosan or methyl-beta-cyclodextrin: A first formulative approach to increase the nose-to-brain transport of deferoxamine mesylate. *J. Control. Release.* 201, 68–77. doi: 10.1016/j.jconrel.2015.01.025

Rathnasamy, G., Ling, E. A., and Kaur, C. (2013). Consequences of iron accumulation in microglia and its implications in neuropathological conditions. *Cns Neurol Disord-Dr.* 12, 785–798. doi: 10.2174/18715273113126660169

Ringbolz, G. M., and Greene, S. R. (2006). The relationship between amyotrophic lateral sclerosis and frontotemporal dementia. *Curr. Neurol. Neurosci.* 6, 387–392. doi: 10.1007/s11910-996-0019-6

Ritchie, C. W., Bush, A. I., Mackinnon, A., Macfarlane, S., Mastwyk, M., MacGregor, L., et al. (2003). Metal-protein attenuation with iodochlorhydroxyquin (clioquinol) targeting A beta amyloid deposition and toxicity in Alzheimer disease - A pilot phase 2 clinical trial. *Arch Neurol-Chicago*. 60, 1685–1691. doi: 10.1001/archneur.60.12.1685

Ritzel, R. M., Doran, S. J., Glaser, E. P., Meadows, V. E., Faden, A. I., Stoica, B. A., et al. (2019). Old age increases microglial senescence, exacerbates secondary neuroinflammation, and worsens neurological outcomes after acute traumatic brain injury in mice. *Neurobiol. Aging*. 77, 194–206. doi: 10.1016/j.neurobiolaging.2019.02.010

Rottkamp, C. A., Raina, A. K., Zhu, X. W., Gaier, E., Bush, A. I., Atwood, C. S., et al. (2001). Redox-active iron mediates amyloid-beta toxicity. *Free Radical Bio Med*. 30, 447–450. doi: 10.1016/S0891-5849(00)00494-9

Rouault, T. A. (2006). The role of iron regulatory proteins in mammalian iron homeostasis and disease. *Nat. Chem. Biol.* 2, 406–414. doi: 10.1038/nchembio807

Sanchez, M., Galy, B., Muckenthaler, M. U., and Hentze, M. W. (2007). Iron-regulatory proteins limit hypoxia-inducible factor-2alpha expression in iron deficiency. *Nat. Struct. Mol. Biol.* 14, 420–426. doi: 10.1038/nsmb1222

Sarutipaiboon, I., Settasatian, N., Komanasin, N., Kukongwiriyapan, U., Sawanyawisuth, K., Intharaphet, P., et al. (2020). Association of genetic variations in NRF2, NQO1, HMOX1, and MT with severity of coronary artery disease and related risk factors. *Cardiovasc. Toxicol.* 20, 176–189. doi: 10.1007/s12012-019-09544-7

Sayan-Ozacmak, H., Ozacmak, V. H., Barut, F., and Jakubowska-Dogru, E. (2012). Rosiglitazone treatment reduces hippocampal neuronal damage possibly through alleviating oxidative stress in chronic cerebral hypoperfusion. *Neurochem. Int*. 61, 287–290. doi: 10.1016/j.neuint.2012.05.011

Schneider, S. A., Hardy, J., and Bhatia, K. P. (2012). Syndromes of neurodegeneration with brain iron accumulation (NBIA): an update on clinical presentations, histological and genetic underpinnings, and treatment considerations. *Movement Disord.* 27, 42–53. doi: 10.1002/mds.23971

Seibt, T. M., Proneth, B., and Conrad, M. (2019). Role of GPX4 in ferroptosis and its pharmacological implication. *Free Radical Bio Med.* 133, 144–152. doi: 10.1016/j.freeradbiomed.2018.09.014

Shih, A. Y., Johnson, D. A., Wong, G., Kraft, A. D., Jiang, L., Erb, H., et al. (2003). Coordinate regulation of glutathione biosynthesis and release by Nrf2-expressing glia potently protects neurons from oxidative stress. *J. Neurosci.* 23, 3394–3406. doi: 10.1523/JNEUROSCI.23-08-03394.2003

Shintoku, R., Takigawa, Y., Yamada, K., Kubota, C., Yoshimoto, Y., Takeuchi, T., et al. (2017). Lipoxygenase-mediated generation of lipid peroxides enhances ferroptosis induced by erastin and RSL3. *Cancer Sci.* 108, 2187–2194. doi: 10.1111/cas.13380

Silvestri, L., and Camaschella, C. (2008). A potential pathogenetic role of iron in Alzheimer's disease. *J. Cell Mol Med.* 12, 1548–50. doi: 10.1111/j.1582-4934.2008.00356.x

Singh, N. (2014). The role of iron in prion disease and other neurodegenerative diseases. *PLoS Pathog.* 10, e1009395. doi: 10.1371/journal.ppat.1004335

Skouta, R., Dixon, S. J., Wang, J. L., Dunn, D. E., Orman, M., Shimada, K., et al. (2014). Ferrostatins inhibit oxidative lipid damage and cell death in diverse disease models. *J. Am. Chem. Soc.* 136, 4551–4556. doi: 10.1021/ja411006a

Spotorno, N., Acosta-Cabronero, J., Stomrud, E., Lampinen, B., Strandberg, O. T., van Westen, D., et al. (2020). Relationship between cortical iron and tau aggregation in Alzheimer's disease. *Brain*. 143, 1341–1349. doi: 10.1093/brain/awaa089

Stockwell, B. R., Angeli, J. P. F., Bayir, H., Bush, A. I., Conrad, M., Dixon, S. J., et al. (2017). Ferroptosis: A regulated cell death nexus linking metabolism, redox biology, and disease. *Cell*. 171, 273–285. doi: 10.1016/j.cell.2017.09.021

Streit, W. J., Rotter, J., Winter, K., Muller, W., Khoshbouei, H., Bechmann, I., et al. (2022). Droplet degeneration of hippocampal and cortical neurons signifies the beginning of neuritic plaque formation. *J. Alzheimers. Dis.* 85, 1701–1720. doi: 10.3233/JAD-215334

Sun, C. Y., Wu, Y., Ling, C., Xie, Z. Y., Kong, Q. L., Fang, X. J., et al. (2020). Deep gray matter iron deposition and its relationship to clinical features in cerebral autosomal dominant arteriopathy with subcortical infarcts and leukoencephalopathy patients A 7.0-T magnetic resonance imaging study. *Stroke*. 51, 1750–1757. doi: 10.1161/STROKEAHA.119.028812

Sun, Y., Zheng, Y. F., Wang, C. X., and Liu, Y. Z. (2018). Glutathione depletion induces ferroptosis, autophagy, and premature cell senescence in retinal pigment epithelial cells. *Cell Death Dis.* 9, 753. doi: 10.1038/s41419-018-0794-4

Sun, Y. R., He, L. B., Wang, T. Y., Hua, W., Qin, H., Wang, J. J., et al. (2020). Activation of p62-Keap1-Nrf2 pathway protects 6-hydroxydopamine-induced ferroptosis in dopaminergic cells. *Mol. Neurobiol.* 57, 4628–4641. doi: 10.1007/s12035-020-02049-3

Takahashi, M., Ko, L. W., Kulathingal, J., Jiang, P. Z., Sevlever, D., Yen, S. H. C., et al. (2007). Oxidative stress-induced phosphorylation, degradation and aggregation of alpha-synuclein are linked to upregulated CK2 and cathepsin D. *Eur. J. Neurosci.* 26, 863–874. doi: 10.1111/j.1460-9568.2007.05736.x

Tao, Y. L., Wang, Y., Rogers, J. T., and Wang, F. D. (2014). Perturbed iron distribution in Alzheimer's disease serum, cerebrospinal fluid, and selected brain regions: a systematic review and meta-analysis. *J. Alzheimers. Dis.* 42, 679–690. doi: 10.3233/JAD-140396

Thomas, G. E. C., Leyland, L. A., Schrag, A. E., Lees, A. J., Acosta-Cabronero, J., Weil, R. S., et al. (2020). Brain iron deposition is linked with cognitive severity in Parkinson's disease. *J Neurol Neurosur Ps.* 91, 418–425. doi: 10.1136/jnnp-2019-322042

Torii, S. (2018). Lipid peroxide accumulation enhances iron-dependent cell death ferroptosis in cancer cells. *Cancer Sci.* 109, 586.

Tripathi, A. K., Haldar, S., Qian, J., Beserra, A., Suda, S., Singh, A., et al. (2015). Prion protein functions as a ferrireductase partner for ZIP14 and DMT1. *Free Radical. Bio. Med.* 84, 322–330. doi: 10.1016/j.freeradbiomed.2015.03.037

Tsatsanis, A., McCorkindale, A. N., Wong, B. X., Patrick, E., Ryan, T. M., Evans, R. W., et al. (2021). The acute phase protein lactoferrin is a key feature of Alzheimer's disease and predictor of A beta burden through induction of APP amyloidogenic processing. *Mol Psychiatr*. 26, 5516–5531. doi: 10.1038/s41380-021-01248-1

Tuo, Q. Z., Lei, P., Jackman, K. A., Li, X. I., Xiong, H., Li, X. L., et al. (2017). Tau-mediated iron export prevents ferroptotic damage after ischemic stroke. *Mol Psychiatr.* 22, 1520–1530. doi: 10.1038/mp.2017.171

van Duijn, S., Bulk, M., van Duinen, S. G., Nabuurs, R. J. A., van Buchem, M. A., van der Weerd, L., et al. (2017). Cortical iron reflects severity of Alzheimer's disease. *J. Alzheimers. Dis.* 60, 1533–1545. doi: 10.3233/JAD-161143

Wan, W. B., Cao, L., Kalionis, B., Murthi, P., Xia, S. J., Guan, Y. T., et al. (2019). Iron deposition leads to hyperphosphorylation of Tau and disruption of insulin signaling. *Front. Neurol.* 2019, 10. doi: 10.3389/fneur.2019.00607

Wang, F., Yu, S. Y., Zuo, L. J., Cao, C. J., Hu, Y., Chen, Z. J., et al. (2016). Excessive iron and alpha-synuclein oligomer in brain are relevant to pure apathy in Parkinson disease. *J. Geriatr. Psychiatry Neurol.* 29, 187–194. doi: 10.1177/0891988716632918

Wang, J. F., Yin, X. M., He, W., Xue, W., Zhang, J., Huang, Y. R., et al. (2021). SUV39H1 deficiency suppresses clear cell renal cell carcinoma growth by inducing ferroptosis. *Acta Pharm. Sin. B*. 11, 406–419. doi: 10.1016/j.apsb.2020.09.015

Wang, T., Wang, C. Y., Shan, Z. Y., Teng, W. P., and Wang, Z. Y. (2012). Clioquinol reduces Zinc accumulation in neuritic plaques and inhibits the amyloidogenic pathway in a beta PP/PS1 transgenic mouse brain. *J. Alzheimers. Dis*. 29, 549–559. doi: 10.3233/JAD-2011-111874

Ward, R., Zucca, F. A., Duyn, J. H., Crichton, R. R., and Zecca, L. (2014). The role of iron in brain ageing and neurodegenerative disorders. *Lancet Neurol*. 13, 1045–1060. doi: 10.1016/S1474-4422(14)70117-6

Ward, R. J., Dexter, D., Florence, A., Aouad, F., Hider, R., Jenner, P., et al. (1995). Brain iron in the ferrocene-loaded rat - its chelation and influence on dopamine metabolism. *Biochem. Pharmacol*. 49, 1821–1826. doi: 10.1016/0006-2952(94)00521-M

Wenzel, S. E., Tyurina, Y. Y., Zhao, J. M., Croix, C. M. S., Dar, H. H., Mao, G. W., et al. (2017). PEBP1 wardens ferroptosis by enabling lipoxygenase generation of lipid death signals. *Cell*. 171, 628. doi: 10.1016/j.cell.2017.09.044

Wullner, U., Loschmann, P. A., Schulz, J. B., Schmid, A., Dringen, R., Eblen, F., et al. (1996). Glutathione depletion potentiates MPTP and MPP(+) toxicity in nigral dopaminergic neurones. *Neuroreport*. 7, 921–923. doi: 10.1097/00001756-199603220-00018

Xie, B. S., Wang, Y. Q., Lin, Y., Mao, Q., Feng, J. F., Gao, G. Y., et al. (2019). Inhibition of ferroptosis attenuates tissue damage and improves long-term outcomes after traumatic brain injury in mice. *CNS Neurosci. Ther*. 25, 465–475. doi: 10.1111/cns.13069

Xiong, W., Li, L. F., Huang, L., Liu, Y., Xia, Z. C., Zhou, X. X., et al. (2020). Different iron deposition patterns in akinetic/rigid-dominant and tremor-dominant Parkinson's disease. *Clin Neurol Neurosur*. 198:106181. doi: 10.1016/j.clineuro.2020.106181

Xu, J. G., Wang, H. D., Ding, K., Zhang, L., Wang, C. X., Li, T., et al. (2014). Luteolin provides neuroprotection in models of traumatic brain injury via the Nrf2-ARE pathway. *Free Radical Bio Med*. 71, 186–195. doi: 10.1016/j.freeradbiomed.2014.03.009

Xu, W., Zhi, Y., Yuan, Y. S., Zhang, B. F., Shen, Y. T., Zhang, H., et al. (2018). Correlations between abnormal iron metabolism and non-motor symptoms in Parkinson's disease. *J. Neural Transm*. 125, 1027–1032. doi: 10.1007/s00702-018-1889-x

Xu, Y., Zhang, Y. T., Zhang, J. H., Han, K., Zhang, X. W., Bai, X., et al. (2020). Astrocyte hepcidin ameliorates neuronal loss through attenuating brain iron deposition and oxidative stress in APP/PS1 mice. *Free Radical Bio Med*. 158, 84–95. doi: 10.1016/j.freeradbiomed.2020.07.012

Yang, J. H., Nguyen, C. D., Lee, G., and Na, C. S. (2022). Insamgobonhwan protects neuronal cells from lipid ROS and improves deficient cognitive function. *Antioxidants-Basel*. 11:295. doi: 10.3390/antiox11020295

Yang, W. S., Kim, K. J., Gaschler, M. M., Patel, M., Shchepinov, M. S., Stockwell, B. R., et al. (2016). Peroxidation of polyunsaturated fatty acids by lipoxygenases drives ferroptosis. *P. Natl. Acad. Sci. USA*. 113, E4966–E75. doi: 10.1073/pnas.1603244113

Yang, X. Y., Park, S. H., Chang, H. C., Shapiro, J. S., Vassilopoulos, A., Sawicki, K. T., et al. (2017). Sirtuin 2 regulates cellular iron homeostasis via deacetylation of transcription factor NRF2. *J. Clin. Invest*. 127, 1505–1516. doi: 10.1172/JCI88574

Yang, Y., Zhang, J. J., Liu, H., and Zhang, L. (2014). Change of Nrf2 expression in rat hippocampus in a model of chronic cerebral hypoperfusion. *Int. J. Neurosci*. 124, 577–584. doi: 10.3109/00207454.2013.863196

Yigitkanli, K., Zheng, Y., Pekcec, A., Lo, E. H., and van Leyen, K. (2017). Increased 12/15-lipoxygenase leads to widespread brain injury following global cerebral ischemia. *Transl. Stroke Res*. 8, 194–202. doi: 10.1007/s12975-016-0509-z

Yoo, M. H., Gu, X., Xu, X. M., Kim, J. Y., Carlson, B. A., Patterson, A. D., et al. (2010). Delineating the role of glutathione peroxidase 4 in protecting cells against lipid hydroperoxide damage and in Alzheimer's disease. *Antioxid. Redox Signal*. 12, 819–827. doi: 10.1089/ars.2009.2891

Yoo, S. E., Chen, L. J., Na, R., Liu, Y. H., Rios, C., Van Remmen, H., et al. (2012). Gpx4 ablation in adult mice results in a lethal phenotype accompanied by neuronal loss in brain. *Free Radical Bio Med*. 52, 1820–1827. doi: 10.1016/j.freeradbiomed.2012.02.043

Zeng, X. Y., An, H. D., Yu, F., Wang, K., Zheng, L. L., Zhou, W., et al. (2021). Benefits of iron chelators in the treatment of Parkinson's disease. *Neurochem. Res*. 46, 1239–1251. doi: 10.1007/s11064-021-03262-9

Zhan, S., Lu, L., Pan, S. S., Wei, X. Q., Miao, R. R., Liu, X. H., et al. (2022). Targeting NQO1/GPX4-mediated ferroptosis by plumbagin suppresses *in vitro* and *in vivo* glioma growth. *Brit. J. Cancer*. 127, 364–376, doi: 10.1038/s41416-022-01800-y

Zhang, Y. H., Wang, D. W., Xu, S. F., Zhang, S., Fan, Y. G., Yang, Y. Y., et al. (2018). alpha-Lipoic acid improves abnormal behavior by mitigation of oxidative stress, inflammation, ferroptosis, and tauopathy in P301S Tau transgenic mice. *Redox Biol*. 14, 535–548. doi: 10.1016/j.redox.2017.11.001

Zhao, Y. Y., Yang, Y. Q., Sheng, H. H., Tang, Q., Han, L., Wang, S. M., et al. (2022). GPX4 plays a crucial role in fuzheng kang'ai decoction-induced non-small cell lung cancer cell ferroptosis. *Front. Pharmacol*. 13, 851680. doi: 10.3389/fphar.2022.851680

Zhou, Z. D., and Tan, E. K. (2017). Iron regulatory protein (IRP)-iron responsive element (IRE) signaling pathway in human neurodegenerative diseases. *Mol. Neurodegener*. 12:75. doi: 10.1186/s13024-017-0218-4

Zhu, K. Y., Zhu, X., Liu, S. Q., Yu, J., Wu, S. W., Hei, M. Y., et al. (2022). Glycyrrhizin attenuates hypoxic-ischemic brain damage by inhibiting ferroptosis and neuroinflammation in neonatal rats via the HMGB1/GPX4 pathway. *Oxid. Med. Cell Longev*. 2022, 8438528. doi: 10.1155/2022/8438528

frontiers | Frontiers in Cellular Neuroscience

TYPE Original Research
PUBLISHED 16 November 2022
DOI 10.3389/fncel.2022.1023947

OPEN ACCESS

EDITED BY
Zhen-Ni Guo,
First Affiliated Hospital of Jilin University, China

REVIEWED BY
Liviu Aron,
Department of Genetics and Harvard Medical School, United States
Jie Jia,
Fudan University, China

*CORRESPONDENCE
Dongdong Qin
qindong108@163.com
Meihua Qiu
1341186480@qq.com
Yong Yin
yyinpmr@126.com

†These authors have contributed equally to this work

SPECIALTY SECTION
This article was submitted to Cellular Neuropathology, a section of the journal Frontiers in Cellular Neuroscience

RECEIVED 20 August 2022
ACCEPTED 31 October 2022
PUBLISHED 16 November 2022

CITATION
Wang B, Fu C, Wei Y, Xu B, Yang R, Li C, Qiu M, Yin Y and Qin D (2022) Ferroptosis-related biomarkers for Alzheimer's disease: Identification by bioinformatic analysis in hippocampus.
Front. Cell. Neurosci. 16:1023947.
doi: 10.3389/fncel.2022.1023947

Ferroptosis-related biomarkers for Alzheimer's disease: Identification by bioinformatic analysis in hippocampus

Binyang Wang[1†], Chenyang Fu[2†], Yuanyuan Wei[2†], Bonan Xu[2], Rongxing Yang[1], Chuanxiong Li[1], Meihua Qiu[1*], Yong Yin[1*] and Dongdong Qin[2*]

[1]Department of Rehabilitation Medicine, The Affiliated Hospital of Yunnan University, Kunming, China, [2]School of Basic Medical Sciences, Yunnan University of Chinese Medicine, Kunming, China

Background: Globally, Alzheimer's Disease (AD) accounts for the majority of dementia, making it a public health concern. AD treatment is limited due to the limited understanding of its pathogenesis. Recently, more and more evidence shows that ferroptosis lead to cell death in the brain, especially in the regions of the brain related to dementia.

Materials and methods: Three microarray datasets (GSE5281, GSE9770, GSE28146) related to AD were downloaded from Gene Expression Omnibus (GEO) datasets. Ferroptosis-related genes were extracted from FerrDb database. Data sets were separated into two groups. GSE5281 and GSE9770 were used to identify ferroptosis-related genes, and GSE28146 was used to verify results. During these processes, protein–protein interaction (PPI), the Gene Ontology (GO), and Kyoto Encyclopedia of Genes and Genomes (KEGG) pathway enrichment analyses were conducted. Finally, the differentiated values of ferroptosis-related genes were determined by receiver operator characteristic (ROC) monofactor analysis to judge their potential quality as biomarkers.

Results: Twenty-four ferroptosis-related genes were obtained. Using STRING (https://cn.string-db.org/) and Cytoscape with CytoHubba, the top 10 genes (*RB1, AGPAT3, SESN2, KLHL24, ALOX15B, CA9, GDF15, DPP4, PRDX1, UBC, FTH1, ASNS, GOT1, PGD, ATG16L1, SLC3A2, DDIT3, RPL8, VDAC2, GLS2, MTOR, HSF1, AKR1C3, NCF2*) were identified as target genes. GO analysis revealed that response to carboxylic acid catabolic process, organic acid catabolic process, alpha-amino acid biosynthetic process and cellular amino acid biosynthetic process were the most highly enriched terms. KEGG analysis showed that these overlapped genes were enriched in p53 signaling pathways, longevity regulating pathway, mTOR signaling pathway, type 2 diabetes mellitus and ferroptosis. Box plots and violine plots were created and verified to confirm the significance of identified target genes. Moreover, ROC monofactor analysis was performed to determine the diagnostic value of identified genes. Two genes (*ASNS*, *SESN2*) were subsequently obtained.

For the tow genes, STRING was used to obtain the five related genes and determined enriched GO terms and KEGG pathways for those genes.

Conclusion: Our results suggest that ASNS and SENS2 may serve as potential diagnostic biomarkers for AD and provide additional evidence regarding the essential role of ferroptosis in AD.

KEYWORDS

ferroptosis, Alzheimer's disease, biomarkers, hippocampus, ASNS, SESN2

Introduction

The number of people suffering from Alzheimer's disease (AD) are increasing globally, and AD influences many aspects from daily lifestyle to family expenditures (Jia et al., 2020; Scheltens et al., 2021). AD is the most common cause of dementia, which may account for approximately 60–80% of cases (Cunningham et al., 2015; Scheltens et al., 2021; Zhang et al., 2021). Clinical characteristics of AD include neurodegeneration with symptoms of cognitive and functional impairment such as decreased memory and ability to perform activities of daily living, and decreased behavioral capacity. Thus, it is important and emergent to figure out how to diagnose and detect AD earlier (Arvanitakis et al., 2019; Scheltens et al., 2021). At present, the pathogenesis of AD focuses mainly on contributions from amyloid β (Aβ) and Tau. AD may be due to the production, aggregation, and accumulation of Aβ leading to neurotoxicity or to changes in normal Tau, or it may be due to Aβ inducing the pathological transmission of Tau (Shaw et al., 2007; Scheltens et al., 2021). Currently, dementia is diagnosed according to associated behavioral traits rather than biological characters, such as brain imaging, due to its complexity and various potential causes, including cerebral cardiovascular diseases, Lewy body disease and frontotemporal dementia (McKhann et al., 2011; Arvanitakis et al., 2019). Therefore, there is a current need to determine specific biomarkers that can be used for the clinical diagnosis of AD, and these biomarkers can also be used for the exploration of future disease mechanisms and to obtain the best therapeutic targets.

Scientists have deemed that the hippocampal brain region is responsible for the function of memory, learning and spatial information in animal and human research (Jarrard, 1995; Knierim, 2015). Exploration between the hippocampal region and AD and dementia is continuing. A research report in 1999 showed that the declination of memory with aging was related to changes in the hippocampal region in AD patients (Small et al., 1999). A review concluded that AD patients suffer impairment in emotional event memory, as viewed in the amygdalohippocampal interconnection, with the amygdala showing damage characteristic of atrophy, plaques and tangles (McDonald and Mott, 2017). Recently, researchers have found new insights into the relationships between AD and the hippocampal region, specifically advancing cell death and neurodegeneration.

In Dixon et al., 2012 officially proposed the conception of ferroptosis (an iron-dependent, oxidative, non-apoptotic cell death) for the first time, which started the formal study of the mechanism between ferroptosis and various diseases. Compared with research on the relationship between ferroptosis and cancer or tumors, the link between ferroptosis and neurological diseases, especially AD, has been poorly studied. Searching ferroptosis and AD in Pubmed revealed that the exploration of ferroptosis and AD began to focus in 2017, and the number of publications in the area has surged in recent years. In 2019, researchers surprisingly found that mice with high dietary iron exhibit neuronal loss by apoptosis, autophagy and ferroptosis, leading to AD (Li et al., 2019). Iron has been reported to accelerate aggregation and pathogenicity of AD-related aberrant proteins, such as β-amyloid, tau, α-synuclein, and TDP (Ashraf and So, 2020). Another study in 2021 found that the loss of Fpn (ferroportin, an iron exporter) in AD mice led to brain atrophy and cognitive impairment, in addition to the morphological and molecular evidence of ferroptosis in hippocampal neurons in Fpn knockout mice (Bao et al., 2021). Restoration of Fpn ameliorated ferroptosis and memory impairment (Bao et al., 2021). Generally, ferroptosis affects AD in terms of iron metabolism, lipid peroxidation, and the glutathione/glutathione peroxidase 4 axis (Chen et al., 2021; Zhang et al., 2021).

Ferroptosis is a unique pattern of cell death that has gained attention in the field of AD research. However, the current studies of AD and ferroptosis lack exploration at the genetic level, although they may help to diagnosis AD and identify therapeutic targets for AD. Therefore, the purpose of the current study was to identify potential biomarkers related to ferroptosis and AD and to provide additional perspective for the research and treatment of AD.

Materials and methods

Datasets and pre-processing

Three AD-related microarrays datasets GSE9770 (Readhead et al., 2018), GSE5281 (Liang et al., 2007), GSE28146

(Blalock et al., 2011) were downloaded from GEO (Gene Expression Omnibus) database. Those datasets shared the same platform, GPL570 (HG-U133_Plus_2) (Affymetrix Human Genome U133 Plus 2.0 Array), which showed in the **Table 1**.

The datasets were processed used R Studio as follows: firstly, after obtaining the raw data of the three datasets, gene expression was normalized and log2-transformed using the LIMMA package (Ritchie et al., 2015) for normalization; then, we removed the no-load and duplicated gene probes to obtain the maximal gene expression probes. GSE9770 and GSE5281 datasets were merged using the Rsva package (Leek et al., 2012), and batch effects were removed. Finally, the LIMMA (Ritchie et al., 2015) package was used to identify DEGs (differentially expression genes) with a log fold change >1 and p-value <0.05. The GSE 28146 dataset underwent the same processing flow with the exception of being merged with any other datasets. DEGs were adjusted by the Benjamini–Hochberg method to process the p-values.

The ferroptosis-related genes from FerrDb and hub-genes from Cytoscape by protein–protein interaction

FerrDb[1] is the world's first database related to ferroptosis that includes genes and substances (Zhou and Bao, 2020). Ferroptosis-related genes, including driver, suppressor and inducer genes, and we removed the duplicated genes, which finally obtain the total 259 genes. These genes intersect with the DEGs from the union set of GSE9770 and GSE5281 and can be visualized in the Venn diagram. After obtaining the shared genes, STRING[2] was used to obtain the PPI (protein–protein interactions) with a 0.4 (medium confidence) minimum required interaction score. Cytoscape V3.9.1 software (Shannon et al., 2003) was then used to visualized the network. Moreover, CytoHubba was used to calculate and visualize the top 10 nodes.

TABLE 1 Alzheimer's disease (AD)-related microarrays datasets in hippocampus.

Dataset	Platform	Total	Alzheimer	Normal
GSE9770	GPL570	34	34	0
GSE5281	GPL570	161	74	87
GSE28146	GPL570	30	22	8

The gene ontology and Kyoto Encyclopedia of Genes and Genomes enrich analysis

The 10 selected genes were used to perform GO (Gene Ontology) analysis to determine BP (biological process), CC (cellular component), and MF (molecular function) term enrichment and perform KEGG (Kyoto Encyclopedia of Genes and Genomes pathway) enrichment. Final significant genes also underwent GO and KEGG enrichment analyses.

1 http://www.zhounan.org/ferrdb/current/

2 https://cn.string-db.org/

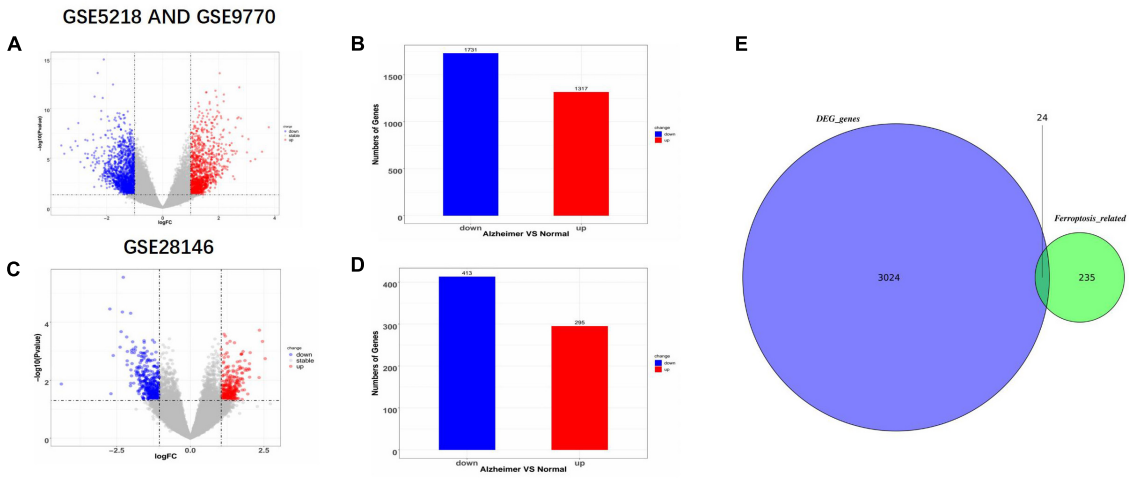

FIGURE 1
Identification of differentially expression genes (DEGs) and ferroptosis-related genes. **(A,B)** Volcano plot and bar plot of AD and non-AD patients in GSE5218 and GSE9770 after merging and removing any batch effects. **(C,D)** Volcano plot and bar plot of AD and non-AD patients in GSE28146. **(E)** Venn diagram showing the intersection of ferroptosis-related DEGs in the combined set. AD, Alzheimer's Disease; DEGs, differentially expressed genes.

Identifying the significant genes and find the clinical and diagnosing value of biomarkers

The significance of the 10 selected genes were checked again by comparing GSE28146 and the union dataset of GSE9770 and GSE5281 and visualized, respectively. Then, ROC monofactor analysis was performed in these two datasets to find the clinical and diagnostic value of ferroptosis-related biomarkers in AD patients. In the GSE28146 dataset, significant genes were identified not only by expression changes in AD but were also associated with the stage of dementia, which provided phenotype information.

Results

Finding and identifying the ferroptosis-related genes

Three datasets, GSE9770, GSE5281, and GSE28146, were downloaded from the GEO database and processed using the LIMMA package (Ritchie et al., 2015) in R studio. First, the GSE9770 and GSE5281 datasets were combined as a union set to identify ferroptosis-related DEGs, after removing no load or duplicated probes and batch effects. **Figures 1A,B** shows the up-regulated and down-regulated genes in the union set as volcano plots. The log fold change was set at 1.0 and p-value at <0.05. As a result, there were 1,731 down-regulated genes and 1,317 up-regulated genes. GSE28146 was similarly processed, and the results are shown in **Figures 1C,D**. There were 413 down-regulated genes and 295 up-regulated genes, with a 1.05 log fold change and p-value <0.05. The total 235 ferroptosis-related genes obtained from the FerrDb database (see text footnote 1) included driver, suppressor, and inducer genes. In **Figure 1E**, the Venn diagram shows the union sets and the ferroptosis-related genes. Finally, 24 ferroptosis-related genes were identified as biomarker candidates.

Protein-protein interaction network and confirming the hub genes

The names and the categories of the 24 ferroptosis-related biomarker candidate genes are shown in **Figure 2A**. The STRING database was used to analyze the PPI network of these genes and Cytoscape V3.9.1 was used for visualization of the network (**Figure 2C**). Cytohubba was applied to calculate the 10 nodes ranked the highest when using the MCC method (**Figure 2D**). *SESN2, ASNS, MTOR, SCL3A2, DDIT3, UBC, GLS2, PRDX1, GOT1,* and *ATG16L1* were identified as hub genes and are shown with their categories in **Figure 2B**.

Gene Ontology and Kyoto Encyclopedia of Genes and Genomes enrichment analysis

Gene Ontology term enrichment was determined for the 10 biomarker candidates and included analysis for enriched BP, MF, and CC (**Figure 3A**). KEGG enrichment analysis was also performed. The GO-BP results showed that these biomarkers are strongly associated with the "response to starvation", "carboxylic acid catabolic process", and "organic acid catabolic process", compared with other process. In the GO-CC, overlapping genes were mostly enriched in the "vacuolar membrane", "melanosome", and "pigment granule" terms. The three most enriched terms in GO-MF were "oxidoreductase activity", "antioxidant activity", and "carboxylic acid binding". Furthermore, KEGG results illustrated that these hub genes were mainly enriched in the "p53 signaling pathway", "longevity regulating pathway", "mTOR signaling pathway", "type 2 diabetes mellitus", and "ferroptosis" pathways (**Figure 3B**).

The expression of overlapped genes and the clinical value in union set

After obtaining the 10 ferroptosis-related genes, we were going to verify whether these genes could have same trend of expression. Firstly, we detected the expression of those 10 overlapped genes in union set and performed by boxplot and barplot. The graph showed that all genes is $p < 0.01$. Surprisingly, all genes showed that the expression is down-regulated in hippocampal region in AD patients vs. health person, except the SESN2 which show the opposite trend (**Figure 4A**). We also used ROC monofactor analysis to perform the diagnostic value of overlapped genes and calculate the AUC area to evaluate the accuracy of these genes' ability in prediction (**Figure 4B**). In the plot, we could see that the lowest AUC area is 0.90 and the maximal AUC is close to the one. As the result, the 10 genes are qualified to select as the biomarker in further verification.

The expression of overlapped genes and the clinical value in GSE28146

After selecting the 10 genes, the GSE28146 dataset was used to verify results. In **Figure 5A**, boxplots and bar plots of the 10 eligible genes are shown. Surprisingly, only two genes were significantly changed (*ANSN* $p < 0.01$, SENS2 $p < 0.05$) in AD patients vs. people without AD. *ASNS* and *SESN2* expression levels in the GSE28146 dataset were similar to that seen in the union set. Phenotypic subgroups were created according to the stage of dementia. There were no gene differences within the subgroups (**Figure 5B**). ROC monofactor analysis was used to

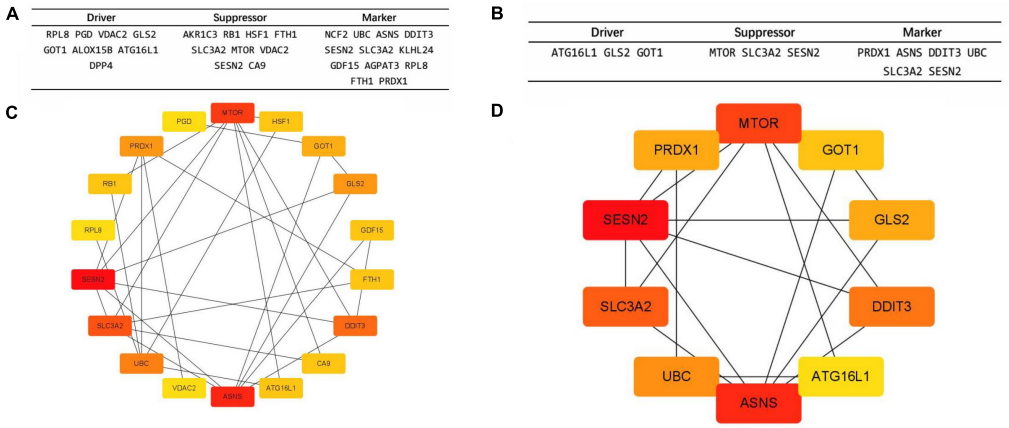

FIGURE 2
The protein–protein interaction (PPI) network and 10 hub gene interaction network analyzed using Cytoscape software. **(A,C)** The 24 Ferroptosis-related DEGs analyzed using STRINGS and Cytohubba (MCC Ranking method). The network includes 18 nodes and 29 edges. (Disconnected nodes are hidden). **(B,D)** Picking the top 10 rank genes (MCC Ranking method). The network includes 10 nodes and 16 edges. Gene to gene interactions are depicted in the graph as edges between two nodes. The different nodes represent the variation of the degrees from high to low, determined by the degree of interaction.

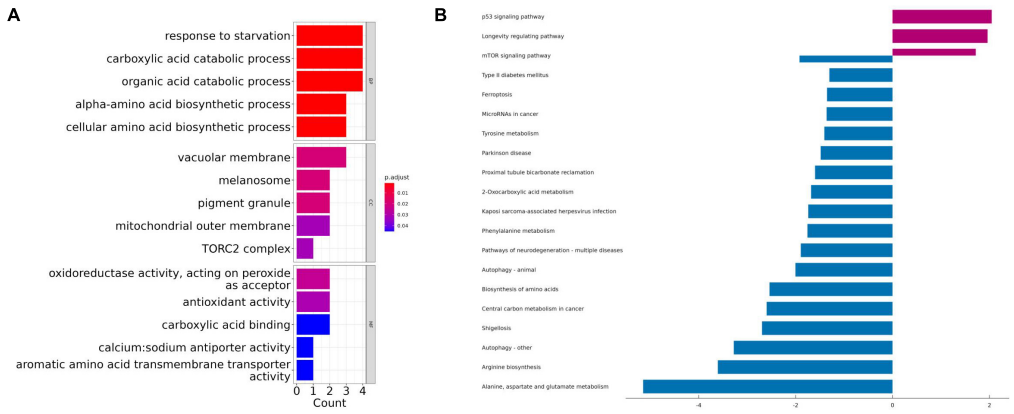

FIGURE 3
The Gene Ontology (GO) and Kyoto Encyclopedia of Genes and Genomes (KEGG) enrichment analyses using the top 10 ranked ferroptosis-related DEGs. **(A)** Gene Ontology (GO) functional analysis shows enriched items in the top 10 ranked ferroptosis-related DEGs. **(B)** Kyoto Encyclopedia of Genes and Genomes (KEGG) analysis shows the enriched items in the top 10 ranked ferroptosis-related DEGs. BP, biological process; CC, cellular component; MF, molecular function.

evaluate clinical value for candidate genes. In Figure 5C, the AUC of *ASNS* and *SESN2* was greater than 0.7 in the m1 curve, and *ATG16L1*, *GOT1*, and *SESN2* exceeded 0.7 in the m2 curve. Thus, *ASNS* and *SESN2* were chosen as biomarker candidates with potential diagnostic value in AD.

The potential mechanism in the selected genes and co-expressed protein network

The STRING database was used to identify the co-expressed protein network of *ASNS* and *SESN2*, and the networks were visualized (Figures 6E,F). Five interactors were identified in these two graphs, respectively. *GOT2*, *CAD*, *ASS1*, *ATF4*, and *CEBPB* are co-expressed with *ASNS*. GO and KEGG analysis results of these six genes are presented in Figures 6C,D. The GO and KEGG enrichment analysis for the co-expressed protein network of *SESN2*, based on the six related genes, is also shown (Figures 6A,B).

Discussion

Aging consists of many processes, including loss of protein homeostasis, DNA damage, lysosomal dysfunction,

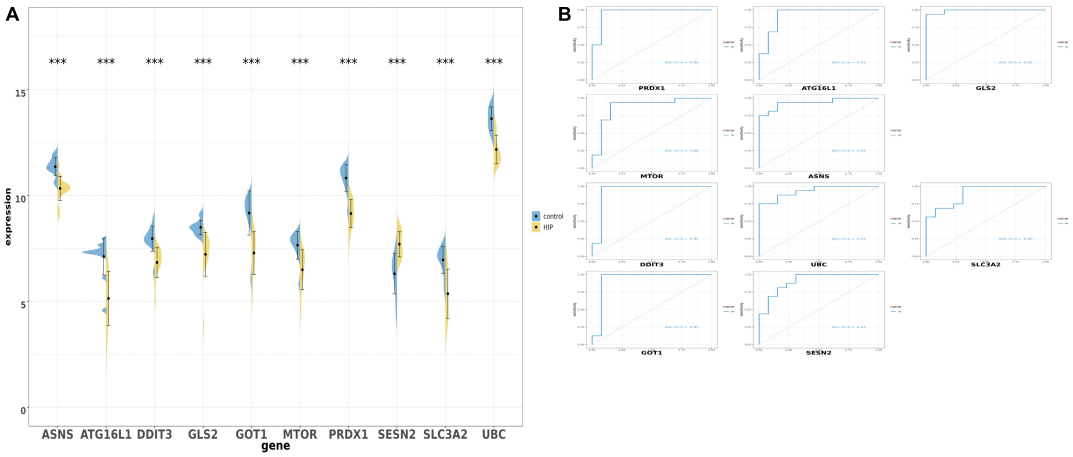

FIGURE 4
The boxplot and violine plot of the expression levels of the top 10 ranked ferroptosis-related differentially expression genes (DEGs), aimed at finding the significance and the ROC curve to illustrate the diagnostic value of ferroptosis-related DEGs by monofactor analysis. **(A)** Expression of the 10 ferroptosis-related genes compared with the non-AD group within the hippocampus region in AD in the combined with GSE5281 and GSE9770 datasets. **(B)** The AUC in the top 10 ranked ferroptosis-related genes in ROC curve in the set combined with GSE5281 and GSE9770. HIP, hippocampus region in Alzheimer's disease; ***, $p < 0.001$. AUC, Area under the curve.

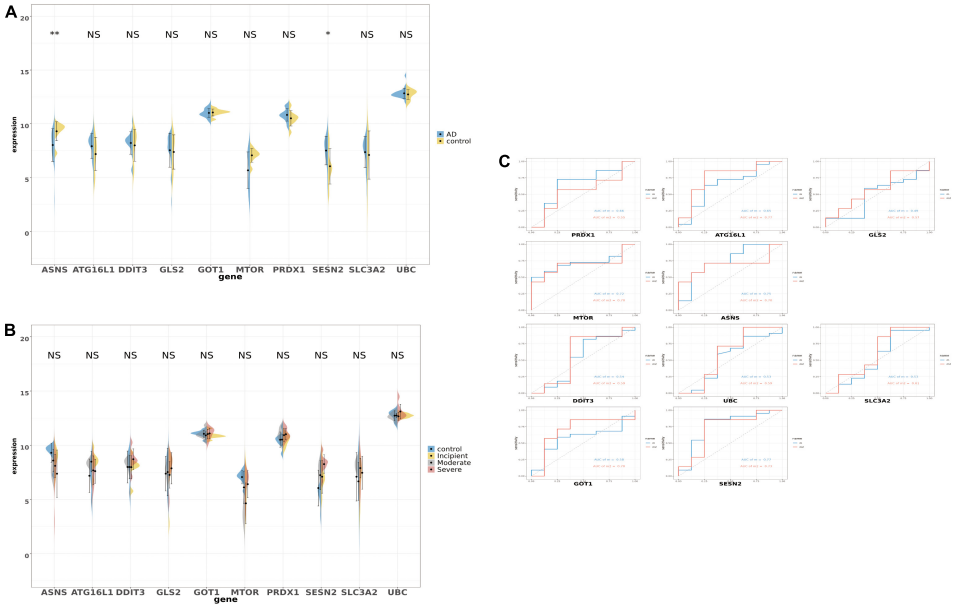

FIGURE 5
The boxplot and violine plot of the expression in the top 10 ranked ferroptosis-related DEGs, aimed at finding the significance and the receiver operator characteristic (ROC) curve in order to illustrate the diagnostic value of ferroptosis-related DEGs by monofactor analysis. **(A)** The expression of the 10 ferroptosis-related genes in AD compared with the non-AD group within the hippocampus region in GSE28146. **(B)** The expression of the 10 ferroptosis-related genes in AD compared with the non-AD group within the hippocampus region in the different stages of dementia in GSE28146. **(C)** AUC in the top 10 ranked ferroptosis-related genes in the ROC curves in GSE28146. *$p < 0.05$; **$p < 0.01$; NS, not significant, $p \geq 0.05$, non-AD control vs. AD; m2, control vs. incipient vs. moderate vs. severe.

epigenetic changes, and immune dysregulation, and it does not mutually and linearly relate to disease (Wyss-Coray, 2016). As normal aging, neurodegeneration and dementia, and cognitive impairment occur along a continuum, it is hard to distinguish the progression from normal aging to disease aging and to find a reliable tool to differentiate these processes, making this area of research a tough and difficult topic (Wyss-Coray, 2016). For the exploration of aging and neurodegenerative diseases, identifying specific cell death patterns and activated signaling pathways in the pathology of disease is crucial (Andreone et al., 2020).

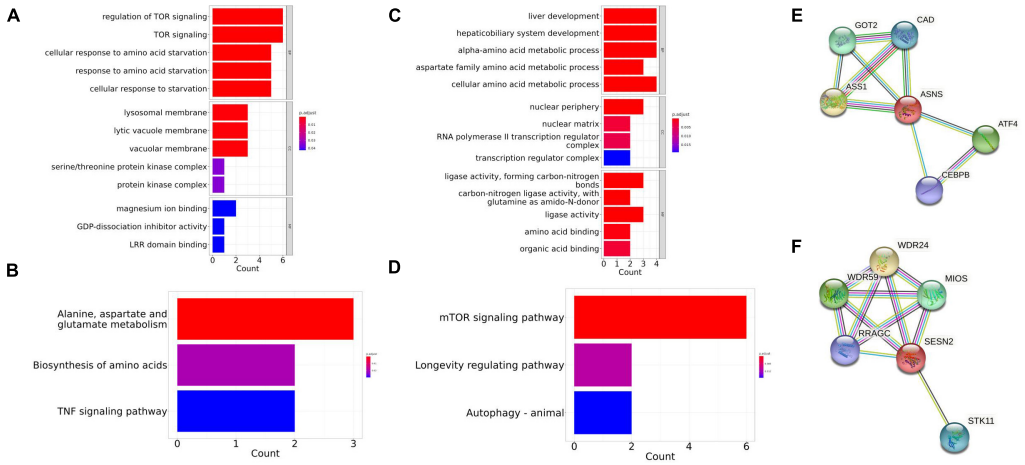

FIGURE 6
Gene Ontology (GO) and Kyoto Encyclopedia of Genes and Genomes (KEGG) enrichment in the co-expressed protein network of ASNS and SESN2. **(A,B)** The GO and KEGG enrichment of the co-expressed protein network of SESN2. **(C,D)** The GO and KEGG enrichment of the co-expressed protein network of ASNS. **(E)** Co-expressed protein network of ASNS. **(F)** Co-expressed protein network of SESN2.

Ferroptosis, which is different from other cell death patterns, is a new horizon for scientists to explore novel biomarkers and therapeutic targets (Andreone et al., 2020). A large cohort study showed that the existence of iron has a strong relationship with the mechanisms involved in neurodegeneration diseases, encouraging research into the interactions and associations between AD and ferroptosis (Ayton et al., 2021). Exploring the relationship between ferroptosis and AD may lead to identification of new biomarkers for AD diagnosis and new targets for AD treatment.

More and more scholars are studying the field of ferroptosis and neurodegenerative diseases. An animal study suggested that *SCL40A1*, a ferroptosis-related gene, is associated with cognitive impairment in type I diabetes (Hao et al., 2021). Moreover, another study found that eriodyctiol produces an anti-ferroptosis effect, thereby alleviating cognitive impairment, and the mechanism of these effects may be related to activation of the Nrf2/HO-1 pathway (Li et al., 2022). In the present study, ASNS and SESN2 were significantly related to AD compared with other ferroptosis-related genes. At present, most studies have focused on the role of ASNS in cancer-related studies, including studies on ovarian cancer, oral squamous cell carcinoma, colorectal cancer cell, T-cell acute lymphoblastic leukemia, and skull base chordoma (Lorenzi et al., 2006; Du et al., 2019; Fu et al., 2021; Shen et al., 2021; Akahane et al., 2022). *ASNS* may be a predictive biomarker in those tumors or cancers; however, assays also indicate an association between *ASNS* and neurodegeneration diseases. *SENS2* shows a similar trend to *ASNS* findings. In the study of carcinoma, *SENS2* was identified as a tumor suppressor gene (Weng et al., 2018). More specifically, *SESN2* may be a prognostic biomarker for hepatocellular cancer (Chen et al., 2017). A mouse study using *SESN2/3* knockout mice may allow characterization of its role in aging and metabolic-related disorders. Furthermore, *SESN2* may inhibit the production of ROS and produce antioxidant effects, making it a potential target for the treatment of AD and neurodegenerative diseases, as AD neuronal death is likely caused by oxidative damage (Wang et al., 2019). Surprisingly, a study for AD and mild cognitive impairment patients has suggested that SESN2 plays an important role in the progression of AD (Rai et al., 2016). In summary, the association between ferroptosis and AD may uncover new insights into diagnosis and therapeutic targets for AD. For example, iron chelators, co-drugs and the antioxidant vitamin E, show effects in the treatment of AD (Yuan et al., 2021). However, both biomarkers and therapeutic drugs need to be confirmed by clinical trials.

In conclusion, after processing and validating, ASNS and SESN2 were identified, which pays little attention on the correlation with AD. In our study, ASNS and SESN2 was regarded as the candidate biomarker of diagnosis of AD and even the therapeutic target in the further study. However, we fail to find the gene providing the clinic value of distinguishing the stage of dementia. Because more ferroptosis-related genes have been finding and more hippocampal region samples are needed.

There are several limitations to the current study. First, the datasets chosen and used for analysis—specifically the merged dataset GSE9770–did not provide specific dementia state information. Therefore, there may be limitations regarding AD patient selection and access to DEGs. In addition, because there are few microarrays in the hippocampus of AD patients and the hippocampus of people without AD, only the three datasets used in the present study were available for continuous verification. Finally, the overlapped genes verified in this

study need to be supported by future studies and verified by laboratory evidence.

Data availability statement

The datasets presented in this study can be found in online repositories. The names of the repositories and accession numbers can be found in the article/supplementary material.

Author contributions

All authors listed have made a substantial, direct, and intellectual contribution to the work, and approved it for publication.

Funding

This study was supported by the National Natural Science Foundation of China (31960178, 82160923, and 81960422); Applied Basic Research Programs of Science and Technology Commission Foundation of Yunnan Province (2019FA007); Key Laboratory of Traditional Chinese Medicine for Prevention and Treatment of Neuropsychiatric Diseases, Yunnan Provincial Department of Education; Scientific Research Projects for High-level Talents of Yunnan University of Chinese Medicine (2019YZG01); Young Top-Notch Talent in 10,000 Talent Program of Yunnan Province (YNWR-QNBJ-2019-235); National Science and Technology Innovation 2030 Major Program (2021ZD0200900); Yunnan Key Research and Development Program (202103AC100005); and Yunnan Province Fabao Gao Expert Workstation Construction Project (202105AF150037).

Conflict of interest

The authors declare that the research was conducted in the absence of any commercial or financial relationships that could be construed as a potential conflict of interest.

Publisher's note

References

Akahane, K., Kimura, S., Miyake, K., Watanabe, A., Kagami, K., Yoshimura, K., et al. (2022). 'Association of allele-specific methylation of the ASNS gene with asparaginase sensitivity and prognosis in T-ALL'. *Blood Adv.* 6, 212–224. doi: 10.1182/bloodadvances.2021004271

Andreone, B. J., Larhammar, M., and Lewcock, J. W. (2020). 'Cell death and neurodegeneration'. *Cold Spring Harb. Perspect. Biol.* 12:a036434. doi: 10.1101/cshperspect.a036434

Arvanitakis, Z., Shah, R. C., and Bennett, D. A. (2019). 'Diagnosis and management of dementia: Review'. *Jama* 322, 1589–1599. doi: 10.1001/jama.2019.4782

Ashraf, A., and So, P. W. (2020). 'Spotlight on ferroptosis: Iron-dependent cell death in Alzheimer's disease'. *Front. Aging Neurosci.* 12:196. doi: 10.3389/fnagi.2020.00196

Ayton, S., Portbury, S., Kalinowski, P., Agarwal, P., Diouf, I., Schneider, J. A., et al. (2021). 'Regional brain iron associated with deterioration in Alzheimer's disease: A large cohort study and theoretical significance'. *Alzheimers Dement.* 17, 1244–1256. doi: 10.1002/alz.12282

Bao, W. D., Pang, P., Zhou, X. T., Hu, F., Xiong, W., Chen, K., et al. (2021). 'Loss of ferroportin induces memory impairment by promoting ferroptosis in Alzheimer's disease'. *Cell Death Differ.* 28, 1548–1562. doi: 10.1038/s41418-020-00685-9

Blalock, E. M., Buechel, H. M., Popovic, J., Geddes, J. W., and Landfield, P. W. (2011). 'Microarray analyses of laser-captured hippocampus reveal distinct gray and white matter signatures associated with incipient Alzheimer's disease'. *J. Chem. Neuroanat.* 42, 118–126. doi: 10.1016/j.jchemneu.2011.06.007

Chen, K., Jiang, X., Wu, M., Cao, X., Bao, W., and Zhu, L. Q. (2021). 'Ferroptosis, a potential therapeutic target in Alzheimer's disease'. *Front. Cell Dev. Biol.* 9:704298. doi: 10.3389/fcell.2021.704298

Chen, S., Yan, W., Lang, W., Yu, J., Xu, L., Xu, X., et al. (2017). 'SESN2 correlates with advantageous prognosis in hepatocellular carcinoma'. *Diagn. Pathol.* 12:13. doi: 10.1186/s13000-016-0591-2

Cunningham, E. L., McGuinness, B., Herron, B., and Passmore, A. P. (2015). 'Dementia'. *Ulster Med. J.* 84, 79–87.

Dixon, S. J., Lemberg, K. M., Lamprecht, M. R., Skouta, R., Zaitsev, E. M., Gleason, C. E., et al. (2012). 'Ferroptosis: An iron-dependent form of nonapoptotic cell death'. *Cell* 149, 1060–1072. doi: 10.1016/j.cell.2012.03.042

Du, F., Chen, J., Liu, H., Cai, Y., Cao, T., Han, W., et al. (2019). 'SOX12 promotes colorectal cancer cell proliferation and metastasis by regulating asparagine synthesis'. *Cell Death Dis.* 10:239. doi: 10.1038/s41419-019-1481-9

Fu, Y., Ding, L., Yang, X., Ding, Z., Huang, X., Zhang, L., et al. (2021). 'Asparagine synthetase-mediated l-Asparagine metabolism disorder promotes the perineural invasion of oral squamous cell carcinoma'. *Front. Oncol.* 11:637226. doi: 10.3389/fonc.2021.637226

Hao, L., Mi, J., Song, L., Guo, Y., Li, Y., Yin, Y., et al. (2021). 'SLC40A1 mediates ferroptosis and cognitive dysfunction in type 1 diabetes'. *Neuroscience* 463, 216–226. doi: 10.1016/j.neuroscience.2021.03.009

Jarrard, L. E. (1995). 'What does the hippocampus really do?'. *Behav. Brain Res.* 71, 1–10. doi: 10.1016/0166-4328(95)00034-8

Jia, L., Quan, M., Fu, Y., Zhao, T., Li, Y., Wei, C., et al. (2020). 'Dementia in China: Epidemiology, clinical management, and research advances'. *Lancet Neurol* 19, 81–92. doi: 10.1016/S1474-4422(19)30290-X

Knierim, J. J. (2015). 'The hippocampus'. *Curr. Biol.* 25, R1116–R1121. doi: 10.1016/j.cub.2015.10.049

Leek, J. T., Johnson, W. E., Parker, H. S., Jaffe, A. E., and Storey, J. D. (2012). 'The sva package for removing batch effects and other unwanted variation

in high-throughput experiments'. *Bioinformatics* 28, 882–883. doi: 10.1093/bioinformatics/bts034

Li, L. B., Chai, R., Zhang, S., Xu, S. F., Zhang, Y. H., Li, H. L., et al. (2019). 'Iron exposure and the cellular mechanisms linked to neuron degeneration in adult mice'. *Cells* 8:198. doi: 10.3390/cells8020198

Li, L., Li, W. J., Zheng, X. R., Liu, Q. L., Du, Q., Lai, Y. J., et al. (2022). 'Eriodictyol ameliorates cognitive dysfunction in APP/PS1 mice by inhibiting ferroptosis via vitamin D receptor-mediated Nrf2 activation'. *Mol. Med.* 28:11. doi: 10.1186/s10020-022-00442-3

Liang, W. S., Dunckley, T., Beach, T. G., Grover, A., Mastroeni, D., Walker, D. G., et al. (2007). 'Gene expression profiles in anatomically and functionally distinct regions of the normal aged human brain'. *Physiol. Genomics* 28, 311–322. doi: 10.1152/physiolgenomics.00208.2006

Lorenzi, P. L., Reinhold, W. C., Rudelius, M., Gunsior, M., Shankavaram, U., Bussey, K. J., et al. (2006). 'Asparagine synthetase as a causal, predictive biomarker for L-asparaginase activity in ovarian cancer cells'. *Mol. Cancer Ther.* 5, 2613–2623. doi: 10.1158/1535-7163.MCT-06-0447

McDonald, A. J., and Mott, D. D. (2017). 'Functional neuroanatomy of amygdalohippocampal interconnections and their role in learning and memory'. *J. Neurosci. Res.* 95, 797–820. doi: 10.1002/jnr.23709

McKhann, G. M., Knopman, D. S., Chertkow, H., Hyman, B. T., Jack, C. R. Jr., Kawas, C. H., et al. (2011). 'The diagnosis of dementia due to Alzheimer's disease: Recommendations from the national institute on Aging-Alzheimer's association workgroups on diagnostic guidelines for Alzheimer's disease'. *Alzheimers Dement.* 7, 263–269. doi: 10.1016/j.jalz.2011.03.005

Rai, N., Kumar, R., Desai, G. R., Venugopalan, G., Shekhar, S., Chatterjee, P., et al. (2016). 'Relative alterations in blood-based levels of sestrin in alzheimer's disease and mild cognitive impairment patients'. *J. Alzheimers Dis.* 54, 1147–1155. doi: 10.3233/JAD-160479

Readhead, B., Haure-Mirande, J. V., Funk, C. C., Richards, M. A., Shannon, P., Haroutunian, V., et al. (2018). 'Multiscale analysis of independent Alzheimer's cohorts finds disruption of molecular, genetic, and clinical networks by human herpesvirus'. *Neuron* 99, 64.e–82.e. doi: 10.1016/j.neuron.2018.05.023

Ritchie, M. E., Phipson, B., Wu, D., Hu, Y., Law, C. W., Shi, W., et al. (2015). 'limma powers differential expression analyses for RNA-sequencing and microarray studies'. *Nucleic Acids Res.* 43:e47. doi: 10.1093/nar/gkv007

Scheltens, P., De Strooper, B., Kivipelto, M., Holstege, H., Chételat, G., Teunissen, C. E., et al. (2021). 'Alzheimer's disease'. *Lancet* 397, 1577–1590. doi: 10.1016/S0140-6736(20)32205-4

Shannon, P., Markiel, A., Ozier, O., Baliga, N. S., Wang, J. T., Ramage, D., et al. (2003). 'Cytoscape: A software environment for integrated models of biomolecular interaction networks'. *Genome Res.* 13, 2498–2504. doi: 10.1101/gr.1239303

Shaw, L. M., Korecka, M., Clark, C. M., Lee, V. M., and Trojanowski, J. Q. (2007). 'Biomarkers of neurodegeneration for diagnosis and monitoring therapeutics'. *Nat. Rev. Drug Discov.* 6, 295–303. doi: 10.1038/nrd2176

Shen, Y., Li, M., Xiong, Y., Gui, S., Bai, J., Zhang, Y., et al. (2021). 'Proteomics analysis identified ASNS as a novel biomarker for predicting recurrence of skull base chordoma'. *Front. Oncol.* 11:698497. doi: 10.3389/fonc.2021.698497

Small, S. A., Perera, G. M., DeLaPaz, R., Mayeux, R., and Stern, Y. (1999). 'Differential regional dysfunction of the hippocampal formation among elderly with memory decline and Alzheimer's disease'. *Ann. Neurol.* 45, 466–472. doi: 10.1002/1531-8249(199904)45:4<466::AID-ANA8>3.0.CO;2-Q

Wang, L. X., Zhu, X. M., and Yao, Y. M. (2019). 'Sestrin2: Its potential role and regulatory mechanism in host immune response in diseases'. *Front. Immunol.* 10:2797. doi: 10.3389/fimmu.2019.02797

Weng, W., Liu, N., Toiyama, Y., Kusunoki, M., Nagasaka, T., Fujiwara, T., et al. (2018). 'Novel evidence for a PIWI-interacting RNA (piRNA) as an oncogenic mediator of disease progression, and a potential prognostic biomarker in colorectal cancer'. *Mol. Cancer* 17:16. doi: 10.1186/s12943-018-0767-3

Wyss-Coray, T. (2016). 'Ageing, neurodegeneration and brain rejuvenation'. *Nature* 539, 180–186. doi: 10.1038/nature20411

Yuan, H., Pratte, J., and Giardina, C. (2021). 'Ferroptosis and its potential as a therapeutic target'. *Biochem. Pharmacol.* 186:114486. doi: 10.1016/j.bcp.2021.114486

Zhang, G., Zhang, Y., Shen, Y., Wang, Y., Zhao, M., and Sun, L. (2021). 'The potential role of ferroptosis in Alzheimer's disease'. *J. Alzheimers Dis.* 80, 907–925. doi: 10.3233/JAD-201369

Zhou, N., and Bao, J. (2020). 'FerrDb: A manually curated resource for regulators and markers of ferroptosis and ferroptosis-disease associations. *Database (Oxford)* 2020:baaa021. doi: 10.1093/database/baaa021

frontiers | Frontiers in Cellular Neuroscience

TYPE Review
PUBLISHED 13 December 2022
DOI 10.3389/fncel.2022.1025708

OPEN ACCESS

EDITED BY
Anwen Shao,
Zhejiang University, China

REVIEWED BY
Amit Kumar,
Burke Neurological Institute (BNI), United States
Zhaohui He,
First Affiliated Hospital of Chongqing Medical University, China

*CORRESPONDENCE
Yuhai Wang
wangyuhai1516@163.com
Kun Xiong
xiongkun2001@163.com

†These authors have contributed equally to this work

SPECIALTY SECTION
This article was submitted to Cellular Neuropathology, a section of the journal Frontiers in Cellular Neuroscience

RECEIVED 30 August 2022
ACCEPTED 08 November 2022
PUBLISHED 13 December 2022

CITATION
Chen J, Li M, Liu Z, Wang Y and Xiong K (2022) Molecular mechanisms of neuronal death in brain injury after subarachnoid hemorrhage.
Front. Cell. Neurosci. 16:1025708.
doi: 10.3389/fncel.2022.1025708

Molecular mechanisms of neuronal death in brain injury after subarachnoid hemorrhage

Junhui Chen[1,2,3†], Mingchang Li[2†], Zhuanghua Liu[3], Yuhai Wang[3*] and Kun Xiong[1*]

[1]Department of Human Anatomy and Neurobiology, School of Basic Medical Science, Central South University, Changsha, Hunan, China, [2]Department of Neurosurgery, Renmin Hospital of Wuhan University, Wuhan, China, [3]Department of Neurosurgery, 904th Hospital of Joint Logistic Support Force of PLA, Wuxi Clinical College of Anhui Medical University, Wuxi, China

Subarachnoid haemorrhage (SAH) is a common cerebrovascular disease with high disability and mortality rates worldwide. The pathophysiological mechanisms involved in an aneurysm rupture in SAH are complex and can be divided into early brain injury and delayed brain injury. The initial mechanical insult results in brain tissue and vascular disruption with hemorrhages and neuronal necrosis. Following this, the secondary injury results in diffused cerebral damage in the peri-core area. However, the molecular mechanisms of neuronal death following an aneurysmal SAH are complex and currently unclear. Furthermore, multiple cell death pathways are stimulated during the pathogenesis of brain damage. Notably, particular attention should be devoted to necrosis, apoptosis, autophagy, necroptosis, pyroptosis and ferroptosis. Thus, this review discussed the mechanism of neuronal death and its influence on brain injury after SAH.

KEYWORDS

cell death, SAH, necrosis, apoptosis, ferroptosis, autophagy, pyroptosis

Introduction

Subarachnoid haemorrhage (SAH) is a common cerebrovascular disease, accounting for approximately 5% of all strokes. According to the latest report by the European Stroke Association, the incidence of SAH is reported to be more than 9/100,000 (Feigin et al., 2009; GBD 2019 Stroke Collaborators, 2021). The incidences of SAH in Asia and Iceland rank the highest, with Japan accounting for approximately 22.7/100,000 cases. Moreover, more than 85% of all SAH cases are caused by intracranial aneurysms, leading to high mortality and disability rates (Steiner et al., 2013). A meta-analysis reported that the short-term mortality of SAH is as high as 8.3–66.7%, the mean median of direct death before admission was 8.3% and the overall favorable prognosis rate was 36–55% (Nieuwkamp et al., 2009). The majority of SAH survivors usually have

long-term cognitive dysfunction, affective disorders, loss of hearing and smell and decreased quality of life after surgery (Rinkel and Algra, 2011). Additionally, >60% of SAH survivors have memory problems, >75% have language problems (Al-Khindi et al., 2010) and almost 95% of patients with SAH have at least one cognitive or affective disorder (Passier et al., 2010). The treatment for patients with SAH is lengthy and expensive, which places a serious burden on the national economy. Since the beginning of the 21st century, the average hospitalization cost of each patient with a SAH aneurysm in the first year in the United States exceeded $65,000 (Qureshi et al., 2007) while those in the United Kingdom paid £510 million a year (Rivero-Arias et al., 2010).

The pathophysiological processes and mechanisms involved in aneurysm rupture in SAH are complex. Nonetheless, a previous study divided the pathological process into two stages: early brain injury (EBI) and delayed brain injury (DBI) (Chen S. et al., 2014). Additionally, various animal and cell experimental studies on SAH report that a large number of red blood cells enter the subarachnoid space, brain parenchyma or ventricle and their subsequent rapid lysis produce a large amount of hemoglobin and corresponding decomposition products (Macdonald, 2014; Lawton and Vates, 2017). These factors exert various neurotoxic effects and can subsequently induce secondary brain injury after SAH (Bulters et al., 2018; Chen et al., 2019c, 2021). Therefore, EBI is considered the most important cause of acute brain damage and neurological dysfunction in patients with SAH. Currently, it is gaining increasing attention as a research hotspot. Neuronal death is considered a major cause of EBI (Macdonald and Schweizer, 2017). Hence, a reduction in the number of neuronal deaths could improve nerve dysfunction and eventually improve the prognosis of patients (Dong et al., 2016; Ding et al., 2022). Thus, further study on the mechanism of EBI and neuronal death is vitally important. In the present review, we discuss the mechanism of neuronal death after SAH and its influence on brain injury (**Table 1**).

Neuronal necrosis

Neuronal necrosis is the death of neurons induced by extreme, chemical or severe pathological factors and is a passive pathological process that does not consume energy (Kroemer et al., 2009). The morphology of necrotic neurons exhibits increased neuronal membrane permeability, neuronal organelle oedema and deformation, nuclear changes, DNA dissolution, intracellular calcium overload, sodium ion influx, potassium ion outflow, plasma concentration changes (Friedrich et al., 2012). Furthermore, degraded lysosomes release various cellular autolysins that eventually destroy the plasma membrane and cause cell death (Kroemer et al., 2009). This pathological process is also an acute passive neuronal death process that is observed after SAH. The specific mechanism and molecular process of neuronal necrosis after SAH are scarce, to the best of our knowledge, as it is a passive, unregulated and irreversible pathological process (Zhu et al., 2012). Friedrich et al. (2012) reported that the activation of endothelial and parenchymal cell apoptosis and neuronal necrosis occurred within 10 min after SAH and is associated with poor outcomes. Thus, the prevention of apoptosis and necrosis could potentially improve impaired functions of the circumventricular organs after SAH (Edebali et al., 2014). However, neuronal necrosis is the most common form of neuronal death in EBI after SAH and is also the main cause of early death, coma and severe neurological dysfunction in patients after SAH (Friedrich et al., 2012). Although neuronal necrosis is a passive and unregulated process, early clinical intervention against its inducing factors can significantly reduce its occurrence (Zhu et al., 2012). Therefore, identifying and inhibiting the inducers of neuronal necrosis is key to regulating this process, which could also be a new research direction for neuronal necrosis after SAH. Additionally, **Figure 1** briefly summarizes the clinical causes of neuronal necrosis after SAH.

Intracranial hypertension

SAH can lead to extensive hemorrhage, including intraventricular hematoma and intracerebral hematoma, and the mass effect directly leads to increased intracranial pressure (ICP) (Macdonald and Schweizer, 2017). Heuer et al. (2004) reported that intracranial hypertension (>20 mmHg) occurs in more than 50% of patients with SAH, with rates as high as 60–70% in poor-grade SAH. Similarly, Zoerle et al. (2015) reported that >80% of patients with SAH had at least one episode of intracranial hypertension following SAH and 36% had an average ICP of >20 mmHg during hospitalization. Increased ICP and complications, such as cerebral ischemia and brain oedema, can directly induce neuronal necrosis, affecting the final prognosis of patients (Said et al., 2021; Narotam et al., 2022). Although the relationship between ICP and prognosis remains unclear, the definite presence of intracranial hypertension after SAH increases the mortality rates and leads to poor outcomes. Moreover, intracranial hypertension and its etiology (hydrocephalus, cerebral oedema, intracerebral hematoma and intraventricular hematoma.) can be used as an independent predictor of poor patient outcome (Claassen et al., 2002; Heuer et al., 2004; Zoerle et al., 2015; Wan et al., 2016).

Currently, there are no recommended guidelines for the treatment of intracranial hypertension after SAH (Svedung Wettervik et al., 2022). From our experience, early-time intraventricular ICP monitoring is a very important therapeutic strategy to relieve ICP in patients with SAH. It is also essential to monitor ICP and cerebral perfusion pressure to avoid severe cerebral ischemia, which can be avoided by maintaining appropriate perfusion pressure regardless of

TABLE 1 Neuronal death pathways and associated morphological and biochemical hallmark features.

Neuronal death	Morphological features and key biochemical pathway components	References
Neuronal necrosis	Plasma membrane rupture, swelling of neuronal organelle, deformation, nucleus changes, DNA dissolution, intracellular calcium overload, sodium ion influx, potassium ion outflow plasma concentration changes, and overspending membrane aquaporin, lack of inter-nucleosomal DNA fragmentation, depletion of ATP, involvement of calpains and cathepsins, release of DAMPs (and in infected cells also PAMPs)	Kroemer et al., 2009; Friedrich et al., 2012
Neuronal apoptosis	Nuclear fragmentation, plasma membrane blebbing, cell shrinkage (pyknosis), formation of apoptotic bodies and phagocytosis by neighboring cells. Pro-apoptotic BCL-2 family members, P53 and caspase activation, cleavage of hundreds of caspase substrates (ICAD, PARP), PS exposure, $\Delta\Psi$m dissipation, MOMP and ROS production	Chen J. H. et al., 2016; Chen et al., 2018b; Chen et al., 2019c
Neuronal pyroptosis	Rupture of the plasma membrane and lack of cell swelling. Inflammatory induced activation of the initiator caspases, caspase-1, -4, -5 and -11, and consequent activation of the effector caspases, caspase-3 and -1. Release of bio-active IL-1β and IL-18 and proteolytic activation of GSDMD	Bergsbaken et al., 2009; Aglietti et al., 2016; Liu et al., 2016; Vande Walle and Lamkanfi, 2016
Neuronal autophagy	Accumulation of autophagic vacuoles, autophagosome, vacuolisation of the cytoplasm, no chromatin condensation. Atg family of gene encoded proteins, LC3-I to LC3-II conversion and cleavage of p62	Ho et al., 2018
Neuronal necroptosis	Cytoplasmic swelling, loss of plasma membrane integrity, swelling of cytoplasmic organelles. RIPK1, RIPK3, MLKL, phosphorylation and ubiquitination of RIPK1, formation of the necrosome complex in the cytosol, phosphorylation and activation of MLKL, the effector of caspases, ROS production and release of DAMPs	Holler et al., 2000; He et al., 2009; Galluzzi et al., 2017
Neuronal ferroptosis	Smaller mitochondria with decreased cristae, disappearance of mitochondrial cristae, thickening of the lipid bilayer membrane, metabolic dysfunction of iron ions, depletion of glutathione (GSH), accumulation of iron-dependent lipid overreactive oxygen species (ROS), inhibited activity, or decreased levels of glutathione peroxidase 4 (GPX4)	Dixon et al., 2012; Zille et al., 2017; Chen et al., 2020c

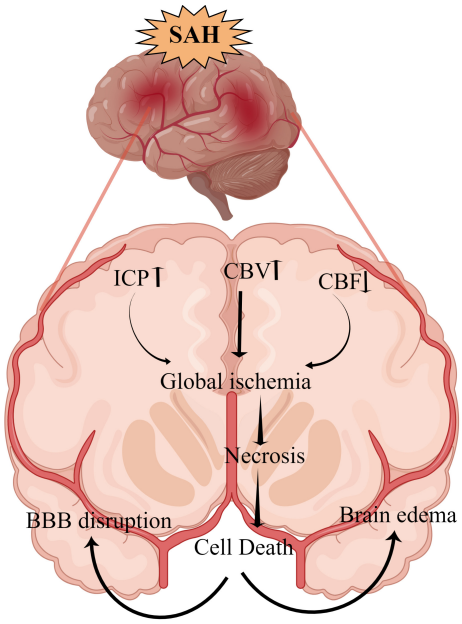

FIGURE 1
The overall scheme of neuronal necrosis from subarachnoid hemorrhage to early brain injury (EBI).

vasospasm (Chen et al., 2018a). Additionally, intraventricular ICP monitoring can aid in properly draining cerebrospinal fluid, reducing ICP, improving obstructive hydrocephalus, draining blood-cerebrospinal fluid to improve vasospasm and reducing toxic brain injury (He et al., 2015; Chen J. et al., 2016). However, not all patients with SAH require ventricular ICP monitoring but it can be considered for poor-grade patients with SAH as the invasive procedure could increase the risk of additional injury and intracranial infection (Chen et al., 2018a). Olson et al. (2013) reported that continuous cerebrospinal fluid drainage and intermittent ICP monitoring increased the incidence of intracranial infection, cerebrospinal fluid leakage and bleeding (clinicaltrials.gov identifier NCT01169454) in a randomized controlled study of 60 patients. Hence, it is necessary to adopt individualized precision therapy to control intracranial hypertension, thereby reducing neuronal necrosis and ameliorating EBI.

Cerebral ischemia

Cerebral ischemia is a common complication after SAH, with >30% of patients experiencing delayed cerebral ischemia (Stienen et al., 2014). Decreased cerebral hypoperfusion leads to cerebral ischemia and cerebral infarction, ultimately inducing severe neurological dysfunction, brain injury and even death (Güresir et al., 2022; Hostettler et al., 2022). Cerebral ischemia is caused by various factors, including cerebral vasospasm, micro thrombosis, blood-brain barrier destruction, inflammatory reactions and cerebral vascular self-regulation dysfunction (Macdonald, 2014). After SAH, a large amount of hemoglobin

enters the subarachnoid space to directly stimulate intracranial blood vessels, thereby activating calcium channels in vascular smooth muscle cells and resulting in smooth muscle contraction and vascular spasm (Pluta, 2005). Endothelin-1 (ET-1) is produced in large quantities by astrocytes and white blood cells during inflammation or cerebral ischemia and has a strong vasoconstriction function (Chen et al., 2018b; Croci et al., 2019). Previous studies have demonstrated that many molecular signaling pathways, such as p38/MAPK (Huang et al., 2017), RhoA (González-Montelongo et al., 2018) and Nrf2-ARE (Zhang et al., 2010; Zhao et al., 2016), are involved in the development of cerebrovascular spasms (CVS) after SAH. Therefore, early diagnosis and treatment of CVS and cerebral ischemia could improve the prognosis of patients. Regrettably, a large number of drugs are effective in basic research but ineffective in clinical trials. For example, clazosentan has been considered for the targeted treatment of CVS; however, a Phase 3 clinical trial found that while it improved CVS, it did not improve the long-term outcomes for patients with SAH (Macdonald et al., 2011). Previous studies report that statins can protect against CVS and EBI after SAH (Chen J. H. et al., 2016; Chen et al., 2018b, 2020a, 2021); however, another study indicates that statins together with nimodipine can reduce CVS and cerebral infarction but have no benefits on 6 months of clinical outcome or 30-day all-cause mortality (Chen et al., 2020b). Additionally, magnesium is gaining widespread attention; however, it has also proven to be ineffective in Phase 2 randomized controlled trials (Mees et al., 2012). Recent clinical studies on cilostazol have demonstrated that it can significantly reduce the incidence of cerebral infarction, delay ischemia after SAH (Sugimoto et al., 2018), reduce the occurrence of secondary stroke and improve the prognosis of patients (Shinohara et al., 2010; Toyoda et al., 2019). However, its effect on ameliorating CVS and micro thrombosis after SAH and improving prognosis require further study using a large sample, multicentre, randomized controlled trial. Additionally, the relationship between CVS and neuronal necrosis after SAH remains unclear and requires further exploration.

Brain oedema

Brain oedema after SAH can be divided into three types: vasogenic cerebral oedema, cytotoxic cerebral oedema, and mixed cerebral oedema (Nag et al., 2009). Vasogenic cerebral oedema is the most common type of brain oedema in the clinical setting, whereas cytotoxic cerebral oedema is caused by increased permeability due to cell membrane disruption and swelling (Kaufmann and Cardoso, 1992). Notably, after SAH, different types of cerebral oedema mainly occur at different periods and stages (Nag et al., 2009). The expression of matrix metalloproteinase-9 is increased after SAH, which leads to the destruction of tight junction proteins between the vascular endothelium and subsequently results in the increased permeability of the blood-brain barrier and aggravated brain oedema (Lee et al., 2007; Sun X. G. et al., 2019). The activation of aquaporin-4 (AQP4) is also an important mechanism affecting brain oedema, wherein water molecules enter brain tissues in large quantities through the activated AQP4 and then aggravate brain oedema and neuronal necrosis in cytotoxic cerebral oedema (Huang et al., 2014; Chen J. H. et al., 2016). In vasogenic cerebral oedema, AQP4 plays an important role in improving oedema, which was confirmed by the significantly reduced rate of resolution of cerebral oedema in AQP4 knockout cells (Papadopoulos et al., 2004; Tourdias et al., 2011). Progressive cerebral oedema leads to increased ICP and malignant intracranial hypertension and subsequently to cerebral ischemia and neuronal necrosis (Bjerring et al., 2011; Halstead and Geocadin, 2019). Therefore, the early management of cerebral oedema after SAH is vitally important in improving the prognosis of patients with SAH, especially those with poor-grade aneurysmal SAH. Powell et al. (1976) also reported that the extent of swelling was significantly decreased with a dehydrating agent (mannitol) treatment and osmolality elevation decreased the extent of eventual myocardial necrosis. Additionally, dehydrating agents also improve brain tissue oxygenation by limiting astrocyte swelling and restoring capillary perfusion, thereby alleviating early brain injury (Halstead and Geocadin, 2019). Hence, exploring the treatment of neuronal necrosis with dehydrating drugs and AQP4-based targeted drugs has therapeutic potential.

Neuronal apoptosis

The mechanical compression of hematoma, toxic damage of hemoglobin and oxidative stress lead to the extensive apoptosis of cortical neurons and hippocampal neurons after SAH (Chen J. H. et al., 2016; Chen et al., 2018b, 2019c). The complex process of neuronal apoptosis involves exogenous death receptor pathways, P53-mediated apoptosis pathways, caspase-dependent and -non-dependent pathways and endogenous mitochondrial pathways (Gao et al., 2000; Sendoel et al., 2010). The BcL-2 gene family promotes the release of cytochrome C from the mitochondrial membrane and its binding with apoptosis protease activating factor 1 (Apaf-1) to regulate mitochondrial membrane permeability (Hasegawa et al., 2011; Jaafaru et al., 2019). The c/Apaf-1 complex further regulates the activation of the apoptosis factor Caspase-3 and induces neuronal apoptosis (Hasegawa et al., 2011). Recent study report that a novel membrane-bound bile acid receptor (TGR5) is involved in the process of oxidative stress and apoptosis, wherein TGR5 and its agonists inhibit neuronal apoptosis and improve neural function via the cAMP/PKCε/ALDH2 pathway in a rat SAH model (Zuo et al., 2019). Furthermore, protein-coupled receptor 30

(GPR30) and its agonist G1 are also involved in neuronal apoptosis after SAH, which can inhibit neuronal apoptosis through the src/EGFR/STAT3 signaling pathway (Peng et al., 2019). A previous study showed that statins can alleviate neuronal apoptosis and EBI by inhibiting caspase-3 after SAH (Chen J. H. et al., 2016). Additionally, Netrin-1 can activate PPARγ and Bcl-2 expressions, inhibit the proapoptotic factors Bax and NF-κB and ameliorate EBI after SAH (Chen et al., 2019c). Similarly, Gao et al. also reported that the early overexpression of PDK4 after SAH has the potential to attenuate neuronal apoptosis by reducing oxidative stress via the ROS/ASK1/P38 pathway (Gao X. et al., 2022). A recent study also demonstrated that early fluoxetine administration can protect against apoptosis by regulating the Notch1/ASK1/p38 MAPK signaling pathway, thereby ameliorating EBI after SAH (Liu M. et al., 2022). Neuronal apoptosis caused by SAH is widely and thoroughly studied, involving many signaling pathways and molecular mechanisms. Future studies need to assess and identify specific molecular mechanisms that can be regulated in the induction of apoptosis, thereby contributing to the development of clinically viable treatment options (**Figure 2**).

Neuronal pyroptosis

Pyroptosis, a newly reported cell death mechanism, is a form of programmed neuronal cell death initiated by Caspase-1 and an important cause of neurological damage (Bergsbaken et al., 2009). Pyroptosis, which was first proposed in 2001, differs from apoptosis with respect to its mechanism, which is associated with inflammation (Aglietti et al., 2016; Liu et al., 2016; Vande Walle and Lamkanfi, 2016). Pyroptosis is a programmed cell death mediated by GSDMD (gasdermin protein family, including Gasdermin A, Gasdermin B, Gasdermin C, DFNA5 and DFNB59), with the inflammasome playing an important role in the pyroptosis process (Kayagaki et al., 2015). Gasdermin, an important element of cell pyrosis, is also widely distributed in the central nervous system (Bergsbaken et al., 2009). Hence, neuronal pyrosis plays an important role in the development of central nervous system-related diseases and is an important mechanism of brain injury (Ito et al., 2015; Van Rossom et al., 2015; An et al., 2019; Kuwar et al., 2019; She et al., 2019; Sun Y. B. et al., 2019). In the classic Caspase-1-induced cell pyroptosis process, inflammasomes (NLRP1, NLRP3, NLRC4 and AIM2) sense the danger signal and induce the connector molecule ASC to activate Caspase-1, thus cleaving GSDMD (Swanson et al., 2019; Chen et al., 2022). Subsequently, cellular pores are formed on the cell membrane, which results in water and ion influx and ultimately cell swelling and death (Shi et al., 2015; Broz and Dixit, 2016). Non-classical pathway-induced cell pyroptosis is activated by the oligomerization of the non-classical inflammasome (in mice, a complex of Caspase-11 precursors and lipopolysaccharides), which binds the intracellular Caspase-11 precursors to lipopolysaccharides (Abu Khweek and Amer, 2020). Following this, GSDMD is cleaved by activation of the Caspase-4/5/11 pathway, which is independent of Caspase-1, to induce cell pyroptosis (Kayagaki et al., 2013; Diamond et al., 2015). Moreover, in animal ischemic stroke experiments, microglial TREM-1 induced the activation of spleen tyrosine kinase (SYK), which increased the level of the N-terminal fragment of GSDMD (Liang et al., 2020). Thereafter, pores were formed in the microglia to promote the release of intracellular inflammatory factors, leading to the pyroptosis of the microglia. Additionally, microglial TREM-1 receptors bind to SYK and induce neuroinflammatory damage after stroke (Xu et al., 2019). Kuwar et al. (2019) also reported that inflammasome inhibitors could significantly inhibit the pyroptosis of neurons and improve brain injury after traumatic brain injury. Additionally, statins have been reported to improve neurological outcomes and reduce neuronal death against neural pyroptosis and neuroinflammation in an animal SAH model (Chen et al., 2021). Gu et al. (2022) demonstrated that the activation of RKIP could attenuate neuronal pyroptosis and brain injury after ICH through the ASC/Caspase-1/GSDMD pathway. Similarly, the inhibition of the pyroptosis of astrocytes and microglia in the central nervous system can also indirectly inhibit the pyroptosis of neurons, thereby protecting neurons and alleviating brain injury (Chavez et al., 2021; Kerr et al., 2022). Collectively, these studies highlight the sophisticated interplay between pyroptosis-related molecules and inflammasome components that could be leveraged to prevent hyperinflammation after SAH (**Figure 3**). Thus, pyroptosis can be a new research direction in the exploration of the mechanism of SAH.

Neuronal autophagy

Autophagy is a cellular repair process that stabilizes the intracellular environment via the lysosomal degradation of selected cytoplasmic components and programmed death of old, dysfunctional or unnecessary cytoplasmic entities (Ho et al., 2018). Autophagy is tightly regulated and involves multiple molecular mechanisms; autophagy plays an important role after SAH (Chen J. et al., 2014; Li et al., 2017; Ho et al., 2018; Sun C. et al., 2019; Sun C. M. et al., 2019). The main morphological changes have been observed in the autophagosomes and autophagolysosomes under an electron microscope (Harris and Rubinsztein, 2012; Chen J. et al., 2014; Li et al., 2017; Ho et al., 2018; Sun C. et al., 2019; Sun C. M. et al., 2019). Lee et al. (2009) reported that neuronal autophagy was significantly activated in the early injury stage of SAH, and different modes of autophagy activation in different parts of SAH indicated different injury mechanisms. Wang et al. (2012) reported that a small amount of autophagy exists in normal brain

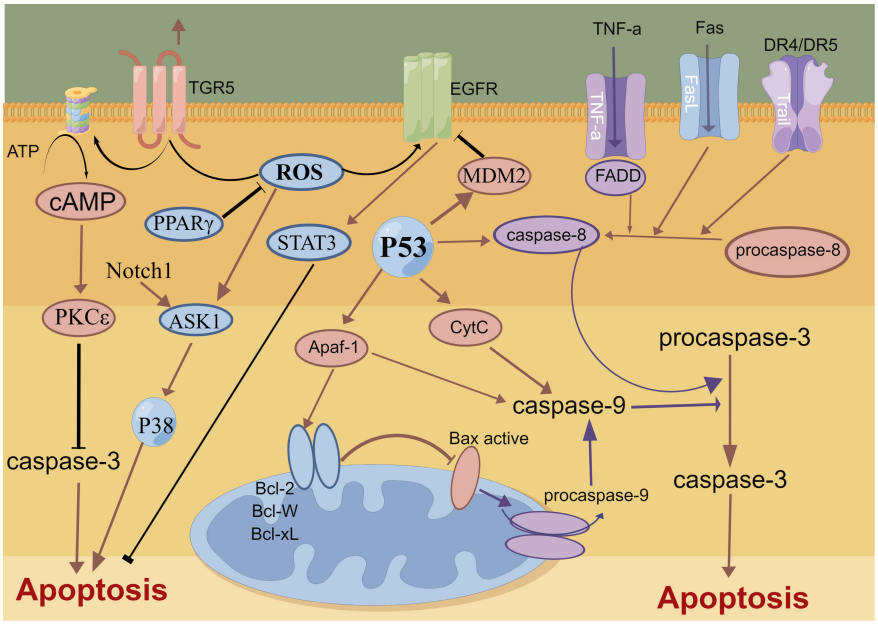

FIGURE 2
Molecular mechanisms of apoptosis from subarachnoid hemorrhage to early brain injury (EBI).

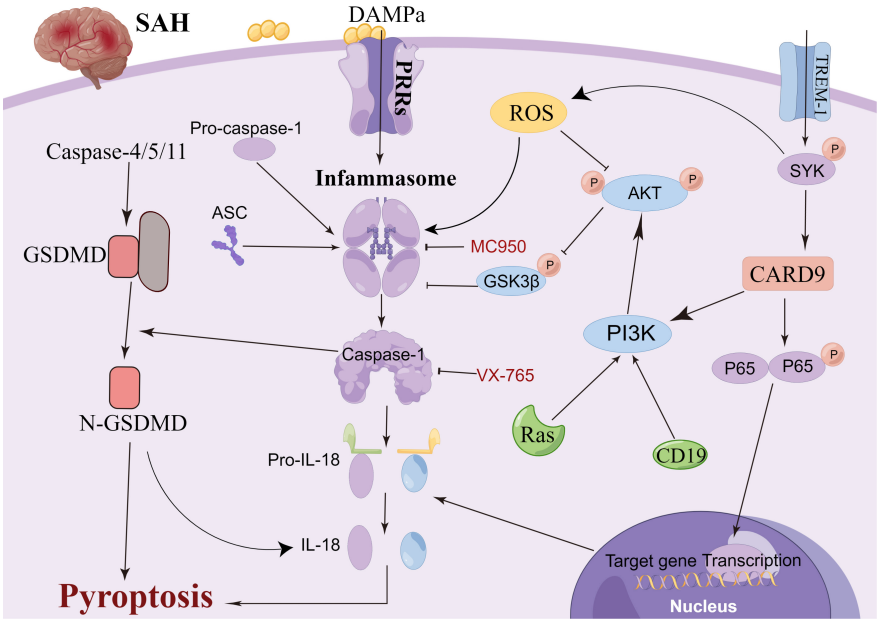

FIGURE 3
Molecular mechanisms of pyroptosis from subarachnoid hemorrhage to early brain injury (EBI).

neurons; however, it is activated in large quantities after SAH. Autophagy can improve cerebral oedema, protect the blood-brain barrier, reduce cortical neuronal apoptosis and improve clinical prognosis after intervention with rapamycin (RAP) and 3-methyladenine (3-MA) (Hu X. et al., 2022; Pang et al., 2022). Lu et al. reported that melatonin enhances autophagy in brain vessel endothelial cells, then protect blood-brain barrier integrity. In the animal CVS model after SAH, the autophagy pathway was activated in the basilar artery wall after SAH, and CysC-induced autophagy played a beneficial role in preventing SAH-induced CVS (Liu et al., 2013). Additionally, many autophagy-related drugs have achieved

good neuroprotective effects in basic research (Li et al., 2017; Chen et al., 2020a; Du et al., 2021; Chang et al., 2022). Sun C. et al. (2019) reported that osteopontin enhanced the autophagy response after SAH via the activation of the FAK-ERK signaling pathway, thereby improving long-term neurological function. Furthermore, Li and Han (2018) confirmed using *in vivo* and *in vitro* models that resveratrol increased the LC3-II/I ratio, AMPK phosphorylation and SIRT1 expression, thereby activating autophagy and reducing the release of inflammatory factors and neuronal apoptosis. Li et al. (2017) reported that fluoxetine significantly decreased the expression of NLRP3 and Caspase-1 and upregulated the expression of Beclin-1, which was reversed by the autophagy inhibitor 3-MA. Additionally, fluoxetine can enhance autophagy by inhibiting the activation of the NLRP3 inflammasome, thus playing a neuroprotective role, which could be attributed to the interaction between autophagy and pyroptosis (Li et al., 2017). Arachidonyl-2-chloroethylamide (ACEA), a highly selective CB1R agonist, was also reported to alleviate oxidative stress and neurological dysfunction by promoting mitophagy after SAH via the CB1R/Nrf1/PINK1 signaling pathway (Liu B. et al., 2022). Similarly, Zeng et al. (2021) demonstrated that the autophagy protein NRBF2 alleviated endoplasmic reticulum stress-associated neuroinflammation and oxidative stress by promoting autophagosome maturation, which occurs through interactions with Rab7 after SAH, and ultimately improving EBI. Hence, autophagy plays an important role in neuronal death, blood?brain barrier and CVS after SAH. Further studies focusing on elucidating the structural basis of the autophagy interaction for pyroptosis induction and developing autophagy-related drugs need to be explored in clinical trials (**Figure 4**).

Neuronal necroptosis

Necroptosis is a regulated form of cell death that relies heavily on receptor interactions of serine-threonine kinase 3 (RIPK3) and the mixed lineage kinase domain (MLKL) and usually presents with morphological characteristics of necrosis (Galluzzi et al., 2017). Unlike apoptosis, necroptosis is a caspase-independent mode of cell death. It is now known that serine/threonine kinases RIPK1, RIPK3 and MLKL are critical for necroptosis induced by the tumour necrosis factor (TNF) (Holler et al., 2000; He et al., 2009)superfamily, TLR3 or TLR4 and interferon receptors (Kaiser et al., 2013). TNF-α-induced necroptosis is the most characteristic signal transduction pathway. TNF-α homotrimer binds to TNF-1 to form a membrane signaling complex-1, which includes TRADD, RIPK1, TRAF2 and cIAP1/cIAP2, and subsequently activates NF-κB and MAP kinases (Chen and Goeddel, 2002). The polyubiquitination of RIPK1 by CIAP1/CIAP2 and LUBC is essential for the activation of the NF-κB signaling pathway (Gerlach et al., 2011). RIPK1 and RIPK3 in the necrosome are phosphorylated by their amino-terminal kinase domains, resulting in cell death through a signaling cascade (He et al., 2009). A previous review summarized that necroptosis is widely associated with various cardiovascular diseases, nerve regeneration diseases, kidney injury and other diseases (Galluzzi et al., 2017). Degterev et al. (2005) observed that necroptosis leads to delayed ischemic brain injury in mice through a mechanism that is different from apoptosis, thereby identifying a previously undescribed basic cell death pathway and providing a new therapeutic target for stroke. Chen et al. (2019a) reported that anti-TNF-α treatment can significantly improve endothelial cell necroptosis and blood-brain barrier damage and further improve nerve function after stroke. In a SAH experimental study, celastrol administration decreased the expression levels of necroptosis-related proteins RIPK3 and MLKL, which exhibited neuroprotective effects on EBI (Xu et al., 2021). Similarly, necrostatin-1, a small-molecule inhibitor of necroptosis, can potentially prevent SAH-induced necroptosis by suppressing the activity of the RIPK3/MLKL signaling pathway (Chen et al., 2019b). Therefore, the inhibition of necroptosis can significantly improve neural function, and its mechanism could be related to the phosphorylation of RIPK1 and RIPK3 (Shen et al., 2017; Yuan et al., 2019). Yang et al. (2018) reported that the specific and potent inhibitor of necroptosis Necrostatin-1 (Nec-1) mitigated SAH-induced synaptic impairments in the hippocampus by inhibiting necroptosis via the CREB-BDNF pathway. Additionally, Nec-1 has been reported to prevent CVS in animals models (Sahin et al., 2021). However, the clinical efficacy of drugs targeting the mechanism of necroptosis remains unclear owing to a lack of relevant clinical studies. Further studies on anti-necroptosis-related drugs that can be used in clinical settings against brain injury after SAH are essential. Additionally, clinical trials should be performed to evaluate the safety and clinical efficacy of anti-necroptosis-related drugs, such as Nec-1 (**Figure 5**).

Neuronal ferroptosis

Recently, a newly identified cell death mechanism called ferroptosis has been widely explored. It is a non-apoptotic form of iron-dependent programmed cell death and differs from traditional cell death processes, such as apoptosis and autophagy (Dixon et al., 2012; Chen et al., 2020c). Moreover, ferroptosis cannot be completely inhibited by necroptosis/apoptosis/autophagy-related inhibitors and intracellular calcium overload (Zille et al., 2017). The classical morphological characteristics of ferroptosis are the disappearance of the mitochondrial cristae, significantly narrowed mitochondria, thickening of the lipid bilayer membrane and reduced cell connections that lead to cell separation (Chen et al., 2020c). Furthermore, the

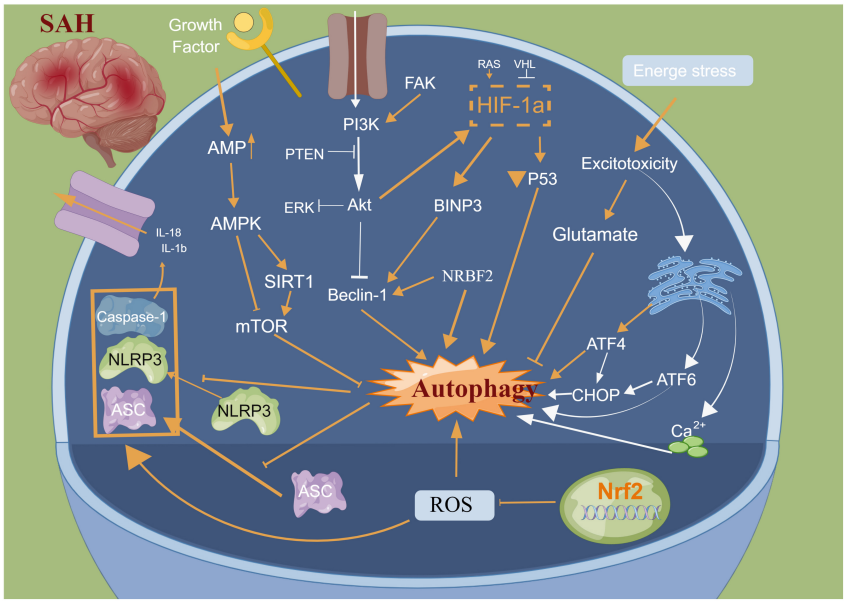

FIGURE 4
Molecular mechanisms of autophagy from subarachnoid hemorrhage to early brain injury (EBI).

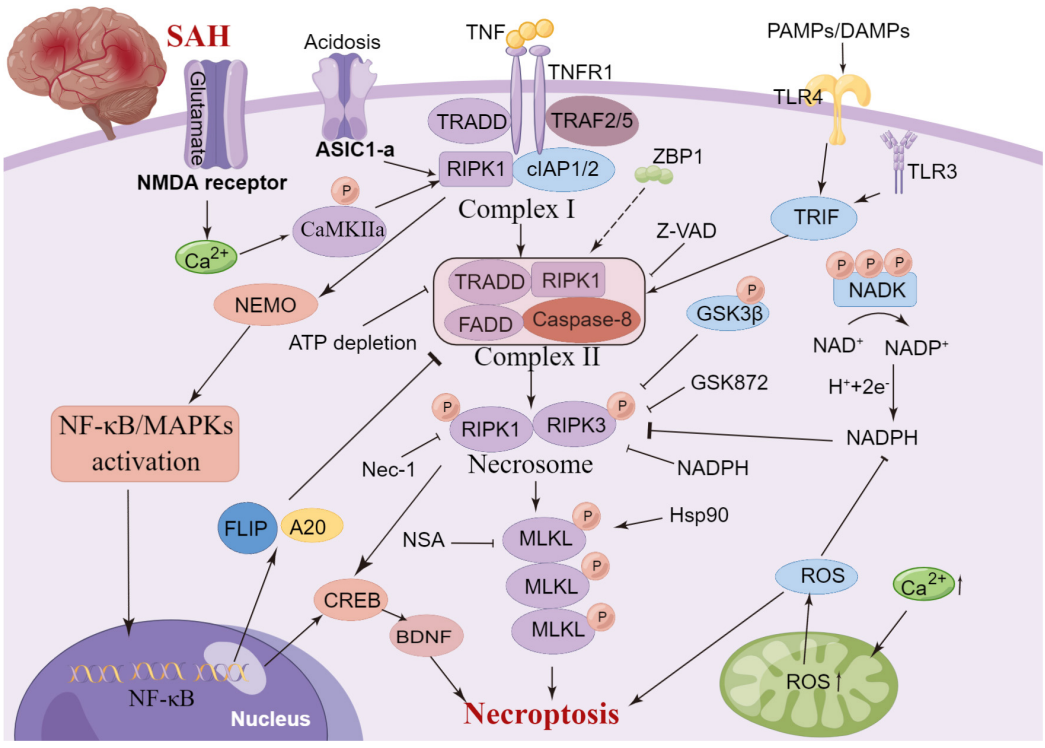

FIGURE 5
Molecular mechanisms of necroptosis from subarachnoid hemorrhage to early brain injury (EBI).

biological characteristics mainly include the metabolic dysfunction of iron ions, depletion of glutathione (GSH), accumulation of iron-dependent lipid reactive oxygen species (ROS) and decreased levels or inhibition of glutathione peroxidase 4 (GPX4) (Chen et al., 2020c). The mechanisms of ferroptosis are complex and involve various cell signaling

pathways (Chen et al., 2020c, 2021). Recent studies have also confirmed that ferroptosis is widely observed in diseases of the central nervous system, including cerebral ischemia/reperfusion (Tuo et al., 2022), SAH (Gao S. et al., 2022), ICH (Dharmalingam et al., 2020) and traumatic brain injury (Rui et al., 2021). The GPX4–GSH–cysteine system, FSP1–CoQ10–NAD (P)H system and GCH1-BH4-DHFR system are the primary anti-ferroptosis systems. A better understanding of three primary anti-ferroptosis systems aids in developing better therapeutic strategies for patients with brain injury after SAH (**Figure 6**).

GPX4–GSH–cysteine system

Ferroptosis was first reported to induce iron-dependent cell death via the small molecules erastin and 1S,3R-RSL3 (RSL3), a classical feature of ferroptosis is that it is independent of Caspase activation after erastin and RSL3 treatment (Dixon et al., 2012; Wang et al., 2016). Erastin targets the Xc- system (comprising SLC3A2 and SLC7A11), which transports cysteine into cells and glutamate out of cells, Cysteine is required for the synthesis of GSH, an important antioxidant that protects cells from oxidative damage (Dixon et al., 2012). Furthermore, erastin inhibits intracellular cysteine, leading to a significant decrease in intracellular GSH levels, ROS levels and oxidative damage (Dixon et al., 2012). GPX4 is the core of ferroptosis and requires GSH as a substrate for lipid repair (Yang et al., 2014). Reduced cysteine levels lead to the depletion of GSH levels and reduction of GPX4 levels and activity, resulting in the accumulation of unrepaired lipid peroxides and ferrous ions (Friedmann Angeli et al., 2014; Stockwell et al., 2017). GSH is a very important component of Fe^{2+} in unstable iron pools, it binds to Fe^{2+} to prevent lipid peroxidation, directly inhibiting GSH biosynthesis and triggering ferroptosis (Hider and Kong, 2011). Additionally, GPX4 can reduce the level of lipid hydrogen peroxide via GSH and convert it to ethanol or free hydrogen peroxide (Stockwell et al., 2017; Gaschler et al., 2018; Forcina and Dixon, 2019), which can be inhibited by RSL-3 (Dixon et al., 2012; Yang et al., 2014), and FINO2 (Gaschler et al., 2018). Conversely, selenium is a key regulator of GPX4 activity (Ingold et al., 2015, 2018; Friedmann Angeli and Conrad, 2018; Alim et al., 2019) and its supplementation after stroke can effectively inhibit ferroptosis and cell death after haemorrhagic or ischemic stroke (Alim et al., 2019).

FSP1–CoQ10–NAD(P)H

Recently, a novel apoptosis-inducing factor mitochondria-associated 2 (AIFM2) gene, also known as AIF homologous mitochondria-related death inducer, has been reported as an anti-ferroptosis gene (Bersuker et al., 2019; Doll et al., 2019). Doll et al. (2019) renamed AIFM2 as FSP1 (ferroptosis suppressor protein 1, FSP1). It has been reported to supplement the anti-iron death effect in the absence of GPX4 by using NAD(P)H to catalyze CoQ10 regeneration and then alleviate lipid peroxidation. Shimada et al. also confirmed that NADPH levels could be used as an important marker of the sensitivity of many cancers cell lines to ferroptosis (Shimada et al., 2016). The FSP1-CoQ10-NAD(P)H pathway is a parallel anti-ferroptosis system independent of the cystine-GSH-GPX4 system that inhibits lipid peroxidation and anti-ferroptosis effects, FSP1 has a dual regulatory role: inducing apoptosis and preventing ferroptosis (Wu et al., 2002; Bersuker et al., 2019; Dar et al., 2021; Tonnus et al., 2021). Furthemore, the C-terminal fragment of FSP1 located in the outer membrane of the mitochondria induced apoptosis while the two N-terminal fragments located in the nucleus cannot induce apoptosis (Wu et al., 2002). Kaku et al. (2015) reported that the translocation of endogenous FSP1 into the nucleus is a necessary step in the apoptosis mechanism. Additionally, FSP1 is an oxidoreductase of CoQ10 (CoQ10), and the nutmeg acylation of the N-terminal of FSP1 is a lipid modification that promotes FSP1 translocation to the plasma membrane, thereby mediating NADH-dependent CoQ reduction on the plasma membrane to inhibit CoQ10 activity (Wu et al., 2002; Bersuker et al., 2019; Dar et al., 2021; Drijvers et al., 2021; Song Z. et al., 2021; Tonnus et al., 2021). Notably, FSP1 still plays an anti-ferroptosis role even after GPX4 knockdown. Therefore, FSP1-CoQ10-NAD(P)H is an independent pathway that cooperates with the cystine-GSH-GPX4 system to inhibit ferroptosis. In a Parkinson's disease model, Song L. M. et al. (2021) demonstrated that inhibiting the upregulation of long-chain acyl-CoA synthase 4 (ACSL4) and downregulation of ferroptosis inhibitor 1 (FSP1) can effectively prevent MPTP-induced ferroptosis, thereby identifying a promising therapeutic target for Parkinson's disease.

GCH1-BH4-DHFR

Exogenous dopamine or melatonin has been shown to inhibit ferroptosis induced by heme (Song L. M. et al., 2021). Tetrahydrobiopterin (BH4) is a natural nutrient that is involved in the biosynthesis of neurotransmitters, for example, 5-hydroxytryptamine, dopamine, adrenaline and melatonin can be used as cofactors of various enzymes, such as tryptophan hydroxylase, nitric oxide (NO) synthase and glycerol ether monooxygenase (Werner et al., 2011). BH4 plays a redox role in the formation of NO, which is catalyzed by L-arginine and NADPH (Hu Q. et al., 2022). The oxidation of BH4 to BH2 leads to the uncoupling of NOS to form $O2^{\cdot-}$, which reacts rapidly with NO to form peroxynitrite and further decouple NOS (Song L. M. et al., 2021). Deng et al. (2020) also

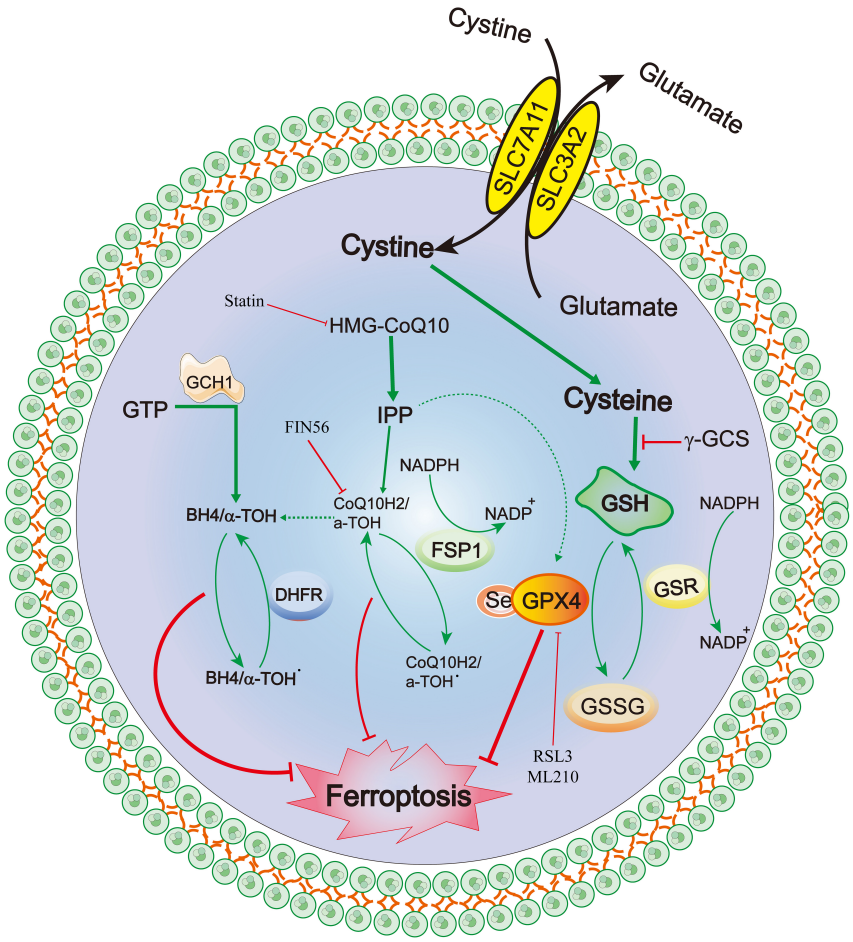

FIGURE 6
Molecular mechanisms of ferroptosis from subarachnoid hemorrhage to early brain injury (EBI).

confirmed that the activation of the NO pathway was associated with tissue damage related to ferroptosis. Additionally, Soula et al. (2020) indicated that BH4 synthesis is a necessary molecule required to protect cells from death. Moreover, the expression of GTP cyclohydrolase 1 (GCH1) determines the effectiveness of BH4 and its dependence on GPX4 inhibition (Kraft et al., 2020; Cronin et al., 2022). BH4 prevents the accumulation of lipid peroxides independently of its cofactor and is an effective free radical trapping agent and antioxidant in the lipid membrane, Dihydrofolate reductase catalyzes BH4 regeneration, methotrexate and GPX4 have been reported to synergistically inhibit ferroptosis (Hu Q. et al., 2022). Additionally, GCH1-mediated BH4 production prevents ferroptosis by inhibiting lipid peroxidation (Kraft et al., 2020; Hu Q. et al., 2022). In the hypertension model reported by Wang et al. (2021), the antihypertensive effect of L-phenylalanine could be mediated by enhancing BH4 biosynthesis and reducing superoxide levels produced by NO synthase, thereby reducing ROS and improving NO levels and protecting blood vessels and renal function. Hence, the GCH1-BH4 signaling pathway, as an endogenous antioxidant pathway, inhibits iron death through a mechanism independent of the GPX4/GSH system (Kuang et al., 2020; Wei et al., 2020).

Conclusions and prospects

The pathological processes and mechanisms of SAH rupture are extremely complex. Regardless of the main mechanism, blood entering the subarachnoid space or brain tissue is considered the inducer. Furthermore, the subsequent red blood cell lysis products release various toxic substances and lead to the death of neurons, ultimately leading to secondary brain injury (Bulters et al., 2018). Increasing basic studies have also demonstrated that ferroptosis-specific inhibitors, including liproxstatin-1 and ferrostatin-1, can decrease lipid peroxidation and neuronal ferroptosis after SAH *in vivo* and *in vitro* by regulating GPX4 and ACSL4 (Cao et al., 2021; Li et al., 2021;

Qu et al., 2021). The present review expounds on the roles and related mechanisms of neuron necrosis, apoptosis, pyroptosis, necroptosis, autophagy and ferroptosis in brain injury after SAH. These mechanisms are interwoven and interact to jointly regulate brain injury after SAH. Furthermore, we explored the interrelated molecular mechanisms and targets to provide new ideas for drug synthesis. This review provides novel research directions that can aid in improving the prognosis of patients with SAH.

Author contributions

JC, KX, and YW designed the study. JC and ML drafted the manuscript. All authors discussed the results and revised the manuscript and read and approved the final manuscript.

Funding

This work was supported by the Jiangsu Provincial Natural Science Foundation (Grant No: BK20201140), Top talent support program for young and middle-aged people of Wuxi Health Committee (HB2020119) and Wuxi Science and Technology Development Foundation (Grant No: N20201008).

Acknowledgments

We thank all the participants in this study.

Conflict of interest

The authors declare that the research was conducted in the absence of any commercial or financial relationships that could be construed as a potential conflict of interest.

Publisher's note

References

Abu Khweek, A., and Amer, A. O. (2020). Pyroptotic and non-pyroptotic effector functions of caspase-11. *Immunol. Rev.* 297, 39–52. doi: 10.1111/imr.12910

Aglietti, R. A., Estevez, A., Gupta, A., Ramirez, M. G., Liu, P. S., Kayagaki, N., et al. (2016). GsdmD p30 elicited by caspase-11 during pyroptosis forms pores in membranes. *Proc. Natl. Acad. Sci. U.S.A.* 113, 7858–7863. doi: 10.1073/pnas.1607769113

Alim, I., Caulfield, J. T., Chen, Y., Swarup, V., Geschwind, D. H., Ivanova, E., et al. (2019). Selenium drives a transcriptional adaptive program to block ferroptosis and treat stroke. *Cell* 177, 1262–1279.e25. doi: 10.1016/j.cell.2019.03.032

Al-Khindi, T., Macdonald, R. L., and Schweizer, T. A. (2010). Cognitive and functional outcome after aneurysmal subarachnoid hemorrhage. *Stroke* 41, e519–e536. doi: 10.1161/strokeaha.110.581975

An, P., Xie, J., Qiu, S., Wang, J., Xiu, X., Li, L., et al. (2019). Hispidulin exhibits neuroprotective activities against cerebral ischemia reperfusion injury through suppressing NLRP3-mediated pyroptosis. *Life Sci.* 232, 116599. doi: 10.1016/j.lfs.2019.116599

Bergsbaken, T., Fink, S., and Cookson, B. T. (2009). Pyroptosis: Host cell death and inflammation. *Nat. Rev. Microbiol.* 7, 99–109. doi: 10.1038/nrmicro2070

Bersuker, K., Hendricks, J. M., Li, Z., Magtanong, L., Ford, B., Tang, P. H., et al. (2019). The CoQ oxidoreductase FSP1 acts parallel to GPX4 to inhibit ferroptosis. *Nature* 575, 688–692. doi: 10.1038/s41586-019-1705-2

Bjerring, P., Eefsen, M., Larsen, F., Bernal, W., and Wendon, J. (2011). Hypermagnesemia does not prevent intracranial hypertension and aggravates cerebral hyperperfusion in a rat model of acute hyperammonemia. *Hepatology* 53, 1986–1994. doi: 10.1002/hep.24274

Broz, P., and Dixit, V. M. (2016). Inflammasomes: Mechanism of assembly, regulation and signalling. *Nat. Rev. Immunol.* 16, 407–420. doi: 10.1038/nri.2016.58

Bulters, D., Gaastra, B., Zolnourian, A., Alexander, S., Ren, D., Blackburn, S. L., et al. (2018). Haemoglobin scavenging in intracranial bleeding: Biology and clinical implications. *Nat. Rev. Neurol.* 14, 416–432. doi: 10.1038/s41582-018-0020-0

Cao, Y., Li, Y., He, C., Yan, F., Li, J. R., Xu, H. Z., et al. (2021). Selective ferroptosis inhibitor liproxstatin-1 attenuates neurological deficits and neuroinflammation after subarachnoid hemorrhage. *Neurosci. Bull.* 37, 535–549. doi: 10.1007/s12264-020-00620-5

Chang, H., Lin, C., Li, Z., Shen, Y., Zhang, G., and Mao, L. (2022). T3 alleviates neuroinflammation and reduces early brain injury after subarachnoid haemorrhage by promoting mitophagy via PINK 1-parkin pathway. *Exp. Neurol.* 357:114175. doi: 10.1016/j.expneurol.2022.114175

Chavez, L., Meguro, J., Chen, S., de Paiva, V. N., Zambrano, R., Eterno, J. M., et al. (2021). Circulating extracellular vesicles activate the pyroptosis pathway in the brain following ventilation-induced lung injury. *J. Neuroinflammation* 18:310. doi: 10.1186/s12974-021-02364-z

Chen, J., Xuan, Y., Chen, Y., Wu, T., Chen, L., Guan, H., et al. (2019c). Netrin-1 alleviates subarachnoid haemorrhage-induced brain injury via the PPARγ/NF-KB signalling pathway. *J. Cell. Mol. Med.* 23, 2256–2262. doi: 10.1111/jcmm.14105

Chen, A. Q., Fang, Z., Chen, X. L., Yang, S., Zhou, Y. F., Mao, L., et al. (2019a). Microglia-derived TNF-α mediates endothelial necroptosis aggravating blood brain-barrier disruption after ischemic stroke. *Cell Death Dis.* 10:487. doi: 10.1038/s41419-019-1716-9

Chen, J., Jin, H., Xu, H., Peng, Y., Jie, L., Xu, D., et al. (2019b). The neuroprotective effects of necrostatin-1 on subarachnoid hemorrhage in rats are possibly mediated by preventing blood-brain barrier disruption and RIP3-mediated necroptosis. *Cell Transplant.* 28, 1358–1372. doi: 10.1177/0963689719867285

Chen, G., and Goeddel, D. V. (2002). TNF-R1 signaling: A beautiful pathway. *Science* 296, 1634–1635. doi: 10.1126/science.1071924

Chen, J. H., Li, M. C., Zhu, X., Yang, S., Zhang, C., Wu, T., et al. (2020a). Atorvastatin reduces cerebral vasospasm and infarction after aneurysmal subarachnoid hemorrhage in elderly Chinese adults. *Aging* 12, 2939–2951. doi: 10.18632/aging.102788

Chen, J. H., Wu, T., Xia, W. Y., Shi, Z. H., Zhang, C. L., Chen, L., et al. (2020b). An early neuroprotective effect of atorvastatin against subarachnoid hemorrhage. *Neural Regen. Res.* 15, 1947–1954. doi: 10.4103/1673-5374.280326

Chen, J., Wang, Y., Wu, J., Yang, J., Li, M., and Chen, Q. (2020c). The potential value of targeting ferroptosis in early brain injury after acute CNS disease. *Front. Mol. Neurosci.* 13:110. doi: 10.3389/fnmol.2020.00110

Chen, J., Zhu, J., He, J., Wang, Y., Chen, L., Zhang, C., et al. (2016). Ultra-early microsurgical treatment within 24 h of SAH improves prognosis of poor-grade aneurysm combined with intracerebral hematoma. *Oncol. Lett.* 11, 3173–3178. doi: 10.3892/ol.2016.4327

Chen, J. H., Yang, L. K., Chen, L., Wang, Y. H., Wu, Y., Jiang, B. J., et al. (2016). Atorvastatin ameliorates early brain injury after subarachnoid hemorrhage via inhibition of AQP4 expression in rabbits. *Int. J. Mol. Med.* 37, 1059–1066. doi: 10.3892/ijmm.2016.2506

Chen, S., Feng, H., Sherchan, P., Klebe, D., Zhao, G., Sun, X., et al. (2014). Controversies and evolving new mechanisms in subarachnoid hemorrhage. *Prog. Neurobiol.* 115, 64–91. doi: 10.1016/j.pneurobio.2013.09.002

Chen, J., Wang, L., Wu, C., Hu, Q., Gu, C., Yan, F., et al. (2014). Melatonin-enhanced autophagy protects against neural apoptosis via a mitochondrial pathway in early brain injury following a subarachnoid hemorrhage. *J. Pineal Res.* 56, 12–19. doi: 10.1111/jpi.12086

Chen, J., Zhang, C., Yan, T., Yang, L., Wang, Y., Shi, Z., et al. (2021). Atorvastatin ameliorates early brain injury after subarachnoid hemorrhage via inhibition of pyroptosis and neuroinflammation. *J. Cell. Physiol.* 236, 6920–6931. doi: 10.1002/jcp.30351

Chen, J.-H., Li, P.-P., Yang, K., Chen, L., Zhu, J., Hu, X., et al. (2018a). Value of ventricular intracranial pressure monitoring for traumatic bifrontal contusions. *World Neurosurg.* 113, E690–E701. doi: 10.1016/j.wneu.2018.02.122

Chen, J. H., Wu, T., Yang, L. K., Chen, L., Zhu, J., Li, P. P., et al. (2018b). Protective effects of atorvastatin on cerebral vessel autoregulation in an experimental rabbit model of subarachnoid hemorrhage. *Mol. Med. Rep.* 17, 1651–1659. doi: 10.3892/mmr.2017.8074

Chen, Y., Zhou, Y., Wang, Q., Chen, J., Chen, H., Xie, H. H., et al. (2022). κConciliatory anti-allergic decoction attenuates pyroptosis in RSV-infected asthmatic mice and lipopolysaccharide (LPS)-induced 16HBE cells by inhibiting TLR3/NLRP3/NF-B/IRF3 signaling pathway. *J. Immunol. Res.* 2022:1800401. doi: 10.1155/2022/1800401

Claassen, J., Carhuapoma, J. R., Kreiter, K. T., Du, E. Y., Connolly, E. S., and Mayer, S. A. (2002). Global cerebral edema after subarachnoid hemorrhage: Frequency, predictors, and impact on outcome. *Stroke* 33, 1225–1232. doi: 10.1161/01.str.0000015624.29071.1f

Croci, D., Nevzati, E., Danura, H., Schöpf, S., Fandino, J., Marbacher, S., et al. (2019). The relationship between IL-6, ET-1 and cerebral vasospasm, in experimental rabbit subarachnoid hemorrhage. *J. Neurosurg. Sci.* 63, 245–250. doi: 10.23736/s0390-5616.16.03876-5

Cronin, S., Rao, S., Tejada, M., Turnes, B. L., Licht-Mayer, S., Omura, T., et al. (2022). Phenotypic drug screen uncovers the metabolic GCH1/BH4 pathway as key regulator of EGFR/KRAS-mediated neuropathic pain and lung cancer. *Sci. Transl. Med.* 14:eabj1531. doi: 10.1126/scitranslmed.abj1531

Dar, H. H., Anthonymuthu, T. S., Ponomareva, L. A., Souryavong, A. B., Shurin, G. V., Kapralov, A. O., et al. (2021). A new thiol-independent mechanism of epithelial host defense against *Pseudomonas aeruginosa*: iNOS/NO(•) sabotage of theft-ferroptosis. *Redox Biol.* 45:102045. doi: 10.1016/j.redox.2021.102045

Degterev, A., Huang, Z., Boyce, M., Jagtap, P., Mizushima, N., Cuny, G. D., et al. (2005). Chemical inhibitor of nonapoptotic cell death with therapeutic potential for ischemic brain injury. *Nat. Chem. Biol.* 1, 112–119. doi: 10.1038/nchembio711

Deng, G., Li, Y., Ma, S., Gao, Z., Zeng, T., Chen, L., et al. (2020). Caveolin-1 dictates ferroptosis in the execution of acute immune-mediated hepatic damage by attenuating nitrogen stress. *Free Radic. Biol. Med.* 148, 151–161. doi: 10.1016/j.freeradbiomed.2019.12.026

Dharmalingam, P., Talakatta, G., Mitra, J., Wang, H., Derry, P. J., Nilewski, L. G., et al. (2020). Pervasive genomic damage in experimental intracerebral hemorrhage: Therapeutic potential of a mechanistic-based carbon nanoparticle. *ACS Nano* 14, 2827–2846. doi: 10.1021/acsnano.9b05821

Diamond, C. E., Khameneh, H. J., Brough, D., and Mortellaro, A. (2015). Novel perspectives on non-canonical inflammasome activation. *Immunotargets Ther.* 4, 131–141. doi: 10.2147/itt.S57976

Ding, P., Zhu, Q., Sheng, B., Yang, H., Xu, H. J., Tao, T., et al. (2022). Alpha-ketoglutarate alleviates neuronal apoptosis induced by central insulin resistance through inhibiting S6K1 phosphorylation after subarachnoid hemorrhage. *Oxid. Med. Cell. Longev.* 2022:9148257. doi: 10.1155/2022/9148257

Dixon, S. J., Lemberg, K. M., Lamprecht, M. R., Skouta, R., Zaitsev, E. M., Gleason, C. E., et al. (2012). Ferroptosis: An iron-dependent form of nonapoptotic cell death. *Cell* 149, 1060–1072. doi: 10.1016/j.cell.2012.03.042

Doll, S., Freitas, F. P., Shah, R., Aldrovandi, M., da Silva, M. C., Ingold, I., et al. (2019). FSP1 is a glutathione-independent ferroptosis suppressor. *Nature* 575, 693–698. doi: 10.1038/s41586-019-1707-0

Dong, Y., Fan, C., Hu, W., Jiang, S., Ma, Z., Yan, X., et al. (2016). Melatonin attenuated early brain injury induced by subarachnoid hemorrhage via regulating NLRP3 inflammasome and apoptosis signaling. *J. Pineal Res.* 60, 253–262. doi: 10.1111/jpi.12300

Drijvers, J. M., Gillis, J. E., Muijlwijk, T., Nguyen, T. H., Gaudiano, E. F., Harris, I. S., et al. (2021). Pharmacologic Screening Identifies Metabolic Vulnerabilities of CD8(+) T Cells. *Cancer Immunol. Res.* 9, 184–199. doi: 10.1158/2326-6066.Cir-20-0384

Du, Y., Lu, Z., Yang, D., Wang, D., Jiang, L., Shen, Y., et al. (2021). MerTK inhibits the activation of the NLRP3 inflammasome after subarachnoid hemorrhage by inducing autophagy. *Brain Res.* 1766, 147525. doi: 10.1016/j.brainres.2021.147525

Edebali, N., Tekin, I., Açıkgöz, B., Açıkgöz, S., Barut, F., Sevinç, N., et al. (2014). Apoptosis and necrosis in the circumventricular organs after experimental subarachnoid hemorrhage as detected with annexin V and caspase 3 immunostaining. *Neurol. Res.* 36, 1114–1120. doi: 10.1179/1743132814y.0000000437

Feigin, V. L., Lawes, C. M., Bennett, D. A., Barker-Collo, S. L., and Parag, V. (2009). Worldwide stroke incidence and early case fatality reported in 56 population-based studies: A systematic review. *Lancet Neurol.* 8, 355–369. doi: 10.1016/s1474-4422(09)70025-0

Forcina, G. C., and Dixon, S. J. (2019). GPX4 at the crossroads of lipid homeostasis and ferroptosis. *Proteomics* 19, e1800311. doi: 10.1002/pmic.201800311

Friedmann Angeli, J. P., and Conrad, M. (2018). Selenium and GPX4, a vital symbiosis. *Free Radic. Biol. Med.* 127, 153–159. doi: 10.1016/j.freeradbiomed.2018.03.001

Friedmann Angeli, J. P., Schneider, M., Proneth, B., Tyurina, Y. Y., Tyurin, V. A., Hammond, V. J., et al. (2014). Inactivation of the ferroptosis regulator Gpx4 triggers acute renal failure in mice. *Nat. Cell Biol.* 16, 1180–1191. doi: 10.1038/ncb3064

Friedrich, V., Flores, R., and Sehba, F. A. (2012). Cell death starts early after subarachnoid hemorrhage. *Neurosci. Lett.* 512, 6–11. doi: 10.1016/j.neulet.2012.01.036

Galluzzi, L., Kepp, O., Chan, F. K., and Kroemer, G. (2017). Necroptosis: Mechanisms and relevance to disease. *Annu. Rev. Pathol.* 12, 103–130. doi: 10.1146/annurev-pathol-052016-100247

Gao, X., Gao, Y. Y., Yan, H. Y., Liu, G.-J., Zhou, Y., Tao, T., et al. (2022). PDK4 decrease neuronal apoptosis via inhibiting ROS-ASK1/P38 pathway in early brain injury after subarachnoid hemorrhage. *Antioxid. Redox Signal.* 36, 505–524. doi: 10.1089/ars.2021.0083

Gao, S., Zhou, L., Lu, J., Fang, Y., Wu, H., Xu, W., et al. (2022). Cepharanthine Attenuates early brain injury after subarachnoid hemorrhage in mice via inhibiting 15-lipoxygenase-1-mediated microglia and endothelial cell ferroptosis. *Oxid. Med. Cell. Longev.* 2022:4295208. doi: 10.1155/2022/4295208

Gao, Y., Ferguson, D., Xie, W., Manis, J. P., Sekiguchi, J., Frank, K. M., et al. (2000). Interplay of p53 and DNA-repair protein XRCC4 in tumorigenesis, genomic stability and development. *Nature* 404, 897–900. doi: 10.1038/35009138

Gaschler, M. M., Andia, A. A., Liu, H., Csuka, J. M., Hurlocker, B., Vaiana, C. A., et al. (2018). FINO(2) initiates ferroptosis through GPX4 inactivation and iron oxidation. *Nat. Chem. Biol.* 14, 507–515. doi: 10.1038/s41589-018-0031-6

GBD 2019 Stroke Collaborators (2021). Global, regional, and national burden of stroke and its risk factors, 1990-2019: A systematic analysis for the Global Burden of Disease Study 2019. *Lancet Neurol.* 20, 795–820. doi: 10.1016/s1474-4422(21)00252-0

Gerlach, B., Cordier, S. M., Schmukle, A. C., Emmerich, C. H., Rieser, E., Haas, T. L., et al. (2011). Linear ubiquitination prevents inflammation and regulates immune signalling. *Nature* 471, 591–596. doi: 10.1038/nature09816

González-Montelongo, M. D. C., Egea-Guerrero, J. J., Murillo-Cabezas, F., González-Montelongo, R., Ruiz de Azúa-López, Z., Rodríguez-Rodríguez, A., et al. (2018). Relation of RhoA in peripheral blood mononuclear cells with severity of aneurysmal subarachnoid hemorrhage and vasospasm. *Stroke* 49, 1507–1510. doi: 10.1161/strokeaha.117.020311

Gu, L., Sun, M., Li, R., Tao, Y., Luo, X., Xu, J., et al. (2022). Activation of RKIP binding ASC attenuates neuronal pyroptosis and Brain Injury via Caspase-1/GSDMD signaling pathway after intracerebral hemorrhage in mice. *Transl. Stroke Res.* 13, 1037–1054. doi: 10.1007/s12975-022-01009-4

Güresir, E., Welchowski, T., Lampmann, T., Brandecker, S., Güresir, A., Wach, J., et al. (2022). Delayed cerebral ischemia after aneurysmal subarachnoid hemorrhage: The results of induced hypertension only after the IMCVS Trial-A prospective cohort study. *J. Clin. Med.* 11:5850. doi: 10.3390/jcm11195850

Halstead, M., and Geocadin, R. G. (2019). The medical management of cerebral edema: Past, present, and future therapies. *Neurotherapeutics* 16, 1133–1148. doi: 10.1007/s13311-019-00779-4

Harris, H., and Rubinsztein, D. C. (2012). Control of autophagy as a therapy for neurodegenerative disease. *Nat. Rev. Neurol.* 8, 108–117. doi: 10.1038/nrneurol.2011.200

Hasegawa, Y., Suzuki, H., Sozen, T., Altay, O., and Zhang, J. H. (2011). apoptotic mechanisms for neuronal cells in early brain injury after subarachnoid hemorrhage. *Acta Neurochir. Suppl.* 110(Pt 1), 43–48.

He, J. Q., Chen, J. H., Zhu, J., Chen, L., Zhang, C. L., Yang, L. K., et al. (2015). Prognosis of ultra-early microsurgery combined with extraventricular drainage in patients with poor-grade aneurysms. *Int. J. Clin. Exp. Med.* 8, 9723–9729.

He, S., Wang, L., Miao, L., Wang, T., Du, F., Zhao, L., et al. (2009). Receptor interacting protein kinase-3 determines cellular necrotic response to TNF-alpha. *Cell* 137, 1100–1111. doi: 10.1016/j.cell.2009.05.021

Heuer, G. G., Smith, M. J., Elliott, J. P., Winn, H. R., and LeRoux, P. D. (2004). Relationship between intracranial pressure and other clinical variables in patients with aneurysmal subarachnoid hemorrhage. *J. Neurosurg.* 101, 408–416. doi: 10.3171/jns.2004.101.3.0408

Hider, R. C., and Kong, X. L. (2011). Glutathione: A key component of the cytoplasmic labile iron pool. *Biometals* 24, 1179–1187. doi: 10.1007/s10534-011-9476-8

Ho, W. M., Akyol, O., Reis, H., Reis, C., McBride, D., Thome, C., et al. (2018). Autophagy after subarachnoid hemorrhage: Can cell death be good? *Curr. Neuropharmacol.* 16, 1314–1319. doi: 10.2174/1570159x15666171123200646

Holler, N., Zaru, R., Micheau, O., Thome, M., Attinger, A., Valitutti, S., et al. (2000). Fas triggers an alternative, caspase-8-independent cell death pathway using the kinase RIP as effector molecule. *Nat. Immunol.* 1, 489–495. doi: 10.1038/82732

Hostettler, I., Kreiser, K., Lange, N., Schwendinger, N., Trost, D., Frangoulis, S., et al. (2022). Treatment during cerebral vasospasm phase-complication association and outcome in aneurysmal subarachnoid haemorrhage. *J. Neurol.* 269, 5553–5560. doi: 10.1007/s00415-022-11212-w

Hu, X., Zhang, H., Zhang, Q., Yao, X., Ni, W., and Zhou, K. (2022). Emerging role of STING signalling in CNS injury: Inflammation, autophagy, necroptosis, ferroptosis and pyroptosis. *J. Neuroinflammation* 19:242. doi: 10.1186/s12974-022-02602-y

Hu, Q., Wei, W., Wu, D., Huang, G., Li, M., Li, W., et al. (2022). Blockade of GCH1/BH4 axis activates ferritinophagy to mitigate the resistance of colorectal cancer to erastin-induced ferroptosis. *Front. Cell. Dev. Biol.* 10:810327. doi: 10.3389/fcell.2022.810327

Huang, J., Lu, W. T., Sun, S. Q., Yang, Z. B., Huang, S. Q., Gan, S. W., et al. (2014). Upregulation and lysosomal degradation of AQP4 in rat brains with bacterial meningitis. *Neurosci. Lett.* 566, 156–161. doi: 10.1016/j.neulet.2014.02.054

Huang, Q., Wang, G., Hu, Y. L., Liu, J. X., Yang, J., Wang, S., et al. (2017). Study on the expression and mechanism of inflammatory factors in the brain of rats with cerebral vasospasm. *Eur. Rev. Med. Pharmacol. Sci.* 21, 2887–2894.

Ingold, I., Aichler, M., Yefremova, E., Roveri, A., Buday, K., Doll, S., et al. (2015). Expression of a catalytically inactive mutant form of glutathione peroxidase 4 (Gpx4) confers a dominant-negative effect in male fertility. *J. Biol. Chem.* 290, 14668–14678. doi: 10.1074/jbc.M115.656363

Ingold, I., Berndt, C., Schmitt, S., Doll, S., Poschmann, G., Buday, K., et al. (2018). Selenium Utilization by GPX4 Is Required to Prevent Hydroperoxide-Induced Ferroptosis. *Cell* 172, 409–422.e421. doi: 10.1016/j.cell.2017.11.048

Ito, M., Shichita, T., Okada, M., Komine, R., Noguchi, Y., Yoshimura, A., et al. (2015). Bruton's tyrosine kinase is essential for NLRP3 inflammasome activation and contributes to ischaemic brain injury. *Nat. Commun.* 6:7360. doi: 10.1038/ncomms8360

Jaafaru, M., Nordin, N., Rosli, R., Shaari, K., Bako, H. Y., Noor, N. M., et al. (2019). Prospective role of mitochondrial apoptotic pathway in mediating GMG-ITC to reduce cytotoxicity in HO-induced oxidative stress in differentiated SH-SY5Y cells. *Biomed. Pharmacother.* 119:109445. doi: 10.1016/j.biopha.2019.109445

Kaiser, W. J., Sridharan, H., Huang, C., Mandal, P., Upton, J. W., Gough, P. J., et al. (2013). Toll-like receptor 3-mediated necrosis via TRIF. RIP3, and MLKL. *J. Biol. Chem.* 288, 31268–31279. doi: 10.1074/jbc.M113.462341

Kaku, Y., Tsuchiya, A., Kanno, T., and Nishizaki, T. (2015). HUHS1015 induces necroptosis and caspase-independent apoptosis of MKN28 human gastric cancer cells in association with AMID accumulation in the nucleus. *Anticancer Agents Med. Chem.* 15, 242–247. doi: 10.2174/1871520614666140922122700

Kaufmann, A., and Cardoso, E. J. J. (1992). Aggravation of vasogenic cerebral edema by multiple-dose mannitol. *J. Neurosurg.* 77, 584–589. doi: 10.3171/jns.1992.77.4.0584

Kayagaki, N., Stowe, I. B., Lee, B. L., O'Rourke, K., Anderson, K., Warming, S., et al. (2015). Caspase-11 cleaves gasdermin D for non-canonical inflammasome signalling. *Nature* 526, 666–671. doi: 10.1038/nature15541

Kayagaki, N., Wong, M. T., Stowe, I. B., Ramani, S. R., Gonzalez, L. C., Akashi-Takamura, S., et al. (2013). Noncanonical inflammasome activation by intracellular LPS independent of TLR4. *Science* 341, 1246–1249. doi: 10.1126/science.1240248

Kerr, N. A., Sanchez, J., O'Connor, G., Watson, B. D., Daunert, S., Bramlett, H. M., et al. (2022). Inflammasome-regulated pyroptotic cell death in disruption of the gut-brain axis after stroke. *Transl. Stroke Res.* 13, 898–912. doi: 10.1007/s12975-022-01005-8

Kraft, V., Bezjian, C. T., Pfeiffer, S., Ringelstetter, L., Müller, C., Zandkarimi, F., et al. (2020). GTP cyclohydrolase 1/tetrahydrobiopterin counteract ferroptosis through lipid remodeling. *ACS Cent. Sci.* 6, 41–53. doi: 10.1021/acscentsci.9b01063

Kroemer, G., Galluzzi, L., Vandenabeele, P., Abrams, J., Alnemri, E. S., Baehrecke, E. H., et al. (2009). Classification of cell death: Recommendations of the Nomenclature Committee on Cell Death 2009. *Cell Death Differ.* 16, 3–11. doi: 10.1038/cdd.2008.150

Kuang, F., Liu, J., Tang, D., and Kang, R. (2020). Oxidative damage and antioxidant defense in ferroptosis. *Front. Cell. Dev. Biol.* 8:586578. doi: 10.3389/fcell.2020.586578

Kuwar, R., Rolfe, A., Di, L., Xu, H., He, L., Jiang, Y., et al. (2019). A novel small molecular NLRP3 inflammasome inhibitor alleviates neuroinflammatory response following traumatic brain injury. *J. Neuroinflammation* 16:81. doi: 10.1186/s12974-019-1471-y

Lawton, M. T., and Vates, G. E. (2017). Subarachnoid Hemorrhage. *N. Engl. J. Med.* 377, 257–266. doi: 10.1056/NEJMcp1605827

Lee, C. Z., Xue, Z., Zhu, Y., Yang, G. Y., and Young, W. L. (2007). Matrix metalloproteinase-9 inhibition attenuates vascular endothelial growth factor-induced intracerebral hemorrhage. *Stroke* 38, 2563–2568. doi: 10.1161/strokeaha.106.481515

Lee, J.-Y., He, Y., Sagher, O., Keep, R., Hua, Y., and Xi, G. (2009). Activated autophagy pathway in experimental subarachnoid hemorrhage. *Brain Res.* 1287, 126–135. doi: 10.1016/j.brainres.2009.06.028

Li, J. R., Xu, H. Z., Nie, S., Peng, Y. C., Fan, L. F., Wang, Z. J., et al. (2017). Fluoxetine-enhanced autophagy ameliorates early brain injury via inhibition of NLRP3 inflammasome activation following subrachnoid hemorrhage in rats. *J. Neuroinflammation* 14:186. doi: 10.1186/s12974-017-0959-6

Li, Y., Liu, Y., Wu, P., Tian, Y., Liu, B., Wang, J., et al. (2021). Inhibition of ferroptosis alleviates early brain injury after subarachnoid hemorrhage *in vitro* and *in vivo* via reduction of lipid peroxidation. *Cell. Mol. Neurobiol.* 41, 263–278. doi: 10.1007/s10571-020-00850-1

Li, Z., and Han, X. (2018). Resveratrol alleviates early brain injury following subarachnoid hemorrhage: Possible involvement of the AMPK/SIRT1/autophagy signaling pathway. *Biol. Chem.* 399, 1339–1350. doi: 10.1515/hsz-2018-0269

Liang, Y., Song, P., Zhu, Y., Xu, J. M., Zhu, P. Z., Liu, R. R., et al. (2020). TREM-1-targeting LP17 attenuates cerebral ischemia-induced neuronal injury by inhibiting oxidative stress and pyroptosis. *Biochem. Biophys. Res. Commun.* 529, 554–561. doi: 10.1016/j.bbrc.2020.05.056

Liu, M., Zhong, W., Li, C., and Su, W. (2022). Fluoxetine attenuates apoptosis in early brain injury after subarachnoid hemorrhage through Notch1/ASK1/p38 MAPK signaling pathway. *Bioengineered* 13, 8396–8411. doi: 10.1080/21655979.2022.2037227

Liu, B., Tian, Y., Li, Y., Wu, P., Zhang, Y., Zheng, J., et al. (2022). ACEA attenuates oxidative stress by promoting mitophagy via CB1R/Nrf1/PINK1 pathway after subarachnoid hemorrhage in rats. *Oxid. Med. Cell. Longev.* 2022:1024279. doi: 10.1155/2022/1024279

Liu, X., Zhang, Z., Ruan, J., Pan, Y., Magupalli, V. G., Wu, H., et al. (2016). Inflammasome-activated gasdermin D causes pyroptosis by forming membrane pores. *Nature* 535, 153–158. doi: 10.1038/nature18629

Liu, Y., Cai, H., Wang, Z., Li, J., Wang, K., Yu, Z., et al. (2013). Induction of autophagy by cystatin C: A potential mechanism for prevention of cerebral vasospasm after experimental subarachnoid hemorrhage. *Eur. J. Med. Res.* 18:21. doi: 10.1186/2047-783x-18-21

Macdonald, R. L. (2014). Delayed neurological deterioration after subarachnoid haemorrhage. *Nat. Rev. Neurol.* 10, 44–58. doi: 10.1038/nrneurol.2013.246

Macdonald, R. L., and Schweizer, T. A. (2017). Spontaneous subarachnoid haemorrhage. *Lancet* 389, 655–666. doi: 10.1016/s0140-6736(16)30668-7

Macdonald, R. L., Higashida, R. T., Keller, E., Mayer, S. A., Molyneux, A., Raabe, A., et al. (2011). Clazosentan, an endothelin receptor antagonist, in patients with aneurysmal subarachnoid haemorrhage undergoing surgical clipping: A randomised, double-blind, placebo-controlled phase 3 trial (CONSCIOUS-2). *Lancet Neurol.* 10, 618–625. doi: 10.1016/s1474-4422(11)70108-9

Mees, S. M. D., Algra, A., Vandertop, W. P., van Kooten, F., Kuijsten, H. A., Boiten, J., et al. (2012). Magnesium for aneurysmal subarachnoid haemorrhage (MASH-2): A randomised placebo-controlled trial. *The Lancet* 380, 44–49. doi: 10.1016/s0140-6736(12)60724-7

Nag, S., Manias, J. L., and Stewart, D. J. (2009). Pathology and new players in the pathogenesis of brain edema. *Acta Neuropathol.* 118, 197–217. doi: 10.1007/s00401-009-0541-0

Narotam, P. K., Garton, A., Morrison, J., Nathoo, N., and Narotam, N. (2022). Brain oxygen-directed management of aneurysmal subarachnoid hemorrhage. Temporal patterns of cerebral ischemia during acute brain attack, early brain injury, and territorial sonographic vasospasm. *World Neurosurg.* 166, e215–e236. doi: 10.1016/j.wneu.2022.06.149

Nieuwkamp, D. J., Setz, L. E., Algra, A., Linn, F. H., de Rooij, N. K., and Rinkel, G. J. (2009). Changes in case fatality of aneurysmal subarachnoid haemorrhage over time, according to age, sex, and region: A meta-analysis. *Lancet Neurol.* 8, 635–642. doi: 10.1016/s1474-4422(09)70126-7

Olson, D. M., Zomorodi, M., Britz, G. W., Zomorodi, A. R., Amato, A., and Graffagnino, C. (2013). Continuous cerebral spinal fluid drainage associated with complications in patients admitted with subarachnoid hemorrhage. *J. Neurosurg.* 119, 974–980. doi: 10.3171/2013.6.Jns122403

Pang, L., Liu, Z., Zhou, K., Chen, P., Pan, E., Che, Y., et al. (2022). ACE2 rescues impaired autophagic flux through the PI3K/AKT pathway after subarachnoid hemorrhage. *Neurochem. Res.* 47, 601–612. doi: 10.1007/s11064-021-03469-w

Papadopoulos, M. C., Manley, G. T., Krishna, S., and Verkman, A. S. (2004). Aquaporin-4 facilitates reabsorption of excess fluid in vasogenic brain edema. *FASEB J.* 18, 1291–1293. doi: 10.1096/fj.04-1723fje

Passier, P. E., Visser-Meily, J. M., van Zandvoort, M. J., Post, M. W., Rinkel, G. J., and van Heugten, C. (2010). Prevalence and determinants of cognitive complaints after aneurysmal subarachnoid hemorrhage. *Cerebrovasc. Dis.* 29, 557–563. doi: 10.1159/000306642

Peng, J., Zuo, Y., Huang, L., Okada, T., Liu, S., Zuo, G., et al. (2019). Activation of GPR30 with G1 attenuates neuronal apoptosis via src/EGFR/stat3 signaling pathway after subarachnoid hemorrhage in male rats. *Exp. Neurol.* 320:113008. doi: 10.1016/j.expneurol.2019.113008

Pluta, R. M. (2005). Delayed cerebral vasospasm and nitric oxide: Review, new hypothesis, and proposed treatment. *Pharmacol. Ther.* 105, 23–56. doi: 10.1016/j.pharmthera.2004.10.002

Powell, W. J. Jr., DiBona, D. R., Flores, J., Frega, N., and Leaf, A. (1976). . Effects of hyperosmotic mannitol in reducing ischemic cell swelling and minimizing myocardial necrosis. *Circulation* 53 (3 Suppl.), I45–I49.

Qu, X. F., Liang, T. Y., Wu, D. G., Lai, N. S., Deng, R. M., Ma, C., et al. (2021). Acyl-CoA synthetase long chain family member 4 plays detrimental role in early brain injury after subarachnoid hemorrhage in rats by inducing ferroptosis. *CNS Neurosci. Ther.* 27, 449–463. doi: 10.1111/cns.13548

Qureshi, A. I., Suri, M. F., Nasar, A., Kirmani, J. F., Ezzeddine, M. A., Divani, A. A., et al. (2007). Changes in cost and outcome among US patients with stroke hospitalized in 1990 to 1991 and those hospitalized in 2000 to 2001. *Stroke* 38, 2180–2184. doi: 10.1161/strokeaha.106.467506

Rinkel, G. J., and Algra, A. (2011). Long-term outcomes of patients with aneurysmal subarachnoid haemorrhage. *Lancet Neurol.* 10, 349–356. doi: 10.1016/s1474-4422(11)70017-5

Rivero-Arias, O., Gray, A., and Wolstenholme, J. (2010). Burden of disease and costs of aneurysmal subarachnoid haemorrhage (aSAH) in the United Kingdom. *Cost Eff. Resour. Alloc.* 8:6. doi: 10.1186/1478-7547-8-6

Rui, T., Wang, H., Li, Q., Cheng, Y., Gao, Y., Fang, X., et al. (2021). Deletion of ferritin H in neurons counteracts the protective effect of melatonin against traumatic brain injury-induced ferroptosis. *J. Pineal Res.* 70:e12704. doi: 10.1111/jpi.12704

Sahin, M. H., Akyuz, E., and Kadioglu, H. H. (2021). The Effects of Necrostatin-1 on Cerebral Vasospasm- Induced Subarachnoid Hemorrhage. *Turk. Neurosurg.* [Epub ahead of print]. doi: 10.5137/1019-5149.Jtn.35167-21.4

Said, M., Gümüs, M., Herten, A., Dinger, T. F., Chihi, M., Darkwah Oppong, M., et al. (2021). Subarachnoid Hemorrhage Early Brain Edema Score (SEBES) as a radiographic marker of clinically relevant intracranial hypertension and unfavorable outcome after subarachnoid hemorrhage. *Eur. J. Neurol.* 28, 4051–4059. doi: 10.1111/ene.15033

Sendoel, A., Kohler, I., Fellmann, C., Lowe, S. W., and Hengartner, M. O. (2010). HIF-1 antagonizes p53-mediated apoptosis through a secreted neuronal tyrosinase. *Nature* 465, 577–583. doi: 10.1038/nature09141

She, Y., Shao, L., Zhang, Y., Hao, Y., Cai, Y., Cheng, Z., et al. (2019). Neuroprotective effect of glycosides in Buyang Huanwu Decoction on pyroptosis following cerebral ischemia-reperfusion injury in rats. *J. Ethnopharmacol.* 242:112051. doi: 10.1016/j.jep.2019.112051

Shen, H., Liu, C., Zhang, D., Yao, X., Zhang, K., Li, H., et al. (2017). Role for RIP1 in mediating necroptosis in experimental intracerebral hemorrhage model both *in vivo* and *in vitro*. *Cell Death Dis.* 8:e2641. doi: 10.1038/cddis.2017.58

Shi, J., Zhao, Y., Wang, K., Shi, X., Wang, Y., Huang, H., et al. (2015). Cleavage of GSDMD by inflammatory caspases determines pyroptotic cell death. *Nature* 526, 660–665. doi: 10.1038/nature15514

Shimada, K., Skouta, R., Kaplan, A., Yang, W. S., Hayano, M., Dixon, S. J., et al. (2016). Global survey of cell death mechanisms reveals metabolic regulation of ferroptosis. *Nat. Chem. Biol.* 12, 497–503. doi: 10.1038/nchembio.2079

Shinohara, Y., Katayama, Y., Uchiyama, S., Yamaguchi, T., Handa, S., Matsuoka, K., et al. (2010). Cilostazol for prevention of secondary stroke (CSPS 2): An aspirin-controlled, double-blind, randomised non-inferiority trial. *Lancet Neurol* 9, 959–968. doi: 10.1016/s1474-4422(10)70198-8

Song, Z., Jia, G., Ma, P., and Cang, S. (2021). Exosomal miR-4443 promotes cisplatin resistance in non-small cell lung carcinoma by regulating FSP1 m6A modification-mediated ferroptosis. *Life Sci.* 276:119399. doi: 10.1016/j.lfs.2021.119399

Song, L. M., Xiao, Z. X., Zhang, N., Zhang, N., Yu, X. Q., Cui, W., et al. (2021). Apoferritin improves motor deficits in MPTP-treated mice by regulating brain iron metabolism and ferroptosis. *iScience* 24:102431. doi: 10.1016/j.isci.2021.102431

Soula, M., Weber, R. A., Zilka, O., Alwaseem, H., La, K., Yen, F., et al. (2020). Metabolic determinants of cancer cell sensitivity to canonical ferroptosis inducers. *Nat. Chem. Biol.* 16, 1351–1360. doi: 10.1038/s41589-020-0613-y

Steiner, T., Juvela, S., Unterberg, A., Jung, C., Forsting, M., Rinkel, G., et al. (2013). European stroke organization guidelines for the management of intracranial aneurysms and subarachnoid haemorrhage. *Cerebrovasc. Dis.* 35, 93–112. doi: 10.1159/000346087

Stienen, M. N., Smoll, N. R., Weisshaupt, R., Fandino, J., Hildebrandt, G., Studerus-Germann, A., et al. (2014). Delayed cerebral ischemia predicts neurocognitive impairment following aneurysmal subarachnoid hemorrhage. *World Neurosurg.* 82, e599–e605. doi: 10.1016/j.wneu.2014.05.011

Stockwell, B. R., Friedmann Angeli, J. P., Bayir, H., Bush, A. I., Conrad, M., Dixon, S. J., et al. (2017). Ferroptosis: A regulated cell death nexus linking metabolism, redox biology, and disease. *Cell* 171, 273–285. doi: 10.1016/j.cell.2017.09.021

Sugimoto, K., Nomura, S., Shirao, S., Inoue, T., Ishihara, H., Kawano, R., et al. (2018). Cilostazol decreases duration of spreading depolarization and spreading ischemia after aneurysmal subarachnoid hemorrhage. *Ann. Neurol.* 84, 873–885. doi: 10.1002/ana.25361

Sun, X. G., Duan, H., Jing, G., Wang, G., Hou, Y., Zhang, M., et al. (2019). Inhibition of TREM-1 attenuates early brain injury after subarachnoid hemorrhage via downregulation of p38MAPK/MMP-9 and preservation of ZO-1. *Neuroscience* 406, 369–375. doi: 10.1016/j.neuroscience.2019.03.032

Sun, Y. B., Zhao, H., Mu, D. L., Zhang, W., Cui, J., Wu, L., et al. (2019). Dexmedetomidine inhibits astrocyte pyroptosis and subsequently protects the brain in in vitro and in vivo models of sepsis. *Cell Death Dis.* 10:167. doi: 10.1038/s41419-019-1416-5

Sun, C., Enkhjargal, B., Reis, C., Zhang, T., Zhu, Q., Zhou, K., et al. (2019). Osteopontin-enhanced autophagy attenuates early brain injury via FAK-ERK pathway and improves long-term outcome after subarachnoid hemorrhage in rats. *Cells* 8:980. doi: 10.3390/cells8090980

Sun, C. M., Enkhjargal, B., Reis, C., Zhou, K. R., Xie, Z. Y., Wu, L. Y., et al. (2019). Osteopontin attenuates early brain injury through regulating autophagy-apoptosis interaction after subarachnoid hemorrhage in rats. *CNS Neurosci. Ther.* 25, 1162–1172. doi: 10.1111/cns.13199

Svedung Wettervik, T., Hånell, A., Howells, T., Ronne Engström, E., Lewén, A., and Enblad, P. (2022). ICP, CPP, and PRx in traumatic brain injury and aneurysmal subarachnoid hemorrhage: Association of insult intensity and duration with clinical outcome. *J. Neurosurg.* [Epub ahead of print]. doi: 10.3171/2022.5.Jns22560

Swanson, K., Deng, M., and Ting, J. P. (2019). The NLRP3 inflammasome: Molecular activation and regulation to therapeutics. *Nat. Rev. Immunol.* 19, 477–489. doi: 10.1038/s41577-019-0165-0

Tonnus, W., Meyer, C., Steinebach, C., Belavgeni, A., von Mässenhausen, A., Gonzalez, N. Z., et al. (2021). Dysfunction of the key ferroptosis-surveilling systems hypersensitizes mice to tubular necrosis during acute kidney injury. *Nat. Commun.* 12:4402. doi: 10.1038/s41467-021-24712-6

Tourdias, T., Mori, N., Dragonu, I., Cassagno, N., Boiziau, C., Aussudre, J., et al. (2011). Differential aquaporin 4 expression during edema build-up and resolution phases of brain inflammation. *J. Neuroinflammation* 8:143. doi: 10.1186/1742-2094-8-143

Toyoda, K., Uchiyama, S., Yamaguchi, T., Easton, J. D., Kimura, K., Hoshino, H., et al. (2019). Dual antiplatelet therapy using cilostazol for secondary prevention in patients with high-risk ischaemic stroke in Japan: A multicentre, open-label, randomised controlled trial. *Lancet Neurol.* 18, 539–548. doi: 10.1016/s1474-4422(19)30148-6

Tuo, Q. Z., Liu, Y., Xiang, Z., Yan, H. F., Zou, T., Shu, Y., et al. (2022). Thrombin induces ACSL4-dependent ferroptosis during cerebral ischemia/reperfusion. *Signal Transduct. Target. Ther.* 7:59. doi: 10.1038/s41392-022-00917-z

Van Rossom, S., Op de Beeck, K., Hristovska, V., Winderickx, J., and Van Camp, G. (2015). The deafness gene DFNA5 induces programmed cell death through mitochondria and MAPK-related pathways. *Front. Cell. Neurosci.* 9:231. doi: 10.3389/fncel.2015.00231

Vande Walle, L., and Lamkanfi, M. (2016). Pyroptosis. *Curr. Biol.* 26, R568–R572. doi: 10.1016/j.cub.2016.02.019

Wan, A., Jaja, B. N., Schweizer, T. A., Macdonald, R. L., and on behalf of the Sahit collaboration (2016). Clinical characteristics and outcome of aneurysmal subarachnoid hemorrhage with intracerebral hematoma. *J. Neurosurg.* 125, 1344–1351. doi: 10.3171/2015.10.Jns151036

Wang, Y., An, R., Umanah, G. K., Nambiar, K., Eacker, S. M., Kim, B., et al. (2016). A nuclease that mediates cell death induced by DNA damage and poly(ADP-ribose) polymerase-1. *Science* 354:aad6872. doi: 10.1126/science.aad6872

Wang, Z., Cheng, C., Yang, X., and Zhang, C. (2021). L-phenylalanine attenuates high salt-induced hypertension in Dahl SS rats through activation of GCH1-BH4. *PLoS One* 16:e0250126. doi: 10.1371/journal.pone.0250126

Wang, Z., Shi, X.-Y., Yin, J., Zuo, G., Zhang, J., Chen, G., et al. (2012). Role of autophagy in early brain injury after experimental subarachnoid hemorrhage. *J. Mol. Neurosci.* 46, 192–202. doi: 10.1007/s12031-011-9575-6

Wei, X., Yi, X., Zhu, X. H., and Jiang, D. S. (2020). Posttranslational modifications in ferroptosis. *Oxid. Med. Cell. Longev.* 2020:8832043. doi: 10.1155/2020/8832043

Werner, E. R., Blau, N., and Thöny, B. (2011). Tetrahydrobiopterin: Biochemistry and pathophysiology. *Biochem. J.* 438, 397–414. doi: 10.1042/bj20110293

Wu, M., Xu, L. G., Li, X., Zhai, Z., and Shu, H. B. (2002). AMID, an apoptosis-inducing factor-homologous mitochondrion-associated protein, induces caspase-independent apoptosis. *J. Biol. Chem.* 277, 25617–25623. doi: 10.1074/jbc.M202285200

Xu, H., Cai, Y., Yu, M., Sun, J., Cai, J., Li, J., et al. (2021). Celastrol protects against early brain injury after subarachnoid hemorrhage in rats through alleviating blood-brain barrier disruption and blocking necroptosis. *Aging* 13, 16816–16833. doi: 10.18632/aging.203221

Xu, P., Zhang, X., Liu, Q., Xie, Y., Shi, X., Chen, J., et al. (2019). Microglial TREM-1 receptor mediates neuroinflammatory injury via interaction with SYK in experimental ischemic stroke. *Cell Death Dis.* 10:555. doi: 10.1038/s41419-019-1777-9

Yang, C., Li, T., Xue, H., Wang, L., Deng, L., Xie, Y., et al. (2018). Inhibition of necroptosis rescues SAH-Induced synaptic impairments in hippocampus via CREB-BDNF Pathway. *Front. Neurosci.* 12:990. doi: 10.3389/fnins.2018.00990

Yang, W. S., SriRamaratnam, R., Welsch, M. E., Shimada, K., Skouta, R., Viswanathan, V. S., et al. (2014). Regulation of ferroptotic cancer cell death by GPX4. *Cell* 156, 317–331. doi: 10.1016/j.cell.2013.12.010

Yuan, S., Yu, Z., Zhang, Z., Zhang, J., Zhang, P., Li, X., et al. (2019). RIP3 participates in early brain injury after experimental subarachnoid hemorrhage in rats by inducing necroptosis. *Neurobiol. Dis.* 129, 144–158. doi: 10.1016/j.nbd.2019.05.004

Zeng, H., Chen, H., Li, M., Zhuang, J., Peng, Y., Zhou, H., et al. (2021). Autophagy protein NRBF2 attenuates endoplasmic reticulum stress-associated neuroinflammation and oxidative stress via promoting autophagosome maturation by interacting with Rab7 after SAH. *J. Neuroinflammation* 18:210. doi: 10.1186/s12974-021-02270-4

Zhang, J., Zhu, Y., Zhou, D., Wang, Z., and Chen, G. (2010). Recombinant human erythropoietin (rhEPO) alleviates early brain injury following subarachnoid hemorrhage in rats: Possible involvement of Nrf2-ARE pathway. *Cytokine* 52, 252–257. doi: 10.1016/j.cyto.2010.08.011

Zhao, X., Wen, L., Dong, M., Dong, M., and Lu, X. (2016). Sulforaphane activates the cerebral vascular Nrf2-ARE pathway and suppresses inflammation to attenuate cerebral vasospasm in rat with subarachnoid hemorrhage. *Brain Res.* 1653, 1–7. doi: 10.1016/j.brainres.2016.09.035

Zhu, X., Tao, L., Tejima-Mandeville, E., Qiu, J., Park, J., Garber, K., et al. (2012). Plasmalemma permeability and necrotic cell death phenotypes after intracerebral hemorrhage in mice. *Stroke* 43, 524–531. doi: 10.1161/strokeaha.111.635672

Zille, M., Karuppagounder, S. S., Chen, Y., Gough, P. J., Bertin, J., Finger, J., et al. (2017). Neuronal death after hemorrhagic stroke *in vitro* and *in vivo* shares features of ferroptosis and necroptosis. *Stroke* 48, 1033–1043. doi: 10.1161/strokeaha.116.015609

Zoerle, T., Lombardo, A., Colombo, A., Longhi, L., Zanier, E. R., Rampini, P., et al. (2015). Intracranial pressure after subarachnoid hemorrhage. *Crit. Care Med.* 43, 168–176. doi: 10.1097/ccm.0000000000000670

Zuo, G., Zhang, T., Huang, L., Araujo, C., Peng, J., Travis, Z., et al. (2019). Activation of TGR5 with INT-777 attenuates oxidative stress and neuronal apoptosis via cAMP/PKCε/ALDH2 pathway after subarachnoid hemorrhage in rats. *Free Radic. Biol. Med.* 143, 441–453. doi: 10.1016/j.freeradbiomed.2019.09.002

frontiers | Frontiers in Cellular Neuroscience

TYPE Original Research
PUBLISHED 04 January 2023
DOI 10.3389/fncel.2022.1057887

OPEN ACCESS

EDITED BY
Anwen Shao,
Zhejiang University, China

REVIEWED BY
Giuseppe Sciamanna,
Saint Camillus International University of Health and Medical Sciences, Italy
Sergio Machado,
Federal University of Santa Maria, Brazil
Clelia Palanza,
Istituto Italiano di Antropologia (ISItA), Italy

*CORRESPONDENCE
Wei Wang
✉ wcnsww@163.com

†These authors have contributed equally to this work

SPECIALTY SECTION
This article was submitted to Cellular Neuropathology, a section of the journal Frontiers in Cellular Neuroscience

RECEIVED 30 September 2022
ACCEPTED 12 December 2022
PUBLISHED 04 January 2023

CITATION
Shi Y, Wang M, Xiao L, Gui L, Zheng W, Bai L, Su B, Li B, Xu Y, Pan W, Zhang J and Wang W (2023) Potential therapeutic mechanism of deep brain stimulation of the nucleus accumbens in obsessive-compulsive disorder. *Front. Cell. Neurosci.* 16:1057887. doi: 10.3389/fncel.2022.1057887

Potential therapeutic mechanism of deep brain stimulation of the nucleus accumbens in obsessive-compulsive disorder

Yifeng Shi[1†], Mengqi Wang[1†], Linglong Xiao[1†], Luolan Gui[2], Wen Zheng[2], Lin Bai[3,4], Bo Su[3], Bin Li[5], Yangyang Xu[1], Wei Pan[1], Jie Zhang[3,4] and Wei Wang[1*]

[1]Department of Neurosurgery, West China Hospital, Sichuan University, Chengdu, Sichuan, China, [2]Laboratory of Clinical Proteomics and Metabolomics, Frontiers Science Center for Disease-Related Molecular Network, National Clinical Research Center for Geriatrics, West China Hospital, Institutes for Systems Genetics, Sichuan University, Chengdu, Sichuan, China, [3]Histology and Imaging Platform, Core Facilities of West China Hospital, Sichuan University, Chengdu, Sichuan, China, [4]Key Laboratory of Transplant Engineering and Immunology, West China Hospital, Sichuan University, Chengdu, Sichuan, China, [5]Mental Health Center, West China Hospital, Sichuan University, Chengdu, Sichuan, China

Deep brain stimulation (DBS) of the nucleus accumbens (NAc) (NAc-DBS) is an effective solution to refractory obsessive-compulsive disorder (OCD). However, evidence for the neurobiological mechanisms of OCD and the effect of NAc-DBS is still lacking. One hypothesis is that the electrophysiological activities in the NAc are modulated by DBS, and another hypothesis is that the activities of neurotransmitters in the NAc are influenced by DBS. To investigate these potential alterations, rats with quinpirole (QNP)-induced OCD were treated with DBS of the core part of NAc. Then, extracellular spikes (SPK) and local field potentials (LFP) in the NAc were recorded, and the levels of relevant neurotransmitters and related proteins were measured. Analysis of SPK revealed that the firing rate was decreased and the firing pattern was changed after NAc-DBS, and analysis of LFP showed that overall power spectral density (PSD) levels were reduced after NAc-DBS. Additionally, we found that the relative powers of the theta band, alpha band and beta band were increased in OCD status, while the relative powers of the delta band and gamma band were decreased. This pathological pattern of power distribution was reformed by NAc-DBS. Furthermore, we found that the local levels of monoamines [dopamine (DA) and serotonin (5-HT)] and amino acids [glutamate (Glu) and gamma-aminobutyric acid (GABA)] in the NAc were increased in OCD status, and that the expression of the two types of DA receptors in the NAc exhibited an opposite change. These abnormalities could be reversed by NAc-DBS. These findings

provide a more comprehensive understanding about the function of the NAc in the pathophysiology of OCD and provide more detailed evidence for the potential effect of NAc-DBS.

KEYWORDS

deep brain stimulation, therapy, nucleus accumbens, obsessive-compulsive disorder, electrophysiology *in vivo*, neurotransmitters

Introduction

Obsessive-compulsive disorder (OCD) is a neuropsychiatric disease that involves obsessions or compulsions that cause distress or impair functioning (Hirschtritt et al., 2017). The prevalence of OCD is 1–3% in general, and 30–40% of OCD patients develop into refractory OCD (Husted and Shapira, 2004; Groth, 2018). Refractory OCD seriously affects the lives of patients and their ability to work, and causes great pain and burden to patients and their families (Pinto et al., 2006; van Oudheusden et al., 2020). Therefore, identifying effective treatments for OCD is very important. As an alternative to medication, psychotherapy and physical therapy, deep brain stimulation (DBS) is gaining increasing attention because it is a reversible and titratable form of neuromodulation (Kumar et al., 2019; Goodman et al., 2020). The nucleus accumbens (NAc) is considered as the limbic-motor interface and plays an important role in brain networks related to motivation and reward processing (Groenewegen et al., 1996; Salamone et al., 2007; Nicola, 2010; Floresco, 2015). It has been suggested that dysfunction of the NAc is associated with various neuropsychiatric disorders (Mavridis, 2015; Park et al., 2019; Gendelis et al., 2021; Bayassi-Jakowicka et al., 2022). The NAc is one of the most commonly used neurosurgical targets in the treatment of OCD (Denys et al., 2010; Greenberg et al., 2010; Huys et al., 2019; Raviv et al., 2020), however, there are still many questions related to the use of DBS of the NAc (NAc-DBS) for the treatment of OCD, because the relevant underlying pathophysiological mechanisms are unclear, including the effect of NAc-DBS on neural electrophysiological activities and neurotransmitters activities.

Spikes (SPK) and local field potentials (LFP) measurements can be taken to assess neuronal firing characteristics and synchronous activity of membrane potentials in a large population of neurons (Buzsáki et al., 2012; Slutzky and Flint, 2017; Hagen et al., 2018; Gonzalez-Escamilla et al., 2020). There are only a few studies which reported some limited evidence on the LFP in OCD (McCracken and Grace, 2007; Neumann et al., 2014; Schüller et al., 2015; Miller et al., 2019), however, the LFP activities were mainly focused on cortex but not on deep NAc region, and the details of LFP and SPK in the NAc in OCD status and even in the DBS condition are still lacking. Moreover, changes in neurotransmitter activity may underlie OCD and the effect of DBS. In case of the NAc, its output patterns are relatively simple and mainly consist of gamma-aminobutyric acid (GABA)ergic projections to the substantia nigra (SN), ventral pallidum (VP), ventral tegmental area (VTA) and entopeduncular nucleus (EP) (**Figure 1K**) (Heimer et al., 1991; Usuda et al., 1998; Tripathi et al., 2010). However, as opposed to its simple output pattern which is mainly consisted of GABAergic projections, its input patterns are quite complicated, the NAc receives various input projections of many different neurotransmitters from wide brain regions, including dopaminergic, serotonergic, histaminergic, cholinergic, glutamatergic projections and so on. To be specific, the dopaminergic projections to the NAc mainly originate from the VTA (**Figure 1A**) (Hadley et al., 2014; Lammel et al., 2014; Cooper et al., 2017), the serotonergic projections to the NAc mainly originate from the raphe nuclei (RN) (**Figure 1C**) (Modell et al., 1989; Kiyasova et al., 2011; Alonso et al., 2013; Kim et al., 2019), histaminergic projections to the NAc mainly originate from the tuberomammillary nucleus (TMN) (**Figure 1E**) (Zhang et al., 2020; Manz et al., 2021), cholinergic projections to the NAc mainly originate from the basal forebrain (BF) and pontomesencephalo-tegmental complex (PTC) (**Figure 1G**) (Mark et al., 2011; Laurent et al., 2014; Luchicchi et al., 2014; Gielow and Zaborszky, 2017), and glutamatergic projections to the NAc mainly originate from the broad cortex, hippocampus (CA) and basolateral amygdala (BLA) (**Figure 1I**) (Walaas, 1981; Tarazi et al., 1998; Saul'skaya and Mikhailova, 2003; Zhu et al., 2022). Recently, some studies have revealed changes in the levels of these neurotransmitters and relevant receptors in OCD, and it is believed that the disturbances of these substances especially in the regions related to the cortico-striato-thalamico-cortical (CSTC) circuitry are normally considered as the basis of OCD (Winslow and Insel, 1990; Fineberg et al., 2011; van Dijk et al., 2012; Haleem et al., 2014; Pittenger, 2015; Ade et al., 2016; Vlček et al., 2018; Zhan et al., 2020; Zai, 2021). Nevertheless, research on the neurotransmitters that play a role in the NAc is lacking, and it is still not clear how the activity of these substances changes in OCD patients after NAc-DBS.

In the present study, a quinpirole (QNP)-induced OCD rat model was adopted, and the open field test (OFT)

10.3389/fncel.2022.1057887

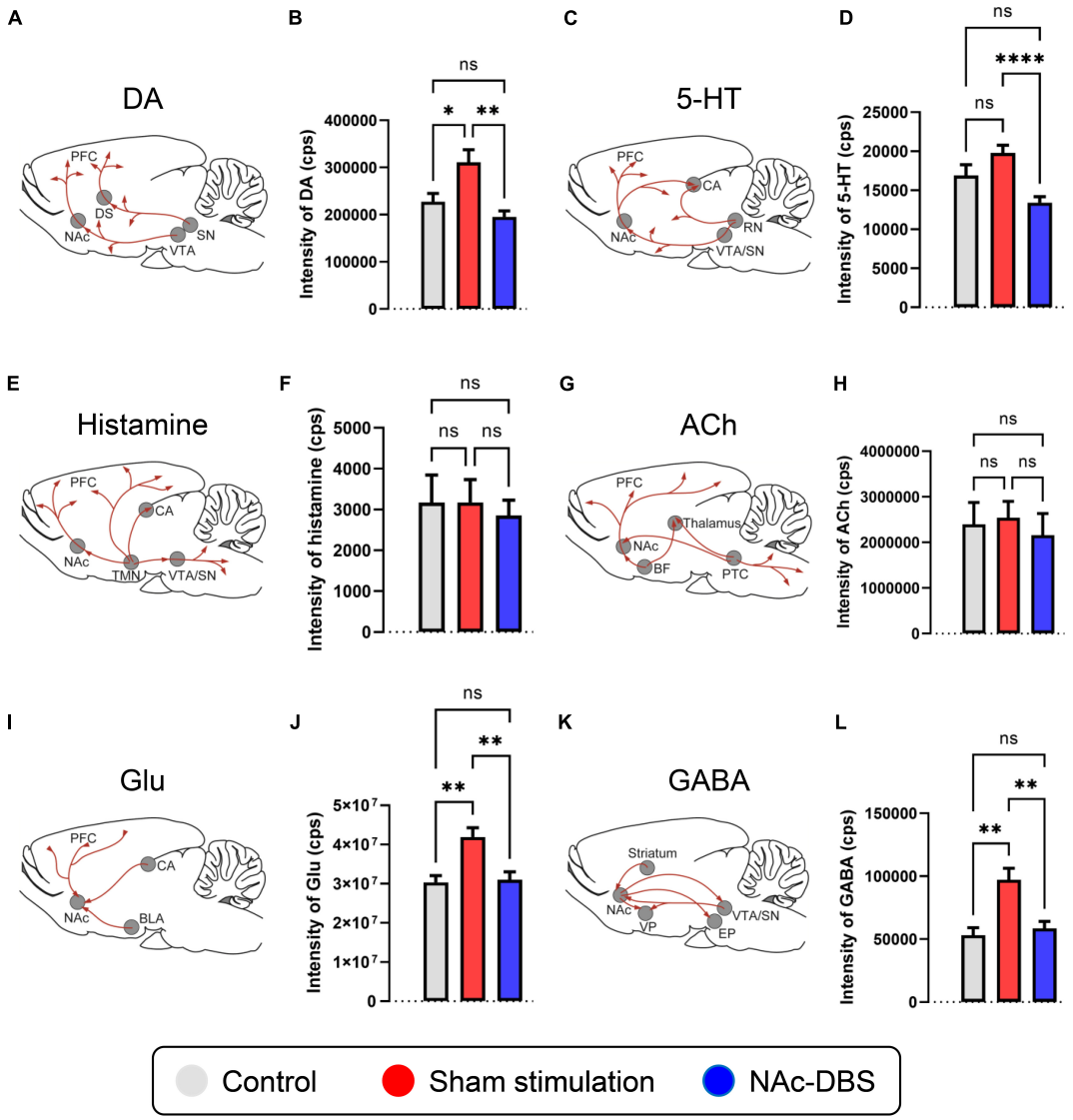

FIGURE 1
Changes in the levels of neurotransmitters of interest in the NAc in the control, sham stimulation and NAc-DBS groups. **(A)** Illustration of dopaminergic projections to the NAc. **(B)** The bar graph represents the mean level of the response intensity indicating the concentration of DA in the NAc. **(C)** Illustration of serotonergic projections to the NAc. **(D)** The bar graph represents the mean level of the intensity of 5-HT in the NAc. **(E)** Illustration of histaminergic projections to the NAc. **(F)** The bar graph represents the mean level of the intensity of histamine in the NAc. **(G)** Illustration of cholinergic projections to the NAc. **(H)** The bar graph represents the mean level of the intensity of ACh in the NAc. **(I)** Illustration of glutamatergic projections to the NAc. **(J)** The bar graph represents the mean level of the intensity of Glu in the NAc. **(K)** Illustration of the GABAergic pathway in the NAc. **(L)** The bar graph represents the mean level of the intensity of GABA in the NAc. All illustrations are modified from the stereotaxic atlas of Paxinos and Watson (6th edition). DA, dopamine; VTA, ventral tegmental area; 5-HT, serotonin; RN, raphe nuclei; TMN, tuberomammillary nucleus; ACh, acetylcholine; BF, basal forebrain; PTC, pontomesencephalo-tegmental complex; Glu, glutamate; BLA, basolateral amygdala; CA, hippocampus; GABA, gamma-aminobutyric acid; VP, ventral pallidum; SN, substantia nigra; EP, entopeduncular nucleus. The data are presented as the mean ± SEM; $n = 11$ vs. $n = 23$ vs. $n = 21$; $^{****}P < 0.0001$, $^{**}P < 0.01$, $^{*}P < 0.05$; ns, no significance.

relevant to compulsive checking behavior and the elevated plus maze (EPM) were used for the behavioral assessment (Szechtman et al., 1998, 2017; Hoffman, 2011). Given that the core of the NAc mediates the control of goal-oriented behaviors and obsessive-compulsive-like behaviors (Di Chiara, 2002; Zhang et al., 2020), micro-electrodes were implanted into the NAc core for stimulation and recording. Then SPK signals were recorded to obtain information about neuronal firing patterns, including the firing rate and indicators of interspike interval (ISI), including the coefficient of variance (CV) and asymmetry index (AI) (Alam et al., 2012, 2015). On the other hand, LFP signals were recorded to obtain

information about synchronous activity through analysis of time-frequency spectrograms and the power spectral density (PSD) (Geng et al., 2016; Salimpour et al., 2022; Wang et al., 2022; Yu et al., 2022). To analyze neurotransmitter activity, dopamine (DA), serotonin (5-HT), histamine, acetylcholine (ACh), glutamate (Glu) and GABA levels in location of the NAc were assessed through high-performance liquid chromatography (HPLC) combined with mass spectrometry (MS). Additionally, immunofluorescence staining for tyrosine hydroxylase (TH) and tryptophan hydroxylase-2 (TPH2) was performed to determine the activity of dopaminergic neurons in the VTA and serotonergic neurons in the RN, and DA receptor (DRD1 and DRD2) levels in the NAc were evaluated by immunohistochemical staining. In general, through the study from the aspects of neural electrophysiology and neurotransmitters, we aimed to provide more abundant evidence for the pathophysiological mechanisms of OCD and therapeutic mechanisms of NAc-DBS.

Materials and methods

Animals

A total of 120 male adult Sprague-Dawley rats (weighing 290–330 g, Huafukang Animal Centre, China) were used in this study. The rats were housed in transparent cages in a temperature- and humidity-controlled environment (25°C, 45%), on a 12 h light/12 h dark cycle, and *ad libitum* access to food and water was provided. All the animal experimental and care procedures were approved by the Biomedical Research Ethics Committee of West China Hospital (Protocol Number: 20211434A).

Experimental design

First, the rats were randomly divided into 2 groups: the control group (subcutaneous injection of saline) and the OCD group (administration of QNP). After OCD animal modeling and behavioral evaluation, the rats in the OCD group were randomly divided into 2 groups: the sham stimulation group (recording but no stimulation) and the NAc-DBS group (DBS at set parameters and recording). The whole procedure is shown in **Figure 2**.

OCD animal model and behavioral assessment

The rats in the OCD group were given subcutaneous injections of QNP (Sigma-Aldrich, US, 0.5 mg/kg) twice a week for 5 weeks. The rats in the control group received subcutaneous injections of saline twice a week for the same time. During the last week, 10 min after each injection, the rats in both groups were subjected to the OFT relevant to compulsive checking behavior. The Visu Track system (XinRuan Technology, China) was used to monitor the rats for 30 min on a 100 × 100 cm table containing four 8 × 8 cm boxes (2 in the center area and 2 in the corner) as potential home bases. The home base was identified as the box with the highest number of visits, and the number of home base visits and total moving distance in the OFT were measured. In addition, the EPM was conducted to evaluated the condition of anxiety, the EPM was composed of two closed arms (50 × 10 cm) and two open arms (50 × 10 cm), the walls surrounded the closed arms were 30 cm high, and the maze was elevated 50 cm above the floor. The rats in each group were placed individually in the central zone of the EPM directing to one open arm, and then the Visu Track system was used to monitor the rats for 5 min. After the monitoring, the percentage of visit times to closed arms and the percentage of total spent time in the closed arms were calculated subsequently. The average measures from 2 experiments in the last week were used as the final results of behavioral evaluation.

Electrode implantation

The stimulation and recording micro-electrodes were constructed based on the semi-finished products (#366-080906-22, Alpha-Omega, Israel). The rats were placed on a stereotaxic apparatus after anesthetization with isoflurane (RWD Life Science, China). According to the stereotaxic atlas of Paxinos and Watson (6th edition), the micro-electrodes were implanted in the core of the left NAc (AP = + 2.00 mm, ML = + 1.60 mm, DV = −7.20 mm), as shown in **Figure 3A**. Moreover, 3 screws were placed on the skull as anchors for the ground wire of the micro-electrodes. The holes were drilled properly after the appropriate locations were measured and marked on the skull. A micro-electrode was attached to the holder and lowered into the NAc perpendicularly through the drilled hole slowly. The micro-electrode and screws were fixed securely with dental cement. After the operation, the rats were given penicillin (Sigma-Aldrich, US, 100 mg/kg, i.p.) and carprofen (Sigma-Aldrich, US, 10 mg/kg, i.p.) every day for 3 days.

Stimulation and electrophysiological signals acquisition

After recovery, a stimulation program based on the most commonly used parameters was administrated to the rats in the NAc-DBS group. A bipolar biphasic current-controlled pulse that was rectangular in shape (90 μs negative/90 μs positive) and had a frequency of 130 Hz and current intensity of 150 μA was delivered for 1 h/day for 5 days. When the stimulation

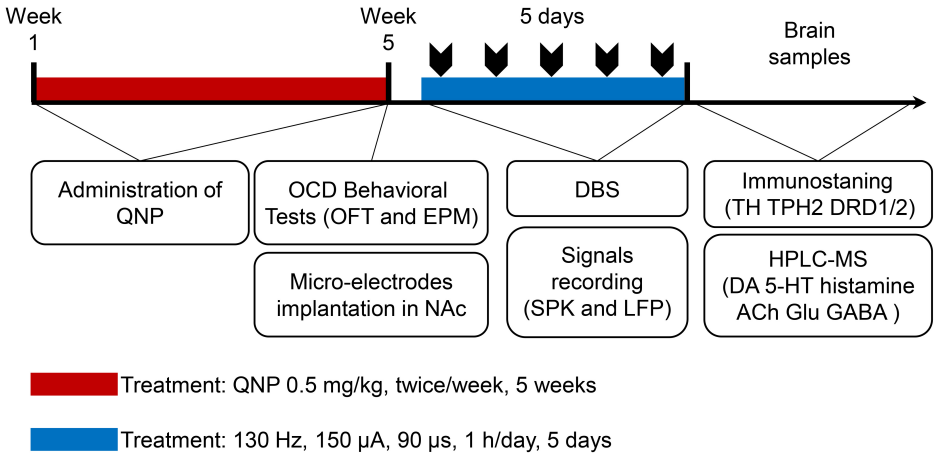

FIGURE 2
Graphical presentation of the timeline of the whole experiment design.

was finished, the *in vivo* neural electrophysiological signals were recorded by the AlphaLab SNR system (Alpha-Omega, Israel). The original signals were split into SPK and LFP activity by digitization at different sampling rates of 22000 and 1375 Hz, and band-pass filtering at 300–9000 and 0.5–200 Hz. The online-sorted SPK signals and the raw LFP signals were both saved for further offline analysis.

The SPK signals were analyzed with Spike2 (Cambridge Electronics Designs, UK) and NeuroExplorer (Nex Technologies, US), and the firing rate and ISI were analyzed to evaluate the firing pattern of the neurons in the NAc. The mean firing rate, which represented the extent of neuronal activity, was defined as the number of spikes divided by the duration of the period; the CV, which represented the whole dispersion, was defined as the standard deviation of the ISI divided by the mean ISI; and the AI, which provides information about the shape of the ISI distribution curves, was defined as the mode of the ISI divided by the mean ISI.

In addition, the LFP signals were analyzed with NeuroExplorer and its extended scripts in MATLAB 2017a (MathWorks, US), and time-frequency spectrogram analysis and PSD analysis were performed to assess the extracellular postsynaptic membrane potential changes in the NAc. It is worth noting that the division of different frequency bands in the present study was as follows: delta band (1–3 Hz), theta band (3–7 Hz), alpha band (7–12 Hz), beta band (12–30 Hz) and gamma band (30–80 Hz).

Slice preparation and immunostaining

After the signals were collected, the rats in each group were sacrificed using a lethal dose of sodium pentobarbital. The rats were perfused with 150 mL 0.01 M phosphate-buffered saline (PBS) and 150 mL of 4% paraformaldehyde (PFA). Then, the rat brains were removed, and tissue blocks containing the NAc, VTA and RN were dissected out. Then, 4 μm coronal paraffin sections were prepared.

Ventral tegmental area (VTA) sections were used for TH immunofluorescence staining, and RN sections were used for TPH2 immunofluorescence staining. After heat-induced antigen retrieval in a water bath (97°C, 40 min) and citrate buffer (pH = 6.0), the sections were blocked with 5% bovine serum albumin (BSA) at 37°C for 1 h and incubated with primary antibodies (anti-TH, Abcam, UK, #ab6211, 1:1000; anti-TPH2, Abcam, UK, #ab288067, 1:300) at 4°C overnight. The sections were then washed with 0.01 M PBS (3 × 10 min) and incubated with the corresponding secondary antibodies (Alexa Fluor® 568, Abcam, UK, #ab175692, 1:200) at 37°C for 1 h. The sections were incubated with DAPI (1:1000) at room temperature for 10 min and then washed with 0.01 M PBS (3 × 10 min).

Nucleus accumbens (NAc) sections were used for immunohistochemical staining of DRD1 and DRD2. After antigen retrieval as described above, endogenous peroxidase activity was blocked with 3% H_2O_2 at room temperature for 30 min. The sections were then blocked with 5% BSA (37°C, 1 h) and incubated with primary antibodies (anti-DRD1, Abcam, UK, #ab279713, 1:500; anti-DRD2, Affinity Biosciences, Australia, #DF10211, 1:100) at 4°C overnight. The sections were then washed with 0.01 M PBS (3 × 10 min) and incubated with the corresponding secondary antibodies (horseradish peroxidase-conjugated anti-rabbit secondary antibodies, Jackson, US, #111-035-003, 1:200) at 37°C for 1 h. Subsequently, the sections were incubated with DAB for chromogenic staining and then washed with 0.01 M PBS (3 × 10 min).

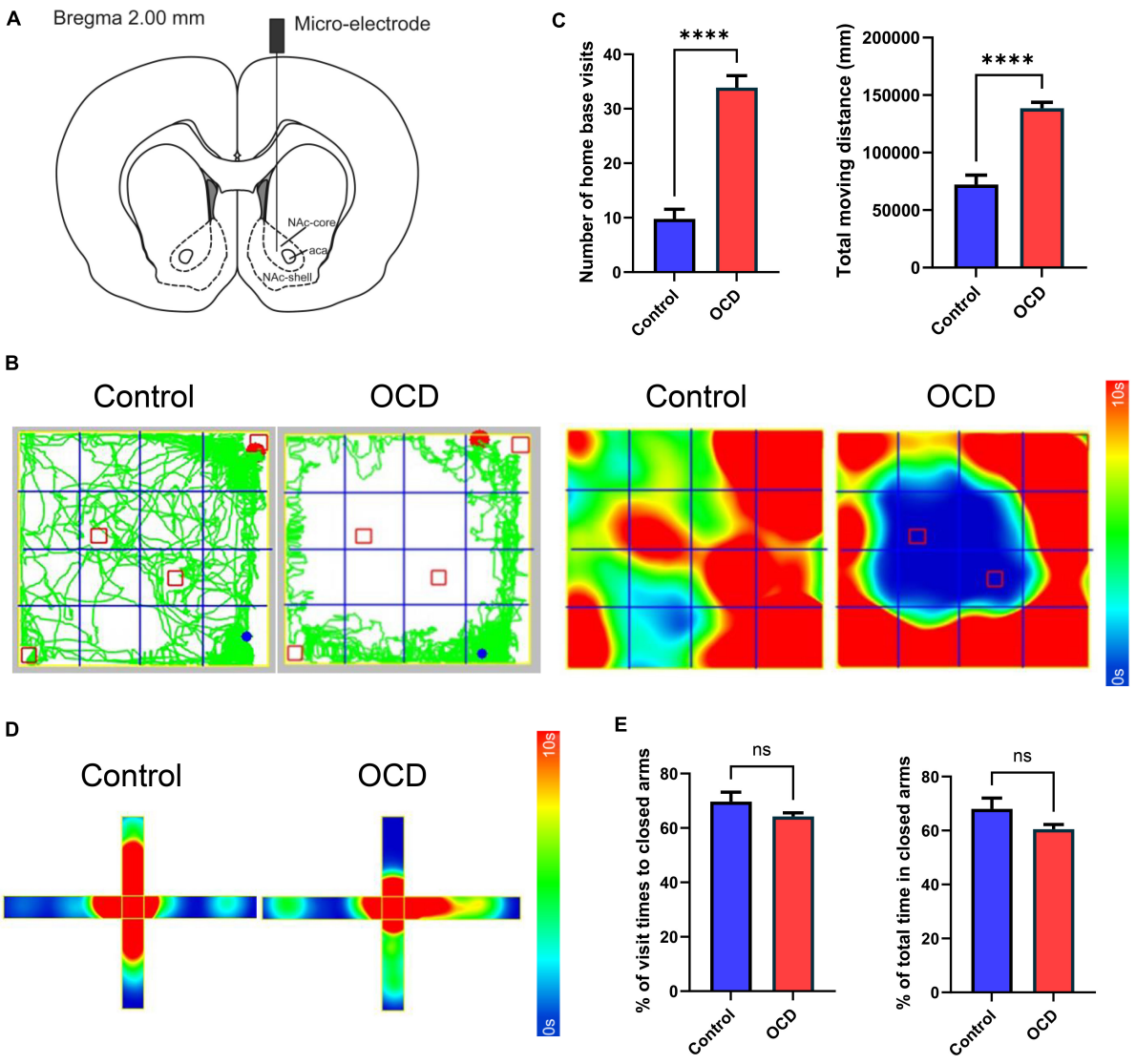

FIGURE 3
Location instruction and behavioral assessments. **(A)** Schematic diagram indicating the location of the micro-electrode in the NAc, modified from the stereotaxic atlas of Paxinos and Watson (6th edition). **(B)** Traces and 2D heatmaps of rats injected with QNP (OCD) and saline (control) in the OFT. **(C)** The bar graphs represent the level of number of home base visits and total moving distance in the OFT, by the control and OCD groups. **(D)** 2D heatmaps of rats in the EPM. The horizontal direction represents the closed arms, and the vertical direction represents the open arms. **(E)** The bar graphs represent the level of percentage of visit times to closed arms and percentage of total spent time in closed arms. OCD, obsessive-compulsive disorder; QNP, quinpirole; OFT, open field test; EPM, elevated plus maze; DBS, deep brain stimulation; HPLC, high-performance liquid chromatography; MS, mass spectrometry; NAc, nucleus accumbens. The data are presented as the mean ± SEM; $n = 8$ vs. $n = 92$; $^{****}P < 0.0001$; ns: no significance.

Immunofluorescence staining images were acquired with an inverted laser confocal microscope (Nikon, Japan, N-STORM & A1). Immunohistochemical staining images were acquired with a multispectral panoramic microscope (PerkinElmer, US, Vectra Polaris). Imaging parameters were kept consistent among sections for the same antibody. The immunofluorescence intensity was measured by NIS-Elements Analysis 5.21.00 (Nikon, Japan), and the integrated optical density (IOD) was measured by Image-Pro Plus (Media Cybernetics, US).

Sample preparation for targeted metabolomics and data collection

After signals were collected, the rats in each group were decapitated, and then brain samples (the ipsilateral NAc) were rapidly harvested, placed in cryogenic vials and frozen in liquid nitrogen. The brain tissues (10 mg) were weighed and homogenized (4°C, 6.5 m/s, 4 × 30 s/cycle) in 200 μL methanol containing internal standards (−80°C,

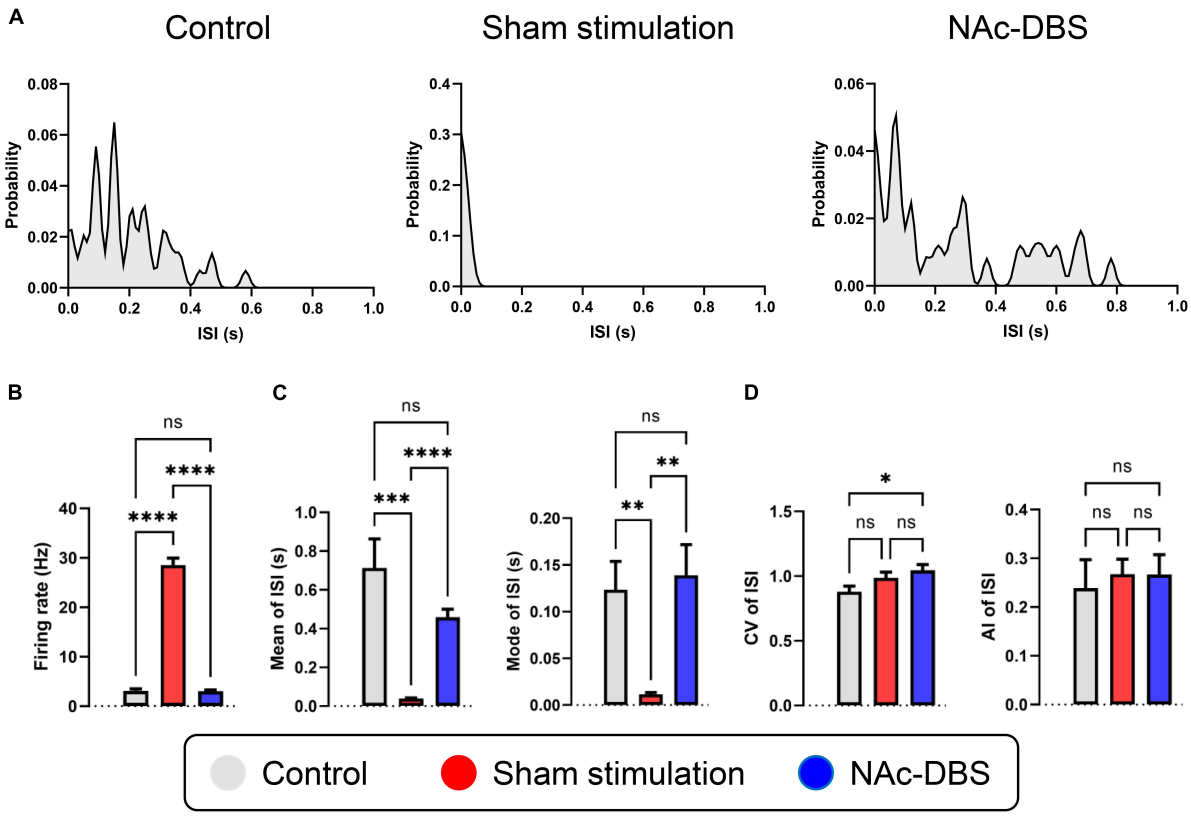

FIGURE 4
Alterations in the firing rate and firing patterns of neurons in the NAc. **(A)** Representative distribution curves of interspike intervals of control, sham stimulation and NAc-DBS groups. **(B)** The bar graph represents the mean level of firing rates. **(C)** The bar graphs represent the mean and the mode of ISI. **(D)** The bar graphs represent the level of CV and AI of ISI. ISI, interspike interval; CV, coefficient of variance; AI, asymmetry index. The data are presented as the mean ± SEM; n = 24 vs. n = 47 vs. n = 48; $^{****}P < 0.0001$, $^{***}P < 0.001$, $^{**}P < 0.01$, $^{*}P < 0.05$; ns, no significance.

^{13}C5-Glutamic acid-^{15}N/^{13}C6-Glucose, Cambridge Isotope Laboratories, UK). Then, 800 μL methanol without internal standards (−80°C) was added, and the mixture was vortexed (4°C, 1500 rpm, 3 min). The samples were sonicated in an ultrasonic water bath (10 min), vortexed (4°C, 1500 rpm, 3 min) again and centrifuged (4°C, 13300 rpm, 15 min). The supernatants (800 μL) were transferred to new centrifuge tubes and dried in a centrifugal vacuum evaporator at 30°C. The samples were reconstituted in 500 μL of mobile phase A (water:acetonitrile = 9:1, 0.2% acetic acid, 10 mM ammonium acetate):mobile phase B (water:acetonitrile = 1:9, 0.2% acetic acid, 10 mM ammonium acetate) (3:7) containing ^{13}C9-L-tyrosine-^{15}N/^{13}C1-lactate (Cambridge Isotope Laboratories, UK), vortexed for 10 min at 1500 rpm and centrifuged for 10 min at 13300 rpm (4°C).

An HPLC system (Shimadzu Corporation, Japan, LC-30AD) coupled with a triple quadrupole MS system (Sciex, US, Q-Trap 5500) equipped with a turbo ion spray source, including scheduled MRM positive mode and negative mode, was used for HPLC–MS analysis. Chromatographic separation was performed at 40°C on a Acquity UPLC BEH Amide column (1.7 μm, 2.1 × 100 mm, Waters, UK). The gradient elution was as follows: 0.0∼0.1 min: 10% A; 0.1∼1.5 min: 10% A; 1.5∼5.0 min: 55% A; 5.0∼10.0 min: 55% A; 10.0∼12.0 min: 10% B; and 12.0∼25.0 min: 10% A. The flow rate was 0.3 mL/min, the autosampler temperature was 6°C, and the sample injection volume was 2 μL for positive mode and 10 μL for negative mode. The ion source parameters: ion spray voltage: ±4000 V; temperature: 650°C; gas-1: 50 psi; gas-2: 40 psi; and curtain gas: 35 psi. The raw data were uploaded to MultiQuant software (Sciex, US, V2.0.3) for pretreatment. Then, data collected for the main neurotransmitters of interest were extracted for further processing.

Statistical analysis

All the data are expressed as the means ± standard errors of the mean. Statistical analyses were conducted using SPSS 22. For comparison between two independent groups, the D'Agostino Pearson method was used to test normality, and homogeneity of variance was tested by F-test, then Student's

t-test was suitable to taken for analyzing. For comparisons among three independent groups, the D'Agostino Pearson method was used to test normality, and homogeneity of variance was tested by Brown-Forsythe method, then one-way analysis of variance (ANOVA) followed by Tukey's *post hoc* test was suitable to taken for analyzing. $P < 0.05$ was considered significant, and $P < 0.01$ was considered highly significant.

Results

Compulsive checking behavior and anxiety behavior

After 10 injections, rats administered QNP exhibited stable compulsive check behavior. Moreover, unlike the saline-treated rats, the QNP-treated rats did not explore the whole open field arena and focused on specific objects as their home base (**Figure 3B**). Compared with the control rats, the QNP-treated rats exhibited increases in the number of home base visits and the total distance traveled ($n = 8$ vs. $n = 92$) (**Figure 3C**). However, there were no significant differences in anxiety-related behaviors (**Figures 3D, E**).

Alterations in SPK activity in the NAc

A total of 24 neurons from the control group, 47 neurons from the sham stimulation group and 48 neurons from the NAc-DBS group were recorded. The neurons from each group were classified as a single type based on the SPK duration and firing properties. Representative distribution curves of ISI are shown in **Figure 4A**. The firing rate was obviously increased in rats in the sham stimulation group compared with those in the control group, and the firing rate in the NAc decreased after application of NAc-DBS (**Figure 4B**). The ISI mean and mode were lower in the sham stimulation group than in the control group and were restored to a certain extent following NAc-DBS (**Figure 4C**). Additionally, we found that the CV of neurons in the NAc-DBS group was increased compared with that of neurons in the control group but did not differ from that of neurons in the sham stimulation group. Moreover, no significant difference in the AI among three groups was found at present (**Figure 4D**).

Alterations in LFP activity in the NAc

Local field potentials (LFP) signals were obtained from each 10 s segment of recordings from the NAc in the control group ($n = 8$), the sham stimulation group ($n = 34$) and the NAc-DBS group ($n = 28$). Visual inspection of representative time-frequency spectrograms and averaged PSD curves with 95% confidence intervals showed that the power of low frequency bands was increased in the OCD model group compared with the control group and that the overall power levels were decreased in rats treated with NAc-DBS (**Figures 5A, B**). For further evaluation of the PSD in the NAc, the relative powers of the different bands were calculated and compared (**Figure 5C**). Compared with those in the control group, rats in the sham stimulation group showed higher relative power in the theta band, alpha band and beta band oscillatory activity in the NAc, and these changes in the alpha band and beta band were reduced in rats treated with NAc-DBS. However, there was no difference in the theta band after NAc-DBS. The rats in the sham stimulation group and NAc-DBS group showed a lower relative power in the delta band than the control group, but there was no noticeable difference between the sham stimulation and NAc-DBS groups. The relative power of the gamma band (30-80 Hz) was lower in the sham stimulation group than in the control group and it was even lower in the NAc-DBS group.

Changes in dopaminergic neurons in the VTA and serotonergic neurons in the RN

Staining for TH was conducted to visualize dopaminergic neurons in the VTA, and staining for TPH2 was performed to visualize serotonergic neurons in the RN. As shown in the immunofluorescence images in **Figures 6A, B**, no noticeable difference in cell morphology was observed among the different groups. Furthermore, analysis of fluorescence intensity did not reveal any significant difference ($n = 10$ vs. $n = 19$ vs. $n = 19$) (**Figures 6E, F**).

Changes in DRD1 and DRD2 expression in the NAc

The core part and shell part of the NAc, which exhibit diffuse expression of DRD1 and DRD2, respectively, were observed separately by immunohistochemical staining. No obvious differences in cell morphology or density were found among the different groups. The intensity of DRD1 staining in the NAc core was weaker in the sham stimulation group and NAc-DBS group than in the control group, and the intensity of DRD2 staining in the NAc core was stronger in the sham stimulation group than in the other two groups (**Figures 6C, D** upper). However, there was no difference in staining intensity in the NAc shell (**Figures 6C, D** lower). Moreover, analysis of the IOD revealed a consistent trend ($n = 8$ vs. $n = 17$ vs. $n = 15$) (**Figures 6G, H**).

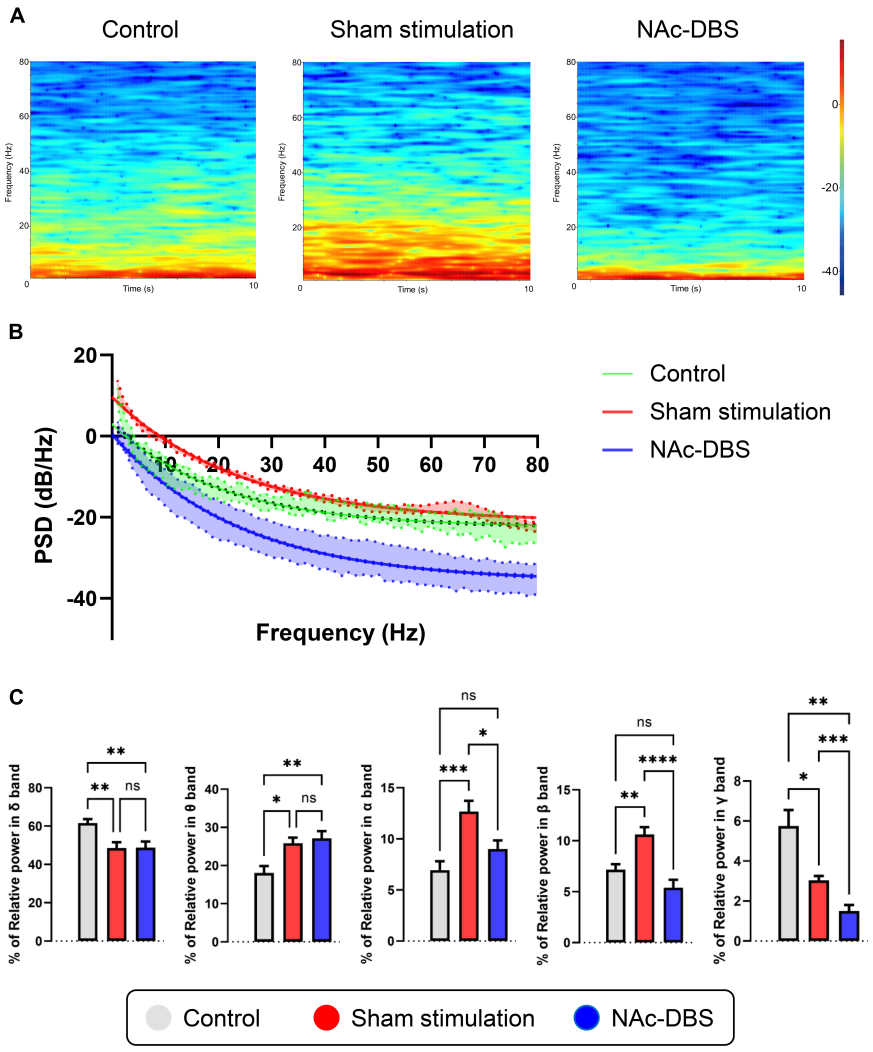

FIGURE 5
Illustrations of the difference in LFP activity in the NAc. **(A)** Representative time-frequency spectrograms in 10 s showing the power level of LFP from 1 to 80 Hz in the NAc of the control, sham stimulation and NAc-DBS groups. **(B)** The mean PSD curve with 95% confidence interval from 1 to 80 Hz. **(C)** The bar graphs represent the mean level of relative LFP powers of the delta band, theta band, alpha band, beta band and gamma band in the NAc in the different group. PSD, power spectral density. The data are presented as the mean ± SEM; n = 8 vs. n = 34 vs. n = 28; $^{****}P < 0.0001$, $^{***}P < 0.001$, $^{**}P < 0.01$, $^{*}P < 0.05$; ns, no significance.

Relative changes of in neurotransmitter levels in the NAc

A total of 11 samples from the control group, 23 samples from the sham stimulation group and 21 samples from the NAc-DBS group were collected. The level of DA in the NAc was increased in the sham stimulation group compared to the control group and decreased in rats treated with NAc-DBS (Figure 1B). The level of 5-HT in the NAc decreased in the NAc-DBS stimulation group compared to the sham stimulation group but did not differ between the control group and the sham stimulation group (Figure 1D). Moreover, we did not detect any significant differences in the levels of histamine and ACh in the NAc among the different groups (Figures 1F, H). Glu and GABA levels were increased in the sham stimulation group compared to the control group and restored to normal levels after NAc-DBS (Figures 1J, L).

Discussion

The hypothesis of this study is that there were some underlying disturbance both in the neural electrophysiological activities and neurotransmitters activities in the NAc, and NAc-DBS could modulate and correct these disturbance both in electrical and chemical ways. To determine the potential

10.3389/fncel.2022.1057887

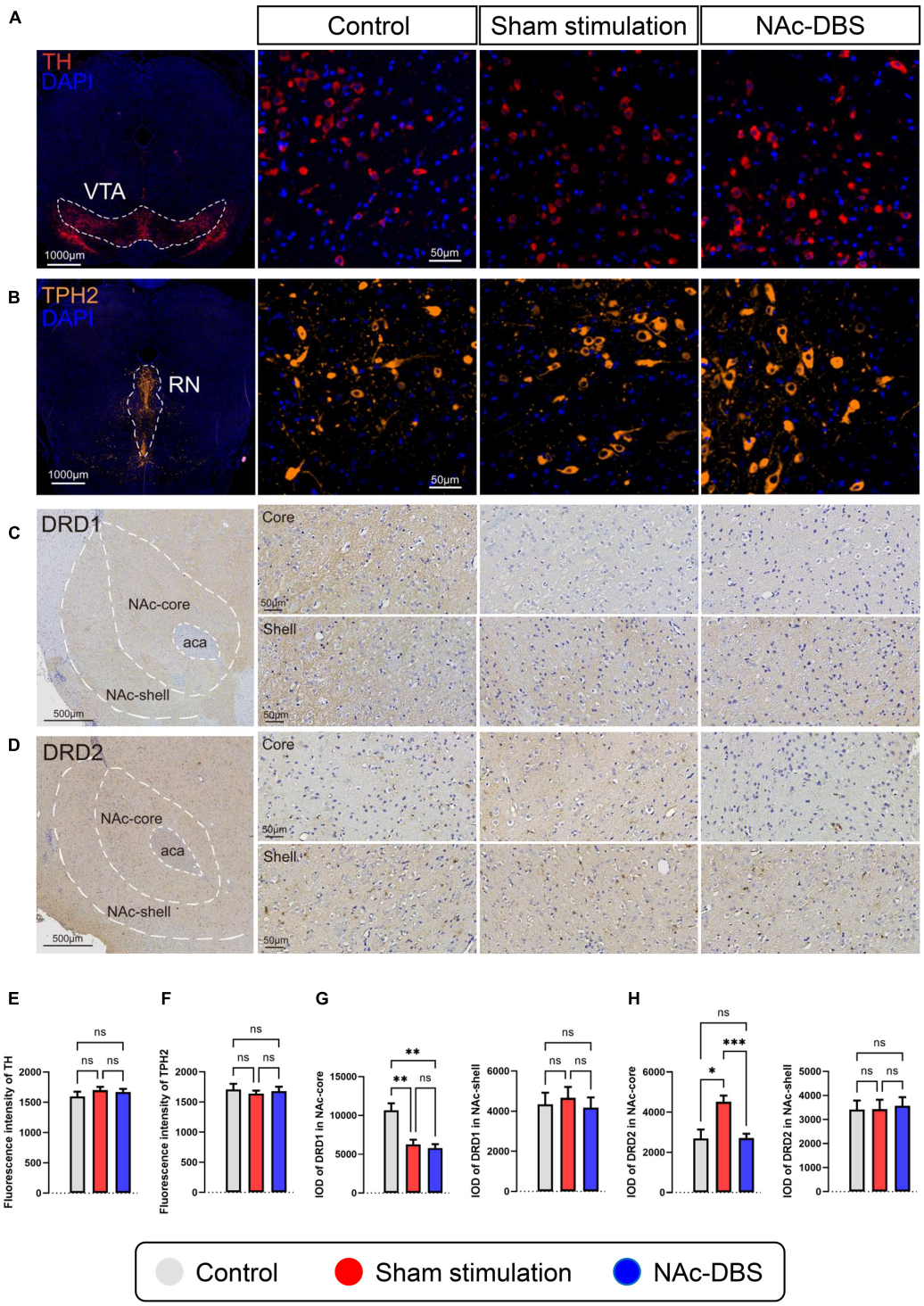

FIGURE 6
Differences in pathological sections among the control, sham stimulation and NAc-DBS groups. **(A)** Immunofluorescence staining for TH was performed to label all dopaminergic neurons in the VTA. **(B)** Immunofluorescence staining for TPH2 was performed to label all serotonergic neurons in the RN. **(C,D)** Immunohistochemical staining for DRD1 and DRD2 in the NAc. The top image is the NAc core, and the bottom image is the NAc shell. **(E)** The bar graph represents the mean level of the immunofluorescence intensity of TH in the VTA. **(F)** The bar graph represents the mean level of the immunofluorescence intensity of TPH2 in the RN. **(G)** The bar graphs represent the mean level of IOD of DRD1 in the core and shell of the NAc. **(H)** The bar graphs represent the mean level of IOD of DRD2 in the core and shell of the NAc. VTA, ventral tegmental area; TH, tyrosine hydroxylase; RN, raphe nuclei; TPH2, tryptophan hydroxylase-2; NAc, nucleus accumbens; DRD1, dopamine receptor-1; DRD2, dopamine receptor-2; IOD, integrated optical density. The data are presented as the mean ± SEM; $n = 10$ vs. $n = 19$ vs. $n = 19$ (immunofluorescence); $n = 8$ vs. $n = 17$ vs. $n = 15$ (immunohistochemistry); $^{***}P < 0.001$, $^{**}P < 0.01$, $^{*}P < 0.05$; ns, no significance.

mechanism by which NAc-DBS can alleviate QNP-induced OCD in rats, we systematically investigated the effect of NAc-DBS on electrophysiological activities *in vivo* and relevant neurotransmitter activities. This study could be the first one to systematically explore the electrophysiological characteristics of the NAc in OCD and DBS conditions not only from LFP but also SPK, and it could also be the first one to roundly explore the neurotransmitter changes in the NAc in OCD and DBS conditions. In general, successful induction of OCD in rats upon chronic administration of QNP was confirmed by relevant behavioral tests. A micro-electrode was implanted into the core part of NAc to obtain information about SPK and LFP in the NAc under different conditions, and the levels of neurotransmitters of interest at the tissue level were measured through HPLC–MS.

This study provides direct evidence that OCD and high-frequency DBS of the NAc core have different effects on neuronal firing patterns and synchronous fluctuations in large populations of neurons in the NAc. The SPK activity of NAc neurons was significantly different between rats in the sham stimulation group and rats in the control group, and the changes induced by QNP administration were substantially reversed by the application of NAc-DBS. The SPK firing rate was markedly increased and the ISI was obviously decreased in OCD model rats, indicating that the NAc was hyperactive, which is a novel finding. Moreover, the SPK firing rate and ISI were altered toward normal levels when electrical stimulation was applied; this finding is in accordance with a previous study that used brain slices (Xie et al., 2014). In the present study, the firing pattern of NAc neurons, as represented by the mean and mode ISI, CV and AI of ISI, was also significantly affected by QNP administration and NAc-DBS.

Abnormalities in the NAc were also revealed by analysis of LFP activity. Our data showed that the low-frequency PSD (especially from 1 to 30 Hz) was enhanced in rats in the sham stimulation group compared to those in the control group but that the high-frequency PSD was not obviously changed; this alteration could be used as a pathological biomarker for OCD. Interestingly, upon administration of NAc-DBS, of the entire PSD, both the low-frequency PSD and high-frequency PSD, was decreased markedly. Through relative power analysis of different frequency bands, more meaningful details were found. Compared with those in the control group, the rats in the sham stimulation group presented higher relative power in the theta band, alpha band and beta band but lower relative power in the delta band and gamma band. These findings provide valuable information for identifying OCD-related biomarkers. After NAc-DBS, the relative power of the alpha band, beta band and gamma band decreased, but there was no significant difference in delta band and theta band. These findings reveal that high-frequency electrical stimulation of the NAc may result in special patterns of neuronal activity, which could be a potential basis for closed-loop stimulation in the future. The findings of this study support previous clinical research. In a study in which DBS of the ventral capsule (VC)/ventral striatum (VS) was applied, the effect of DBS was correlated with the activity of the alpha, beta and gamma bands (Olsen et al., 2020). Another study in which DBS of the bed nucleus of the stria terminalis (BNST) was administered found that the normalized delta, beta and gamma band power in the right BNST was specifically correlated with compulsive behaviors (Wu et al., 2016). There is also some evidence suggesting that the activities of the alpha band and beta band are related to depression (Neumann et al., 2014). In addition, some research has indicated that oscillatory activity of the theta band in the striatal area may be a potential biomarker for OCD (Neumann et al., 2014; Miller et al., 2019; Schwabe et al., 2021), and studies in which DBS of the subthalamic nucleus (STN) was applied to treat OCD have shown that theta band activity is correlated with the severity of OCD symptoms (Rappel et al., 2018; Buot et al., 2021). Our data are generally consistent with these previous results and provide more detailed and comprehensive information about SPK and LFP activity in the NAc in OCD and after NAc-DBS, filling a knowledge gap.

The present study also showed that OCD and NAc-DBS have different influences on the neurotransmitter system in the NAc. Immunofluorescence revealed that dopaminergic neurons in the VTA, the main dopaminergic projections to the NAc, did not exhibit changes. However, we found that the level of DA in the NAc was increased in the sham stimulation group and decreased upon NAc-DBS. In addition, we found that the expression of DRD1 was decreased and the expression of DRD2 was increased in the NAc core in the sham stimulation group; this change did not occur in the NAc shell. This finding is in line with the previous research (Varatharajan et al., 2015; Servaes et al., 2019), however, in a study in which the NAc shell was stimulated rather than the NAc core, the level of DA was increased after DBS (Sesia et al., 2010). This may have been due to the differences in the functions of the core and shell. Immunofluorescence revealed no change in serotonergic neurons in the RN, but the level of 5-HT in the NAc was reduced upon NAc-DBS treatment. This finding is inconsistent with the results of previous research (Sesia et al., 2010), possibly due to differences in stimulation location. Furthermore, an early study in which unilateral DBS of the NAc core was applied showed no change in local monoamine release (van Dijk et al., 2011), there may be many reasons for this inconsistency, especially differences in stimulation parameters. Interestingly, in another relevant study, DA, 5-HT and noradrenaline levels in the prefrontal cortex (PFC) were increased upon NAc-DBS (van Dijk et al., 2012). This finding indicates that stimulation of a particular brain area may have different effects on the level of the same neurotransmitter in different brain regions. No significant alterations in the level of histamine or ACh was observed in this study; nevertheless, these two substances have important functions in the NAc. The NAc core receives direct

histaminergic projections from the TMN, and the symptoms of OCD and anxiety are influenced by the activity of the presynaptic H3 histamine receptor on glutamatergic afferent terminals from the prelimbic PFC to the core of the NAc (Zhang et al., 2020). More detailed information about this pathway is needed. Moreover, cholinergic interneurons are essential components of the NAc (Xie et al., 2014), they generally exert mutual antagonistic effects with DA, but whether this is the case in the NAc is still unclear. Finally, the levels of Glu and GABA should be evaluated because an imbalance between Glu and GABA levels is thought to be responsible for neuronal hyperexcitability in neuropsychiatric disorders. In the present study, we found that both Glu levels and GABA levels in the NAc were increased after sham stimulation and that this change could be markedly reversed through NAc-DBS. However, the results of this study are somewhat different from those of previous reports. Glu is the most prominent excitatory amino acid in the brain, and elevation of the extracellular level of Glu is thought to be related to many neuropsychiatric disorders (Dahchour et al., 2000; Tokuyama et al., 2001; Hanna et al., 2002; Arnold et al., 2004). Consistent with this research, some studies have shown that the level of Glu is increased in OCD (Egashira et al., 2008; Yan et al., 2013). Furthermore, GABA is the most important inhibitory amino acid in the brain, and it is commonly accepted that GABAergic medium spiny neurons projecting to the VP are inhibited by excess DA release in the NAc, which is a key node in reward circuitry (Smith et al., 2009). Other research has demonstrated that the extracellular level of GABA in the NAc decreases when reward circuitry is disturbed and increases upon DBS (Yan et al., 2013; Varatharajan et al., 2015), which is not in line with our results. Notably, GABAergic projection neurons are the main neurons in the NAc (Smith and Villalba, 2008), but extracellular GABA in the NAc is predominantly derived from VS and VTA collaterals that project to the VP (Brog et al., 1993; Pennartz et al., 1994). Differences in methods between these previous studies (*in situ* microdialysis) and the present study (tissue homogenates) may have caused the inconsistencies in findings, or there may be deeper mechanisms involved that need to be further explored.

There are some limitations in this study. First, the micro-electrodes were just implanted into the NAc, the neural electrophysiological information we could obtain was confined to single region. The follow-up studies which have more comprehensive recording of multiple brain regions may reveal more valuable hints. On the other hand, the analyzing of neurotransmitters was based on tissue homogenates which has less temporal resolution and stable performance, like the first one, the analyzing of neurotransmitters should be also expanded to more areas simultaneously to form a more overall view to brain network in OCD and DBS conditions. Last but not least, the applying of evidences obtained from rats to humans truly should be carefully evaluated. Eventhough there could be some possible similar mechanisms, the functioning of the human mind compared to that of rat is still different. More in-depth research at primate especially human level is necessary.

In conclusion, our study shows that DBS of the NAc core apparently alters neuronal firing patterns as well as LFP activity in the NAc. Moreover, NAc-DBS decreases monoamine and amino acid neurotransmitter levels in the NAc, reversing the effect of OCD. All these results suggest that high-frequency electrical stimulation of the NAc core inhibits the activity of neurons in the NAc, and this change could underlie the ability of NAc-DBS to alleviate OCD. All these findings of this study provide a chance to exert the full potential of the application of NAc-DBS. Moreover, these findings also provide a new insight into the possible candidate biomarkers for OCD and electrochemical targets for developing closed-loop neurostimulation.

Data availability statement

The original contributions presented in this study are included in the article/supplementary material, further inquiries can be directed to the corresponding author.

Ethics statement

All the animal experimental and care procedures were approved by the Biomedical Research Ethics Committee of West China Hospital (Protocol Number: 20211434A).

Author contributions

YS, JZ, and WW designed the research. YS, MW, LX, LG, LB, and BS conducted the research. YS, LG, and WZ performed statistical analysis. YS, MW, and LX wrote the manuscript. BL, YX, WP, and WW reviewed and edited the manuscript. WW supervised the work, acquired funding, and had primary responsibility for the final content. All authors contributed to the manuscript writing.

Funding

This study was supported by 1·3·5 Project for Disciplines of Excellence-Clinical Research Incubation Project, West China Hospital, Sichuan University (ZY2017307).

Conflict of interest

The authors declare that the research was conducted in the absence of any commercial or financial relationships that could be construed as a potential conflict of interest.

Publisher's note

References

Ade, K., Wan, Y., Hamann, H., O'Hare, J., Guo, W., Quian, A., et al. (2016). Increased metabotropic glutamate receptor 5 signaling underlies obsessive-compulsive disorder-like behavioral and striatal circuit abnormalities in mice. *Biol. Psychiatry* 80, 522–533. doi: 10.1016/j.biopsych.2016.04.023

Alam, M., Angelov, S., Stemmler, M., von Wrangel, C., Krauss, J., and Schwabe, K. (2015). Neuronal activity of the prefrontal cortex is reduced in rats selectively bred for deficient sensorimotor gating. *Prog. Neuropsychopharmacol. Biol. Psychiatry*. 56, 174–184. doi: 10.1016/j.pnpbp.2014.08.017

Alam, M., Heissler, H., Schwabe, K., and Krauss, J. (2012). Deep brain stimulation of the pedunculopontine tegmental nucleus modulates neuronal hyperactivity and enhanced beta oscillatory activity of the subthalamic nucleus in the rat 6-hydroxydopamine model. *Exp. Neurol.* 233, 233–242. doi: 10.1016/j.expneurol.2011.10.006

Alonso, A., Merchán, P., Sandoval, J., Sánchez-Arrones, L., Garcia-Cazorla, A., Artuch, R., et al. (2013). Development of the serotonergic cells in murine raphe nuclei and their relations with rhombomeric domains. *Brain Struct. Funct.* 218, 1229–1277. doi: 10.1007/s00429-012-0456-8

Arnold, P., Rosenberg, D., Mundo, E., Tharmalingam, S., Kennedy, J., and Richter, M. (2004). Association of a glutamate (n.d.) subunit receptor gene (GRIN2B) with obsessive-compulsive disorder: A preliminary study. *Psychopharmacology* 174, 530–538. doi: 10.1007/s00213-004-1847-1

Bayassi-Jakowicka, M., Lietzau, G., Czuba, E., Patrone, C., and Kowiański, P. (2022). More than addiction-the nucleus accumbens contribution to development of mental disorders and neurodegenerative diseases. *Int. J. Mol. Sci.* 23:2618. doi: 10.3390/ijms23052618

Brog, J., Salyapongse, A., Deutch, A., and Zahm, D. (1993). The patterns of afferent innervation of the core and shell in the "accumbens" part of the rat ventral striatum: Immunohistochemical detection of retrogradely transported fluoro-gold. *J. Comp. Neurol.* 338, 255–278. doi: 10.1002/cne.903380209

Buot, A., Karachi, C., Lau, B., Belaid, H., Fernandez-Vidal, S., Welter, M., et al. (2021). Emotions modulate subthalamic nucleus Activity: New evidence in obsessive-compulsive disorder and Parkinson's disease patients. *Biol. Psychiatry Cogn. Neurosci. Neuroimaging* 6, 556–567. doi: 10.1016/j.bpsc.2020.08.002

Buzsáki, G., Anastassiou, C., and Koch, C. (2012). The origin of extracellular fields and currents–EEG, ECoG, LFP and spikes. *Nat. Rev. Neurosci.* 13, 407–420. doi: 10.1038/nrn3241

Cooper, S., Robison, A., and Mazei-Robison, M. (2017). Reward Circuitry in Addiction. *Neurotherapeutics* 14, 687–697.

Dahchour, A., Hoffman, A., Deitrich, R., and de Witte, P. (2000). Effects of ethanol on extracellular amino acid levels in high-and low-alcohol sensitive rats: A microdialysis study. *Alcohol Alcohol.* 35, 548–553. doi: 10.1093/alcalc/35.6.548

Denys, D., Mantione, M., Figee, M., van den Munckhof, P., Koerselman, F., Westenberg, H., et al. (2010). Deep brain stimulation of the nucleus accumbens for treatment-refractory obsessive-compulsive disorder. *Arch. Gen. Psychiatry* 67, 1061–1068.

Di Chiara, G. (2002). Nucleus accumbens shell and core dopamine: Differential role in behavior and addiction. *Behav. Brain Res.* 137, 75–114.

Egashira, N., Okuno, R., Harada, S., Matsushita, M., Mishima, K., Iwasaki, K., et al. (2008). Effects of glutamate-related drugs on marble-burying behavior in mice: Implications for obsessive-compulsive disorder. *Eur. J. Pharmacol.* 586, 164–170. doi: 10.1016/j.ejphar.2008.01.035

Fineberg, N., Chamberlain, S., Hollander, E., Boulougouris, V., and Robbins, T. (2011). Translational approaches to obsessive-compulsive disorder: From animal models to clinical treatment. *Br. J. Pharmacol.* 164, 1044–1061.

Floresco, S. (2015). The nucleus accumbens: An interface between cognition, emotion, and action. *Annu. Rev. Psychol.* 66, 25–52.

Gendelis, S., Inbar, D., and Kupchik, Y. (2021). The role of the nucleus accumbens and ventral pallidum in feeding and obesity. *Prog. Neuropsychopharmacol. Biol. Psychiatry* 111:110394.

Geng, X., Xie, J., Wang, X., Wang, X., Zhang, X., Hou, Y., et al. (2016). Altered neuronal activity in the pedunculopontine nucleus: An electrophysiological study in a rat model of Parkinson's disease. *Behav. Brain Res.* 305, 57–64. doi: 10.1016/j.bbr.2016.02.026

Gielow, M., and Zaborszky, L. (2017). The input-output relationship of the cholinergic basal forebrain. *Cell Rep.* 18, 1817–1830.

Gonzalez-Escamilla, G., Muthuraman, M., Ciolac, D., Coenen, V., Schnitzler, A., and Groppa, S. (2020). Neuroimaging and electrophysiology meet invasive neurostimulation for causal interrogations and modulations of brain states. *NeuroImage* 220:117144. doi: 10.1016/j.neuroimage.2020.117144

Goodman, W., Storch, E., Cohn, J., and Sheth, S. (2020). Deep brain stimulation for intractable obsessive-compulsive disorder: Progress and opportunities. *Am. J. Psychiatry* 177, 200–203. doi: 10.1176/appi.ajp.2020.20010037

Greenberg, B., Gabriels, L., Malone, D. Jr., Rezai, A., Friehs, G., Okun, M., et al. (2010). Deep brain stimulation of the ventral internal capsule/ventral striatum for obsessive-compulsive disorder: Worldwide experience. *Mol. Psychiatry* 15, 64–79. doi: 10.1038/mp.2008.55

Groenewegen, H., Wright, C., and Beijer, A. (1996). The nucleus accumbens: Gateway for limbic structures to reach the motor system? *Prog. Brain Res.* 107, 485–511. doi: 10.1016/s0079-6123(08)61883-x

Groth, C. (2018). Tourette syndrome in a longitudinal perspective. Clinical course of tics and comorbidities, coexisting psychopathologies, phenotypes and predictors. *Dan. Med. J.* 65:B5465.

Hadley, J., Nenert, R., Kraguljac, N., Bolding, M., White, D., Skidmore, F., et al. (2014). Ventral tegmental area/midbrain functional connectivity and response to antipsychotic medication in schizophrenia. *Neuropsychopharmacology* 39, 1020–1030.

Hagen, E., Næss, S., Ness, T., and Einevoll, G. (2018). Multimodal modeling of neural network activity: Computing LFP, ECoG, EEG, and MEG signals with LFPy 2.0. *Front. Neuroinform.* 12:92. doi: 10.3389/fninf.2018.00092

Haleem, D., Ikram, H., and Haleem, M. (2014). Inhibition of apomorphine-induced conditioned place preference in rats co-injected with buspirone: Relationship with serotonin and dopamine in the striatum. *Brain Res.* 1586, 73–82. doi: 10.1016/j.brainres.2014.06.022

Hanna, G., Veenstra-VanderWeele, J., Cox, N., Boehnke, M., Himle, J., Curtis, G., et al. (2002). Genome-wide linkage analysis of families with obsessive-compulsive disorder ascertained through pediatric probands. *Am. J. Med. Genet.* 114, 541–552. doi: 10.1002/ajmg.10519

Heimer, L., Zahm, D., Churchill, L., Kalivas, P., and Wohltmann, C. (1991). Specificity in the projection patterns of accumbal core and shell in the rat. *Neuroscience* 41, 89–125.

Hirschtritt, M., Bloch, M., and Mathews, C. (2017). Obsessive-compulsive disorder: Advances in diagnosis and treatment. *JAMA* 317, 1358–1367.

Hoffman, K. (2011). Animal models of obsessive compulsive disorder: Recent findings and future directions. *Expert Opin. Drug Discov.* 6, 725–737. doi: 10.1517/17460441.2011.577772

Husted, D., and Shapira, N. (2004). A review of the treatment for refractory obsessive-compulsive disorder: From medicine to deep brain stimulation. *CNS Spectr.* 9, 833–847.

Huys, D., Kohl, S., Baldermann, J., Timmermann, L., Sturm, V., Visser-Vandewalle, V., et al. (2019). Open-label trial of anterior limb of internal capsule-nucleus accumbens deep brain stimulation for obsessive-compulsive disorder: Insights gained. *J. Neurol. Neurosurg. Psychiatry* 90, 805–812. doi: 10.1136/jnnp-2018-318996

Kim, M., Kwak, S., Yoon, Y., Kwak, Y., Kim, T., Cho, K., et al. (2019). Functional connectivity of the raphe nucleus as a predictor of the response to selective serotonin reuptake inhibitors in obsessive-compulsive disorder. *Neuropsychopharmacology* 44, 2073–2081. doi: 10.1038/s41386-019-0436-2

Kiyasova, V., Fernandez, S., Laine, J., Stankovski, L., Muzerelle, A., Doly, S., et al. (2011). A genetically defined morphologically and functionally unique subset of 5-HT neurons in the mouse raphe nuclei. *J. Neurosci.* 31, 2756–2768. doi: 10.1523/JNEUROSCI.4080-10.2011

Kumar, K., Appelboom, G., Lamsam, L., Caplan, A., Williams, N., Bhati, M., et al. (2019). Comparative effectiveness of neuroablation and deep brain stimulation for treatment-resistant obsessive-compulsive disorder: A meta-analytic study. *J. Neurol. Neurosurg. Psychiatry* 90, 469–473. doi: 10.1136/jnnp-2018-319318

Lammel, S., Lim, B., and Malenka, R. (2014). Reward and aversion in a heterogeneous midbrain dopamine system. *Neuropharmacology* 76, 351–359. doi: 10.1016/j.neuropharm.2013.03.019

Laurent, V., Bertran-Gonzalez, J., Chieng, B., and Balleine, B. (2014). δ-opioid and dopaminergic processes in accumbens shell modulate the cholinergic control of predictive learning and choice. *J. Neurosci.* 34, 1358–1369. doi: 10.1523/JNEUROSCI.4592-13.2014

Luchicchi, A., Bloem, B., Viaña, J., Mansvelder, H., and Role, L. (2014). Illuminating the role of cholinergic signaling in circuits of attention and emotionally salient behaviors. *Front. Synaptic Neurosci.* 6:24. doi: 10.3389/fnsyn.2014.00024

Manz, K., Becker, J., Grueter, C., and Grueter, B. (2021). Histamine H(3) receptor function biases excitatory gain in the nucleus accumbens. *Biol. Psychiatry* 89, 588–599. doi: 10.1016/j.biopsych.2020.07.023

Mark, G., Shabani, S., Dobbs, L., and Hansen, S. (2011). Cholinergic modulation of mesolimbic dopamine function and reward. *Physiol. Behav.* 104, 76–81.

Mavridis, I. (2015). [The role of the nucleus accumbens in psychiatric disorders]. *Psychiatrike* 25, 282–294.

McCracken, C., and Grace, A. (2007). High-frequency deep brain stimulation of the nucleus accumbens region suppresses neuronal activity and selectively modulates afferent drive in rat orbitofrontal cortex *in vivo*. *J. Neurosci.* 27, 12601–12610. doi: 10.1523/JNEUROSCI.3750-07.2007

Miller, K., Prieto, T., Williams, N., and Halpern, C. (2019). Case studies in neuroscience: The electrophysiology of a human obsession in nucleus accumbens. *J. Neurophysiol.* 121, 2336–2340. doi: 10.1152/jn.00096.2019

Modell, J., Mountz, J., Curtis, G., and Greden, J. (1989). Neurophysiologic dysfunction in basal ganglia/limbic striatal and thalamocortical circuits as a pathogenetic mechanism of obsessive-compulsive disorder. *J. Neuropsychiatry Clin. Neurosci.* 1, 27–36. doi: 10.1176/jnp.1.1.27

Neumann, W., Huebl, J., Brücke, C., Gabriëls, L., Bajbouj, M., Merkl, A., et al. (2014). Different patterns of local field potentials from limbic DBS targets in patients with major depressive and obsessive compulsive disorder. *Mol. Psychiatry* 19, 1186–1192. doi: 10.1038/mp.2014.2

Nicola, S. (2010). The flexible approach hypothesis: Unification of effort and cue-responding hypotheses for the role of nucleus accumbens dopamine in the activation of reward-seeking behavior. *J. Neurosci.* 30, 16585–16600. doi: 10.1523/JNEUROSCI.3958-10.2010

Olsen, S., Basu, I., Bilge, M., Kanabar, A., Boggess, M., Rockhill, A., et al. (2020). Case report of dual-site neurostimulation and chronic recording of cortico-striatal circuitry in a patient with treatment refractory obsessive compulsive disorder. *Front. Hum. Neurosci.* 14:569973. doi: 10.3389/fnhum.2020.569973

Park, Y., Sammartino, F., Young, N., Corrigan, J., Krishna, V., and Rezai, A. (2019). Anatomic review of the ventral capsule/ventral striatum and the nucleus accumbens to guide target selection for deep brain stimulation for obsessive-compulsive disorder. *World Neurosurg.* 126, 1–10. doi: 10.1016/j.wneu.2019.01.254

Pennartz, C., Groenewegen, H., and Lopes da Silva, F. (1994). The nucleus accumbens as a complex of functionally distinct neuronal ensembles: An integration of behavioural, electrophysiological and anatomical data. *Prog. Neurobiol.* 42, 719–761. doi: 10.1016/0301-0082(94)90025-6

Pinto, A., Mancebo, M., Eisen, J., Pagano, M., and Rasmussen, S. (2006). The brown longitudinal obsessive compulsive study: Clinical features and symptoms of the sample at intake. *J. Clin. Psychiatry* 67, 703–711. doi: 10.4088/jcp.v67n0503

Pittenger, C. (2015). Glutamatergic agents for OCD and related disorders. *Curr. Treat. Opt. Psychiatry* 2, 271–283.

Rappel, P., Marmor, O., Bick, A., Arkadir, D., Linetsky, E., Castrioto, A., et al. (2018). Subthalamic theta activity: A novel human subcortical biomarker for obsessive compulsive disorder. *Transl. Psychiatry* 8:118. doi: 10.1038/s41398-018-0165-z

Raviv, N., Staudt, M., Rock, A., MacDonell, J., Slyer, J., and Pilitsis, J. G. (2020). A Systematic review of deep brain stimulation targets for obsessive compulsive disorder. *Neurosurgery* 87, 1098–1110.

Salamone, J., Correa, M., Farrar, A., and Mingote, S. (2007). Effort-related functions of nucleus accumbens dopamine and associated forebrain circuits. *Psychopharmacology* 191, 461–482. doi: 10.1007/s00213-006-0668-9

Salimpour, Y., Mills, K., Hwang, B., and Anderson, W. (2022). Phase- targeted stimulation modulates phase-amplitude coupling in the motor cortex of the human brain. *Brain Stimul.* 15, 152–163.

Saul'skaya, N., and Mikhailova, M. (2003). The effects of motivational and emotional factors in glutamate release in the nucleus accumbens of the rat brain during food consumption. *Neurosci. Behav. Physiol.* 33, 151–156. doi: 10.1023/a:1021769814069

Schüller, T., Gruendler, T., Jocham, G., Klein, T., Timmermann, L., Visser-Vandewalle, V., et al. (2015). Rapid feedback processing in human nucleus accumbens and motor thalamus. *Neuropsychologia* 70, 246–254. doi: 10.1016/j.neuropsychologia.2015.02.032

Schwabe, K., Alam, M., Saryyeva, A., Lütjens, G., Heissler, H., Winter, L., et al. (2021). Oscillatory activity in the BNST/ALIC and the frontal cortex in OCD: Acute effects of DBS. *J. Neural Transm.* 128, 215–224. doi: 10.1007/s00702-020-02297-6

Servaes, S., Glorie, D., Stroobants, S., and Staelens, S. (2019). Neuroreceptor kinetics in rats repeatedly exposed to quinpirole as a model for OCD. *PLoS One* 14:e0213313. doi: 10.1371/journal.pone.0213313

Sesia, T., Bulthuis, V., Tan, S., Lim, L., Vlamings, R., Blokland, A., et al. (2010). Deep brain stimulation of the nucleus accumbens shell increases impulsive behavior and tissue levels of dopamine and serotonin. *Exp. Neurol.* 225, 302–309. doi: 10.1016/j.expneurol.2010.06.022

Slutzky, M., and Flint, R. (2017). Physiological properties of brain-machine interface input signals. *J. Neurophysiol.* 118, 1329–1343. doi: 10.1152/jn.00070.2017

Smith, K., Tindell, A., Aldridge, J., and Berridge, K. (2009). Ventral pallidum roles in reward and motivation. *Behav. Brain Res.* 196, 155–167.

Smith, Y., and Villalba, R. (2008). Striatal and extrastriatal dopamine in the basal ganglia: An overview of its anatomical organization in normal and Parkinsonian brains. *Mov. Disord.* 23:S534–S547. doi: 10.1002/mds.22027

Szechtman, H., Ahmari, S., Beninger, R., Eilam, D., Harvey, B., Edemann-Callesen, H., et al. (2017). Obsessive-compulsive disorder: Insights from animal models. *Neurosci. Biobehav. Rev.* 76, 254–279.

Szechtman, H., Sulis, W., and Eilam, D. (1998). Quinpirole induces compulsive checking behavior in rats: A potential animal model of obsessive-compulsive disorder (OCD). *Behav. Neurosci.* 112, 1475–1485.

Tarazi, F., Campbell, A., Yeghiayan, S., and Baldessarini, R. (1998). Localization of ionotropic glutamate receptors in caudate-putamen and nucleus accumbens septi of rat brain: Comparison of NMDA, AMPA, and kainate receptors. *Synapse* 30, 227–235.

Tokuyama, S., Zhu, H., Oh, S., Ho, I., and Yamamoto, T. (2001). Further evidence for a role of NMDA receptors in the locus coeruleus in the expression of withdrawal syndrome from opioids. *Neurochem. Int.* 39, 103–109.

Tripathi, A., Prensa, L., Cebrián, C., and Mengual, E. (2010). Axonal branching patterns of nucleus accumbens neurons in the rat. *J. Comp. Neurol.* 518, 4649–4673.

Usuda, I., Tanaka, K., and Chiba, T. (1998). Efferent projections of the nucleus accumbens in the rat with special reference to subdivision of the nucleus: Biotinylated dextran amine study. *Brain Res.* 797, 73–93. doi: 10.1016/s0006-8993(98)00359-x

van Dijk, A., Klompmakers, A., Feenstra, M., and Denys, D. (2012). Deep brain stimulation of the accumbens increases dopamine, serotonin, and noradrenaline in the prefrontal cortex. *J. Neurochem.* 123, 897–903. doi: 10.1111/jnc.12054

van Dijk, A., Mason, O., Klompmakers, A., Feenstra, M., and Denys, D. (2011). Unilateral deep brain stimulation in the nucleus accumbens core does not affect local monoamine release. *J. Neurosci. Methods* 202, 113–118.

van Oudheusden, L., van de Schoot, R., Hoogendoorn, A., van Oppen, P., Kaarsemaker, M., Meynen, G., et al. (2020). Classification of comorbidity in obsessive-compulsive disorder: A latent class analysis. *Brain Behav.* 10:e01641.

Varatharajan, R., Joseph, K., Neto, S., Hofmann, U., Moser, A., and Tronnier, V. (2015). Electrical high frequency stimulation modulates GABAergic activity in the nucleus accumbens of freely moving rats. *Neurochem. Int.* 90, 255–260.

Vlček, P., Polák, J., Brunovskı, M., and Horáèek, J. (2018). Role of glutamatergic system in obsessive-compulsive disorder with possible therapeutic implications. *Pharmacopsychiatry* 51, 229–242.

Walaas, I. (1981). Biochemical evidence for overlapping neocortical and allocortical glutamate projections to the nucleus accumbens and rostral caudatoputamen in the rat brain. *Neuroscience* 6, 399–405. doi: 10.1016/0306-4522(81)90132-9

Wang, X., Li, M., Xie, J., Chen, D., Geng, X., Sun, S., et al. (2022). Beta band modulation by dopamine D2 receptors in the primary motor cortex and pedunculopontine nucleus in a rat model of Parkinson's disease. *Brain Res. Bull.* 181, 121–128. doi: 10.1016/j.brainresbull.2022.01.012

Winslow, J., and Insel, T. (1990). Neurobiology of obsessive compulsive disorder: A possible role for serotonin. *J. Clin. Psychiatry* 51, 27–31.

Wu, H., Tambuyzer, T., Nica, I., Deprez, M., van Kuyck, K., Aerts, J., et al. (2016). Field potential oscillations in the bed nucleus of the stria terminalis correlate with compulsion in a rat model of obsessive-compulsive disorder. *J. Neurosci.* 36, 10050–10059. doi: 10.1523/JNEUROSCI.1872-15.2016

Xie, Y., Heida, T., Stegenga, J., Zhao, Y., Moser, A., Tronnier, V., et al. (2014). High-frequency electrical stimulation suppresses cholinergic accumbens interneurons in acute rat brain slices through GABA(B) receptors. *Eur. J. Neurosci.* 40, 3653–3662. doi: 10.1111/ejn.12736

Yan, N., Chen, N., Zhu, H., Zhang, J., Sim, M., Ma, Y., et al. (2013). High-frequency stimulation of nucleus accumbens changes in dopaminergic reward circuit. *PLoS One* 8:e79318. doi: 10.1371/journal.pone.0079318

Yu, Y., Han, F., and Wang, Q. (2022). Exploring phase-amplitude coupling from primary motor cortex-basal ganglia-thalamus network model. *Neural Netw.* 153, 130–141. doi: 10.1016/j.neunet.2022.05.027

Zai, G. (2021). Pharmacogenetics of obsessive-compulsive disorder: An evidence-update. *Curr. Top. Behav. Neurosci.* 49, 385–398. doi: 10.1007/7854_2020_205

Zhan, Y., Xia, J., and Wang, X. (2020). Effects of glutamate-related drugs on anxiety and compulsive behavior in rats with obsessive-compulsive disorder. *Int. J. Neurosci.* 130, 551–560. doi: 10.1080/00207454.2019.1684276

Zhang, X., Peng, S., Shen, L., Zhuang, Q., Li, B., Xie, S., et al. (2020). Targeting presynaptic H3 heteroreceptor in nucleus accumbens to improve anxiety and obsessive-compulsive-like behaviors. *Proc. Natl. Acad. Sci. U.S.A.* 117, 32155–32164. doi: 10.1073/pnas.2008456117

Zhu, W., Wu, F., Li, J., Meng, L., Zhang, W., Zhang, H., et al. (2022). Impaired learning and memory generated by hyperthyroidism is rescued by restoration of AMPA and NMDA receptors function. *Neurobiol. Dis.* 171:105807. doi: 10.1016/j.nbd.2022.105807

frontiers | Frontiers in Cellular Neuroscience

TYPE Review
PUBLISHED 11 January 2023
DOI 10.3389/fncel.2022.1067570

OPEN ACCESS

EDITED BY
Zhen-Ni Guo,
First Affiliated Hospital of Jilin University, China

REVIEWED BY
Frederick Colbourne,
University of Alberta, Canada
Jun Yan,
Guangxi Medical University Cancer Hospital, China

*CORRESPONDENCE
Chencen Wang
✉ w1150988@163.com

SPECIALTY SECTION
This article was submitted to Cellular Neuropathology, a section of the journal Frontiers in Cellular Neuroscience

RECEIVED 12 October 2022
ACCEPTED 13 December 2022
PUBLISHED 11 January 2023

CITATION
Pan F, Xu W, Ding J and Wang C (2023) Elucidating the progress and impact of ferroptosis in hemorrhagic stroke.
Front. Cell. Neurosci. 16:1067570.
doi: 10.3389/fncel.2022.1067570

Elucidating the progress and impact of ferroptosis in hemorrhagic stroke

Feixia Pan[1], Weize Xu[1], Jieying Ding[2] and Chencen Wang[3]*

[1]Department of Cardiac Surgery, The Children's Hospital, Zhejiang University School of Medicine, National Clinical Research Center for Child Health, Hangzhou, China, [2]Department of Pharmacy, The Children's Hospital, Zhejiang University School of Medicine, National Clinical Research Center for Child Health, Hangzhou, China, [3]Department of Pediatrics, The First People's Hospital of Yongkang Affiliated to Hangzhou Medical College, Jinhua, China

Hemorrhagic stroke is a devastating cerebrovascular disease with high morbidity and mortality, for which effective therapies are currently unavailable. Based on different bleeding sites, hemorrhagic stroke can be generally divided into intracerebral hemorrhage (ICH) and subarachnoid hemorrhage (SAH), whose pathogenesis share some similarity. Ferroptosis is a recently defined programmed cell deaths (PCDs), which is a critical supplement to the hypothesis on the mechanism of nervous system injury after hemorrhagic stroke. Ferroptosis is characterized by distinctive morphological changes of mitochondria and iron-dependent accumulation of lipid peroxides. Moreover, scientists have successfully demonstrated the involvement of ferroptosis in animal models of ICH and SAH, indicating that ferroptosis is a promising target for hemorrhagic stroke therapy. However, the studies on ferroptosis still faces a serious of technical and theoretical challenges. This review systematically elaborates the role of ferroptosis in the pathogenesis of hemorrhagic stroke and puts forward some opinions on the dilemma of ferroptosis research.

KEYWORDS

stroke, intracerebral hemorrhage, subarachnoid hemorrhage, ferroptosis, target, lipid peroxidation

1. Introduction

Hemorrhagic stroke is an acute disease caused by the sudden rupture of a specific blood vessel in the brain. It refers to two main diseases based on bleeding sites: bleeding within brain parenchyma termed intracerebral hemorrhage (ICH) or within the subarachnoid space called subarachnoid hemorrhage (SAH) (Doria and Forgacs, 2019; Fang et al., 2020). Hemorrhagic stroke accounts for 10–20% of all strokes and is responsible for more than 40% of stroke-related deaths caused by severe primary and complicated secondary brain injury (Doria and Forgacs, 2019). Currently, the treatment of hemorrhagic stroke has not been well-established. Apart from the recognized supportive care, the efficacy of antihypertensive therapy, complication prevention, surgery, and hemostatic therapy to reduce primary brain injury remain controversial

(Grysiewicz et al., 2008; Xu Y. et al., 2022). Moreover, despite the considerable pre-clinical efficacy of several pharmacological agents targeting pathological events of hemorrhagic stroke, they failed to perform in clinical trials as factors such as the short half-life periods of agents and the role of the blood-brain barrier (BBB) complicated the scenario (Grysiewicz et al., 2008). Further efforts are necessary to develop potential drugs against novel pathological targets to facilitate functional recovery for hemorrhagic stroke patients. Numerous pathological processes during the secondary brain injury lead to the death of neuronal cells after hemorrhagic stroke. In addition to extensively researched apoptosis, many other modes of cell death, including ferroptosis, have been explored in ICH and SAH animal models in recent years (Fang et al., 2020; Shen et al., 2020).

Based on previous studies, Dixon et al. (2012), defined a mode of programmed cell death (PCD) caused by iron overload-dependent accumulation of lethal lipid peroxides as "ferroptosis" (Dixon et al., 2012). Morphologically, ferroptosis is characterized by mitochondrial shrinkage, loss of mitochondrial cristae, and increased mitochondrial membrane density. Biochemically, the ferroptosis-mediated changes include defective glutathione (GSH) activity, excessive accumulation of lethal lipid reactive oxygen species (ROS) on the plasma membrane, the inactivation of glutathione peroxidase 4 (GPX4), and the abnormal activation of some lipid metabolism regulatory molecules (Dixon et al., 2012; Stockwell et al., 2017; Wang et al., 2021). Before the concept was proposed, most of these ferroptosis-associated biochemical changes were detected in animal models of hemorrhagic stroke (Chang et al., 2014; Gao et al., 2020; Cao et al., 2021; Duan et al., 2021; Qu et al., 2021). Several recent studies have systematically examined these markers and monitored key targets regulating ferroptosis, confirming the presence of ferroptosis in hemorrhagic stroke diseases (Alim et al., 2019; Cao et al., 2021). More importantly, many studies demonstrated that inhibition or negative modulation of ferroptosis in neuronal cells was promising as a potential therapy for treating hemorrhagic stroke (Chang et al., 2014; Shao et al., 2019; Qu et al., 2021; Ren et al., 2022). However, limited by the objective reasons of experimental technological challenges, many critical issues still remain to be discussed and resolved. Therefore, in this review, we explored the current status of ferroptosis research advances in animal models of SAH and ICH. We also summarized the findings of the studies on the drugs or inhibitors targeting ferroptosis and further discussed their feasibility as potential therapies for treating hemorrhagic stroke.

Search strategy: A systematic search was implemented on two databases PubMed and Web of Science. The overall retrieval terms are "intracerebral hemorrhage AND ferroptosis," and "subarachnoid hemorrhage AND ferroptosis." In the part of Iron overload, retrieval terms "(intracerebral hemorrhage or subarachnoid hemorrhage) AND (iron OR iron disorder OR iron overload)" were used. In the part of Lipid peroxidation, retrieval terms "(intracerebral hemorrhage or subarachnoid hemorrhage) AND (lipid peroxidation OR reactive oxygen species)" were used. In the part of antioxidant system Lipid peroxidation, retrieval terms "(intracerebral hemorrhage or subarachnoid hemorrhage) AND (FSP1/CoQ10 OR GSH/GPX4)" were used. All the references were loaded into Zotero (version 5.0.96) and combined to exclude duplicate and triplicate.

2. Essential characteristics and mechanisms of ferroptosis

A decade before the term "ferroptosis" was defined, the basic features of ferroptosis were identified in quick succession (**Figure 1**). The two most used drugs for inducing ferroptosis, erastin, and Ras-selective lethal small molecules 3 (RSL3), were identified by the same research team in 2003 and 2008, respectively (Dolma et al., 2003; Yang and Stockwell, 2008). This group reported that they induce a form of PCD different from apoptosis. It was shown that iron chelator (deferoxamine) and certain antioxidants explicitly inhibit this type of cell death. Based on previous studies, Dixon et al. (2012) named this form of PCD as "ferroptosis" in 2012 and systematically described its biological, biochemical, and genetic characteristics. After about 5 years, studies from several different laboratories comprehensively summarized the morphological features of ferroptosis, which manifest as damaged mitochondria including mitochondrial shrinkage, reduced amounts of cristae, and outer membrane rupturing (Kagan et al., 2017). Mitochondrial structure monitoring by transmission electron microscope (TEM) is crucial for determining the occurrence of ferroptosis in the cells (Dixon et al., 2012). From the biochemical standpoint, ferroptosis involves a complex molecular biological network leading to the overproduction and accumulation of lipid peroxidation products and disrupting the antioxidant systems (Dixon et al., 2012; Stockwell et al., 2017). These include landmarks that are widely recognized by researchers like GPX4, SLC7A11 (xCT), and acyl-CoA synthetase long-chain family member 4 (ACSL4). Moreover, there are also many new targets that have been successively proven to be related to ferroptosis in recent years (Lei et al., 2022). In this review, we attempt to make a succinct summary of all such information below.

2.1. Disorders of iron metabolism

Ferroptosis is inhibited by iron chelators, which have led scientists to initially name it a new PCD with a root "ferr-" representing the then-popular belief that iron is indispensable in this process. However, this led to a misconception for future research, whereby people believed that ferroptosis must be accompanied by the disturbance of iron metabolism or even

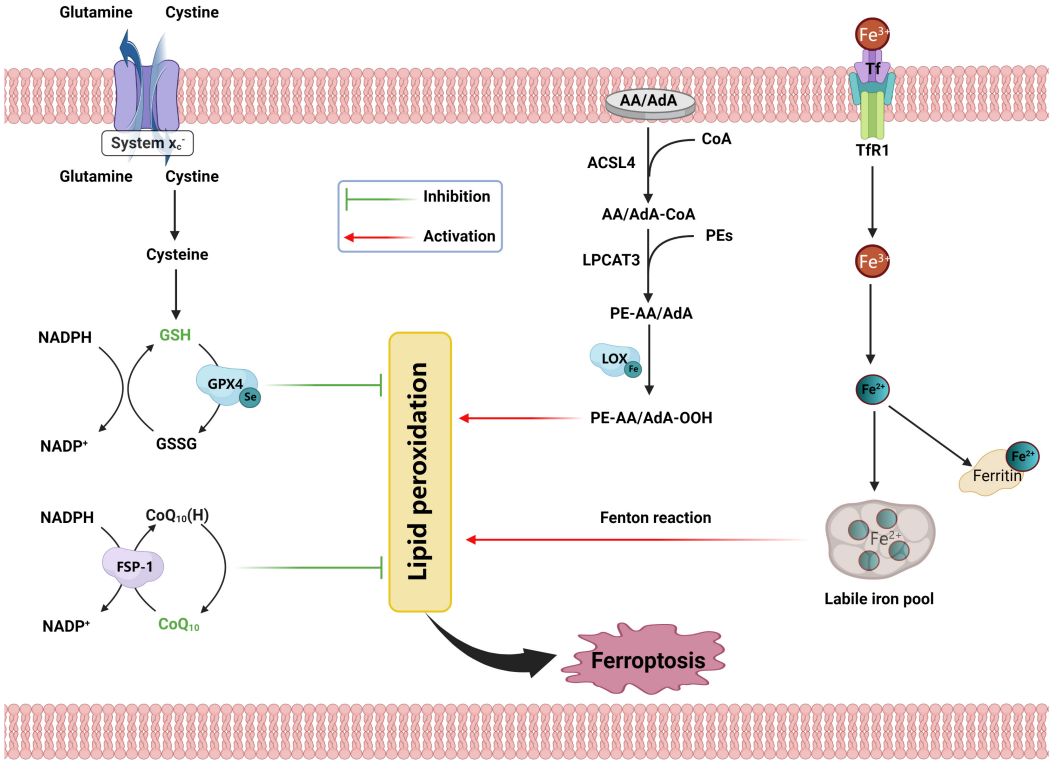

FIGURE 1
Schematic representation for the mechanism of ferroptosis, including antioxidant systems, iron disorder, and lipid peroxidation. SLC7A11, solute carrier family 7 member 11; SLC3A2, solute carrier family 3 member 2; GSH, glutathione; GSSG, oxidized glutathione; GPX4, glutathione peroxidase 4; NADPH, nicotinamide adenine dinucleotide phosphate; GPX4, glutathione peroxidase 4; CoQ10, coenzyme Q10; FSP1, ferroptosis suppressor protein 1; AA, arachidonic acid; AdA, adrenic acid; CoA, coenzyme A; ACSL4, acyl-CoA synthetase long-chain family member 4; AA/AdA-CoA, adrenic acid/arachidonic acid-CoA; PEs, phosphatidylethanolamines; LPCAT3, lysophosphatidylcholine acyltransferase 3; PE-AA/AdA, phosphatidylethanolamine-adrenic acid/arachidonic acid; LOX, lipoxygenase; PE-AA/AdA-OOH, phosphatidylethanolamine-adrenic acid/arachidonic acid bis/trioxide; Tf, transferrin; TFR1, transferrin receptor 1.

iron overload. Many subsequent landmark studies did not pay attention to iron metabolism-related factors because lethal lipid-related ROS and disruption of the antioxidant system are the key factors mediating ferroptosis (Li and Li, 2020). Moreover, the construction of many *in vitro* ferroptosis models does not depend on any form of iron (Ding et al., 2020; Liu et al., 2020). Despite no apparent link between iron overload and ferroptosis, substantial attention is warranted to investigate the possibility of ferroptosis during iron overload.

Under normal circumstances, ferrous ($Fe2^+$) ions from physiological or pathological origin get oxidized to ferric ($Fe3^+$) ions. They combine with free transferrin (TF), which is recognized by membrane protein transferrin receptor 1 (TFR1). Then the TF/TFR1 complex will be taken up in a manner of endocytosis. Because of the acidic environment in endosome, $Fe3^+$ will immediately be reduced to $Fe2^+$ by ferric reductase sixtransmembrane epithelial antigen of prostate 3 (STEAP3) after being released from TF (Louandre et al., 2013). After that, divalent metal transporter 1 (DMT1) transports $Fe2^+$ into the labile iron pool in the cytoplasm (Katsarou and Pantopoulos, 2020). It is noteworthy that ferroportin-1 (FPN1) on the cell membrane is currently the only known molecule to actively transport $Fe2^+$ from the intracellular to the extracellular region, maintaining the stability of the intracellular iron pool (Troadec et al., 2010). The change in the function or content of the above-mentioned iron regulatory molecules may cause the iron overload in cells, inducing ferroptosis. A recent study found that activation of nuclear receptor coactivator 4 (NCOA4) destabilizes ferritin in an autophagy-dependent manner, increasing the labile iron level and promoting ferroptosis (Zhang Y. et al., 2021).

2.2. Excessive accumulation of lipid peroxides

Lipid peroxides not removed in time are the most direct executors of ferroptosis. The following three pathways generate the free radical reactions mediating the formation of lethal lipid peroxides: (i) non-enzymatic Fenton reaction; (ii) iron-catalyzed auto-oxidation, and (iii) oxidase- and esterase-mediated peroxidation of polyunsaturated fatty acids (PUFA)

(Yang and Stockwell, 2016; Li and Li, 2020). The polyolefinic structure of PUFAs, especially arachidonic acid (AA) and adrenic acid (ADA), makes them susceptible to oxidation to form lipid peroxides. However, studies show that excess peroxidation of PUFAs (AA/ADA-OOH) does not explicitly indicate ferroptosis. AA/ADA must be catalyzed by acyl-CoA synthetase long-chain family member 4 (ACSL4) to form AA/ADA-CoA, followed by esterification into membrane phospholipids before becoming a crucial precursor of lethal lipid-related ROS (Kagan et al., 2017; Wenzel et al., 2017). Two independent groups have implicated using lipid metabolomics screening that the product of phosphatidylethanolamines (PEs)-AA/ADA, namely, PEs-AA/ADA-OOH, oxidized by lipoxygenase, as the critical substance mediating ferroptosis. There are numerous ways of catalyzing PEs-AA/ADA to form peroxides (Kagan et al., 2017; Wenzel et al., 2017). It has been shown that the rate-limiting steps in acetylation and esterification make ACSL4 and lysophosphatidylcholine acyltransferase 3 (LPCAT3) the critical promoters in the regulation of ferroptosis (Feng et al., 2022). Multiple studies have confirmed the roles of these enzymes. Numerous recent studies have indicated how inhibition of ACSL4 and LPCAT3 might be promising therapeutic strategies for treating ferroptosis-related injuries (Cui et al., 2021a; Sha et al., 2021; Reed et al., 2022). However, how PEs-AA/ADA-OOH relay the signals for ferroptosis remains to be interpreted. Plausible underlying mechanisms include binding excess lipid peroxides to the membrane, causing lethal changes in membrane permeability and ion concentrations. It is also believed that the downstream products of these lipid peroxides, like malondialdehyde (MDA) and 4-hydroxy-nonenal (4-HNE), exert ferroptotic damage by degrading proteins or nucleic acids (Liu et al., 2020, 2021). Many studies have implicated MDA and 4-HNE as markers of ferroptosis.

2.3. GSH/GPX4 antioxidant system

GPX4 is an important peroxide-decomposing enzyme ubiquitously present in the body. GSH can complete the conversion of lipid peroxides to non-toxic lipids (Fraternale et al., 2009). This property protects cell membranes made up of large lipid molecules from peroxides interference and damage. GSH/GPX4 antioxidant system is one of the most crucial endogenous factors against ferroptosis (Li F. et al., 2022). GSH is synthesized by three amino acids: glutamate, cysteine, and glycine. Cysteine, mainly derived from extracellular cystine after entering the cell and being reduced, is present in the lowest concentration in the cell, making it the critical rate-limiting factor for the *de novo* synthesis of GSH. The cystine/glutamate antiporter (system X_C^-) on the cell membrane transports the extracellular cysteine into the cell in a 1:1 form while transporting out the intracellular glutamate (Yuan Y. et al., 2022). The system X_C^- on the cell membrane is a heterodimer consisting of the substrate-specific subunit SLC7A11 (xCT) and the regulatory subunit SLC3A2 (Koppula et al., 2021). GPX4 converts the reduced form of GSH into oxidized glutathione (GSSG) and promotes the reduction reaction from lipid peroxides (L–OOH) to corresponding alcohols (L–OH) (Li F. et al., 2022).

In many pathological conditions or artificial interventions, increased extracellular glutamate and disrupted xCT structure or function lead to intracellular GSH depletion, thereby inducing ferroptosis (Chen et al., 2017; Yadav et al., 2021). Meanwhile, the down-regulation or functional disruption of GPX is also essential for promoting ferroptosis. The most used inducers of ferroptosis, erastin, and RSL3, are inhibitors of system X_C^- and direct inhibitors of GPX4, respectively (Stockwell et al., 2017). In addition, there are many compounds that can induce ferroptosis by inhibiting GPX4, like DPI7 and DPI10 in a directing binding manner and FIN56 in a form that induces GPX4 degradation (Mou et al., 2019; Sun et al., 2021). On the other hand, selenium promotes GPX4 transcription and prevents it from irreversible degradation, thereby inhibiting ferroptosis (Alim et al., 2019; Yao et al., 2021). Increasing evidence delineate the role of the GSH/GPX4 antioxidant system in the mechanism of ferroptosis.

2.4. FSP1/CoQ10 and its related antioxidant system

The ferroptosis suppressor protein 1 (FSP1)/coenzyme Q10 (CoQ10) pathway is another efficient endogenous antioxidant system independent of GPX4/GSH system, that critically regulates cellular sensitivity toward ferroptosis. FSP1, alternatively known as apoptosis-inducing factor mitochondria 2 (AIFM2), has significantly high homology with apoptosis-inducing factor (AIF) (Miriyala et al., 2016). The name and homology details of AIFM2 indicate how it was identified by its function to induce apoptosis by releasing cytochrome c and caspase 9 (Miriyala et al., 2016). However, a recent study found that AIFM2 had a marked inhibitory effect on GPX4 deficiency that leads to ferroptosis, renamed "FSP1" (Doll et al., 2019). The lethal lipid peroxidation event in ferroptosis mainly starts at the plasma membrane, leading to the transfer of FSP1 by myristoylation for subsequent free radical scavenging (Doll et al., 2019). FSP1 uses the reducing equivalents of nicotinamide adenine dinucleotide phosphate [NAD(P)H] to reduce CoQ10 to ubiquinol, which acts as a lipophilic radical-trapping antioxidant (RTA) to remove lipid peroxides from phospholipid bilayers (Bersuker et al., 2019).

NAD(P)H is also indispensable for reducing GSSG to GSH. Therefore, involved in two important antioxidant systems, the level of NAD(P)H have also been indicated by several studies as a predictor of cellular susceptibility to ferroptosis

(Bersuker et al., 2019). This molecular crosstalk means that the intracellular defenses against lipid peroxides are not dependent on a single system. FSP1 was also recently reported to inhibit ferroptosis in endosomal required transport (ESCRT)-III-dependent manner (Dai et al., 2020). ESCRT-III is a membrane-associated protein complex enhancing plasma membrane repair by activating subtypes of charged multivesicular body proteins (Dai et al., 2020). In addition, tetrahydrobiopterin (BH4) and its synthetic rate-limiting enzyme Guanosine triphosphate cyclohydrolase 1 (GCH1) are involved in the ferroptosis-resistant oxidative network by regulating CoQ10 synthesis (Mishima and Conrad, 2022). However, more investigation is required to confirm these systems' effectiveness and underlying mechanisms.

3. The role of ferroptosis in hemorrhagic stroke

According to the bleeding site, a hemorrhagic stroke can be divided into two subtypes, ICH and SAH (Doria and Forgacs, 2019). Their pathological mechanisms occur in two steps and involve multiple similarities. The first stage involves primary brain injury dominated by mechanical damage caused by the traction of the hematoma, accompanied by increased intracranial pressure and secondary cerebral infarction (Magid-Bernstein et al., 2022). The second stage consists of pathophysiological events caused by blood components and their metabolites, including BBB destruction, neural excitatory events, ion disturbances, oxidative stress, neuroinflammation, cell death, etc (Magid-Bernstein et al., 2022). In SAH, early brain injury (EBI) is crucial, indicating the pathological damage within 3 days after SAH (Kusaka et al., 2004; Fujii et al., 2013). The recovery degree of the pathological damage during EBI will substantially impact the recovery of subsequent neurological functions.

Several animal models were adopted for hemorrhagic stroke research. For ICH, collagenase injection or autologous blood injection at the basal ganglia are two common modeling methods (Krafft et al., 2012; Lei et al., 2014). The former causes cerebral hemorrhage by decomposing collagen on the cell matrix and vascular basement membrane, which has the advantage of high efficiency and convenience. While the latter can better simulate the pathophysiological changes of patients with cerebral hemorrhage. For SAH, the endovascular perforation model is widely used because it can simulate SAH caused by rupture of aneurysm (Du et al., 2016). These models can cause a large amount of instantaneous hemorrhage in specific regions of the brain, and are valuable experimental models of hemorrhagic stroke in preclinical research.

Degradation products of hemoglobin (ferrous iron and heme) play an essential initiating role in the induction of these pathophysiological events. Among them, the abnormal accumulation of iron ions leads to severe tissue damage (Gaasch et al., 2007). It generates a large amount of ROS, providing a solid foundation for ferroptosis to set in Gaasch et al. (2007). This validates the hypothesis that ferroptosis plays a critical pathological role after a hemorrhagic stroke. A series of subsequent studies also confirmed the occurrence of ferroptosis in animal and *in vitro* models of ICH and SAH (Karuppagounder et al., 2018; Chen et al., 2019; Cao et al., 2021; Qu et al., 2021). Li et al. (2018) first observed specific mitochondrial morphology of ferroptosis in perihematoma neurons in a collagenase-induced mouse ICH model. Then in 2020, ferroptotic mitochondria were first observed in temporal cortical neurons in a mouse model of SAH (Li Y. et al., 2021). The TEM pictures of mitochondria provide strong evidence supporting ferroptosis. In addition, the down-regulation of the antioxidant molecule GPX4 and upregulation of ACSL4 and lipid peroxides were also validated in these two models by various groups (Zhang et al., 2018; Gao et al., 2020; Jin et al., 2021; Qu et al., 2021). These results demonstrate how ferroptosis, an essential complement to other PCDs, plays a vital role in hemorrhagic stroke. Moreover, two critical inhibitors of ferroptosis, Ferrostatin-1 (fer-1) and Liproxstatin-1 (Lip-1), inhibited neuronal ferroptosis and neuroinflammation in animal models of hemorrhagic stroke, reducing neurological impairment (Li et al., 2017a; Zhang et al., 2018; Cao et al., 2021). In addition, various chemical agents and natural medicines improve neurological damage in animals with ICH or SAH by inhibiting ferroptosis, suggesting ferroptosis as a promising potential target for therapeutic strategies for hemorrhagic stroke (Li et al., 2019; Duan et al., 2021; Gao et al., 2022).

However, the knowledge about ferroptosis in hemorrhagic stroke is still minimal. To achieve clinical translation, sufficient preclinical experiments must identify effective therapeutic agents and the exact molecular mechanisms.

4. Crosstalk between ferroptosis and other PCDs in hemorrhagic stroke

In addition to ferroptosis, other PCDs such as apoptosis, pyroptosis, necroptosis, and autophagy are also widely studied in the field of hemorrhagic stroke. There are also various crosstalk between ferroptosis and these PCDs. Apoptosis is the most well-studied forms of PCD in hemorrhagic stroke, which mainly induced by two pathways: extrinsic and intrinsic pathways (Sekerdag et al., 2018). The characteristic features of apoptotic neuron include chromatin condensation, nuclear shrinkage, and DNA fragmentation, which is completely different from ferroptosis (Weiland et al., 2019). Hence, apoptosis, being considered as the main form of neuronal death after hemorrhagic stroke, is mainly studied as an exclusionary form in iron death related studies. A recent study suggests

that there may be a certain correlation between ferroptosis and necroptosis through NADPH (Hou et al., 2019). Since autophagy can regulate intracellular iron homeostasis and ROS synthesis, current research indicates that many ferroptosis are autophagic dependent (Ma et al., 2022; Tao et al., 2022). The latest research of Tao et al. (2022) indicates that S100A8 can mediate autophagy-dependent ferroptosis of microglia after SAH. In addition, mitophagy has also been reported to mediate ferroptosis (Li J. et al., 2022), which has not been verified in hemorrhagic stroke, indicating it may be a valuable research direction in the future.

5. The research status in ferroptosis in hemorrhagic stroke

Subarachnoid hemorrhage (SAH) and intracerebral hemorrhage (ICH) share many pathological similarities, and similar hypotheses have been formed to identify the mechanism of ferroptosis in these two hemorrhagic strokes. However, to date, the underlying mechanisms of ferroptosis have not been understood to the same extent in ICH and SAH, triggered by differential research investments. Because the incidence of SAH is much lower than ICH worldwide, the progress of basic research in decoding the mechanisms of ferroptosis is also relatively inadequate in SAH (Doria and Forgacs, 2019). However, the advances in research to decode ferroptosis mechanisms in SAH have not been summarized. Therefore, in this part, we will systematically review the research progress in understanding ferroptosis mechanisms in ICH and SAH.

5.1. Iron overload in ICH

The direct accumulation of blood components in the injured area is a critical pathogenic symptom of hemorrhagic disease. Therefore, since the discovery of ICH, researchers have long been critically concerned about the disturbance of iron metabolism (Uselis, 1970). As early as 2004, a study identified iron deposition in the basal ganglia in a rat model of ICH (Nakamura et al., 2004). This deposited iron is mainly derived from the lysed red blood cell hemoglobin, which is degraded into heme and free iron. In addition, Nakamura et al. (2005) indicated that holo-transferrin interacts with thrombin to exacerbate brain damage upon the onset of ICH. Iron accumulation and ferritin upregulation also cause long-term neurological impairment in animal models of ICH (Nakamura et al., 2005). Deferoxamine (DFO) is a drug that eliminates iron accumulation and has been validated by multiple research groups in various animal models. Its therapeutic mechanism has been hypothesized to involve DNA oxidative damage repair, neuronal apoptosis inhibition, and brain edema reduction (Farr and Xiong, 2021). In addition, Zhao et al. (2011) reported another potent iron chelator, minocycline, which alleviates neuronal apoptosis after ICH by inhibiting the pathways that upregulate iron handling proteins of the brain. DFO and minocycline have been selected for clinical trials because of their excellent efficacy in animal experiments. Unfortunately, no drug targeting iron chelation has successfully achieved clinical translation (Selim et al., 2011). Moreover, the specific mechanism underlying cellular damage due to ROS generation by iron overload has not been elucidated.

Introducing the concept of ferroptosis provides insights into a new pathogenic mechanism of iron-mediated diseases, encouraging researchers to delve deep into it. Hemorrhage leads to iron deposition and regulates iron's entry and exit pathways by several vital molecules, including TF, TFR1, DMT1, and FPN1 (Vogt et al., 2021). Hepcidin has received more attention in recent years due to its ability to change intracellular iron content by regulating the expression of TF, TFR1, DMT1, and FPN1 (Camaschella et al., 2020). TF, TFR1, and DMT1 are responsible for iron uptake, while FPN1 is the only regulatory molecule aiding in the transport of iron out of the cells (Vogt et al., 2021). Yang et al. (2021) have demonstrated how ICH mice exhibited less iron overload, brain edema, and neuronal damage after adeno-associated virus-mediated overexpression of hepcidin. Down-regulating TF and TFR1 mainly achieve this effect after ICH. In recent years, many new iron chelators have been tested on animal models of ICH and achieved considerable preclinical efficacy. VK-28, Deferiprone (DFP), and Deferasirox (DFX) are some representative drugs (Wang et al., 2016; Li et al., 2017b; Imai et al., 2021). However, it is worth pointing out that although most studies of ferroptosis in ICH involve some iron deposition, few studies have directly explored the association between iron deposition and ferroptosis. We believe this action stems from the lack of a specific mechanism of iron-mediated ferroptosis.

The STICH II trial showed that withdrawal after open surgery didn't significantly reduce the mortality of cerebral hemorrhage compared with the initial conservative treatment (Mendelow et al., 2013). However, the subgroup of MISTIE III trial showed that compared with the conservative treatment group, the patients whose blood clot size decreased less than 15 ml after minimally invasive surgery live with better neurological recovery (Hanley et al., 2019). In addition to iron chelating agent drugs, surgical removal of hematoma or endogenous phagocytosis of ectopic erythrocyte from the source to reduce the degradation products of erythrocyte are effective treatments for hemorrhagic stroke (Zheng et al., 2022). The phagocytosis of erythrocytes is mainly completed by microglia and macrophages, which are regulated by several signal pathways. Peroxisome proliferator-activated receptor γ (PPAR-γ) is one of the most widely studied regulatory molecules, and its activation can promote the phagocytosis of microglia on hematoma. Drugs including monascin, simvastatin, wogonin can activate PPAR-γ, thus promoting phagocytosis (Wang et al., 2018; Fu et al., 2020; Zhuang et al., 2021). In addition, the activation of nuclear factor erythroid 2-related

factor2 (Nrf2) pathway has also been proved to promote hematoma phagocytosis (Zheng et al., 2022). Xu C. et al. (2022) demonstrated that CD47 also plays an important role in the process of hematoma phagocytosis in the SAH model.

5.2. Iron overload in SAH

Before the concept of early brain injury was proposed, the academic research on the pathogenesis of SAH mainly focused on secondary ischemia caused by vasospasm (Lin et al., 2004). In 1988, the non-glucocorticoid 21-aminosteroid U74006F, an inhibitor of iron-dependent lipid peroxidation, alleviated the acutely progressive hypoperfusion state in a cat SAH model (Hall and Travis, 1988). In the early 1990s, Utkan et al. (1996) demonstrated for the first time that the iron chelator DFO could prevent SAH-induced vasospasm in a rabbit model (Utkan et al., 1996). They also hypothesized that the underlying mechanism might involve the inhibition of iron-induced ROS and lipid peroxides (Utkan et al., 1996). Subsequent studies have repeatedly demonstrated the reduction of vasospasm by iron chelation (Luo et al., 1995). Smith et al. (1996) primarily focused on iron-induced neuronal damage. They elucidated how a lipid peroxidation inhibitor, tirilazad mesylate (U-74006F), and its metabolites attenuated early BBB damage and attenuated iron-induced neuronal lipid peroxidative damage. This may be the earliest proof of the underlying mechanism of ferroptosis in hemorrhagic stroke.

Similar to studies on ICH, around 2004, researchers systematically studied the metabolism and role of hemoglobin, heme, and iron in SAH and also pointed out the predictive effect of serum ferritin content on the severity of SAH (O'Connell and Watson, 2003; Suzuki et al., 2003). In addition, the up-regulation of TF and TFR1 and ferritin in brain tissue was also verified by Lee et al. (2010) in a rat model of SAH. Their team also showed that iron overload in the acute phase of SAH leads to oxidative stress and neuronal damage, which can be reversed by the application of DFO (Lee et al., 2010). However, since the advent of the concept of ferroptosis, few studies have systematically verified the association between iron overload and cellular ferroptosis in SAH models. Moreover, no study has investigated the neurological rescue effect of various iron chelators achieved by inhibiting ferroptosis. However, many studies have reported a positive correlation between iron accumulation and ferroptosis in ischemic stroke. One study indicated that tau-mediated iron export could reduce ferroptosis after ischemic stroke (Tuo et al., 2017). Mitochondrial ferritin has also been upregulated in the brain of mice with ischemic stroke upon FPN1 upregulation to attenuate ferroptosis and achieve neuroprotective effects (Wang P. et al., 2022). Recently, Zhang H. et al. (2021) pointed out that hepcidin can promote ferroptosis after SAH by regulating iron metabolism, and this effect may be performed by upregulating DMT1. Their research on iron metabolism regulation lacks comprehensiveness, warranting more in-depth studies to explore the correlation between iron overload and ferroptosis.

5.3. Lipid peroxidation in ICH

Oxidative stress is essential in ICH pathogenesis, primarily mediated by excessive accumulation of ROS and reactive nitrogen species (RNS) (Li et al., 2011). ROS is a group of partially reduced oxygen-containing molecules or radicals, and its simple form mainly includes hydrogen peroxide (H_2O_2) and some radicals such as hydroxyl radical (·OH) and superoxide anion (O^{2-}) (Zhu et al., 2021). Lipid peroxidation involves ROS-mediated electron loss, forming various reactive intermediates. Before introducing the concept of ferroptosis, numerous studies demonstrated how ROS and end-products of lipid peroxidation like MDA damage proteins and DNA, resulting in cell injury (Wang et al., 2011). Some classic antioxidant drugs, such as metformin and melatonin, provide neuroprotective effects to ICH mice by reducing ROS and MDA levels (Lekic et al., 2010; Wu et al., 2016). However, the mechanisms underlying the pathogenicity of lipid peroxides remain unclear. The synthesis of lipid peroxides relies on several specific regulatory processes, which are thought to be critical factors regulating the initiation of ICH ferroptosis.

The high level of PUFAs in the brain is beneficial for inducing ferroptosis signaling in ICH. 20-hydroxyeicosatetraenoic acid (20-HETE), a metabolite of ADA, was recently shown to be involved in neuronal ferroptosis upon ICH induction in mice (Han et al., 2021). And reduction of its production with the specific inhibitor HET0016 significantly inhibited lipid peroxidation levels and cell death in an *in vitro* model of ICH (Han et al., 2021). This significantly contributed to research on lipid peroxidation in ferroptosis after ICH due to limited previous research exploring this direct relationship. Previous studies indicated that N-acetylcysteine could neutralize the peroxidative toxicity of arachidonic acid catalyzed by 5-lipoxygenase to inhibit ferroptosis after ICH (Karuppagounder et al., 2018). Moreover, baicalin, a non-specific inhibitor of 12/15-lipoxygenase, significantly increases the detection indices related to ferroptosis after ICH (Duan et al., 2021), suggesting that 12/15-lipoxygenase may play a critical role in the process of ferroptosis after ICH.

ACSL4 has also been implicated in the process of ferroptosis in ICH by two recent independent studies (Chen et al., 2021; Jin et al., 2021). It is highly expressed in the brain tissue surrounding the hematoma of ICH mice. Moreover, ACSL4 can also be regulated by long non-coding RNAs (LncRNAs). LncRNA H19 positively regulates ACSL4 expression upon ICH onset (Chen et al., 2021). Another study pointed out that LncRNA HOX transcript antisense RNA (HOTAIR) can bind to UPF1 to degrade ACSL4, thereby inhibiting ferroptosis and the impairment of neurological function in ICH mice (Jin et al., 2021).

5.4. Lipid peroxidation in SAH

As early as the 1980s, a team led by Asano explored the roles of lipid peroxides in SAH (Suzuki et al., 1983). They used a combination of high-performance liquid chromatography (HPLC) and gas chromatography-mass spectrometry (GC-MS) techniques to identify hydroperoxy HETEs (HPETEs) and HETEs in the cerebrospinal fluid (CSF) of SAH patients as well as healthy individuals (Suzuki et al., 1983). The results showed that compared with the average population, the content of 5-HETE in the CSF of SAH patients was significantly increased. However, the knowledge about SAH at that time led them to hypothesize that the content of this 5-HETE was related to the degree of vasospasm (Suzuki et al., 1983). Their follow-up studies also showed that 5-HETE levels were also elevated in the walls of blood vessels and the temporal cortex adjacent to SAH blood clots (Sakaki et al., 1986). Later, another group reported the up-regulation of another class of lipid peroxides, phosphatidylcholine hydroperoxide, and cholesteryl ester hydroperoxide, in the CSF of SAH patients (Kamezaki et al., 2002). However, our current knowledge indicates that neither of these two lipid peroxides mediates ferroptosis. After an extended period, there has been a lacuna in studies on lipid peroxidation in patients or animals with SAH. It is worth pointing out that 5-HETE is formed when 5-lipoxygenase catalyzes ADA (Stockwell et al., 2017). Unfortunately, no studies have investigated the mechanism of action and role of 5-lipoxygenase in SAH. In animal models of ICH and ischemic stroke, 5-lipoxygenase has been demonstrated to induce ferroptosis induction critically. 15-lipoxygenase performs a similar function as 5-lipoxygenase, only differing in the site of oxidized PUFAs (Çolakoğlu et al., 2018). It is highly expressed in microglia upon the onset of SAH. Reduction of 15-lipoxygenase level by drug application inhibits microglial ferroptosis (Gao et al., 2022). Moreover, applying its inhibitor baicalin can reduce ferroptosis after SAH and thus alleviate EBI (Zhang et al., 2020). Such lines of research on lipoxygenase may be valuable in depicting SAH pathogenesis.

Qu et al. (2021) verified the essential role of ASCL4 in ferroptosis induction in the SAH mice model for the first time. They found that the down-regulation of ACSL4 significantly inhibits lipid peroxidation and neurological damage in SAH. Two subsequent studies also examined the role of ACSL4 as a protein-level biomarker for ferroptosis (Huang et al., 2022; Yuan B. et al., 2022). The alteration of ASCL4 has higher stability than other marker molecules and has a better significance in detection. This characteristic has been confirmed in various disease models.

5.5. Antioxidant system in ICH

Moreover, GSH/GPX antioxidant system received attention simultaneously as more studies on lipid peroxidation were performed. In the ICH disease model, the role of GSH was first revealed by the team led by Dhandapani, who successively reported that GSH depletion leads to cell damage and death in hemin-induced astrocytes and endothelial cells (Laird et al., 2008; Sukumari-Ramesh et al., 2010). However, these forms of cell death do not accord with the features of ferroptosis. Zhang et al. (2018), for the first time, explored the expression changes and effects of GPX4 in a mouse model of ICH and showed how its levels in mouse brain tissue surrounding the hematoma were significantly reduced 2 days after ICH. Moreover, overexpression of GPX4 with adeno-associated virus significantly attenuated neuronal cell death and improved mice behavior (Zhang et al., 2018). Unfortunately, the identification of ferroptosis was not rigorous enough. In 2019, a cellular study found that selenium upregulates GPX4 by activating the transcription factors TFAP2c and Sp1 of GPX4 (Alim et al., 2019). Upregulated GPX4 can protect neurons from ferroptosis. They reported that GPX4 was upregulated in hemin-induced primary neurons, which may be related to the negative feedback regulation after ferroptosis. GSH and GPX have been repeatedly verified as critical negative regulators of oxidative stress in subsequent ICH studies. Most studies demonstrated how GSH content and the expression of GPX4 are downregulated, subject to reversing by regulating antioxidant drugs like dauricine or microRNAs to exert neuroprotective effects (Zhang et al., 2018; Peng et al., 2022).

A recent study showed in the FSP1/CoQ10 antioxidant system that the level of FSP1 was significantly reduced in the brain tissue surrounding hematomas in ICH mice, which could be treated with the drug dexpramipexole to reverse this harmful change (Wang B. et al., 2022). However, the expression pattern and the underlying mechanism with the potential role of CoQ10 have not been adequately investigated.

5.6. Antioxidant system in SAH

In SAH, the GSH/GPX4 antioxidant system research has been significantly more robust than in ICH, due to the early successful identification of lipid peroxides in CSF and the correlation between its content and disease prognosis (Suzuki et al., 1983; Sakaki et al., 1986). Lipid peroxidation in CSF also revealed decreased GPX activity and decreased GSH content in CSF of SAH patients (Suzuki et al., 1983). Another animal experiment showed reduced superoxide-dismutase (SOD) and GPX levels could be observed in the hippocampus of the SAH rat model (Sakaki et al., 1986). Based on such observations, the imbalance of this antioxidant system in the temporal cortex of SAH patients have also been elucidated.

Moreover, a multicenter, double-blind clinical trial showed how a seleno-organic compound, ebselen, alleviate neurological deficits in SAH patients through a GPX-like mechanism of

TABLE 1 Ferroptosis in different cell types in the central nervous system (CNS).

Disease model	Cell type	Means for identification	Potential mechanisms	References
Collagenase-induced mouse model of ICH; Hemin-induced primary cortical neurons.	Neuron	***In vivo:*** FJB staining; Measurement of eicosanoids; Metabolic analysis of lipoxygenase. ***In vitro:*** Adenoviral overexpression of antioxidant enzymes; Measurement of eicosanoids.	Neuronal ferroptosis may be involved in neurological impairment after ICH.	Karuppagounder et al., 2018
Collagenase-induced mouse model of ICH; Hb/ferrous iron-induced OHSCs.		***In vivo:*** FJB/FJC staining; PI staining; TEM; Perls' staining; Biomarker analysis (COX-2; GPX-4); 4-HNE and MDA measurement. ***In vitro***: DIPY 581/591 C11; Biomarker analysis.	Neuronal ferroptosis may contribute to neurological defects after ICH; Fer-1 treatment can alleviate neuronal ferroptosis.	Li et al., 2017a
Endovascular perforation mouse model of SAH; Hemin-induced HT22 cells.		***In vivo:*** FJC staining; GSH, GPX4, MDA measurement; TEM; Biomarker analysis (ACSL4; GPX-4; xCT; COX-2). ***In vitro:*** Cell viability analysis; Mitochondrial functions evaluation; DIPY 581/591 C11.	Neuronal ferroptosis may contribute to neurological defects after SAH; Lip-1 treatment can alleviate neuronal ferroptosis.	Cao et al., 2021
Endovascular perforation rat model of SAH; Oxyhemoglobin-induced SH-SY5Y cells.		***In vivo:*** FJC staining; GSH and GPX4 activity measurement; TEM; Biomarker analysis (GPX-4; FPN; TfR1); Iron stain assay. ***In vitro:*** Cell viability analysis; DIPY 581/591 C11.	Neuronal ferroptosis may contribute to neurological defects after SAH; Fer-1 treatment can alleviate neuronal ferroptosis.	Li Y. et al., 2021
Endovascular perforation mouse model of SAH; Hemin-induced BV2 cells.	Microglia	***In vivo:*** GSH, GPX4 activity, and MDA measurement; TEM; Biomarker analysis (ALOX-15; GPX-4; xCT); ***In vitro:*** Cell viability analysis; DIPY 581/591 C11.	M2-type microglia may be more sensitive to ferroptosis after SAH than M1-type microglia.	Gao et al., 2022
I.p. injection of LPS -induced inflammation model; LPS-induced primary neonatal microglia.		***In vivo:*** DCFH-DA for intracellular ROS; MDA measurement. ***In vitro:*** Cell viability analysis; LDH release assay; DIPY 581/591 C11.	RSL3 inhibited LPS-induced inflammation of microglia in a Nrf2-dependent way.	Cui et al., 2021b
Endovascular perforation rat model of SAH; Oxyhemoglobin-induced BV2 microglia.		***In vivo:*** FJB staining; MDA measurement; Biomarker analysis (GPX-4; FPN; Tf; xCT; TfR1; COX-2). ***In vitro:*** Cell viability analysis; DIPY 581/591 C11.	Upregulated iNOS may mediate the defense effect of M1-type microglia against ferroptosis after SAH.	Qu et al., 2022
I.v. injection of autologous blood induced IVH model; Hemin induced primary OPCs.	Oligodendrocyte progenitor cells	***In vivo:*** PI staining; Perls' staining; TEM; Biomarker analysis (GPX-4; xCT; COX-2); ***In vitro:*** GSH and GPX4 activity measurement; DIPY 581/591 C11.	Ferroptosis is the primary cell death form in Hemin-induced and hemorrhagic stroke-induced OPCs death.	Shen et al., 2022
Autologous blood-induced mouse model of ICH.	Oligodendrocytes	***In vivo:*** Dihydroethidium staining for ROS identification; Perls' staining; MDA measurement; TEM; Biomarker analysis (FSP1; GPX-4).	Some degree of ferroptosis in oligodendrocytes after ICH, which can be alleviated by treatment with dexpramipexole.	Wang B. et al., 2022
RSL-3 induced ONL-93 oligodendrocytes.		***In vitro:*** PI staining; Cell viability analysis; ROS identification; Biomarker analysis (ACSL4; xCT; GPX4; FSP1); GSH, GPX4 activity, and MDA measurement; Mitochondrial lipid peroxidation detection.	Lip-1 can inhibit RSL-3-induced ferroptosis in ONL-93 oligodendrocytes by upregulating GPX4.	Jhelum et al., 2020
Mbp knockout *Shiverer* mice; Primary Oligodendrocytes from Pelizaeus-Merzbacher patient.		***In vivo:*** Click-iT® lipid peroxidation detection; TEM; CellROX® ROS sensor; Biomarker analysis (GPX-4; FPN; Tf; xCT; TfR1). *In vitro*: CellROX® ROS sensor; Biomarker analysis.	Iron Chelation can reduce oligodendrocyte ferroptosis in Pelizaeus-Merzbacher disease.	Nobuta et al., 2019
APP/PS1 double-transgenic mice	Astrocyte	***In vivo:*** Mitochondrial ROS analysis; GSH, the ratio of GSH/GSSG and GSSG	Astrocyte ferroptosis in Alzheimer's disease is promoted by upregulated NADPH oxidase 4.	Park et al., 2021

(Continued)

TABLE 1 (Continued)

Disease model	Cell type	Means for identification	Potential mechanisms	References
model of AD.		measurement; glutamate-cysteine ligase catalytic subunit measurement.		
Angiotensin II-induced primary astrocyte.		***In vitro:*** Cell viability analysis; Biomarker analysis (GPX-4; Nrf2; HO-1; COX-2); LDH release assay; Intracellular total iron assay.	Fer-1 reduced Angiotensin II-induced ferroptosis in astrocytes.	Li S. et al., 2021
High glucose-induced human retinal capillary endothelial cells (HRCECs).	Endothelial cells	***In vitro:*** Cell viability analysis; PI staining; SOD, GPX4 activity, and MDA measurement; Biomarker analysis (GPX-4); DIPY 581/591 C11.	High glucose-induced HRCECs ferroptosis can be facilitated by TRIM46-induced GPX4 ubiquitination.	Qin et al., 2021

action (Handa et al., 2000). Later, more antioxidant drugs, such as melatonin and N-acetylcysteine, upregulated the antioxidant activity of GSH/GPX, causing neuroprotection in SAH experimental animals (Ayer et al., 2008; Lu et al., 2009). Notably, any of these neuroprotective effects involve inhibition of neuronal apoptosis.

After introducing the ferroptosis concept, the main focus of the research was on a subtype of the GPX family, GPX4, which also acts as a biomarker in SAH ferroptosis. Gao et al. (2020) were the first to explore the role of GPX4 in SAH. They showed that SAH significantly reduced GPX4, which is mainly expressed in neurons, and overexpression of GPX4 alleviated lipid peroxidation-mediated cell death. Most drug-related studies also focus on the up-regulation of GPX4 and whether it can be achieved as a criterion for determining whether a drug is effective for ferroptosis treatment (Huang et al., 2022; Yuan B. et al., 2022). SLC7A11, as the critical target regulating GSH synthesis, was also found to be impaired in SAH models (Liu et al., 2022). But in terms of protein expression, the reduction is not as significant as GPX4.

A recent study also validated the inhibition of the FSP1/CoQ10 antioxidant system *in vivo* and *in vitro* SAH models. They highlighted how the activation of a well-known epigenetic regulator, Sirtuin 1 (SIRT1), alleviates neuronal ferroptosis in SAH by upregulating the expression of FSP1 and CoQ10B (Yuan B. et al., 2022). Their finding adds critically to the existing knowledge about the antioxidant mechanism underlying ferroptosis after a hemorrhagic stroke and deserves more investment in future research.

6. The research dilemma and prospects of ferroptosis

6.1. Technical barrier of ferroptosis marker detection

Apoptosis, pyroptosis, and autophagy involve hallmark molecules that can execute the cell death program, enabling researchers to detect these PCDs by simple but specific techniques (Fang et al., 2020). In addition, technical means such as TUNNEL staining and annexin v-pi staining help to locate the apoptotic cells (Luchetti et al., 2023). For autophagy, the autophagic-lysosome is its identification marker (Rodgers et al., 2022). However, the currently established markers for ferroptosis, GPX4, SLC7A11, ACSL4, and several iron metabolism-related indicators fail to point to ferroptosis directly. In 2017, two independent groups established that PEs-AA/ADA-OOH are the direct executor of ferroptosis, providing a novel yet convincing biomarker for validating ferroptosis (Kagan et al., 2017; Wenzel et al., 2017). However, separating and purifying this specific phospholipid is challenging as the tedious and elaborate process involves high-performance liquid chromatography and mass spectrometry with high-purity standards for comparison. Very few laboratories worldwide accurately detect PEs-AA/ADA-OOH. Hence minimal testing has been performed to evaluate its content in brain tissue after a hemorrhagic stroke. Moreover, no ferroptosis-specific tissue staining techniques or flow cytometry have been developed. Therefore, the identification of ferroptosis still involves evaluating morphological changes observed by TEM and verifying many biomarkers.

6.2. The diversity of ferroptotic cell types

Evidence from most of the current studies suggests that the cell types undergoing ferroptosis after hemorrhagic stroke mainly involve neurons (Zhang et al., 2018; Gao et al., 2020; Huang et al., 2022). The recovery of neural function is largely due to the repair of neurons. Moreover, the primary regulators of ferroptosis, ACSL4, and GPX4, were mainly localized in neurons, further validating the hypothesis that ferroptosis occurs in neurons after an injury. Mitochondrial ferroptotic damage within neurons under TEM observation is critical for identification. However, multiple other cell types in the brain have also been reported to undergo ferroptosis.

Several studies have reported the role of ferroptosis in microglia, which put forward by Kapralov et al.'s (2020) research on macrophage ferroptosis. They found M2-type macrophages to be more sensitive than M1-type macrophages to ferroptosis. Studies have shown that ferroptosis is prevalent in SAH microglia, and the sensitivity of M1 and M2 microglia to ferroptosis is also similar to that of peripheral macrophages (Wu et al., 2020). Two subsequent studies indicated that this sensitivity of microglia to ferroptosis may be regulated by the expression of intracellular NRF2 or iNOS (Cui et al., 2021b; Qu et al., 2022). Nevertheless, the specific role of microglia upon the onset of ferroptosis has not been fully explored.

Li et al. (2018) used TEM to observe mitochondria characteristics of ferroptosis in axons of oligodendrocytes. Subsequently, they further systematically presented ample evidence of ferroptosis in oligodendrocytes after ICH (Shen et al., 2022). Dexpramipexole has also been reported to attenuate white matter damage caused by oligodendrocyte ferroptosis in mice after ICH, thereby improving spatial localization and motor function (Wang B. et al., 2022). Moreover, ferroptosis has also been reported to be involved in white matter damage after spinal cord injury, which can be suppressed by the application of Fer-1 (Chen et al., 2022).

In an Alzheimer's disease study, ferroptosis was shown to occur in astrocytes and is positively regulated by NADPH oxidase 4-mediated impairment of mitochondrial metabolism (Park et al., 2021). Another study identified ferroptosis in cultured astrocytes. Although the validation evidence for ferroptosis in this *in vitro* experiment is not comprehensive (Li S. et al., 2021), it still provides an outlook for the existence of ferroptosis in astrocytes.

In addition, some studies or reviews have proposed the feasibility and essential role of ferroptosis in endothelial cells (Qin et al., 2021). However, evidence for it, especially in the central nervous system (CNS), still appears to be lacking. In summary, studying the ferroptosis of cells other than neurons holds great promise in the CNS. The lack of practical means makes this line of research somewhat challenging to identify the specific ferroptotic cell localization. We have presented the current studies for various types of ferroptosis in the CNS in **Table 1**.

6.3. Uncertainty about the magnitude and duration of ferroptotic action

Developing clinically effective drugs against ferroptosis is a crucial goal of our research. The elucidation of the molecular mechanism of ferroptosis after hemorrhagic new stroke will facilitate the development of novel and more efficacious drugs. There is electron microscopic evidence that ferrotropis existed earlier in ICH than necrossis and autophagy (Li et al., 2018). However, a significant challenge in this area of research involves the failure to define the contribution of ferroptosis to neurological impairment after hemorrhagic stroke and the difficulty of determining which specific period after hemorrhagic stroke plays a vital role in the ferroptosis effect. The crucial questions remain: faced with various PCDs after injury, which one aspect of research should we focus on? Is it possible to target in combination some of these forms of death to achieve the highest therapeutic effect? Are the dominant PCDs different across periods after hemorrhagic stroke? In fact, a large amount of basic studies related to ferroptosis are lack of reliable experimental evidence. For example, many articles have not provided evidence of TEM, or arbitrarily concluded that ferroptosis changes only through the changes in the end products of lipid peroxidation. And most of studies have not been repeatedly verified or even can't be reproduced at all. It has to be admitted that in view of the above problems, there is no treatment based on iron death that can be carried out in a phase I clinical trial. These issues are of paramount importance to be addressed in the clinical translation of preclinical drug research for hemorrhagic stroke. In the face of the above problems, using single cell sequencing technology to classify dying cells in biology may be a direction worth trying. Combining with the pseudotime analysis, we may classify the outcomes of these cells by detecting the marker molecules of PCDs, so as to solve the difficult problems of time point after stroke and proportion of ferroptosis in PCDs.

Author contributions

FP and CW designed and wrote the manuscript. WX and JD contributed to the literature searches and analyses. FP and WX critically revised the manuscript. All authors approved the final manuscript.

Conflict of interest

The authors declare that the research was conducted in the absence of any commercial or financial relationships that could be construed as a potential conflict of interest.

Publisher's note

References

Alim, I., Caulfield, J. T., Chen, Y., Swarup, V., Geschwind, D. H., Ivanova, E., et al. (2019). Selenium drives a transcriptional adaptive program to block ferroptosis and treat stroke. *Cell* 177, 1262.e–1279.e. doi: 10.1016/j.cell.2019.03.032

Ayer, R. E., Sugawara, T., Chen, W., Tong, W., and Zhang, J. H. (2008). Melatonin decreases mortality following severe subarachnoid hemorrhage. *J. Pineal Res.* 44, 197–204. doi: 10.1111/j.1600-079X.2007.00508.x

Bersuker, K., Hendricks, J. M., Li, Z., Magtanong, L., Ford, B., Tang, P. H., et al. (2019). The CoQ oxidoreductase FSP1 acts parallel to GPX4 to inhibit ferroptosis. *Nature* 575, 688–692. doi: 10.1038/s41586-019-1705-2

Camaschella, C., Nai, A., and Silvestri, L. (2020). Iron metabolism and iron disorders revisited in the hepcidin era. *Haematologica* 105, 260–272. doi: 10.3324/haematol.2019.232124

Cao, Y., Li, Y., He, C., Yan, F., Li, J., Xu, H., et al. (2021). Selective ferroptosis inhibitor liproxstatin-1 attenuates neurological deficits and neuroinflammation after subarachnoid hemorrhage. *Neurosci. Bull.* 37, 535–549. doi: 10.1007/s12264-020-00620-5

Chang, C. F., Cho, S. and Wang, J. (2014). (-)-Epicatechin protects hemorrhagic brain via synergistic Nrf2 pathways. *Ann. Clin. Transl. Neurol.* 1, 258–271. doi: 10.1002/acn3.54

Chen, B., Chen, Z., Liu, M., Gao, X., Cheng, Y., Wei, Y., et al. (2019). Inhibition of neuronal ferroptosis in the acute phase of intracerebral hemorrhage shows long-term cerebroprotective effects. *Brain Res. Bull.* 153, 122–132. doi: 10.1016/j.brainresbull.2019.08.013

Chen, B., Wang, H., Lv, C., Mao, C., and Cui, Y. (2021). Long non-coding RNA H19 protects against intracerebral hemorrhage injuries via regulating microRNA-106b-5p/acyl-CoA synthetase long chain family member 4 axis. *Bioengineered* 12, 4004–4015. doi: 10.1080/21655979.2021.1951070

Chen, D., Fan, Z., Rauh, M., Buchfelder, M., Eyupoglu, I. Y., and Savaskan, N. (2017). ATF4 promotes angiogenesis and neuronal cell death and confers ferroptosis in a xCT-dependent manner. *Oncogene* 36, 5593–5608. doi: 10.1038/onc.2017.146

Chen, Y., Zuliyaer, T., Liu, B., Guo, S., Yang, D., Gao, F., et al. (2022). Sodium selenite promotes neurological function recovery after spinal cord injury by inhibiting ferroptosis. *Neural. Regen. Res.* 17, 2702–2709. doi: 10.4103/1673-5374.314322

Çolakoğlu, M., Tunçer, S., Banerjee, S. (2018). , Emerging cellular functions of the lipid metabolizing enzyme 15-Lipoxygenase-1. *Cell Prolif.* 51:e12472. doi: 10.1111/cpr.12472

Cui, Y., Zhang, Y., Zhao, X., Shao, L., Liu, G., Sun, C., et al. (2021a). ACSL4 exacerbates ischemic stroke by promoting ferroptosis-induced brain injury and neuroinflammation. *Brain Behav. Immun.* 93, 312–321. doi: 10.1016/j.bbi.2021.01.003

Cui, Y., Zhang, Z., Zhou, X., Zhao, Z., Zhao, R., Xu, X., et al. (2021b). Microglia and macrophage exhibit attenuated inflammatory response and ferroptosis resistance after RSL3 stimulation via increasing Nrf2 expression. *J. Neuroinflammation* 18:249. doi: 10.1186/s12974-021-02231-x

Dai, E., Zhang, W., Cong, D., Kang, R., Wang, J., Tang, D., et al. (2020). AIFM2 blocks ferroptosis independent of ubiquinol metabolism. *Biochem. Biophys. Res. Commun.* 523, 966–971. doi: 10.1016/j.bbrc.2020.01.066

Ding, C., Ding, X., Zheng, J., Wang, B., Li, Y., Xiang, H., et al. (2020). miR-182-5p and miR-378a-3p regulate ferroptosis in I/R-induced renal injury. *Cell Death Dis.* 11:929. doi: 10.1038/s41419-020-03135-z

Dixon, S. J., Lemberg, K. M., Lamprecht, M. R., Skouta, R., Zaitsev, E. M., Gleason, C. E., et al. (2012). Ferroptosis: An iron-dependent form of nonapoptotic cell death. *Cell* 149, 1060–1072. doi: 10.1016/j.cell.2012.03.042

Doll, S., Freitas, F. P., Shah, R., Aldrovandi, M., Silva, M. C., Ingold, I., et al. (2019). FSP1 is a glutathione-independent ferroptosis suppressor. *Nature* 575, 693–698. doi: 10.1038/s41586-019-1707-0

Dolma, S., Lessnick, S. L., Hahn, W. C., and Stockwell, B. R. (2003). Identification of genotype-selective antitumor agents using synthetic lethal chemical screening in engineered human tumor cells. *Cancer Cell* 3, 285–296. doi: 10.1016/S1535-6108(03)00050-3

Doria, J. W., and Forgacs, P. B. (2019). Incidence, implications, and management of seizures following ischemic and hemorrhagic stroke. *Curr. Neurol. Neurosci. Rep.* 19:37. doi: 10.1007/s11910-019-0957-4

Du, G. J., Lu, G., Zheng, Z. Y., Poon, W. S., and Wong, K. C. (2016). Endovascular perforation murine model of subarachnoid hemorrhage. *Acta Neurochir. Suppl.* 121, 83–88. doi: 10.1007/978-3-319-18497-5_14

Duan, L., Zhang, Y., Yang, Y., Su, S., Zhou, L., Lo, P., et al. (2021). Baicalin inhibits ferroptosis in intracerebral hemorrhage. *Front. Pharmacol.* 12:629379. doi: 10.3389/fphar.2021.629379

Fang, Y., Gao, S., Wang, X., Cao, Y., Lu, J., Chen, S., et al. (2020). Programmed cell deaths and potential crosstalk with blood-brain barrier dysfunction after hemorrhagic stroke. *Front. Cell Neurosci.* 14:68. doi: 10.3389/fncel.2020.00068

Farr, A. C., and Xiong, M. P. (2021). Challenges and opportunities of deferoxamine delivery for treatment of Alzheimer's Disease, Parkinson's Disease, and intracerebral hemorrhage. *Mol. Pharm.* 18, 593–609. doi: 10.1021/acs.molpharmaceut.0c00474

Feng, H., Liu, Q., Deng, Z., Li, H., Zhang, H., Song, J., et al. (2022). Human umbilical cord mesenchymal stem cells ameliorate erectile dysfunction in rats with diabetes mellitus through the attenuation of ferroptosis. *Stem Cell Res. Ther.* 13:450. doi: 10.1186/s13287-022-03147-w

Fraternale, A., Paoletti, M. F., Casabianca, A., Nencioni, L., Garaci, E., Palamara, A. T., et al. (2009). GSH and analogs in antiviral therapy. *Mol. Aspects Med.* 30, 99–110. doi: 10.1016/j.mam.2008.09.001

Fu, P., Liu, J., Bai, Q., Sun, X., Yao, Z., Liu, L., et al. (2020). Long-term outcomes of monascin - a novel dual peroxisome proliferator-activated receptor γ/nuclear factor-erythroid 2 related factor-2 agonist in experimental intracerebral hemorrhage. *Ther. Adv. Neurol. Disord.* 13:1756286420921083. doi: 10.1177/1756286420921083

Fujii, M., Yan, J., Rolland, W. B., Soejima, Y., Caner, B., and Zhang, J. H. (2013). Early brain injury, an evolving frontier in subarachnoid hemorrhage research. *Transl. Stroke Res.* 4, 432–446. doi: 10.1007/s12975-013-0257-2

Gaasch, J. A., Lockman, P. R., Geldenhuys, W. J., Allen, D. D., and Schyf, C. J. (2007). Brain iron toxicity: Differential responses of astrocytes, neurons, and endothelial cells. *Neurochem. Res.* 32, 1196–1208. doi: 10.1007/s11064-007-9290-4

Gao, S., Liu, J., Han, Y., Deji, Q., Zhaba, W., Deng, H., et al. (2020). Neuroprotective role of glutathione peroxidase 4 in experimental subarachnoid hemorrhage models. *Life Sci.* 257:118050. doi: 10.1016/j.lfs.2020.118050

Gao, S., Zhou, L., Lu, J., Fang, Y., Wu, H., Xu, W., et al. (2022). Cepharanthine attenuates early brain injury after subarachnoid hemorrhage in mice via inhibiting 15-Lipoxygenase-1-Mediated microglia and endothelial cell ferroptosis. *Oxid. Med. Cell Longev.* 2022:4295208. doi: 10.1155/2022/4295208

Grysiewicz, R. A., Thomas, K., and Pandey, D. K. (2008). Epidemiology of ischemic and hemorrhagic stroke: Incidence, prevalence, mortality, and risk factors. *Neurol. Clin.* 26, 871–895. doi: 10.1016/j.ncl.2008.07.003

Hall, E. D., and Travis, M. A. (1988). Effects of the nonglucocorticoid 21-aminosteroid U74006F on acute cerebral hypoperfusion following experimental subarachnoid hemorrhage. *Exp. Neurol.* 102, 244–248. doi: 10.1016/0014-4886(88)90100-8

Han, R., Wan, J., Han, X., Ren, H., Falck, J. R., Munnuri, S., et al. (2021). 20-HETE participates in intracerebral hemorrhage-induced acute injury by promoting cell ferroptosis. *Front. Neurol.* 12:763419. doi: 10.3389/fneur.2021.763419

Handa, Y., Kaneko, M., Takeuchi, H., Tsuchida, A., Kobayashi, H., and Kubota, T. (2000). Effect of an antioxidant, ebselen, on development of chronic cerebral vasospasm after subarachnoid hemorrhage in primates. *Surg. Neurol.* 53, 323–329. doi: 10.1016/S0090-3019(00)00168-3

Hanley, D. F., Thompson, R. E., Rosenblum, M., Yenokyan, G., Lane, K., McBee, N., et al. (2019). Efficacy and safety of minimally invasive surgery with thrombolysis in intracerebral haemorrhage evacuation (MISTIE III): A randomised, controlled, open-label, blinded endpoint phase 3 trial. *Lancet* 393, 1021–1032. doi: 10.1016/S0140-6736(19)30195-3

Hou, L., Huang, R., Sun, F., Zhang, L., and Wang, Q. (2019). NADPH oxidase regulates paraquat and maneb-induced dopaminergic neurodegeneration through ferroptosis. *Toxicology* 417, 64–73. doi: 10.1016/j.tox.2019.02.011

Huang, Y., Wu, H., Hu, Y., Zhou, C., Wu, J., Wu, Y., et al. (2022). Puerarin attenuates oxidative stress and ferroptosis via AMPK/PGC1α/Nrf2 pathway after subarachnoid hemorrhage in rats. *Antioxidants* 11:1259 doi: 10.3390/antiox11071259

Imai, T., Tsuji, S., Matsubara, H., Ohba, T., Sugiyama, T., Nakamura, S., et al. (2021). Deferasirox, a trivalent iron chelator, ameliorates neuronal damage in hemorrhagic stroke models. *Naunyn Schmiedebergs Arch. Pharmacol.* 394, 73–84. doi: 10.1007/s00210-020-01963-6

Jhelum, P., Santos-Nogueira, E., Teo, W., Haumont, A., Lenoël, I., Stys, P. K., et al. (2020). Ferroptosis mediates cuprizone-induced loss of oligodendrocytes and demyelination. *J. Neurosci.* 40, 9327–9341. doi: 10.1523/JNEUROSCI.1749-20.2020

Jin, Z., Gao, W., Liao, S., Yu, T., Shi, Q., Yu, S., et al. (2021). Paeonol inhibits the progression of intracerebral haemorrhage by mediating the HOTAIR/UPF1/ACSL4 axis. *ASN Neuro.* 13:17590914211010647. doi: 10.1177/17590914211010647

Kagan, V. E., Mao, G., Qu, F., Angeli, J. P., Doll, S., Croix, C. S., et al. (2017). Oxidized arachidonic and adrenic PEs navigate cells to ferroptosis. *Nat. Chem. Biol.* 13, 81–90. doi: 10.1038/nchembio.2238

Kamezaki, T., Yanaka, K., Nagase, S., Fujita, K., Kato, N., and Nose, T. (2002). Increased levels of lipid peroxides as predictive of symptomatic vasospasm and poor outcome after aneurysmal subarachnoid hemorrhage. *J Neurosurg* 97, 1302–1305. doi: 10.3171/jns.2002.97.6.1302

Kapralov, A. A., Yang, Q., Dar, H. H., Tyurina, Y. Y., Anthonymuthu, T. S., Kim, R., et al. (2020). Redox lipid reprogramming commands susceptibility of macrophages and microglia to ferroptotic death. *Nat. Chem. Biol.* 16, 278–290. doi: 10.1038/s41589-019-0462-8

Karuppagounder, S. S., Alin, L., Chen, Y., Brand, D., Bourassa, M. W., Dietrich, K., et al. (2018). N-acetylcysteine targets 5 lipoxygenase-derived, toxic lipids and can synergize with prostaglandin E(2) to inhibit ferroptosis and improve outcomes following hemorrhagic stroke in mice. *Ann. Neurol.* 84, 854–872. doi: 10.1002/ana.25356

Katsarou, A., and Pantopoulos, K. (2020). Basics and principles of cellular and systemic iron homeostasis. . *Mol. Aspects Med.* 75:100866. doi: 10.1016/j.mam.2020.100866

Koppula, P., Zhuang, L., and Gan, B. (2021). Cystine transporter SLC7A11/xCT in cancer: Ferroptosis, nutrient dependency, and cancer therapy. *Protein Cell* 12, 599–620. doi: 10.1007/s13238-020-00789-5

Krafft, P. R., Rolland, W. B., Duris, K., Lekic, T., Campbell, A., Tang, J., et al. (2012). Modeling intracerebral hemorrhage in mice: Injection of autologous blood or bacterial collagenase. *J. Vis. Exp.* 67:e4289. doi: 10.3791/4289

Kusaka, G., Ishikawa, M., Nanda, A., Granger, D. N., and Zhang, J. H. (2004). Signaling pathways for early brain injury after subarachnoid hemorrhage. *J. Cereb Blood Flow Metab.* 24, 916–925. doi: 10.1097/01.WCB.0000125886.48838.7E

Laird, M. D., Wakade, C., Jr, C. H., and Dhandapani, K. M. (2008). Hemin-induced necroptosis involves glutathione depletion in mouse astrocytes. *Free Radic. Biol. Med.* 45, 1103–1114. doi: 10.1016/j.freeradbiomed.2008.07.003

Lee, J., Keep, R. F., He, Y., Sagher, O., Hua, Y., and Xi, G. (2010). Hemoglobin and iron handling in brain after subarachnoid hemorrhage and the effect of deferoxamine on early brain injury. *J. Cereb Blood Flow Metab.* 30, 1793–1803. doi: 10.1038/jcbfm.2010.137

Lei, B., Rolland, W. B., Duris, K., Lekic, T., Campbell, A., Tang, J., et al. (2014). Intrastriatal injection of autologous blood or clostridial collagenase as murine models of intracerebral hemorrhage. *J. Vis. Exp.* 89, 1–7. doi: 10.3791/51439

Lei, G., Zhuang, L., and Gan, B. (2022). Targeting ferroptosis as a vulnerability in cancer. *Nat. Rev. Cancer* 22, 381–396. doi: 10.1038/s41568-022-00459-0

Lekic, T., Hartman, R., Rojas, H., Manaenko, A., Chen, W., Ayer, R., et al. (2010). Protective effect of melatonin upon neuropathology, striatal function, and memory ability after intracerebral hemorrhage in rats. *J. Neurotrauma* 27, 627–637. doi: 10.1089/neu.2009.1163

Li, D., and Li, Y. (2020). The interaction between ferroptosis and lipid metabolism in cancer. *Signal Transd. Target Ther.* 5:108. doi: 10.1038/s41392-020-00216-5

Li, F., Long, H., Zhou, Z., Luo, H., Xu, S., and Gao, L. (2022). System X(c) (-)/GSH/GPX4 axis: An important antioxidant system for the ferroptosis in drug-resistant solid tumor therapy. *Front. Pharmacol.* 13:910292. doi: 10.3389/fphar.2022.910292

Li, J., Li, M., Ge, Y., Chen, J., Ma, J., Wang, C., et al. (2022). β-amyloid protein induces mitophagy-dependent ferroptosis through the CD36/PINK/PARKIN pathway leading to blood-brain barrier destruction in Alzheimer's disease. *Cell Biosci.* 12:69. doi: 10.1186/s13578-022-00807-5

Li, N., Worthmann, H., Deb, M., Chen, S., and Weissenborn, K. (2011). Nitric oxide (NO) and asymmetric dimethylarginine (ADMA): Their pathophysiological role and involvement in intracerebral hemorrhage. *Neurol. Res.* 33, 541–548. doi: 10.1179/016164111X13007856084403

Li, Q., Han, X., Lan, X., Gao, Y., Wan, J., Durham, F., et al. (2017a). Inhibition of neuronal ferroptosis protects hemorrhagic brain. *JCI Insight* 2:e90777. doi: 10.1172/jci.insight.90777

Li, Q., Li, Q., Jia, J., Sun, Q., Zhou, H., Jin, W., et al. (2019). Baicalein exerts neuroprotective effects in fecl(3)-induced posttraumatic epileptic seizures via suppressing ferroptosis. *Front. Pharmacol.* 10:638. doi: 10.3389/fphar.2019.00638

Li, Q., Wan, J., Lan, X., Han, X., Wang, Z., and Wang, J. (2017b). Neuroprotection of brain-permeable iron chelator VK-28 against intracerebral hemorrhage in mice. *J. Cereb Blood Flow Metab.* 37, 3110–3123. doi: 10.1177/0271678X17709186

Li, Q., Weiland, A., Chen, X., Lan, X., Han, X., Durham, F., et al. (2018). Ultrastructural characteristics of neuronal death and white matter injury in mouse brain tissues after intracerebral hemorrhage: Coexistence of ferroptosis. autophagy, and necrosis. *Front. Neurol.* 9:581. doi: 10.3389/fneur.2018.00581

Li, S., Zhou, C., Zhu, Y., Chao, Z., Sheng, Z., Zhang, Y., et al. (2021). Ferrostatin-1 alleviates angiotensin II (Ang II)- induced inflammation and ferroptosis in astrocytes. *Int. Immunopharmacol.* 90:107179. doi: 10.1016/j.intimp.2020.107179

Li, Y., Liu, Y., Wu, P., Tian, Y., Liu, B., Wang, J., et al. (2021). Inhibition of ferroptosis alleviates early brain injury after subarachnoid hemorrhage in vitro and in vivo via reduction of lipid peroxidation. *Cell Mol. Neurobiol.* 41, 263–278. doi: 10.1007/s10571-020-00850-1

Lin, C., Jeng, A. Y., Howng, S., and Kwan, A. (2004). Endothelin and subarachnoid hemorrhage-induced cerebral vasospasm: Pathogenesis and treatment. *Curr. Med. Chem.* 11, 1779–1791. doi: 10.2174/0929867043364919

Liu, L., Li, Y., Cao, D., Qiu, S., Li, Y., Jiang, C., et al. (2021). SIRT3 inhibits gallbladder cancer by induction of AKT-dependent ferroptosis and blockade of epithelial-mesenchymal transition. *Cancer Lett.* 510, 93–104. doi: 10.1016/j.canlet.2021.04.007

Liu, P., Feng, Y., Li, H., Chen, X., Wang, G., Xu, S., et al. (2020). Ferrostatin-1 alleviates lipopolysaccharide-induced acute lung injury via inhibiting ferroptosis. *Cell Mol. Biol. Lett.* 25:10. doi: 10.1186/s11658-020-00205-0

Liu, Z., Zhou, Z., Ai, P., Zhang, C., Chen, J., and Wang, Y. (2022). Astragaloside IV attenuates ferroptosis after subarachnoid hemorrhage via Nrf2/HO-1 signaling pathway. *Front. Pharmacol.* 13:924826. doi: 10.3389/fphar.2022.924826

Louandre, C., Ezzoukhry, Z., Godin, C., Barbare, J., Mazière, J., Chauffert, B., et al. (2013). Iron-dependent cell death of hepatocellular carcinoma cells exposed to sorafenib. *Int. J. Cancer* 133, 1732–1742. doi: 10.1002/ijc.28159

Lu, H., Zhang, D., Chen, H., Lin, Y., Hang, C., Yin, H., et al. (2009). N-acetylcysteine suppresses oxidative stress in experimental rats with subarachnoid hemorrhage. *J. Clin. Neurosci.* 16, 684–688. doi: 10.1016/j.jocn.2008.04.021

Luchetti, F., Carloni, S., Nasoni, M. G., Reiter, R. J., and Balduini, W. (2023). Melatonin, tunneling nanotubes, mesenchymal cells, and tissue regeneration. *Neural. Regen. Res.* 18, 760–762. doi: 10.4103/1673-5374.353480

Luo, Z., Harada, T., London, S., Gajdusek, C., and Mayberg, M. R. (1995). Antioxidant and iron-chelating agents in cerebral vasospasm. *Neurosurgery* 37, 1154–8;discussion1158–9. doi: 10.1097/00006123-199512000-00015

Ma, H., Liu, Y., Miao, Z., Cheng, S., Zhu, Y., Wu, Y., et al. (2022). Neratinib inhibits proliferation and promotes apoptosis of acute myeloid leukemia cells by activating autophagy-dependent ferroptosis. *Drug Dev. Res.* 83, 1641-1653. doi: 10.1002/ddr.21983

Magid-Bernstein, J., Girard, R., Polster, S., Srinath, A., Romanos, S., Awad, I. A., et al. (2022). Cerebral hemorrhage: Pathophysiology. Treatment, and future directions. *Circ Res* 130, 1204–1229. doi: 10.1161/CIRCRESAHA.121.319949

Mendelow, A. D., Gregson, B. A., Rowan, E. N., Murray, G. D., Gholkar, A., Mitchell, P. M., et al. (2013). Early surgery versus initial conservative treatment in patients with spontaneous supratentorial lobar intracerebral haematomas (STICH II): A randomised trial. *Lancet* 382, 397–408. doi: 10.1016/S0140-6736(13)60986-1

Miriyala, S., Thippakorn, C., Chaiswing, L., Xu, Y., Noel, T., Tovmasyan, A., et al. (2016). Novel role of 4-hydroxy-2-nonenal in AIFm2-mediated mitochondrial stress signaling. *Free Radic. Biol. Med.* 91, 68–80. doi: 10.1016/j.freeradbiomed.2015.12.002

Mishima, E., and Conrad, M. (2022). Nutritional and metabolic control of ferroptosis. *Annu. Rev. Nutr.* 42, 275–309. doi: 10.1146/annurev-nutr-062320-114541

Mou, Y., Wang, J., Wu, J., He, D., Zhang, C., Duan, C., et al. (2019). Ferroptosis, a new form of cell death: Opportunities and challenges in cancer. *J. Hematol. Oncol.* 12:34. doi: 10.1186/s13045-019-0720-y

Nakamura, T., Keep, R. F., Hua, Y., Schallert, T., Hoff, J. T., and Xi, G. (2004). Deferoxamine-induced attenuation of brain edema and neurological deficits in a rat model of intracerebral hemorrhage. *J. Neurosurg.* 100, 672–678. doi: 10.3171/jns.2004.100.4.0672

Nakamura, T., Xi, G., Park, J., Hua, Y., Hoff, J. T., and Keep, R. F. (2005). Holo-transferrin and thrombin can interact to cause brain damage. *Stroke* 36, 348–352. doi: 10.1161/01.STR.0000153044.60858.1b

Nobuta, H., Yang, N., Han, Y., Marro, S. G., Sabeur, K., and Chavali, M. (2019). Oligodendrocyte death in pelizaeus-merzbacher disease is rescued by iron chelation. *Cell Stem Cell* 25, 531–541. doi: 10.1016/j.stem.2019.09.003

O'Connell, D. M., and Watson, I. D. (2003). Definitive angiographic detection of subarachnoid haemorrhage compared with laboratory assessment of intracranial bleed in CT-negative patients. *Ann. Clin. Biochem.* 40(Pt 3), 269–273. doi: 10.1258/000456303321610592

Park, M. W., Cha, H. W., Kim, J., Kim, J. H., Yang, H., Yoon, S., et al. (2021). NOX4 promotes ferroptosis of astrocytes by oxidative stress-induced lipid peroxidation via the impairment of mitochondrial metabolism in Alzheimer's diseases. *Redox Biol.* 41:101947. doi: 10.1016/j.redox.2021.101947

Peng, C., Fu, X., Wang, K., Chen, L., Luo, B., Huang, N., et al. (2022). Dauricine alleviated secondary brain injury after intracerebral hemorrhage by upregulating GPX4 expression and inhibiting ferroptosis of nerve cells. *Eur. J. Pharmacol.* 914:174461. doi: 10.1016/j.ejphar.2021.174461

Qin, X., Zhang, J., Wang, B., Xu, G., Yang, X., Zou, Z., et al. (2021). Ferritinophagy is involved in the zinc oxide nanoparticles-induced ferroptosis of vascular endothelial cells. *Autophagy* 17, 4266–4285. doi: 10.1080/15548627.2021.1911016

Qu, W., Cheng, Y., Peng, W., Wu, Y., Rui, T., Luo, C., et al. (2022). Targeting iNOS alleviates early brain injury after experimental subarachnoid hemorrhage via promoting ferroptosis of M1 microglia and reducing neuroinflammation. *Mol. Neurobiol.* 59, 3124–3139. doi: 10.1007/s12035-022-02788-5

Qu, X., Liang, T., Wu, D., Lai, N., Deng, R., Ma, C., et al. (2021). Acyl-CoA synthetase long chain family member 4 plays detrimental role in early brain injury after subarachnoid hemorrhage in rats by inducing ferroptosis. *CNS Neurosci. Ther.* 27, 449–463. doi: 10.1111/cns.13548

Reed, A., Ichu, T., Milosevich, N., Melillo, B., Schafroth, M. A., Otsuka, Y., et al. (2022). LPCAT3 inhibitors remodel the polyunsaturated phospholipid content of human cells and protect from ferroptosis. *ACS Chem. Biol.* 17, 1607–1618. doi: 10.1021/acschembio.2c00317

Ren, S., Chen, Y., Wang, L., and Wu, G. (2022). Neuronal ferroptosis after intracerebral hemorrhage. *Front. Mol. Biosci.* 9:966478. doi: 10.3389/fmolb.2022.966478

Rodgers, S. J., Jones, E., Mitchell, C. A., and McGrath, M. J. (2022). Sequential conversion of PtdIns3P to PtdIns(3,5)P(2) via endosome maturation couples nutrient signaling to lysosome reformation and basal autophagy. *Autophagy*. doi: 10.1080/15548627.2022.2124499 [Epub ahead of print].

Sakaki, S., Kuwabara, H., and Ohta, S. (1986). Biological defence mechanism in the pathogenesis of prolonged cerebral vasospasm in the patients with ruptured intracranial aneurysms. *Stroke* 17, 196–202. doi: 10.1161/01.STR.17.2.196

Sekerdag, E., Solaroglu, I., and Gursoy-Ozdemir, Y. (2018). Cell death mechanisms in stroke and novel molecular and cellular treatment options. *Curr. Neuropharmacol.* 16, 1396–1415. doi: 10.2174/1570159X16666180302115544

Selim, M., Yeatts, S., Goldstein, J. N., Gomes, J., Greenberg, S., Morgenstern, L. B., et al. (2011). Safety and tolerability of deferoxamine mesylate in patients with acute intracerebral hemorrhage. *Stroke* 42, 3067–3074. doi: 10.1161/STROKEAHA.111.617589

Sha, R., Xu, Y., Yuan, C., Sheng, X., Wu, Z., Peng, J., et al. (2021). Predictive and prognostic impact of ferroptosis-related genes ACSL4 and GPX4 on breast cancer treated with neoadjuvant chemotherapy. *EBioMedicine* 71:103560. doi: 10.1016/j.ebiom.2021.103560

Shao, Z., Tu, S., and Shao, A. (2019). Pathophysiological mechanisms and potential therapeutic targets in intracerebral hemorrhage. *Front. Pharmacol.* 10:1079. doi: 10.3389/fphar.2019.01079

Shen, D., Wu, W., Liu, J., Lan, T., Xiao, Z., Gai, K., et al. (2022). Ferroptosis in oligodendrocyte progenitor cells mediates white matter injury after hemorrhagic stroke. *Cell Death Dis.* 13:259. doi: 10.1038/s41419-022-04712-0

Shen, L., Lin, D., Li, X., Wu, H., Lenahan, C., Pan, Y., et al. (2020). Ferroptosis in acute central nervous system injuries: The future direction? *Front. Cell Dev. Biol.* 8:594. doi: 10.3389/fcell.2020.00594

Smith, S. L., Scherch, H. M., and Hall, E. D. (1996). Protective effects of tirilazad mesylate and metabolite U-89678 against blood-brain barrier damage after subarachnoid hemorrhage and lipid peroxidative neuronal injury. *J. Neurosurg.* 84, 229–233. doi: 10.3171/jns.1996.84.2.0229

Stockwell, B. R., Angeli, J. P., Bayir, H., Bush, A. I., Conrad, M., Dixon, S. J., et al. (2017). Ferroptosis: A regulated cell death nexus linking metabolism. *Redox Biol. Dis. Cell* 171, 273–285. doi: 10.1016/j.cell.2017.09.021

Sukumari-Ramesh, S., Laird, M. D., Singh, N., Vender, J. R., Jr, C. H., and Dhandapani, K. M. (2010). Astrocyte-derived glutathione attenuates hemin-induced apoptosis in cerebral microvascular cells. *Glia* 58, 1858–1870. doi: 10.1002/glia.21055

Sun, Y., Berleth, N., Wu, W., Schlütermann, D., Deitersen, J., Stuhldreier, F., et al. (2021). Fin56-induced ferroptosis is supported by autophagy-mediated GPX4 degradation and functions synergistically with mTOR inhibition to kill bladder cancer cells. *Cell Death Dis.* 12:1028. doi: 10.1038/s41419-021-04306-2

Suzuki, H., Muramatsu, M., Kojima, T., and Taki, W. (2003). Intracranial heme metabolism and cerebral vasospasm after aneurysmal subarachnoid hemorrhage. *Stroke* 34, 2796–2800. doi: 10.1161/01.STR.0000103743.62248.12

Suzuki, N., Nakamura, T., Imabayashi, S., Ishikawa, Y., Sasaki, T., and Asano, T. (1983). Identification of 5-hydroxy eicosatetraenoic acid in cerebrospinal fluid after subarachnoid hemorrhage. *J. Neurochem.* 41, 1186–1189. doi: 10.1111/j.1471-4159.1983.tb09071.x

Tao, Q., Qiu, X., Li, C., Zhou, J., Gu, L., Zhang, L., et al. (2022). S100A8 regulates autophagy-dependent ferroptosis in microglia after experimental subarachnoid hemorrhage. *Exp. Neurol.* 357:114171. doi: 10.1016/j.expneurol.2022.114171

Troadec, M., Ward, D. M., Lo, E., Kaplan, J., and Domenico, I. D. (2010). Induction of FPN1 transcription by MTF-1 reveals a role for ferroportin in transition metal efflux. *Blood* 116, 4657–4664. doi: 10.1182/blood-2010-04-278614

Tuo, Q., Lei, P., Jackman, K. A., Li, X., Xiong, H., Li, X., et al. (2017). Tau-mediated iron export prevents ferroptotic damage after ischemic stroke. *Mol. Psychiatry* 22, 1520–1530. doi: 10.1038/mp.2017.171

Uselis, J. (1970). [Iron-binding capacity of serum proteins and the degree of their saturation by iron in a selected group of shipyard welders]. *Pol. Tyg Lek.* 25, 755–757.

Utkan, T., Sarioglu, Y., Kaya, T., Akgün, M., Göksel, M., and Solak, O. (1996). Effect of deferoxamine and sympathectomy on vasospasm following subarachnoid hemorrhage. *Pharmacology* 52, 353–361. doi: 10.1159/000139402

Vogt, A. S., Arsiwala, T., Mohsen, M., Vogel, M., Manolova, V., and Bachmann, M. F. (2021). On iron metabolism and its regulation. *Int. J. Mol. Sci.* 22:4591. doi: 10.3390/ijms22094591

Wang, B., Zhang, X., Zhong, J., Wang, S., Zhang, C., Li, M., et al. (2022). Dexpramipexole attenuates white matter injury to facilitate locomotion and motor coordination recovery via reducing ferroptosis after intracerebral hemorrhage. *Oxid. Med. Cell Longev.* 2022:6160701. doi: 10.1155/2022/6160701

Wang, G., Hu, W., Tang, Q., Wang, L., Sun, X., Chen, Y., et al. (2016). Effect comparison of both iron chelators on outcomes. iron deposit, and iron transporters after intracerebral hemorrhage in rats. *Mol. Neurobiol.* 53, 3576–3585. doi: 10.1007/s12035-015-9302-3

Wang, G., Li, T., Duan, S., Dong, L., Sun, X., and Xue, F. (2018). PPAR-γ promotes hematoma clearance through haptoglobin-hemoglobin-CD163 in a rat model of intracerebral hemorrhage. *Behav. Neurol.* 2018:7646104. doi: 10.1155/2018/7646104

Wang, G., Yang, Q., Li, G., Wang, L., Hu, W., Tang, Q., et al. (2011). Time course of heme oxygenase-1 and oxidative stress after experimental intracerebral hemorrhage. *Acta Neurochir (Wien)* 153, 319–325. doi: 10.1007/s00701-010-0750-2

Wang, H., Lin, D., Yu, Q., Li, Z., Lenahan, C., Dong, Y., et al. (2021). A promising future of ferroptosis in tumor therapy. *Front. Cell Dev. Biol.* 9:629150. doi: 10.3389/fcell.2021.629150

Wang, P., Cui, Y., Liu, Y., Li, Z., Bai, H., Zhao, Y., et al. (2022). Mitochondrial ferritin alleviates apoptosis by enhancing mitochondrial bioenergetics and stimulating glucose metabolism in cerebral ischemia reperfusion. *Redox Biol.* 57:102475. doi: 10.1016/j.redox.2022.102475

Weiland, A., Wang, Y., Wu, W., Lan, X., Han, X., Li, Q., et al. (2019). Ferroptosis and its role in diverse brain diseases. *Mol. Neurobiol.* 56, 4880–4893. doi: 10.1007/s12035-018-1403-3

Wenzel, S. E., Tyurina, Y., Zhao, J., Cm, S. C., Dar, H. H., Mao, G., et al. (2017). PEBP1 wardens ferroptosis by enabling lipoxygenase generation of lipid death signals. *Cell* 171, 628–641e26. doi: 10.1016/j.cell.2017.09.044

Wu, T. Y., Campbell, B. C., Strbian, D., Yassi, N., Putaala, J., Tatlisumak, T., et al. (2016). Impact of pre-stroke sulphonylurea and metformin use on mortality of intracerebral haemorrhage. *Eur. Stroke J.* 1, 302–309. doi: 10.1177/2396987316666617

Wu, T., Liang, X., Liu, X., Li, Y., Wang, Y., Kong, L., et al. (2020). Induction of ferroptosis in response to graphene quantum dots through mitochondrial oxidative stress in microglia. *Part Fibre Toxicol.* 17:30. doi: 10.1186/s12989-020-00363-1

Xu, C., Li, J., Jiang, S., Wan, L., Zhang, X., Xia, L., et al. (2022). CD47 blockade accelerates blood clearance and alleviates early brain injury after experimental subarachnoid hemorrhage. *Front. Immunol.* 13:823999. doi: 10.3389/fimmu.2022.823999

Xu, Y., Chen, A., Wu, J., Wan, Y., You, M., Gu, X., et al. (2022). Nanomedicine: An emerging novel therapeutic strategy for hemorrhagic stroke. *Int. J. Nanomed.* 17, 1927–1950. doi: 10.2147/IJN.S357598

Yadav, P., Sharma, P., Sundaram, S., Venkatraman, G., Bera, A. K., and Karunagaran, D. (2021). SLC7A11/ xCT is a target of miR-5096 and its restoration partially rescues miR-5096-mediated ferroptosis and anti-tumor effects in human breast cancer cells. *Cancer Lett.* 522, 211–224. doi: 10.1016/j.canlet.2021.09.033

Yang, G., Qian, C., Zhang, C., Bao, Y., Liu, M., Jiang, F., et al. (2021). Hepcidin attenuates the iron-mediated secondary neuronal injury after intracerebral hemorrhage in rats. *Transl. Res.* 229, 53–68. doi: 10.1016/j.trsl.2020.09.002

Yang, W. S., and Stockwell, B. R. (2008). Synthetic lethal screening identifies compounds activating iron-dependent, nonapoptotic cell death in oncogenic-RAS-harboring cancer cells. *Chem. Biol.* 15, 234–245. doi: 10.1016/j.chembiol.2008.02.010

Yang, W. S., and Stockwell, B. R. (2016). Ferroptosis: Death by lipid peroxidation. *Trends Cell Biol.* 26, 165–176. doi: 10.1016/j.tcb.2015.10.014

Yao, Y., Chen, Z., Zhang, H., Chen, C., Zeng, M., Yunis, J., et al. (2021). Selenium-GPX4 axis protects follicular helper T cells from ferroptosis. *Nat. Immunol.* 22, 1127–1139. doi: 10.1038/s41590-021-00996-0

Yuan, B., Zhao, X., Shen, J., Chen, S., Huang, H., Zhou, X., et al. (2022). Activation of SIRT1 alleviates ferroptosis in the early brain injury after subarachnoid hemorrhage. *Oxid. Med. Cell Longev.* 2022:9069825. doi: 10.1155/2022/9069825

Yuan, Y., Yucai, L., Lu, L., Hui, L., Yong, P., and Haiyang, Y. (2022). Acrylamide induces ferroptosis in HSC-T6 cells by causing antioxidant imbalance of the XCT-GSH-GPX4 signaling and mitochondrial dysfunction. *Toxicol Lett.* 368, 24–32. doi: 10.1016/j.toxlet.2022.08.007

Zhang, H., Ostrowski, R., Jiang, D., Zhao, Q., Liang, Y., Che, X., et al. (2021). Hepcidin promoted ferroptosis through iron metabolism which is associated with DMT1 signaling activation in early brain injury following subarachnoid hemorrhage. *Oxid Med. Cell Longev.* 2021:9800794. doi: 10.1155/2021/9800794

Zhang, H., Tu, X., Song, S., Liang, R., and Shi, S. (2020). Baicalin reduces early brain injury after subarachnoid hemorrhage in rats. *Chin. J. Integr. Med.* 26, 510–518. doi: 10.1007/s11655-020-3183-7

Zhang, Y., Kong, Y., Ma, Y., Ni, S., Wikerholmen, T., Xi, K., et al. (2021). Loss of COPZ1 induces NCOA4 mediated autophagy and ferroptosis in glioblastoma cell lines. *Oncogene* 40, 1425–1439. doi: 10.1038/s41388-020-01622-3

Zhang, Z., Wu, Y., Yuan, S., Zhang, P., Zhang, J., Li, H., et al. (2018). Glutathione peroxidase 4 participates in secondary brain injury through mediating ferroptosis in a rat model of intracerebral hemorrhage. *Brain Res.* 1701, 112–125. doi: 10.1016/j.brainres.2018.09.012

Zhao, F., Hua, Y., He, Y., Keep, R. F., and Xi, G. (2011). Minocycline-induced attenuation of iron overload and brain injury after experimental intracerebral hemorrhage. *Stroke* 42, 3587–3593. doi: 10.1161/STROKEAHA.111.623926

Zheng, Y., Tan, X., and Cao, S. (2022). The critical role of erythrolysis and microglia/macrophages in clot resolution after intracerebral hemorrhage: A review of the mechanisms and potential therapeutic targets. *Cell Mol. Neurobiol.* doi: 10.1007/s10571-021-01175-3 [Epub ahead of print].

Zhu, F., Zi, L., Yang, P., Wei, Y., Zhong, R., Wang, Y., et al. (2021). Efficient Iron and ROS Nanoscavengers for brain protection after intracerebral hemorrhage. *ACS Appl. Mater Interfaces* 13, 9729–9738. doi: 10.1021/acsami.1c00491

Zhuang, J., Peng, Y., Gu, C., Chen, H., Lin, Z., Zhou, H., et al. (2021). Wogonin accelerates hematoma clearance and improves neurological outcome via the PPAR-γ pathway after intracerebral hemorrhage. *Transl. Stroke Res.* 12, 660–675. doi: 10.1007/s12975-020-00842-9

frontiers | Frontiers in Cellular Neuroscience

TYPE Review
PUBLISHED 06 February 2023
DOI 10.3389/fncel.2023.1080344

OPEN ACCESS

EDITED BY
Anwen Shao,
Zhejiang University, China

REVIEWED BY
Sheng-Yu Zhou,
The First Affiliated Hospital of Jilin University, China
Abdel Ali Belaidi,
The University of Melbourne, Australia

*CORRESPONDENCE
Yi Zeng
✉ zengyi_xyneuro@csu.edu.cn

SPECIALTY SECTION
This article was submitted to Cellular Neuropathology, a section of the journal Frontiers in Cellular Neuroscience

RECEIVED 26 October 2022
ACCEPTED 16 January 2023
PUBLISHED 06 February 2023

CITATION
Cao Y, Xiao W, Liu S and Zeng Y (2023) Ferroptosis: Underlying mechanism and the crosstalk with other modes of neuronal death after intracerebral hemorrhage.
Front. Cell. Neurosci. 17:1080344.
doi: 10.3389/fncel.2023.1080344

Ferroptosis: Underlying mechanism and the crosstalk with other modes of neuronal death after intracerebral hemorrhage

Yuan Cao[1], Wenbiao Xiao[1], Shuzhen Liu[2] and Yi Zeng[1]*

[1]Department of Geriatrics, The Second Xiangya Hospital of Central South University, Changsha, Hunan, China, [2]Department of Radiology, The Second Xiangya Hospital of Central South University, Changsha, Hunan, China

Intracerebral hemorrhage (ICH) is a serious cerebrovascular disease with high rates of morbidity, mortality, and disability. Optimal treatment of ICH is a major clinical challenge, as the underlying mechanisms remain unclear. Ferroptosis, a newly identified form of non-apoptotic programmed cell death, is characterized by the iron-induced accumulation of lipid reactive oxygen species (ROS), leading to intracellular oxidative stress. Lipid ROS causes damage to nucleic acids, proteins, and cell membranes, eventually resulting in ferroptosis. In the past 10 years, ferroptosis has resulted in plenty of discoveries and breakthroughs in cancer, neurodegeneration, and other diseases. Some studies have also reported that ferroptosis does occur after ICH *in vitro* and *in vivo* and contribute to neuronal death. However, the studies on ferroptosis following ICH are still in the preliminary stage. In this review, we will summarize the current evidence on the mechanism underlying ferroptosis after ICH. And review the traditional modes of neuronal death to identify the crosstalk with ferroptosis in ICH, including apoptosis, necroptosis, and autophagy. Additionally, we also aim to explore the promising therapeutic application of ferroptosis in cell death-based ICH.

KEYWORDS

intracerebral hemorrhage, ferroptosis, apoptosis, necroptosis, autophagy

1. Introduction

Intracerebral hemorrhage constitutes 10–15% of all strokes but accounts for almost 50% of stroke mortality worldwide (Thrift et al., 2017). For patients with ICH, the rupture of blood vessels in the brain results in primary brain injury and secondary brain injury (SBI) (Qureshi et al., 2009). These patients suffer from a lack of effective treatments to overcome harmful brain symptoms and research efforts lag behind those for ischemic stroke (Donnan et al., 2010; Hemphill et al., 2015). In general, it is thought that the main mechanisms of neuronal death in ICH are excitotoxicity, the toxicity of blood, oxidative stress, mitochondrial death pathways, the release of free radicals, protein misfolding, apoptosis, necroptosis, necrosis, autophagy, and inflammation (Wang, 2010; Aronowski and Zhao, 2011). Such mechanisms occur around the hematoma and in remote areas of the brain, not necessarily in contact with the bleeding. These all lead to neuronal death and dissipation of function which are particularly crucial because adult neurons have a limited ability to proliferate or replace. In the past, common neuronal death modalities following ICH included apoptosis, necroptosis, pyroptosis, autophagy, and parthanatos (Zhang et al., 2022c). Until, Li et al. (2017b) confirmed the occurrence of ferroptosis

through the ICH mouse model, which was the earliest report of neuronal ferroptosis after ICH. They also showed that ferrostatin-1 (Fer-1), a ferroptosis inhibitor, improved the neurological functions of mice after acute ICH (Li et al., 2017b). In Zille et al. (2017) reported that necroptosis and ferroptosis inhibitors each abrogated neuronal death by >80% after ICH and had similar therapeutic windows *in vitro*. So, Ferroptosis may provide new insights into neuronal death after ICH. Subsequently, many researchers have investigated the mechanism of ferroptosis in ICH, intending to identify new directions and targets for treating SBI after ICH (Li et al., 2018, 2020; Bao et al., 2020). Multiple modes of cell death after ICH have been identified. However, the crosstalk between cell death post-ICH is ambiguous, which makes it difficult for scientific researchers to explore the prevention and treatment of ICH (Fricker et al., 2018). In this review, we specifically focus on the mechanism of ferroptosis in neuronal death after ICH and compare the similarities and differences between ferroptosis and several dominant modes of neuronal death, such as apoptosis, necroptosis, and autophagy which exactly can be observed in the pathogenesis of ICH. Additionally, inhibiting neuronal death is a critical component of future therapeutic strategies for ICH. we also search for promising therapeutic applications to improve nerve function after ICH.

2. Ferroptosis in ICH

Ferroptosis, a newly identified iron-dependent concept of regulated cell death (RCD) type, was first proposed by Dixon et al. (2012). It is associated with iron, amino acid, and lipid metabolism. The iron-dependent accumulation of lipid peroxidation is the key trigger (Dixon et al., 2014; Conrad et al., 2018; Fujii et al., 2020). The Nomenclature Committee on Cell Death (NCCD) defined ferroptosis as "a form of RCD initiated by oxidative perturbations of the intracellular microenvironment that is under constitutive control by glutathione peroxidase 4 (GPX4) and can be inhibited by iron chelators and lipophilic antioxidants" (Galluzzi et al., 2018). During intracerebral hemorrhage, there is a high flow of iron originating from hemoglobin and hemoglobin, which contributes to cell death that may occur hours or days after the bleeding, and other factors released from blood may also play a role. In Zille et al. (2017), reported that the ICH model treated with Hb had an increased level of extracellular regulated protein kinases (ERK1/2). ERK1/2 is a critical signal in the RAS-RAF-MEK pathway in the process of ferroptosis providing sufficient evidence for the occurrence of neuronal ferroptosis after ICH. In another study, Zhang et al. (2018) showed that the expression of GPX4 was markedly reduced during acute ICH. GPX4 is an important antioxidant that protects neurons against oxidative stress and ferroptosis. Many studies have also revealed that the administration of ferrostatin-1 (Fer-1), a specific inhibitor of ferroptosis, prevented neuronal death and improved neurological function after ICH *in vitro* and *in vivo* (Wu et al., 2011; Li et al., 2017b; Stokum et al., 2020). Li et al. (2017b) also used transmission electron microscopy to find mitochondrial morphological atrophy characteristic of ferroptosis in perihematoma neuronal cells, which may provide strong evidence for the occurrence of ferroptosis after intracerebral hemorrhage. These findings fill an important gap in ferroptosis after ICH and provide a vital foundation for cell death-based ICH treatment in the future.

3. The underlying mechanisms of ferroptosis in ICH

So far, the metabolic mechanisms of ferroptosis after ICH seems to be tightly linked to three main categories: the metabolism of amino acids, iron, and lipids, which involve a complex network to shape oxidative stress (**Figure 1**). Metabolic dysregulation of any one of them may influence ferroptosis. Any molecular change or pharmacological intervention that regulates any of these elements may affect the final consequences of ferroptosis (Liu and Gu, 2022). Strategies targeting ferroptosis pathways have resulted in neuroprotection in preclinical models and some of these have shown promise for patients with ICH (Stockwell et al., 2017). Understanding the mechanisms of ferroptosis after ICH will provide a vital foundation for cell death-based ICH treatment and diagnosis.

3.1. Amino acid metabolic pathway

Amino acid metabolism is tightly linked to the regulation of ferroptosis (Angeli et al., 2017). Upregulating GPX4 expression in the ICH model can inhibit ferroptosis and treat ICH (Peng et al., 2022). The GPX4 is currently recognized as a central repressor of ferroptosis, and its activity depends on antioxidant glutathione (GSH). The GSH is a tripeptide composed of glutamic acid, cysteine, and glycine. The three kinds of amino acids are from different pathways. The system xc- antiporter, comprised of SLC7A11 and SLC3A2, is responsible for the transmembrane import of extracellular cystine, which is reduced back to intracellular cysteine. Due to the limited concentration of cysteine in cells, cysteine is considered to be the rate-limiting precursor for GSH synthesis. Glutamate and glutamine are also important regulators of ferroptosis (Gao et al., 2015). Researchers have found in mice, rabbits, and patients with ICH that glutamate levels in brain tissue surrounding the hematoma were elevated (Li et al., 2017b; Epping et al., 2022). The addition of human glutamate to the culture medium of HT22 hippocampal neurons resulted in a significant increase in cell death (Chen et al., 2022a). Li et al. (2017b) found that the application of glutaminase inhibitors could inhibit the decomposition of glutamine into glutamate, and significantly reduce the number of degenerate nerve cells around hematoma. These all confirmed that poor clinical outcomes and increased volume of the residual cavity after ICH are associated with high concentrations of glutamate in blood within the first 24 h from symptom onset (Li et al., 2017a). The presence of large amounts of glutamate will be the rate-limiting precursor for GSH synthesis which is the key to ferroptosis (Leasure et al., 2021). Some study has also highlighted the role that selenium plays in modulating ferroptosis *via* its co-translational incorporation into selenocysteine in GPX4 (Ingold et al., 2018). A single dose of Se delivered into the brain drives antioxidant GPX4 expression, protects neurons, and improves behavior in an intracerebral hemorrhage model. These all findings give us some insights into the treatment of ICH by inhibiting ferroptosis based on amino acid metabolism.

3.2. Iron metabolism

Iron metabolism disorder is thought to be a key factor in ferroptosis. While lipid peroxidation causes ferroptosis, an increase

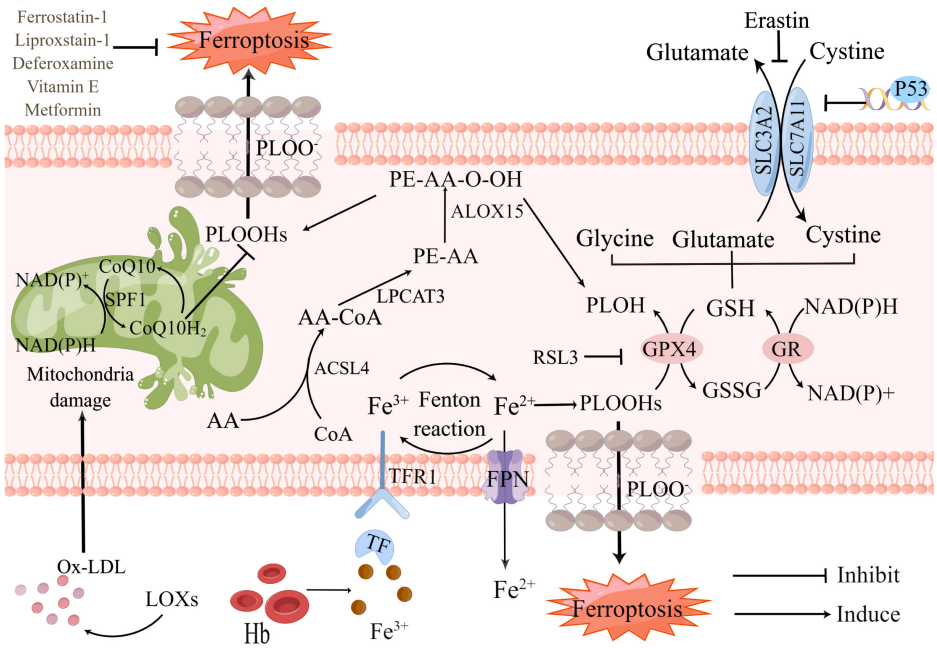

FIGURE 1
Core mechanisms and signaling pathways of ferroptosis in Intracerebral hemorrhage (ICH). Ferroptosis is driven by the accumulation of PLOOHs, which is tightly linked to the metabolism of amino acids, iron, and lipids. Iron overload and antioxidants lacking as the major component of lipid peroxidation, which contribute to ferroptosis. Fe3+, released from hemoglobin after ICH, converts into Fe2+ by Fenton reaction. Too much Fe2+ causes iron overload in neurons, accelerating intracellular reactive oxygen species (ROS) production and promoting ferroptosis. GSH-GPX4 and FSP1-CoQ are the two main pathways against ferroptosis. Restriction of either pathway will promote ferroptosis. PLOH, phospholipid alcohol; PLOOHs, phospholipid hydroperoxides; FSP1, ferroptosis suppressor protein 1; CoQ10, coenzyme Q10; CoQ10H2, ubiquinol-10; Ox-LDL, oxidized low-density lipoprotein; LOXs, lipoxygenases; Hb, hemoglobin; Fe3+, ferric iron; Fe2+, ferrous iron; ACSL4, Acyl-CoA synthase long-chain family member 4; AA-CoA, arachidonoyl-CoA; LPCAT3, lysophosphatidylcholine acyltransferase 3; FPN, ferroportin; RSL3, RAS-selective lethal 3; GPX4, glutathione peroxidase 4; GSH, glutathione; GSSG, glutathione disulfide; GR, glutathione reductase; ALOX15, arachidonate 15-lipoxygenase; SLC3A2, solute carrier family 3 member 2; SLC7A11, solute carrier family 7 member 11.

in intracellular iron is a risk factor for ferroptosis, and the level of damage is greater when iron is raised. Iron, a putative neurotoxin, is a major product of lysed erythrocytes in hematoma after ICH. It can be engulfed by microglia and infiltrating macrophages in the perihematomal zone and metabolized into ferrous/ferric iron, which induces the formation of lethal ROS and lipid peroxidation contributing to ferroptosis and SBI (Zhang et al., 2022a). Since intraparenchymal hematomas and red blood cells are the main sources of free iron in the ICH brain, resolution of hematoma and the clearance and phagocytosis of red blood cells might reduce iron-induced ferroptosis. Further research is necessary to examine these methods for treating iron-induced ferroptosis. Deferasirox (DFR), a trivalent iron chelator, suppressed microglia/macrophage activation in peri-hematoma area at 3 days after ICH and significantly suppressed the intracellular Fe2+ accumulation and cell death caused by hemin exposure. It might be a useful therapeutic agent for the therapy of ICH (Imai et al., 2021). Excessive iron form highly toxic hydroxyl radicals and trigger ROS formation to attack DNA, proteins, and lipid membranes, thereby disrupting cellular functions and causing neuronal death (Magtanong and Dixon, 2018; Zhang et al., 2022c). Wu et al. have shown that iron ions overload occurs in the posterior brain of ICH which accumulates within 3 days after ICH causing brain edema and cell death (Urday et al., 2015; Selim, 2022). Mechanistically, following ICH, excessive ferric irons from red blood cells (RBC) bind to transferrin (TF) in serum transported into cells through receptor-mediated effects (Schwartz-Duval and Sokolov, 2022). Ferric irons are reduced to ferrous ions by divalent metal transporter 1 (DMT1) and accumulation in nerve cells. Ferrous ions induce excessive lethal ROS and lipid peroxide formation. In a previous study of ICH in mice, two kinds of iron chelators, deferoxamine (DFX) and VK28, reduced the number of nerve cell death, iron ion accumulation, microglia activation and improved the neural function of mice eventually (Li et al., 2017a). Iron-dependent Fenton chain reaction is likely the key to ferroptosis. When GPX4 is lacking, phospholipid hydroperoxides (PLOOHs) in the cell cannot be removed in time and will react with iron to trigger the Fenton chain reaction, generating more PLOOHs. This is also a hallmark of ferroptosis (Conrad and Pratt, 2019). This reaction not only damages lipids and proteins but also causes oxidative damage to DNA, including DNA base modifications and DNA strand breaks (Gu et al., 2022; Wu et al., 2022). While an iron overload does not always induce ferroptosis, it will enhance cell death when it occurs. The mechanisms of brain iron metabolism are still poorly understood, which greatly limits the development of therapeutic drugs targeting brain iron efflux after ICH. Therefore, elucidating the mechanisms underlying iron metabolism is crucial to developing effective therapeutic strategies to reduce iron accumulation in ICH (Bao et al., 2020).

3.3. Lipid metabolism

In the physiological state, the dynamic balance between oxidation and antioxidant reactions helps to keep the body operating normally.

Polyunsaturated fatty acids (PUFAs), an integral component of the plasma membrane, may be oxidized *in vivo* enzymatically. Excess oxidized PUFA is converted by GPX4 to a non-toxic form. PUFAs can also be generated with fenton chemistry but a functional GPX4/GSH axis should be able to maintain homeostasis. One of the features of ferroptosis is the accumulation of LPO which causes a variety of damage to the structure and function of cells and membranes (Dixon et al., 2012). LPO is a lipid with a peroxide group formed after the reaction of unsaturated fatty acid chains with free radicals or ROS. Under normal conditions, the level of LPO is extremely low, but in pathological conditions, increased lipid peroxidation can lead to an increase. It has been illuminated as a clear mechanism to produce highly LPO with ROS up-regulation through the fenton chemistry (Liang et al., 2019; Lei et al., 2020). After ICH, ferrous ions overload, GPX4 deficiency, and PLOOHs cannot be cleared in time pointing to the susceptibility of the fenton chemistry. Overload ROS that exceeds the antioxidant capacity of cells leads to an enhanced oxidative stress response, which directly or indirectly damages proteins, nucleic acids, lipids, and other macromolecular substances (Tan et al., 2022). Finally, the membrane is damaged and the cell collapses and dies due to the lipid peroxidation inside the phospholipid of the cell membrane. In addition, GPX4, a selenoprotein, implies that selenium availability impacts the sensitivity to ferroptosis. It functions to reduce PLOOHs to lipid alcohols (L-OH) and to reduce H_2O_2 to H_2O then reduce the damage to membrane function (Tang et al., 2019). Delivery of selenium to cells or animals to upgrade GPX4 level can suppress ferroptosis, including in a mouse model of ICH (Friedmann Angeli and Conrad, 2018; Ingold et al., 2018; Alim et al., 2019). However, abnormal amino acid metabolism after ICH results in GPX4 deficiency as mentioned above. Other research has shown that the suppression of GPX4 is related to cyclooxygenase-2 (COX-2) and the increased expression of 15-lipoxygenase (ALOX15) (Meng et al., 2022). Li et al. (2017b) observed in a collagenase-induced ICH model that COX-2, encoded by-product cyclooxygenase-2 (PTGDS-2), was highly expressed in post-ICH neurons. High expression of COX-2 contributes to ferroptosis by inhibiting the antioxidant effect of GPX4. In addition, ALOX15 participates in the programmed degradation of organelles by binding to the membranes of various organelles in cells. *In vitro* ALOX15 is found to bind to mitochondria leading to membrane disintegration and ROS production (Choudhary et al., 2022). Currently, increased ALOX was observed after ICH in both humans and mice (Karuppagounder et al., 2018). Lipoxygenases (LOXs) have been also implicated as central players in ferroptosis (Shah et al., 2018). 5-lipoxygenase (5-LOX) inhibitor Zileuton could inhibit ferroptosis and play a protective role in nerve cells through the reduction of lipid peroxides (LPO) production (Gao et al., 2015; Shah et al., 2018). Therefore, the regulation of enzymes in lipid metabolism and enhancement of cellular antioxidant effects are other potential targets for inhibiting ferroptosis.

4. The crosstalk between ferroptosis and other traditional cell death pathways in ICH

There are various forms of cell death have been identified in ICH earlier except for ferroptosis (Chen et al., 2012; Zille et al., 2017; Zhang et al., 2018, 2020; Djulbegovic and Uversky, 2019), including apoptosis (de Oliveira Manoel, 2020; Gan et al., 2021; Tarantini et al., 2021; Grootaert and Bennett, 2022; Kuramoto et al., 2022), necroptosis (Yuan et al., 2019; Meng et al., 2021), autophagy (Chen et al., 2012; Cao and Mu, 2021; Zhang et al., 2022b) and so on in humans and experimental animals. Ferroptosis is mainly characterized by lipid peroxidation-induced cell death, which is morphologically, biochemically, and genetically distinct from apoptosis, necroptosis, and autophagy[14]. Cell death pathways have long been considered to function in parallel with little or no overlap. However, it is currently clear that apoptosis, necroptosis, autophagy, and ferroptosis are tightly connected and can cross-regulation each other. Gao et al. (2016), found that during ferroptosis ferritin is actively degraded *via* an autophagy pathway and the iron is released from ferritin to actively promote ferroptosis and hence he demonstrated that autophagy is important for ferroptosis initiation. Hou et al. also demonstrated experimentally that autophagy promotes ferroptosis by degrading ferritin in fibroblasts and cancer cells. And the erastin-induced ferroptosis could be inhibited by Atg5 (autophagy-related 5) and Atg7 knockouts or knockdowns, which resulted in lower intracellular ferrous iron levels and reduced lipid peroxidation (Hou et al., 2016). Briefly, modes of cell death following ICH are varied and overlapping. The mechanisms involved need to be supported by more research. Here will show the overview and comparison of different neuronal cell death types: apoptosis, necroptosis, and autophagy. Each type, along with its characteristics and mechanisms, and their potential roles in brain damage after ICH, are discussed below and are compared with the corresponding features of ferroptosis (**Table 1**).

4.1. Ferroptosis and apoptosis

Apoptosis is an active process that is subject to strict gene activation, expression, and regulation, demarcated by permeabilization of the mitochondrial outer membrane and promoted by executioner caspases (Sekerdag et al., 2018). Studies on the regulation of apoptosis after ICH have been conducted earlier. In Young et al. (1989) reported that leukocytes infiltrating the brain in ICH can release harmful substances, such as proteolytic and oxidizing agents as well as cytokines, which can injure or kill cells through caspase-dependent or independent pathways (Zhang et al., 2022c). In a rabbit ICH model, the levels of active caspase-3, Fas, FasL, and active caspase-8 were upregulated in neurons near the hematoma driving neuronal apoptosis after ICH (Deng et al., 2018). Wang et al. (2022) reported that histone deacetylase 6 (HDAC6) inhibition protects against brain injury post-ICH by reducing neuron apoptosis and apoptosis-related protein expression levels by acetylation of malate dehydrogenase 1 (MDH1). Studies of tumors have shown that the ferroptosis inducer erastin activates the p53-dependent CHOP/PUMA axis and increases sensitivity to apoptosis induced by the tumor necrosis factor-related apoptosis-inducing ligand (TRAIL) (Hong et al., 2018). Ferroptosis has been shown to inhibit apoptosis through the JNK signaling pathway activity (Liu et al., 2012). Thus, there are some crosstalk between ferroptosis and apoptosis.

4.2. Ferroptosis and necroptosis

Necroptosis combines both necrosis and apoptosis, hence the term necroptosis (Vanden Berghe et al., 2014). It is a regulated form of necrotic cell death mediated by receptor-interacting kinase 1 (RIPK1), receptor-interacting protein kinase 3

TABLE 1 The main feature of apoptosis, necroptosis, autophagy, ferroptosis.

Type of cell death	Morphological feature	Regulators	Relationship with ferroptosis
Apoptosis	Plasma membrane blebbing, exposure of membrane phosphatidylserine, cellular and nuclear volume reduction. Nuclear shrink, nuclear fragmentation, chromatin condensation and margination	Bax, Bak, p53, Bcl-2, Bcl-XL	Ferroptosis inhibit apoptosis through the JNK signaling pathway activity
Necroptosis	Rupture of plasma membrane. Organelle swelling. Moderate chromatin condensation	RIP1/3, MLKL	Ferroptosis is always accompanied by necroptosis. NADPH might be a link between them
Autophagy	Formation of double-membraned autolysosomes	PI3K-AKT-mTOR, MAPK-ERK1/2-mTOR signal pathway	Autophagy regulates intracellular iron homeostasis and ROS synthesis to promote ferroptosis
Ferroptosis	The cell membrane did not rupture and blisters. Mitochondrial crests are reduced or disappeared, and the outer mitochondrial membrane ruptures. Normal nuclear size and chromatin	NOX, GPX4, p53, HO-1 DHODH, FSP1, BH4, GOT1, NRF2	

(RIPK3), and mixed lineage kinase domain-like (MLKL) (Conrad et al., 2016; Cao et al., 2022). RIPK1 activates RIPK3 and thereby recruits MLKL at the cell membrane, which causes membrane rupture and eventually triggers necroptosis (Samson et al., 2021; Gupta et al., 2022). Necroptosis is involved in cell death associated with ICH (Galluzzi et al., 2018). Neurovascular injury and related hemolysis of extravasated erythrocytes post-ICH producing hemoglobin degradation metabolites may trigger the neuroinflammatory response of surrounding astroglia resulting in activation of the necroptotic pathway. Meanwhile, Necrostatin-1, a specific RIPK1 inhibitor, has been shown to reduce cell death, hematoma volume, and neurobehavioral outcomes in a mouse model of ICH (Gupta et al., 2022). Numerous reports have suggested that ferroptosis is always accompanied by necroptosis (Lv et al., 2021). The major ultrastructural characteristics of hemin-induced neuron death are related to ferroptosis and not necroptosis. In contrast, molecular marker levels of both ferroptosis (ferric iron, GSH, and GPX4) and necroptosis (MLKL and RIPK3) may increase after ICH. NADPH might be a link between ferroptosis and necroptosis (Hou et al., 2019). However, such studies regarding ICH are lacking (Lin et al., 2016; Newton et al., 2016; Minagawa et al., 2020; Chen et al., 2022b).

4.3. Ferroptosis and autophagy

Some research has revealed the important role of autophagy in ferroptosis, especially selective types of autophagy (e.g., ferritinophagy, lipophagy, clockophagy, and chaperone-mediated autophagy) (Liu et al., 2020). Ferritinophagy is the process of autophagic degradation of the iron storage protein ferritin, which is critical for the regulation of cellular iron levels. ferritinophagy promotes ferroptosis by releasing free iron from ferritin. Inhibition of Ferritinophagy inhibits ferritin degradation and therefore reduces free iron levels and thus limits subsequent oxidative injury during ferroptosis (Gao et al., 2016; Hou et al., 2016). Moreover, deficient ferritinophagy may increase the activity of iron-responsive element binding protein 2 (IREB2/IRP2) to promote ferroptosis (Dixon et al., 2012). According to Gao et al. (2016) autophagy regulates intracellular iron homeostasis and ROS synthesis to promote ferroptosis. *In vitro* experiments showed that Erastin, a synthetic small-molecule compound, which induces ferroptosis and activates autophagy, led to intracellular ferritin degradation to further increase the level of intracellular iron ions through autophagy, resulting in rapid accumulation of intracellular ROS, which promote ferroptosis. Hou et al. (2016) also demonstrated that the activation of autophagy further promoted ferroptosis by degrading ferritin in tumor cells. Suppressing autophagy is one of the ways to inhibit ferroptosis. Lipophagy, the autophagic digestion of lipid droplets can release free fatty acids. The level of lipid droplets is negatively related to oxidative stress-induced ferroptosis (Cho et al., 2022). Increased lipid droplet formation suppresses RSL3-induced ferroptosis in hepatocytes (Cho et al., 2022). In contrast, increased lipophagy promotes lipid droplet degradation and therefore increases lipid peroxidation-mediated ferroptosis (Cho et al., 2022). Chaperone-mediated autophagy (CMA) is a type of selective autophagy that uses molecular chaperones to deliver certain cytosolic proteins to lysosomes for degradation based on the recognition of specific amino acid sequences. ER stress-associated molecular chaperone, can limit erastin-induced GPX4 degradation and therefore protects against ferroptosis in pancreatic cancer cells (Zhu et al., 2017). These findings establish a model of interaction between CMA and autophagy to determine GPX4 protein stability in ferroptosis. In brief, ferroptosis and autophagy are inseparable and both contribute to neuronal death in ICH. Understanding the mechanism of autophagy and inhibiting it is one of the ways to inhibit neuronal ferroptosis.

5. Therapeutic application

Although the efficacy of medical interventions targeting pathological pathways of ICH has been verified in several preclinical studies, their promise has not translated to clinical trials in patients with ICH (Jin et al., 2021). Further efforts are needed to improve these limited medicinal approaches, mitigate neuronal death, and facilitate functional recovery during and after ICH. Ferroptosis has been shown to mediate the damage processes in patients with ICH (Li et al., 2020). Many previously reported neuroprotectants that showed protective effects in ICH models and patients were validated as ferroptosis inhibitors recently. Here we summarized the therapeutic targets of inhibitors of ferroptosis in ICH models (**Figure 2** and **Table 2**).

5.1. Selenium supplementation

Neurons respond to ferroptosis stimuli by induction of selenoproteins, including antioxidant GPX4. A single dose of Se

delivered into the brain drives antioxidant GPX4 expression, protects neurons, and improves behavior in an ICH model. According to Tuo et al. (2021), certain selenocompounds are selective anti-ferroptotic medications that can cross the blood-brain barrier and prevent neuronal death in ischemic stroke. Recent studies demonstrated that selenium can drive protective transcriptional responses, including the transcriptional activators TFAP2c and Sp1, to upregulate GPX4 and suppress ferroptosis (Alim et al., 2019). Pharmacological Se supplementation effectively inhibits GPX4-dependent ferroptosis. The inhibition of ferroptosis and neuronal protection of selenium *via* transcriptional regulation have been verified in mouse models of ICH and ischemic stroke (Alim et al., 2019). *In vitro* and *in vivo* results highlight the potential of the pharmacological administration of selenium for the treatment of both hemorrhagic and ischemic stroke. It is also noteworthy that the Tat SelPep (a peptide that can increase GPX4 expression in the brain) can overcome the narrow therapeutic window of direct intracerebroventricular injections of sodium selenite, providing a novel strategy to deliver selenium with minimal toxicity (Alim et al., 2019).

5.2. Iron chelators

Intracerebral hemorrhage leads to iron overload and the upregulation of iron-handling proteins, resulting in a brain injury that can be reduced by DFX, an iron chelator, indicating that

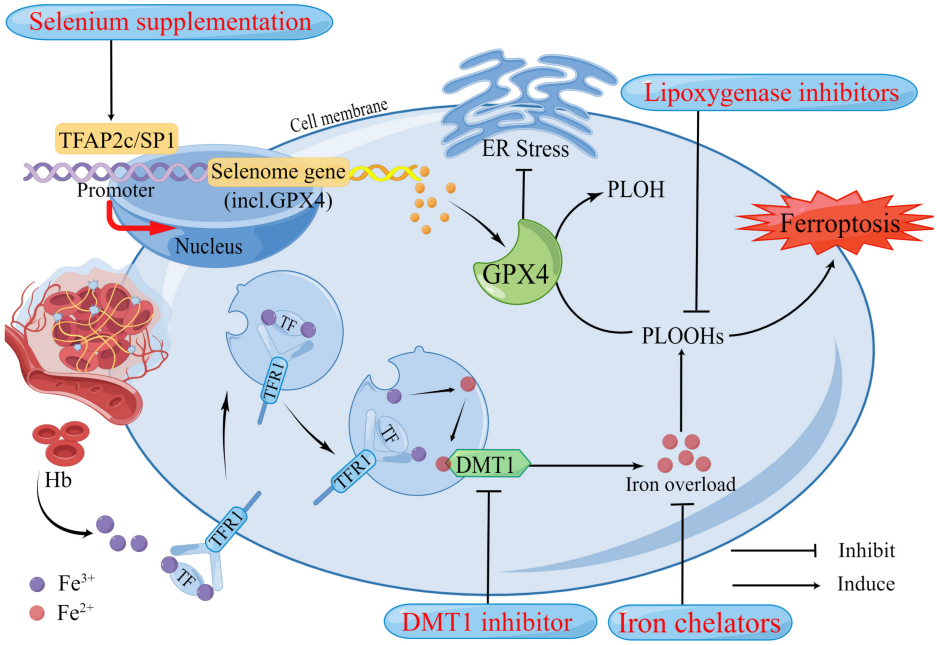

FIGURE 2
Potential therapeutic strategies based on neuronal ferroptosis after Intracerebral hemorrhage (ICH). Several regulators in the ferroptosis pathway are highlighted in the treatment of ICH. These regulators have been confirmed to play roles in ferroptosis. After ICH, in addition to the primary brain injury caused by the hematoma compressing the surrounding brain tissue, Hb, iron, and other neurotoxic substances released by the hematoma also contribute to the increase of reactive oxygen species (ROS), resulting in ferroptosis and cause secondary brain injury. DMT1 and Iron chelators could reduce iron overload from two aspects, respectively. GPX4 acts as an antioxidant that inhibits ER stress and reduces lipid peroxides in cells to harmless PLOH to inhibit ferroptosis. It has been well established that GPX4 deficiency causes neuronal ferroptosis after ICH. Selenium supplementation augments GPX4 and other genes in this transcriptional program, the selenome, *via* coordinated activation of the transcription factors TFAP2c and Sp1 to protect neurons. Hb, hemoglobin; Fe3+, ferric iron; Fe2+, ferrous iron; TF, transferrin; TFR1, transferrin receptor 1; DMT1, divalent metal transporter 1; Gpx4, glutathione peroxidase 4; PLOH, phospholipid alcohol; PLOOHs, phospholipid hydroperoxides; ER, endoplasmic reticulum.

TABLE 2 Reagent associated with ferroptosis.

Reagent	Target/function	Impact on ferroptosis	Mechanism
Selenium	Selenoproteins, GPX4	Stimulates the expression of the selenoproteins, such as antioxidant GPX4	GPX4 availability
DFX	Iron	Function as iron chelator, depletes iron, and prevent iron-dependent lipid peroxidation	Reduced iron overload
VK-28	Iron	Function as iron chelator, depletes iron, and prevent iron-dependent lipid peroxidation	Reduced iron overload
Deferiprone	Iron	Function as iron chelator, depletes iron, and prevent iron-dependent lipid peroxidation	Reduced iron overload
LOX inhibitors	Lipid peroxidation	Inhibits cytosolic ROS production and blocks lipid peroxidation	Radical trapping
Ebselen (DMT1 inhibitors)	Iron	Reduced the iron ion transport activity of DMT1 and prevents iron-dependent lipid peroxidation	Reduced iron overload

iron imbalance is an essential initiator of ferroptosis and can provide new insights into the neuroprotective activity of iron chelators (Xue et al., 2022). DFX inhibits the overactivation of microglia by forming an iron amine chelate with iron ions around the hematoma, preventing iron ions from providing electrons to oxygen to form ROS (Dixon and Stockwell, 2014; Li et al., 2017b). This processing alleviates cerebral edema, neurological deficit, and brain atrophy after ICH in rats (Selim et al., 2019). Several iron chelators have been developed. DFX was approved by the FDA in 1968 as an iron chelator that concentrates in the brain following subcutaneous injection. By sequestering nonheme iron, DFX effectively diminishes hydroxyl radical formation and reduces brain damage after subarachnoid hemorrhage (SAH) (Pandya et al., 2021). In addition to SAH, studies have reported favorable effects of DFX in various hemorrhage models, including reduced iron overload, attenuated brain–blood barrier (BBB) disruption, reduced dendritic and white matter damage, improved neurological behavior, and lower rates of mortality (Selim et al., 2019). However, according to Selim et al. (2019), the Intracerebral Hemorrhage Deferoxamine (i-DEF) trial failed to demonstrate that using DFX to treat ICH patients was sufficient enough and further research is needed to determine its effectiveness. Compared with DFX, VK-28 has a greater advantage in that it can penetrate the intact BBB which is a more effective and safer advantage. Therefore, VK-28 may act at lower concentrations in the brain, making it more suitable for clinical (Li et al., 2017a). Deferiprone, an iron chelator that can cross the blood-brain barrier, is utilized for transfusion-dependent thalassemia as well as in Parkinson's disease clinical trials (Devos et al., 2022). These results may stimulate further development of iron chelators for ICH treatment.

5.3. Lipoxygenase inhibitors

Lipoxygenases inhibitors with radical trapping can function as terminators of the radical chain reactions of lipid autoxidation to inhibit ferroptosis (Poon et al., 2021). For LOX inhibitors that lack radical trapping ability, those targeting 15-LOX-1, exhibit a degree of anti-ferroptosis activity (Kagan et al., 2017). 15-LOX-1 has been regarded as a potent target for stroke treatment. Among the six LOXs isoforms (15-LOX-1, 15-LOX-2, 12S-LOX, 12R-LOX, eLOX3, and 5-LOX), 15-LOX-1 levels increase under pathological conditions in both human and mice following stroke (Yigitkanli et al., 2013; Watanabe et al., 2022). Moreover, 15-LOX-1-KO mice exhibited a protective ability against ischemic injury in several experimental stroke models (Shen et al., 2020a), highlighting the benefits of inhibiting 15-LOX-1 during stroke treatment. Targeting 15-LOX-1 during both ischemic and hemorrhagic stroke treatment showed effective and potent neuroprotective activity in several mouse models (Yigitkanli et al., 2013; Shen et al., 2020b). 15-LOX-1 inhibitors lacking radical-trapping activity might block ferroptosis by directly inhibiting the complexes. This provides a novel direction for the future development of such inhibitors.

5.4. DMT1 inhibitor

Divalent metal transporter 1 is a divalent metal ion transporter and is the only protein that transports ferrous iron from endosomes into the cytosol (Gao et al., 2015). In endosomes, upon release of ferric iron from transferrin following acidification, ferric iron is reduced to ferrous iron by a specific reductase and then ferrous iron is pumped in the cytosol by DMT1. After ICH, the expression of DMT1 is significantly increased. Ferrous ions induce the formation of excessive ROS and LPO, which are important factors causing ferroptosis in nerve cells (Nogueira et al., 2021). Pretreatment with the DMT1 inhibitor, ebselen, significantly reduced the iron ion transport activity of DMT1 and inhibited the production of ROS (Cheng et al., 2022). Research demonstrated that ebselen further attenuated DMT1 by inhibiting ferroptosis of neuronal cells after SAH in rats. At present, it is necessary to further strengthen the study of ebselen in cerebral hemorrhage.

6. Conclusion and perspectives

In recent years, the study of ferroptosis has gradually increased, and it is significant in exploring the direction of treatment and intervention for ICH. Ferroptosis is considered to be a form of regulated necrosis, which is strictly controlled at multiple levels (Stockwell et al., 2020; Chen et al., 2021). In general, ferroptosis is closely related to the intracellular iron ion, GSH, LPO, and so on factors. Selenium, iron chelators, lipoxygenase inhibitors, and DMT1 inhibitors can be used to inhibit cellular ferroptosis after ICH. It is expected to provide a new direction for the clinical treatment of ICH. Ferroptosis has more probing value in brain protection and improving neurologic function after ICH. However, more in-depth research is needed on how to translate these basic research results into clinical applications and reduce associated adverse effects.

In this review, we explored and summarized the modes of cell death after ICH, including apoptosis, autophagy, necroptosis, and ferroptosis. However, whether there is a sequential, synergistic, or other relationship between those modes of cell death is unknown and many mechanisms and regulatory factors of ferroptosis remain undiscovered. We discovered the existence of ferroptosis in neuronal cells following ICH by reviewing the literature, and also found some pathways and factors involved in regulating ferroptosis. But which plays a major role in the ferroptosis of neuronal cells after ICH, and are there other pathways of regulation? Many doubts remain to be resolved. In summary, although there are a large number of regulators that directly or indirectly affect the iron accumulation and lipid peroxidation to regulate ferroptosis post-ICH, there are still many questions that have not been answered. Further functional investigations into the complicated machinery and regulation of ferroptosis will provide a new way to effectively treat neuronal death after ICH.

Author contributions

YZ determined the structure of the review. YC selected the references and contributed to the writing. WX contributed to the revision and finalization of the manuscript. SL prepared the all figures. All authors contributed to the article and approved the submitted version.

Funding

This research was supported by the National Science and Technology Fundamental Resources Investigation Program of China (No. 2018FY100900), the National Natural Science Foundation of China (Nos. 815771151 and 82201614), and the Hunan Provincial Natural Science Foundation of China (No. 2021JJ30923).

Acknowledgments

We thank Jueyi Mao for her help on article submission. We also thank Figdraw (www.figdraw.com) for expert assistance in the pattern drawing.

Conflict of interest

The authors declare that the research was conducted in the absence of any commercial or financial relationships that could be construed as a potential conflict of interest.

Publisher's note

All claims expressed in this article are solely those of the authors and do not necessarily represent those of their affiliated organizations, or those of the publisher, the editors and the reviewers. Any product that may be evaluated in this article, or claim that may be made by its manufacturer, is not guaranteed or endorsed by the publisher.

References

Alim, I., Caulfield, J. T., Chen, Y., Swarup, V., Geschwind, D. H., Ivanova, E., et al. (2019). Selenium drives a transcriptional adaptive program to block ferroptosis and treat stroke. *Cell* 126:e1225.

Angeli, J. P. F., Shah, R., Pratt, D. A., and Conrad, M. (2017). Ferroptosis inhibition: Mechanisms and opportunities. *Trends Pharmacol. Sci.* 38, 489–498.

Aronowski, J., and Zhao, X. (2011). Molecular pathophysiology of cerebral hemorrhage: Secondary brain injury. *Stroke* 42, 1781–1786. doi: 10.1016/j.tips.2017.02.005

Bao, W. D., Zhou, X. T., Zhou, L. T., Wang, F., Yin, X., Lu, Y., et al. (2020). Targeting miR-124/Ferroportin signaling ameliorated neuronal cell death through inhibiting apoptosis and ferroptosis in aged intracerebral hemorrhage murine model. *Aging Cell* 19:e13235. doi: 10.1161/STROKEAHA.110.596718

Cao, L., and Mu, W. (2021). Necrostatin-1 and necroptosis inhibition: Pathophysiology and therapeutic implications. *Pharmacol Res* 163:105297. doi: 10.1111/acel.13235

Cao, T., Ni, R., Ding, W., Ji, X., Li, L., Liao, G., et al. (2022). MLKL-mediated necroptosis is a target for cardiac protection in mouse models of type-1 diabetes. *Cardiovasc. Diabetol.* 21:165. doi: 10.1016/j.phrs.2020.105297

Chen, C. W., Chen, T. Y., Tsai, K. L., Lin, C. L., Yokoyama, K. K., Lee, W. S., et al. (2012). Inhibition of autophagy as a therapeutic strategy of iron-induced brain injury after hemorrhage. *Autophagy* 8, 1510–1520. doi: 10.1186/s12933-022-01602-9

Chen, J., Li, X., Ge, C., Min, J., and Wang, F. (2022a). The multifaceted role of ferroptosis in liver disease. *Cell Death Differ.* 29, 467–480. doi: 10.4161/auto.21289

Chen, X., Li, J., Kang, R., Klionsky, D., and Tang, D. (2021). Ferroptosis: Machinery and regulation. *Autophagy* 17, 2054–2081. doi: 10.1038/s41418-022-00941-0

Chen, X., Zhu, R., Zhong, J., Ying, Y., Wang, W., Cao, Y., et al. (2022b). Mosaic composition of RIP1-RIP3 signalling hub and its role in regulating cell death. *Nat. Cell. Biol.* 24, 471–482. doi: 10.1080/15548627.2020.1810918

Cheng, H., Wang, N., Ma, X., Wang, P., Dong, W., Chen, Z., et al. (2022). Spatial-temporal changes of iron deposition and iron metabolism after traumatic brain injury in mice. *Front. Mol. Neurosci.* 15:949573. doi: 10.1038/s41556-022-00854-7

Cho, S., Hong, S. J., Kang, S. H., Park, Y., and Kim, S. K. (2022). Alpha-lipoic acid attenuates apoptosis and ferroptosis in cisplatin-induced ototoxicity via the reduction of intracellular lipid droplets. *Int. J. Mol. Sci.* 23:427 doi: 10.3389/fnmol.2022.949573

Choudhary, R., Kumar, M., and Katyal, A. (2022). 12/15-Lipoxygenase debilitates mitochondrial health in intermittent hypobaric hypoxia induced neuronal damage: An in vivo study. *Redox. Biol.* 49:102228. doi: 10.3390/ijms231810981

Conrad, M., and Pratt, D. A. (2019). The chemical basis of ferroptosis. *Nat. Chem. Biol.* 15, 1137–1147. doi: 10.1016/j.redox.2021.102228

Conrad, M., Angeli, J. P., Vandenabeele, P., and Stockwell, B. R. (2016). Regulated necrosis: Disease relevance and therapeutic opportunities. *Nat. Rev. Drug Discov.* 15, 348–366. doi: 10.1038/s41589-019-0408-1

Conrad, M., Kagan, V. E., Bayir, H., Pagnussat, G. C., Head, B., Traber, M. G., et al. (2018). Regulation of lipid peroxidation and ferroptosis in diverse species. *Gen. Dev.* 32, 602–619. doi: 10.1038/nrd.2015.6

de Oliveira Manoel, A. L. (2020). Surgery for spontaneous intracerebral hemorrhage. *Crit. Care* 24:45. doi: 10.1101/gad.314674.118

Deng, T., Yan, G., Song, X., Xie, L., Zhou, Y., Li, J., et al. (2018). Deubiquitylation and stabilization of p21 by USP11 is critical for cell-cycle progression and DNA damage responses. *Proc. Natl. Acad. Sci. U.S.A.* 115, 4678–4683. doi: 10.1186/s13054-020-2749-2

Devos, D., Labreuche, J., Rascol, O., Corvol, J. C., Duhamel, A., Guyon Delannoy, P., et al. (2022). Trial of Deferiprone in Parkinson's Disease. *N. Engl. J. Med.* 387, 2045–2055. doi: 10.1073/pnas.1714938115

Dixon, S. J., and Stockwell, B. R. (2014). The role of iron and reactive oxygen species in cell death. *Nat. Chem. Biol.* 10, 9–17. doi: 10.1056/NEJMoa2209254

Dixon, S. J., Lemberg, K. M., Lamprecht, M. R., Skouta, R., Zaitsev, E. M., Gleason, C. E., et al. (2012). Ferroptosis: An iron-dependent form of nonapoptotic cell death. *Cell* 149, 1060–1072. doi: 10.1038/nchembio.1416

Dixon, S. J., Patel, D. N., Welsch, M., Skouta, R., Lee, E. D., Hayano, M., et al. (2014). Pharmacological inhibition of cystine-glutamate exchange induces endoplasmic reticulum stress and ferroptosis. *Elife* 3:e02523. doi: 10.1016/j.cell.2012.03.042

Djulbegovic, M. B., and Uversky, V. N. (2019). Ferroptosis - An iron- and disorder-dependent programmed cell death. *Int. J. Biol. Macromol.* 135, 1052–1069. doi: 10.7554/eLife.02523

Donnan, G., Hankey, G., and Davis, S. (2010). Intracerebral haemorrhage: A need for more data and new research directions. *Lancet Neurol.* 9, 133–134. doi: 10.1016/j.ijbiomac.2019.05.221

Epping, L., Schroeter, C. B., Nelke, C., Bock, S., Gola, L., Ritter, N., et al. (2022). Activation of non-classical NMDA receptors by glycine impairs barrier function of brain endothelial cells. *Cell. Mol. Life Sci.* 79:479. doi: 10.1016/S1474-4422(10)70001-6

Fricker, M., Tolkovsky, A., Borutaite, V., Coleman, M., and Brown, G. (2018). Neuronal cell death. *Physiol. Rev.* 98, 813–880. doi: 10.1007/s00018-022-04502-z

Friedmann Angeli, J. P., and Conrad, M. (2018). Selenium and GPX4, a vital symbiosis. *Free Radic. Biol. Med.* 127, 153–159. doi: 10.1152/physrev.00011.2017

Fujii, J., Homma, T., and Kobayashi, S. (2020). Ferroptosis caused by cysteine insufficiency and oxidative insult. *Free Radic. Res.* 54, 969–980. doi: 10.1016/j.freeradbiomed.2018.03.001

Galluzzi, L., Vitale, I., Aaronson, S. A., Abrams, J. M., Adam, D., Agostinis, P., et al. (2018). Molecular mechanisms of cell death: Recommendations of the Nomenclature Committee on Cell Death 2018. *Cell Death Differ.* 25, 486–541. doi: 10.1080/10715762.2019.1666983

Gan, H., Zhang, L., Chen, H., Xiao, H., Wang, L., Zhai, X., et al. (2021). The pivotal role of the NLRC4 inflammasome in neuroinflammation after intracerebral hemorrhage in rats. *Exp. Mol. Med.* 53, 1807–1818. doi: 10.1038/s41418-017-0012-4

Gao, M., Monian, P., Pan, Q., Zhang, W., Xiang, J., and Jiang, X. (2016). Ferroptosis is an autophagic cell death process. *Cell Res.* 26, 1021–1032. doi: 10.1038/s12276-021-00702-y

Gao, M., Monian, P., Quadri, N., Ramasamy, R., and Jiang, X. (2015). Glutaminolysis and Transferrin Regulate Ferroptosis. *Mol. Cell* 59, 298–308.

Grootaert, M. O. J., and Bennett, M. R. (2022). Sirtuins in atherosclerosis: Guardians of healthspan and therapeutic targets. *Nat. Rev. Cardiol.* 19, 668–683.

Gu, R., Xia, Y., Li, P., Zou, D., Lu, K., Ren, L., et al. (2022). Ferroptosis and its Role in Gastric Cancer. *Front. Cell Dev. Biol.* 10:860344. doi: 10.1016/j.molcel.2015.06.011

Gupta, K., Brown, K. A., Hsieh, M. L., Hoover, B. M., Wang, J., Khoury, M. K., et al. (2022). Necroptosis is associated with Rab27-independent expulsion of extracellular vesicles containing RIPK3 and MLKL. *J. Extracell Vesicles* 11:e12261. doi: 10.1038/s41569-022-00685-x

Hong, S. H., Lee, D. H., Lee, Y. S., Jo, M. J., Jeong, Y. A., Kwon, W. T., et al. (2018). Correction: Molecular crosstalk between ferroptosis and apoptosis: Emerging role of ER

stress-induced p53-independent PUMA expression. *Oncotarget* 9:24869. doi: 10.3389/fcell.2022.860344

Hou, L., Huang, R., Sun, F., Zhang, L., and Wang, Q. (2019). NADPH oxidase regulates paraquat and maneb-induced dopaminergic neurodegeneration through ferroptosis. *Toxicology* 417, 64–73. doi: 10.1002/jev2.12261

Hou, W., Xie, Y., Song, X., Sun, X., Lotze, M. T., Zeh, H. J. III, et al. (2016). Autophagy promotes ferroptosis by degradation of ferritin. *Autophagy* 12, 1425–1428. doi: 10.18632/oncotarget.25365

Imai, T., Tsuji, S., Matsubara, H., Ohba, T., Sugiyama, T., Nakamura, S., et al. (2021). Deferasirox, a trivalent iron chelator, ameliorates neuronal damage in hemorrhagic stroke models. *Naunyn Schmiedebergs Arch. Pharmacol.* 394, 73–84. doi: 10.1016/j.tox.2019.02.011

Ingold, I., Berndt, C., Schmitt, S., Doll, S., Poschmann, G., Buday, K., et al. (2018). Selenium Utilization by GPX4 Is required to prevent Hydroperoxide-induced ferroptosis. *Cell* 40:e421.

Jin, Y., Zhuang, Y., Liu, M., Che, J., and Dong, X. (2021). Inhibiting ferroptosis: A novel approach for stroke therapeutics. *Drug Discov. Today* 26, 916–930.

Kagan, V. E., Mao, G., Qu, F., Angeli, J., Doll, S., Croix, C., et al. (2017). Oxidized arachidonic and adrenic PEs navigate cells to ferroptosis. *Nat. Chem. Biol.* 13, 81–90. doi: 10.1007/s00210-020-01963-6

Karuppagounder, S. S., Alin, L., Chen, Y., Brand, D., Bourassa, M., Dietrich, K., et al. (2018). N-acetylcysteine targets 5 lipoxygenase-derived, toxic lipids and can synergize with prostaglandin E2 to inhibit ferroptosis and improve outcomes following hemorrhagic stroke in mice. *Ann. Neurol.* 84, 854–872. doi: 10.1016/j.cell.2017.11.048

Kuramoto, Y., Fujita, M., Takagi, T., Takeda, Y., Doe, N., Yamahara, K., et al. (2022). Early-phase administration of human amnion-derived stem cells ameliorates neurobehavioral deficits of intracerebral hemorrhage by suppressing local inflammation and apoptosis. *J. Neuroinflammation* 19:48. doi: 10.1016/j.drudis.2020.12.020

Leasure, A. C., Kuohn, L. R., Vanent, K. N., Bevers, M. B., Kimberly, W. T., Steiner, T., et al. (2021). Association of Serum IL-6 (Interleukin 6) with functional outcome after intracerebral hemorrhage. *Stroke* 52, 1733–1740. doi: 10.1038/nchembio.2238

Lei, G., Zhang, Y., Koppula, P., Liu, X., Zhang, J., Lin, S., et al. (2020). The role of ferroptosis in ionizing radiation-induced cell death and tumor. *Cell Res.* 30, 146–162. doi: 10.1002/ana.25356

Li, J., Cao, F., Yin, H., Huang, Z., Lin, Z., Mao, N., et al. (2020). Ferroptosis: Past, present and future. *Cell Death Dis.* 11:88. doi: 10.1186/s12974-022-02411-3

Li, Q., Han, X., Lan, X., Gao, Y., Wan, J., Durham, F., et al. (2017b). Inhibition of neuronal ferroptosis protects hemorrhagic brain. *JCI Insight* 2:e90777. doi: 10.1161/STROKEAHA.120.032888

Li, Q., Wan, J., Lan, X., Han, X., Wang, Z., and Wang, J. (2017a). Neuroprotection of brain-permeable iron chelator VK-28 against intracerebral. *J. Cereb. Blood Flow Metab.* 37, 3110–3123. doi: 10.1038/s41422-019-0263-3

Li, Q., Weiland, A., Chen, X., Lan, X., Han, X., Durham, F., et al. (2018). Ultrastructural characteristics of neuronal death and white matter injury in mouse brain tissues after intracerebral hemorrhage: Coexistence of ferroptosis. autophagy, and necrosis. *Front. Neurol.* 9:581. doi: 10.1038/s41419-020-2298-2

Liang, C., Zhang, X., Yang, M., and Dong, X. (2019). Recent progress in ferroptosis inducers for cancer therapy. *Adv. Mater.* 31:e1904197.

Lin, J., Kumari, S., Kim, C., Van, T. M., Wachsmuth, L., Polykratis, A., et al. (2016). RIPK1 counteracts ZBP1-mediated necroptosis to inhibit inflammation. *Nature* 540, 124–128.

Liu, F., Du, Z. Y., He, J. L., Liu, X. Q., Yu, Q. B., and Wang, Y. X. (2012). FTH1 binds to Daxx and inhibits Daxx-mediated cell apoptosis. *Mol. Biol. Rep.* 39, 873–879. doi: 10.1177/0271678X17709186

Liu, J., Kuang, F., Kroemer, G., Klionsky, D. J., Kang, R., and Tang, D. (2020). Autophagy-dependent ferroptosis: Machinery and regulation. *Cell Chem. Biol.* 27, 420–435. doi: 10.3389/fneur.2018.00581

Liu, Y., and Gu, W. (2022). p53 in ferroptosis regulation: The new weapon for the old guardian. *Cell Death Differ.* 29, 895–910. doi: 10.1002/adma.201904197

Lv, Z., Xiong, L. L., Qin, X., Zhang, H., Luo, X., Peng, W., et al. (2021). Role of GRK2 in trophoblast necroptosis and spiral artery remodeling: Implications for preeclampsia pathogenesis. *Front. Cell Dev. Biol.* 9:694261. doi: 10.1038/nature20558

Magtanong, L., and Dixon, S. J. (2018). Ferroptosis and Brain Injury. *Dev. Neurosci.* 40, 382–395. doi: 10.1007/s11033-011-0811-5

Meng, H., Wu, G., Zhao, X., Wang, A., Li, D., Tong, Y., et al. (2021). Discovery of a cooperative mode of inhibiting RIPK1 kinase. *Cell Discov.* 7:41. doi: 10.1016/j.chembiol.2020.02.005

Meng, Y., Sun, H., Li, Y., Zhao, S., Su, J., Zeng, F., et al. (2022). Targeting ferroptosis by ubiquitin system enzymes: A potential therapeutic strategy in cancer. *Int. J. Biol. Sci.* 18, 5475–5488. doi: 10.1038/s41418-022-00943-y

Minagawa, S., Yoshida, M., Araya, J., Hara, H., Imai, H., and Kuwano, K. (2020). Regulated necrosis in pulmonary disease. a focus on necroptosis and ferroptosis. *Am. J. Respir. Cell Mol. Biol.* 62, 554–562. doi: 10.3389/fcell.2021.694261

Newton, K., Dugger, D. L., Maltzman, A., Greve, J. M., Hedehus, M., Martin-McNulty, B., et al. (2016). RIPK3 deficiency or catalytically inactive RIPK1 provides greater benefit than MLKL deficiency in mouse models of inflammation and tissue injury. *Cell Death Differ.* 23, 1565–1576. doi: 10.1159/000496922

Nogueira, C. W., Barbosa, N. V., and Rocha, J. B. T. (2021). Toxicology and pharmacology of synthetic organoselenium compounds: An update. *Arch. Toxicol.* 95, 1179–1226. doi: 10.1038/s41421-021-00278-x

Pandya, C. D., Vekaria, H., Joseph, B., Slone, S. A., Gensel, J. C., Sullivan, P. G., et al. (2021). Hemoglobin induces oxidative stress and mitochondrial dysfunction in oligodendrocyte progenitor cells. *Transl. Res.* 231, 13–23. doi: 10.7150/ijbs.73790

Peng, C., Fu, X., Wang, K., Chen, L., Luo, B., Huang, N., et al. (2022). Dauricine alleviated secondary brain injury after intracerebral hemorrhage by upregulating GPX4 expression and inhibiting ferroptosis of nerve cells. *Eur. J. Pharmacol.* 914:174461. doi: 10.1165/rcmb.2019-0337TR

Poon, J. F., Farmer, L. A., Haidasz, E. A., and Pratt, D. A. (2021). Temperature-dependence of radical-trapping activity of phenoxazine, phenothiazine and their aza-analogues clarifies the way forward for new antioxidant design. *Chem. Sci.* 12, 11065–11079. doi: 10.1038/cdd.2016.46

Qureshi, A. I., Mendelow, A. D., and Hanley, D. F. (2009). Intracerebral haemorrhage. *Lancet* 373, 1632–1644. doi: 10.1007/s00204-021-03003-5

Samson, A. L., Fitzgibbon, C., Patel, K. M., Hildebrand, J. M., Whitehead, L. W., Rimes, J. S., et al. (2021). A toolbox for imaging RIPK1, RIPK3, and MLKL in mouse and human cells. *Cell Death Differ.* 28, 2126–2144. doi: 10.1016/j.trsl.2021.01.005

Schwartz-Duval, A. S., and Sokolov, K. V. (2022). Prospecting cellular gold nanoparticle biomineralization as a viable alternative to prefabricated gold nanoparticles. *Adv. Sci.* 9:e2105957. doi: 10.1016/j.ejphar.2021.174461

Sekerdag, E., Solaroglu, I., and Gursoy-Ozdemir, Y. (2018). Cell Death Mechanisms in Stroke and Novel Molecular and Cellular Treatment. *Curr. Neuropharmacol.* 16, 1396–1415. doi: 10.1039/D1SC02976B

Selim, M. (2022). Building the case for targeting the secondary injury after intracerebral hemorrhage: Slowly but surely. *Stroke* 53, 2036–2037. doi: 10.1016/S0140-6736(09)60371-8

Selim, M., Foster, L. D., Moy, C. S., Xi, G., Hill, M. D., Morgenstern, L. B., et al. (2019). Deferoxamine mesylate in patients with intracerebral haemorrhage (i-DEF): A multicentre, randomised, placebo-controlled, double-blind phase 2 trial. *Lancet Neurol.* 18, 428–438. doi: 10.1038/s41418-021-00742-x

Shah, R., Shchepinov, M., and Pratt, D. (2018). Resolving the role of Lipoxygenases in the Initiation and execution of ferroptosis. *ACS Cent. Sci.* 4, 387–396. doi: 10.1002/advs.202105957

Shen, B., Zhou, P., Jiao, X., Yao, Z., Ye, L., and Yu, H. (2020a). Fermentative production of Vitamin E tocotrienols in Saccharomyces cerevisiae under cold-shock-triggered temperature control. *Nat. Commun.* 11:5155. doi: 10.2174/1570159X16666180302115544

Shen, L., Lin, D., Li, X., Wu, H., Lenahan, C., Pan, Y., et al. (2020b). Ferroptosis in acute central nervous system injuries: The future direction? *Front. Cell Dev. Biol.* 8:594. doi: 10.1161/STROKEAHA.122.038321

Stockwell, B. R., Friedmann, A. J., Bayir, H., Bush, A., Conrad, M., Dixon, S., et al. (2017). Ferroptosis: A regulated cell death nexus linking metabolism, redox biology, and disease. *Cell* 171, 273–285. doi: 10.1016/S1474-4422(19)30069-9

Stockwell, B. R., Jiang, X., and Gu, W. (2020). Emerging mechanisms and disease relevance of ferroptosis. *Trends Cell Biol.* 30, 478–490. doi: 10.1021/acscentsci.7b00589

Stokum, J. A., Gerzanich, V., Sheth, K. N., Kimberly, W. T., and Simard, J. M. (2020). Emerging pharmacological treatments for cerebral edema: Evidence from clinical studies. *Annu. Rev. Pharmacol. Toxicol.* 60, 291–309. doi: 10.1038/s41467-020-18958-9

Tan, S., Kong, Y., Xian, Y., Gao, P., Xu, Y., Wei, C., et al. (2022). The mechanisms of ferroptosis and the applications in tumor treatment: Enemies or friends? *Front. Mol. Biosci.* 9:938677. doi: 10.3389/fcell.2020.00594

Tang, D., Kang, R., Berghe, T. V., Vandenabeele, P., and Kroemer, G. (2019). The molecular machinery of regulated cell death. *Cell Res.* 29, 347–364. doi: 10.1016/j.cell.2017.09.021

Tarantini, S., Yabluchanskiy, A., Lindsey, M. L., Csiszar, A., and Ungvari, Z. (2021). Effect of genetic depletion of MMP-9 on neurological manifestations of hypertension-induced intracerebral hemorrhages in aged mice. *Geroscience* 43, 2611–2619. doi: 10.1016/j.tcb.2020.02.009

Thrift, A. G., Thayabaranathan, T., Howard, G., Howard, V. J., Rothwell, P. M., Feigin, V. L., et al. (2017). Global stroke statistics. *Int. J. Stroke* 12, 13–32. doi: 10.1146/annurev-pharmtox-010919-023429

Hemphill, J. C., Greenberg, S. M., Anderson, C. S., Becker, K., Bendok, B. R., Cushman, M., et al. (2015). Guidelines for the management of spontaneous intracerebral hemorrhage: A guideline for healthcare professionals from the american heart association/american stroke association. *Stroke* 46, 2032–2060. doi: 10.3389/fmolb.2022.938677

Tuo, Q. Z., Masaldan, S., Southon, A., Mawal, C., Ayton, S., Bush, A. I., et al. (2021). Characterization of selenium compounds for anti-ferroptotic activity in neuronal cells and after cerebral ischemia-reperfusion injury. *Neurotherapeutics* 18, 2682–2691. doi: 10.1038/s41422-019-0164-5

Urday, S., Kimberly, W. T., Beslow, L. A., Vortmeyer, A. O., Selim, M. H., Rosand, J., et al. (2015). Targeting secondary injury in intracerebral haemorrhage–perihaematomal oedema. *Nat. Rev. Neurol.* 11, 111–122. doi: 10.1007/s11357-021-00402-5

Vanden Berghe, T., Linkermann, A., Jouan-Lanhouet, S., Walczak, H., and Vandenabeele, P. (2014). Regulated necrosis: The expanding network of non-apoptotic cell death pathways. *Nat. Rev. Mol. Cell Biol.* 15, 135–147. doi: 10.1177/1747493016676285

Wang, J. (2010). Preclinical and clinical research on inflammation after intracerebral hemorrhage. *Prog. Neurobiol.* 92, 463–477. doi: 10.1161/STR.0000000000000069

Watanabe, A., Hama, K., Watanabe, K., Fujiwara, Y., Yokoyama, K., Murata, S., et al. (2022). Controlled tetradeuteration of straight-chain fatty acids: Synthesis, application, and insight into the metabolism of oxidized linoleic acid. *Angew. Chem. Int. Ed. Engl.* 61:e202202779. doi: 10.1007/s13311-021-01111-9

Wu, T., Wu, H., Wang, J., and Wang, J. (2011). Expression and cellular localization of cyclooxygenases and prostaglandin E synthases in the hemorrhagic brain. *J. Neuroinflammation* 8:22. doi: 10.1038/nrneurol.2014.264

Wu, Y., Ma, Z., Mai, X., Liu, X., Li, P., Qi, X., et al. (2022). Identification of a novel inhibitor of TfR1 from designed and synthesized muriceidine a derivatives. *Antioxidants* 11:834. doi: 10.1038/nrm3737

Xue, T., Ji, J., Sun, Y., Huang, X., Cai, Z., Yang, J., et al. (2022). Sphingosine-1-phosphate, a novel TREM2 ligand, promotes microglial phagocytosis to protect against ischemic brain injury. *Acta Pharm. Sin. B* 12, 1885–1898. doi: 10.1016/j.pneurobio.2010.08.001

Yigitkanli, K., Pekcec, A., Karatas, H., Pallast, S., Mandeville, E., Joshi, N., et al. (2013). Inhibition of 12/15-lipoxygenase as therapeutic strategy to treat stroke. *Ann. Neurol.* 73, 129–135. doi: 10.1002/anie.202202779

Young, L. H., Klavinskis, L. S., Oldstone, M. B., and Young, J. D. (1989). *In vivo* expression of perforin by CD8+ lymphocytes during an acute viral infection. *J. Exp. Med.* 169, 2159–2171. doi: 10.1084/jem.169.6.2159

Yuan, J., Amin, P., and Ofengeim, D. (2019). Necroptosis and RIPK1-mediated neuroinflammation in CNS diseases. *Nat. Rev. Neurosci.* 20, 19–33. doi: 10.1186/1742-2094-8-22

Zhang, P., Chen, L., Zhao, Q., Du, X., Bi, M., Li, Y., et al. (2020). Ferroptosis was more initial in cell death caused by iron overload and its underlying mechanism in Parkinson's disease. *Free Radic. Biol. Med.* 152, 227–234. doi: 10.3390/antiox1105 0834

Zhang, Y., Khan, S., Liu, Y., Zhang, R., Li, H., Wu, G., et al. (2022c). Modes of brain cell death following intracerebral hemorrhage. *Front. Cell Neurosci.* 16:799753. doi: 10.1016/j.apsb.2021.10.012

Zhang, R., Yong, V. W., and Xue, M. (2022a). Revisiting minocycline in intracerebral hemorrhage: Mechanisms and clinical translation. *Front. Immunol.* 13:844163. doi: 10.1002/ana.23734

Zhang, Y., Khan, S., Liu, Y., Wu, G., Yong, V. W., and Xue, M. (2022b). Oxidative stress following intracerebral hemorrhage: From molecular mechanisms to therapeutic targets. *Front. Immunol.* 13:847246. doi: 10.1038/s41583-018-0093-1

Zhang, Z., Wu, Y., Yuan, S., Zhang, P., Zhang, J., Li, H., et al. (2018). Glutathione peroxidase 4 participates in secondary brain injury through mediating ferroptosis in a rat model of intracerebral hemorrhage. *Brain Res.* 1701, 112–125. doi: 10.1016/j.freeradbiomed.2020.03.015

Wang, M., Chao, Z., Lu, Y., Delian, K., Weijing, M., Bingchen, L, et al. (2022). Upregulation of MDH1 acetylation by HDAC6 inhibition protects against oxidative stress-derived neuronal apoptosis following intracerebral hemorrhage. *Cell Mol. Life Sci.* 79:356. doi: 10.3389/fncel.2022.799753

Zhu, S., Zhang, Q., Sun, X., Zeh, H. J. III, Lotze, M. T., Kang, R., et al. (2017). HSPA5 regulates ferroptotic cell death in cancer cells. *Cancer Res* 77, 2064–2077. doi: 10.3389/fimmu.2022.844163

Zille, M., Karuppagounder, S. S., Chen, Y., Gough, P. J., Bertin, J., Finger, J., et al. (2017). Neuronal death after hemorrhagic stroke in vitro and in vivo shares features of ferroptosis and necroptosis. *Stroke* 48, 1033–1043. doi: 10.3389/fimmu.2022.847246

frontiers | Frontiers in Neuroscience

TYPE Original Research
PUBLISHED 02 March 2023
DOI 10.3389/fnins.2023.1113216

OPEN ACCESS

EDITED BY
Weilin Xu,
Zhejiang University, China

REVIEWED BY
Menattallah Elserafy,
Zewail City of Science and Technology, Egypt
Eman Badr,
Zewail City of Science and Technology, Egypt

*CORRESPONDENCE
Yongzhi Xie
✉ yzxiexy3@163.com
Zuneng Lu
✉ lzn196480@126.com

SPECIALTY SECTION
This article was submitted to Neurodegeneration, a section of the journal Frontiers in Neuroscience

RECEIVED 01 December 2022
ACCEPTED 10 February 2023
PUBLISHED 02 March 2023

CITATION
Fu X, He Y, Xie Y and Lu Z (2023) A conjoint analysis of bulk RNA-seq and single-nucleus RNA-seq for revealing the role of ferroptosis and iron metabolism in ALS.
Front. Neurosci. 17:1113216.
doi: 10.3389/fnins.2023.1113216

A conjoint analysis of bulk RNA-seq and single-nucleus RNA-seq for revealing the role of ferroptosis and iron metabolism in ALS

Xiujuan Fu[1], Yizi He[2], Yongzhi Xie[3]* and Zuneng Lu[1]*

[1]Department of Neurology, Renmin Hospital of Wuhan University, Wuhan, China, [2]Department of Lymphoma and Hematology, Hunan Cancer Hospital, The Affiliated Cancer Hospital of Xiangya School of Medicine, Central South University, Changsha, China, [3]Department of Radiology, The Third Xiangya Hospital, Central South University, Changsha, China

Amyotrophic lateral sclerosis (ALS) is a neurodegenerative disease characterized by progressive and selective degeneration of motor neurons in the motor cortex of brain and spinal cord. Ferroptosis is a newly discovered form of cell death and reported to mediate selective motor neuron death in the mouse model of ALS. The growing awareness of ferroptosis and iron metabolism dysfunction in ALS prompted us to investigate the expression pattern of ferroptosis and iron metabolism-related genes (FIRGs) in ALS. Here, we performed a conjoint analysis of bulk-RNA sequence and single-nucleus RNA sequence data using the datasets from Gene Expression Omnibus (GEO) to reveal the role of FIRGs in ALS, especially in selective motor neuron death of ALS. We first investigated the differentially expressed genes (DEGs) between ALS and non-neurological controls. Weighted gene co-expression network analysis constructed the gene co-expression network and identified three modules closely associated with ALS. Fifteen FIRGs was identified as target genes based on least absolute shrinkage and selection operator regression analysis as follows: ACSL4, ANO6, ATP6V0E1, B2M, CD44, CHMP5, CYBB, CYBRD1, HIF1A, MOSPD1, NCF2, SDCBP, STEAP2, TMEM14C, ULK1. These genes could differentiate ALS patients from non-neurological controls ($p < 2.2e{-}16$) and had a valid value in predicting and diagnosing ALS (AUC = 0.881 in primary dataset and AUC = 0.768 in validation dataset). Then we performed the functional enrichment analysis of DEGs between ALS cases, the most significantly influenced by target genes, and non-neurological controls. The result indicated that the most significantly influenced functions in ALS pathogenesis by these identified FIRGs are synapse pathways, calcium signaling pathway, cAMP signaling pathway, and phagosome and several immune pathways. At last, the analysis of single- nuclear seq found that CHMP5, one of the 15 FIRGs identified by bulk single-nucleus RNA-seq data, was expressed significantly higher in ALS than pathologically normal (PN),

specifically in excitatory neuron populations with layer 2 and layer 3 markers (Ex L2_L3), layer 3 and layer 5 markers (Ex L3_L5). Taken together, our study indicates the positive correlation between FIRGs and ALS, presents potential markers for ALS diagnosis and provides new research directions of CHMP5 function in selective motor neuron death in ALS.

KEYWORDS

amyotrophic lateral sclerosis, ferroptosis, iron metabolism, single nuclear analysis, WGCNA, LASSO

Introduction

Amyotrophic lateral sclerosis (ALS) is a severe neurodegenerative disease characterized by progressive and relatively selective loss of upper and lower motor neurons. It was brought into the spotlight due to its lethality and complexity. However, foggy pathogenesis and uncontrolled progression still confuse the world.

Growing evidences indicate that iron affects cell death pathways and brain homeostasis in neurodegenerative diseases. Ferroptosis is a type of cell death triggered by the built up of lipid peroxides, defined as an iron-dependent regulated necrosis that can affect neurons (Stockwell et al., 2017). Since iron is a redox ion, it can induce free radicals, including reactive oxygen species (ROS), which participates in the regulation of cell survival and death. ROS can cause cell damage by destroying the iron homeostasis of cells, leading to a vicious circle (Sirabella et al., 2018). Evidence from past decades links iron homeostasis to neuronal cell death in ALS (Matsuo et al., 2021). In ALS patients, MRI reveals increased iron accumulation in motor cortex (Kwan et al., 2012). The markers of lipid oxidation and iron status are correlated with clinical function decline in ALS (Devos et al., 2019). Another study showed that moderate iron chelation regimen may incorporate a novel curative option for neuroprotection in ALS (Moreau et al., 2018). ALS is the most common motor neuron disorder, and show selective vulnerability of motor neurons in cortex (Hammer et al., 1979; Cronin et al., 2007). Excitingly, the research in utilizing ALS $SOD1^{G93A}$ mice model showed that ferroptosis could mediate selective motor neuron death (Wang et al., 2022). Focus on ferroptosis and iron metabolism in ALS may provide new targets to uncover the pathogenesis of selective vulnerability of motor neurons and reduce dysfunction.

Here we did a conjoint analysis of bulk RNA-seq and single-nucleus RNA-seq based on the publicly available mRNA expression data. In bulk RNA-seq analysis, we focused on differentially expressed genes and altered pathways related to ferroptosis and iron metabolism in ALS to uncover the involvement of ferroptosis and iron metabolism in ALS and provide potential targets for further investigation. In single-nucleus RNA-seq analysis, we explored the expression of hub genes in primary cortex motor neurons in ALS to explore the role of ferroptosis and iron metabolism in motor neurons and provide potential pathogenesis of selective vulnerability of motor neurons in ALS.

Materials and methods

Data preparation for bulk RNA-seq

Transcriptome data were obtained from Gene Expression Omnibus (GEO). Specifically, the bulk RNA-seq dataset is from GSE153960 (Prudencio et al., 2020), from which we extracted two parts of the data. A total of 684 ALS spectrum motor neuron disease (MND) patients and 190 non-neurological controls were selected in the primary dataset for hub genes screening, grounded on the platform of GPL24676. Another dataset based on the platform of GPL16791 including 546 ALS spectrum MND patients and 90 non-neurological controls for validation. The raw count matrices were normalized and transformed into fragments per kilobase of sequence per million mapped reads (FPKM) values for further analysis.

Screening of differentially expressed genes (DEGs)

The raw counts of expression profiles were extracted from the primary dataset (GPL24676), generating the heatmap using the R package "pheatmap." The DEGs were screened using the DESeq2 R package with a threshold of $|\log2FC| \geq 0.5$ and FDR < 0.05 (Love et al., 2014). A volcano plot was used to visualize the distribution of DEGs.

Ferroptosis and iron metabolism-related genes screening and analysis

The ferroptosis-related genes were downloaded from FerrDb database (FerrDb)[1] (Zhou and Bao, 2020; Zhou et al., 2022). A total of thirty-two iron metabolism-related gene sets were extracted from the Molecular Signatures Database (MsigDB)[2] and Gene Ontology with keywords "iron" and "heme." We combined the ferroptosis-related genes and iron metabolism-related genes and removed the repeated genes. Finally, a total of 763 ferroptosis and iron

1 http://zhounan.org/

2 https://www.gsea-msigdb.org/gsea/msigdb/index.jsp

metabolism-related genes (FIRGs) were screened out (as shown in the **Supplementary Table 1**).

WGCNA

Weighted gene co-expression network analysis (WGCNA) was performed on the DEGs extracted from the primary dataset, based on the WCGNA analysis in the R package (Zhang and Horvath, 2005; Li et al., 2020). The log2 transformed gene expression data was used to calculate the Pearson correlation matrix. We used R function "pickSoftThreshold" for module building and screened the soft threshold power β to achieve a scale-free topology. The minimum number of genes per gene module was set to 30, and genes were grouped into modules with similar expression patterns. Finally, we identified modules associated with ALS by assessing correlations between phenotypes and modules by Pearson correlation. Besides, a WGCNA integrated function (module Preservation) was applied to calculate module preservation statistics. Zsummary was used to assess the significance of observed statistics by distinguishing preserved from non-preserved modules *via* permutation testing 200 times (Langfelder et al., 2011). Preservation analysis was performed in primary dataset (GPL24676) as 1:1 divided into training set and test set, and also performed between primary dataset (GPL24676) and validation dataset (GPL16791).

Module membership (MM): MM(i) = cor (x, ME) is defined to measure the importance of a gene in one module. Gene Significance (GS) is defined as the correlation between the individual genes and the trait. In this study, a gene with MM > 0.8 and GS > 0.2 was defined as candidate gene among modules associated with ALS. The identified WGCNA ALS-related genes were crossed with 763 FIRGs (**Supplementary Table 1**) to obtain the overlapped FIRGs for further analysis.

LASSO analysis and validation

Least Absolute Shrinkage and Selection Operator (LASSO) is considered appropriate for high-dimensional data and has strong predictive value and can prevent model overfitting (Tibshirani, 1996). In order to identify ALS from non-neurological controls, the "glmnet" package in R was used to conduct LASSO Regression Analysis (Tibshirani, 1996) on log2 (FPKM + 1) transformed data of overlapped FIRGs. With the LASSO regression analysis, FIRGs with non-zero coefficients were selected as hub genes. A LASSO model (Binomial Lasso) with hub genes expression profiles was incorporated. The risk score (RS) of each sample was calculated using the formula: risk score = $\Sigma \beta i$ x expression value of genei.

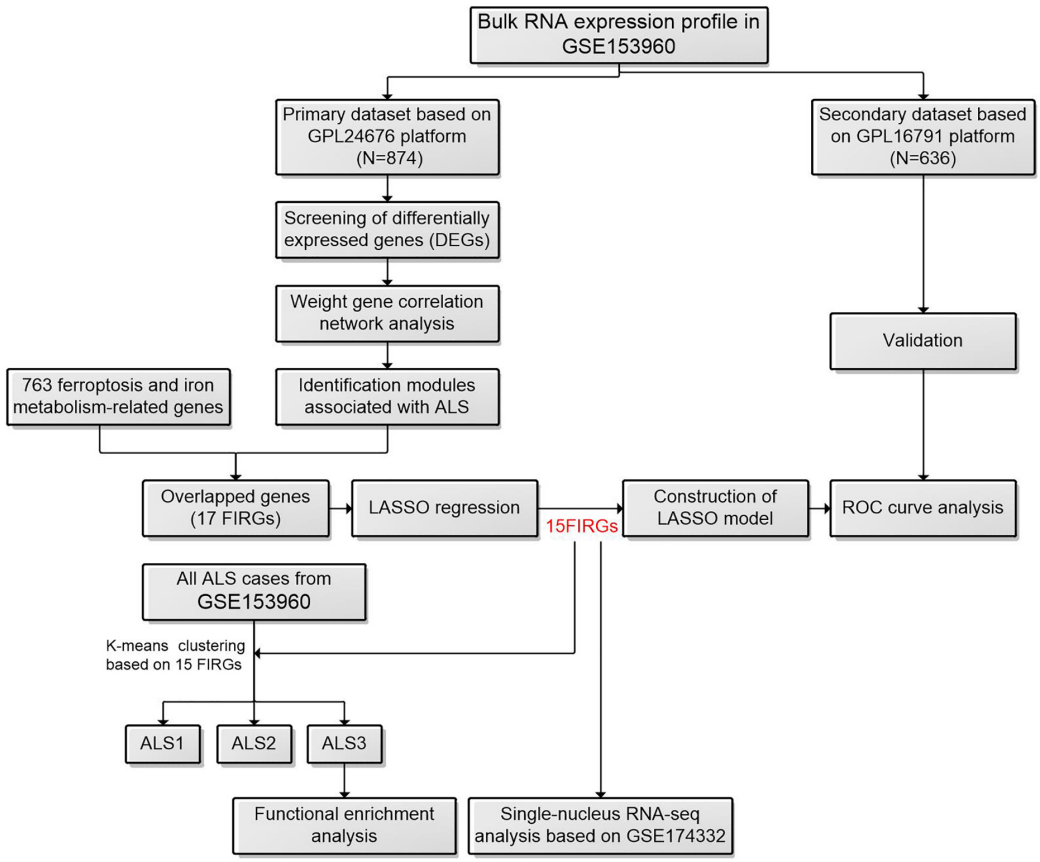

FIGURE 1
The workflow of this study. ALS, amyotrophic lateral sclerosis; FIRGs, ferroptosis and iron metabolism-related genes; LASSO, least absolute shrinkage and selection operator; ROC, receiver operating characteristic.

For the validation of LASSO model, the primary cohort from GPL24676 was used for the training set and secondary cohort from GPL16791 were used to validate the model. The pROC package in the R package was used to perform receiver operating characteristic (ROC) curve analysis (Robin et al., 2011).

KEGG pathway analysis

Amyotrophic lateral sclerosis samples from GSE153960 and GSE174332 were clustered into three groups by K-means clustering using an expression matrix (Shabalin, 2012) of hub FIRGs identified by LASSO analysis. Differentially expressed genes between each ALS group and controls were analyzed with DESeq2. Functional enrichment analysis was done by Enrichr (Chen et al., 2013), $p < 0.05$ was considered as significantly enriched.

Single-nucleus RNA-seq analysis

Motor cortex neuron single-nucleus RNA-sequencing dataset came from GSE174332, including 17 sporadic ALS cases and 17 pathologically normal controls with similar sex distribution (Pineda et al., 2021). Sporadic ALS is defined as no family history and no defined genetic risk factors (SOD1, C9orf72, TBK1, etc.). The analysis was done with R package Seurat (Hao et al., 2021). Low-quality cells with less than 100 detected genes were removed. DEGs expressed in at least 10% of cells were detected with a fold change of >0.25 (log scale) and tested by non-parameteric Wilcoxon rank sum test.

Results

Screening of differentially expressed genes (DEGs)

A flowchart of the study is shown in Figure 1. We first investigated the DEGs between ALS patients and non-neurological controls in the primary dataset. As Figure 2 shows, there are 1,767 genes downregulated and 987 genes upregulated in ALS patients, compared with controls. And there are 17,249 genes has no change between ALS patients and controls.

WGCNA identified critical modules correlating with ALS

To construct the gene co-expression network, WGCNA was used to analyze the expression profiles of DEGs in the primary dataset. On the basis of scale-free $R^2 > 0.9$, the soft thresholding power was determined as $\beta = 14$, and then a scale-free network was constructed (Figure 3A). The module eigengenes were counted and classified into 8 modules designated by a distinctive color (Figure 3B). We explored the correlation of each signature gene with the disease phenotype, as shown in Figure 3C, the yellow (cor = 0.4, p = 2e−35), green (cor = 0.43, p = 1e−41) and blue (cor = 0.23, p = 2e−12) modules were positively related to ALS. The connection between gene significance and module membership for all 3 modules as follows: yellow (cor = 0.51, p = 1.9e−12), green (cor = 0.31, p = 0.0026) blue: (cor = 0.24,

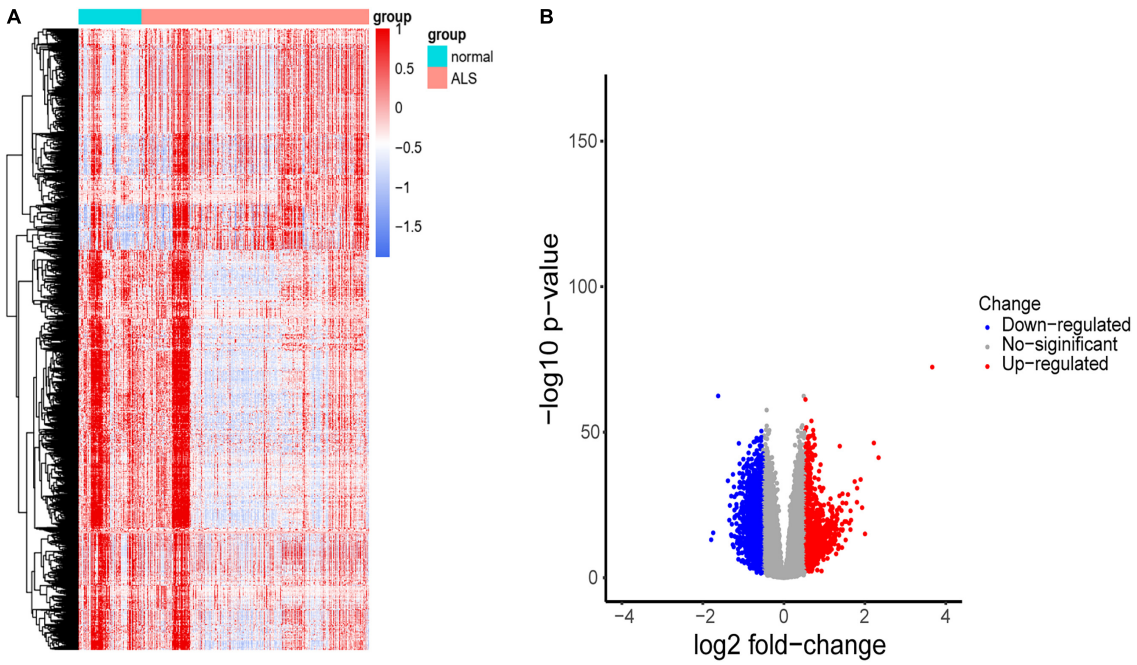

FIGURE 2
Identification of DEGs between ALS cases and non-neurological controls. **(A)** Heatmap profiling of the genes enrichment analysis between ALS patients and non-neurological controls. **(B)** Volcano plot of DEGs between ALS patients and non-neurological controls. Blue dots represent downregulated genes (1,767 genes), red dots represent upregulated genes (987 genes), and gray dots represent no significantly differentially expressed genes (17,249 genes).

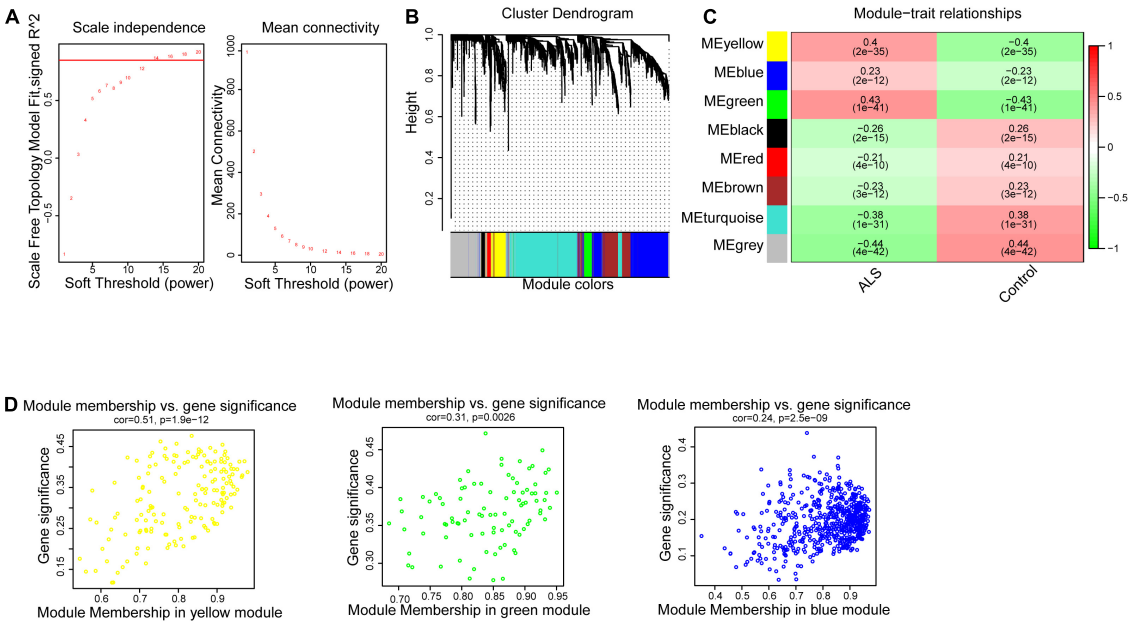

FIGURE 3
Weighted gene correlation network analysis (WGCNA). **(A)** The scale-free fit index for soft-thresholding powers. The scale-free $R^2 > 0.9$ was used as a criterion to construct a soft threshold power for appropriate networks. **(B)** A dendrogram of co-expressed gene modules. The branches in the graph are clustered into eight modules, designated by each color below. **(C)** A heatmap shows the association between each module eigengene and phenotype. The coefficient in each cell is the correlation, decreasing from red to green. Yellow, green, and blue three modules are positively correlated with ALS. **(D)** Scatter plot of module eigengenes in the yellow, green and blue modules. All these three modules were significantly associated with ALS ($p < 0.05$).

p = 2.5e−09) (Figure 3D). To test the stability of the indicated modules, preservation analysis was performed in primary dataset as 1:1 divided into training set and test set (Supplementary Figure 1A), and also performed primary dataset and secondary dataset (Supplementary Figure 1B). Both of the results show green, yellow and blue modules are preserved stably in individual datasets as all of these modules' Zsummary value of >10 (Supplementary Figures 1A, B). Although blue module's cor value is smaller than yellow and green modules, its Zsummary value is highest in all modules. There are 860 genes from yellow, green and blue modules. A total of 481 genes that associated with ALS were further identified by MM > 0.8 and GS > 0.2 among three modules. Subsequently, overlap analysis was performed on 481 DEGs identified by WGCNA and 763 FIRGs, and finally 17 overlapped genes were identified (Figure 4A).

Construction and validation of the LASSO model

The LASSO regression analysis was performed to recognize the optimal linear model of crucial genes for predicting the occurrence of ALS (Figure 4B). A total of 15 FIRGs with non-zero coefficients were selected for model construction. The risk score was calculated as follows:

Risk score=(0.1567×expression value of ANO6)+(0.3361×expression value of CD44)+(0.0333×expression value of CHMP5) +(1.3087×expression value of MOSPD1)+(1.6129×expression value of NCF2)+(1.8261×expression value of SDCBP)+(0.4153×expression value of STEAP2)+(1.1168×expression value of TMEM14C)+(0.0040×expression value of ULK1)-(0.2332×expression value of ACSL4)-(0.8929×expression value of ATP6V0E1)-(0.5481×expression value of B2M)-(0.917×expression value of CYBB)-(0.0261×expression value of CYBRD1)-(0.0096×expression value of HIF1A).

We performed a predictive score based on LASSO analysis, which is helpful in effectively discriminating ALS patients from non-neurological controls (p < 2.2e−16, Wilcoxon test) (Figure 4C). Then the ROC curve analysis was implemented on the primary dataset, showing that the area under the ROC curve (AUC) of the model was 0.881 (Figure 4D). Simultaneously, ROC analysis in the secondary validated dataset indicated the AUC value of 0.768 (Figure 4E). These results illustrated that the model based on these 15 hub FIRGs had a valid value in predicting and diagnosing ALS.

Functional enrichment analysis based on cases that significantly associated with hub FIRGs in ALS

To detect the most significantly influenced function in ALS pathogenesis by 15 hub FIRGs, we clustered all ALS samples from GSE153960 and GSE174332 into three groups by K-means clustering using an expression matrix of 15 FIRGs (Figure 5A). Analysis of DEGs between each ALS group and controls indicated that ALS3 subgroup was the most strongly associated with these 15 FIRGs and closely related with ALS (Figures 5B, C). KEGG pathway analysis of the downregulated genes in ALS3 subgroup mainly enriched in synaptically important pathways involving different synapse types (glutamatergic, serotonergic, cholinergic,

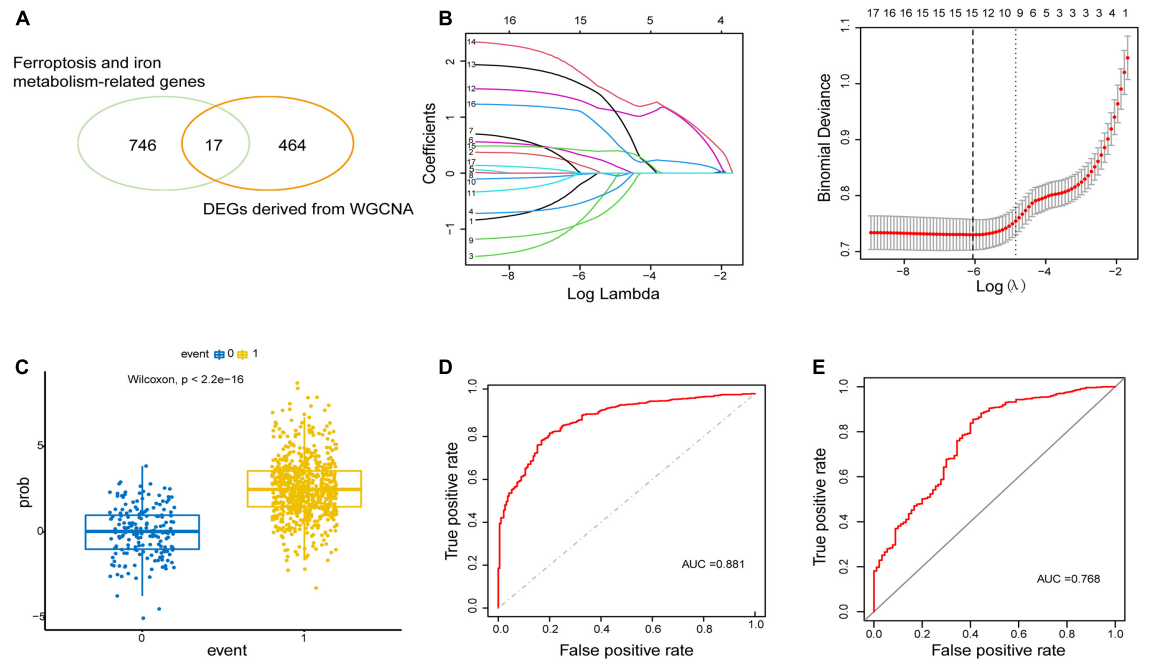

FIGURE 4
Construction and validation of LASSO model. **(A)** 17 overlapping genes were identified between ferroptosis-related genes and ALS-related DEGs derived from WGCNA. **(B)** Construction of LASSO model. **(C)** Boxplot: visualization of the predictive property of model. Each dot represented each individual's predicted score. **(D,E)** ROC curve analysis of predicting the occurrence of ALS in the primary dataset and secondary dataset.

and dopaminergic) and known ALS-related pathways like the calcium signaling pathway and cAMP signaling pathway. The upregulated DEGs in ALS3 mainly enriched in phagosome and several immune pathways (Figure 5D).

Single-nucleus RNA-seq analysis investigate the role of FIRGs in primary motor cortex neurons

To further investigate the role of FIRGs in primary motor cortex neurons in ALS, this study further extracted primary motor cortex neurons' single-nucleus RNA-seq data from GSE174332, including 17 sporadic ALS and 17 pathologically normal controls (PN). UMAP analysis done with R package Seurat divided the motor neurons into 20 clusters (Figure 6A). Based on the annotation analysis of cell subpopulations, there are 7 subtypes characterized in the Excitatory neurons (Neuron_Ex) and Inhibitory neurons (Neuron_In), respectively (Figures 6B, C). Thereafter, we studied the expression analysis of the 15 hub FIRGs in cell subpopulations in ALS and PN, and found that CHMP5, one of the 15 hub FIRGs, was expressed significantly higher in excitatory neuron populations of ExL2_L3 and ExL3_L5 in ALS than PN (Figure 6D).

Discussion

Amyotrophic lateral sclerosis is a multifactorial and highly heterogeneous disease. Although multiple mechanisms have been identified in the pathogenesis of ALS, for example, impaired axonal transport, mitochondrial dysfunction and oxidative stress, immune dysregulation (Mejzini et al., 2019), many mysteries remain in the understanding of ALS pathogenesis. Ferroptosis is a newly identified type of cell death triggered by the accumulation of lipid peroxides, defined as an iron-dependent regulated necrosis that could affect neurons (Stockwell et al., 2017). Previous study raised the hypothesis that the ferroptosis was involved in the pathogenesis of ALS. In $SOD1^{G93A}$ transgenic mice, reduction of iron level by iron chelators could increase the mean life span (Wang et al., 2011). In ALS patients, increased serum ferritin was positively correlated with a faster progression and shorter survival (Paydarnia et al., 2021).

Here we first investigate the DEGs between ALS patients and non-neurological controls. Using WGCNA, we identify 3 modules DEGs in correlation with ALS. After overlapping with FIRGs, there is a total of 17 FIRGs associated with ALS. Finally, with LASSO analysis, 15 hub FIRGs (ACSL4, ANO6, ATP6V0E1, B2M, CD44, CHMP5, CYBB, CYBRD1, HIF1A, MOSPD1, NCF2, SDCBP, STEAP2, TMEM14C, ULK1) have been screened out as target genes. These hub genes display good predictive value in distinguishing ALS from non-neurological controls, which were validated by secondary dataset.

Ferritinophagy plays an important role in driving some pathological processes in neurodegenerative diseases (Tang et al., 2018). In a lysosomal transport pathway for ferritin, ULK1/2-FIP200 complex regulates ferritin turnover at basal state, and its loss results in TBK1 activation and regulation of ferritin transport (Goodwin et al., 2017). (ULK)1/2 complex, which is also an initial inducer of autophagy. In a recent study of ALS/FTD associated C9orf72, the protein product of C9orf72

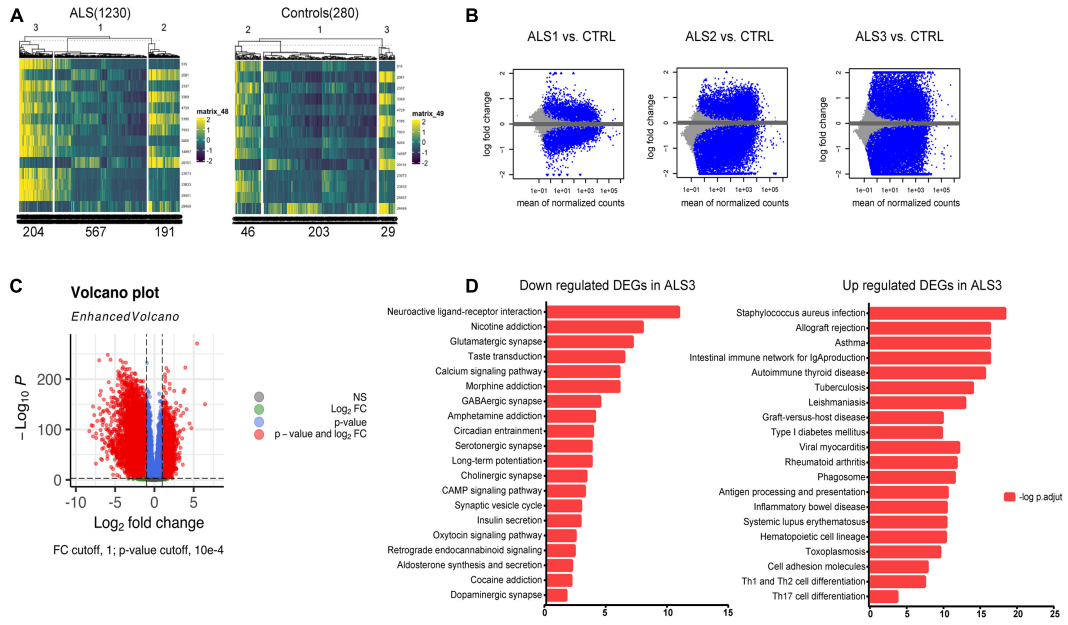

FIGURE 5
KEGG pathway analysis based on FIRGs that significantly altered in ALS. **(A)** Sample clusters based on expression matrix of 15 hub genes. **(B)** MA plot of DEGs of each ALS subgroup vs. controls. **(C)** Volcano plot of DEGs between ALS3 and controls. **(D)** KEGG pathway analysis of downregulated and upregulated DEGs in ALS3 subgroup, compared with non-neurological controls.

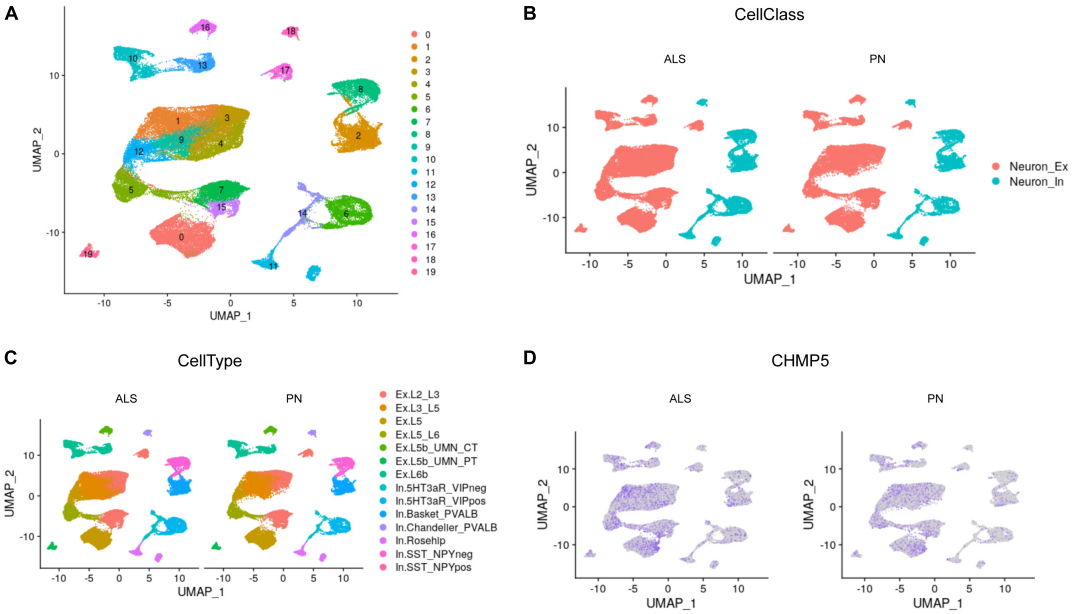

FIGURE 6
Single-nucleus RNA-seq analysis. **(A)** UMAP plot for the analysis of cell subpopulations in the motor cortex neuron, which were divided into 20 cell subsets. **(B)** The neurons of ALS and PN are classified into excitatory neurons (Neuron_Ex) and inhibitory neurons (Neuron_In), PN: pathologically normal controls. **(C)** Detailed submap of transcriptional isoforms annotated by motor cortex segment excitatory neurons and inhibitory neurons. **(D)** The expression analysis of CHMP5 in motor cortex neuron populations of ALS and PN.

could control the initiation of autophagy by regulating ULK1 complex trafficking (Higginbottom, 2016). As a pro-survival factor of ferroptosis, HIF1A is a major transcription factor that can regulate the homeostatic responses to reduced oxygen level in microenvironment (Yang et al., 2019). Moreau et al. (2011) reported that the HIF-1 signaling pathway exhibited significant abnormalities during hypoxia in sporadic ALS cases. The expression of ACSL4 determines sensitivity to ferroptosis. Knockout or inhibition of ACSL4 caused a dramatic reduction in the content of polyunsaturated fatty acids (PUFAs) in membranes, and targeted inhibitors of ACSL4 improved tissue death in a mouse model of ferroptosis (Doll et al., 2017). It is reported that ACSL4

plays important roles in Aβ-induced changes in cell survival, myocardial dysfunction, and lipid peroxidation in AD mice model (Zhu et al., 2022). CYBB (also known as NOX2) participated in the transmission of electrons across the plasma membrane to produce superoxide and other downstream ROS (Bedard and Krause, 2007). In ALS patients, NOX2 activity presented a negative correlation with survival time, while inactivation of NOX2 delayed the progression of neurodegeneration in ALS SOD1 transgenic mice (Sorce et al., 2017). NCF2 is responsible for the synthesis of superoxide in neutrophils. As an oxidative stress gene, NCF2 has been considered as a potential biomarker for Friedreich's ataxia disease progression and drug action (Hayashi and Cortopassi, 2016). ANO6 is one of the anoctamins, a family of Ca2 + -activated chloride channels and phospholipid scramblases. ANO6 can lead to the activation of lipid peroxidation as a mechanism proposed earlier in ferroptosis (Ousingsawat et al., 2019). In ALS mice model, the ANO6/TMEM16F loss of function reduces denervation and motor decline (Soulard et al., 2020). In contrast, CD44 can inhibit oxidative stress and ferroptosis through regulating GPX4. CD44 can enhance the stability of SLC7A11, which is a protective factor for cells through synthesizes reduced glutathione (GSH) by promoting the uptake of cystine (Liu et al., 2019). Study in SOD1 (G93A) mice showed the expression of CD44 in astrocytes and microglia was accompanied by the pathogenesis of ALS (Matsumoto et al., 2012). CHMP5, a core component of ESCRT-III pathway, has been shown to gather in the plasma membrane during ferroptosis. ESCRT-III could participate in the inversely modulated ferroptosis, mediating plasma membrane repair and decreasing lipid peroxidation. Genetic inhibition of CHMP5 enhanced ferroptosis *in vivo* and *in vitro* (Dai et al., 2020). Previous study showed that higher CHMP5 level in whole blood was positively associated with shorter survival of ALS patients, with potential as a biomarker for ALS prognosis (Zhang et al., 2022). B2M localizes to the cell membrane and is a member of major histocompatibility complex-1 (MHC-1), which participates in synaptic function and axonal regeneration. Widely expressed in human brain, B2M has been shown to play a role in neurodegenerative diseases (Gupta et al., 2017) and has previously been described in sporadic ALS studies (Baciu et al., 2012). SDCBP can interact with a variety of signal proteins, and regulate the different signaling transduction pathways (Pradhan et al., 2020). It is reported that individuals with AD had increased SDCBP expression (Lark and LaRocca, 2022). In addition, CYBRD1, STEAP2 and TMEM14C are significantly involved in iron transport and HEME metabolism. Dysfunction of these genes could cause iron accumulation and iron homeostasis disorders (Ji and Kosman, 2015; Kleven et al., 2015; Harding et al., 2020). However, it's still unclear about the MOSPD1 and ATP6VE01 involved in the process of ferroptosis, and there is no evidence to support their role in ALS. Overall, these findings may provide a new perspective for exploring the molecular mechanism underlying ALS pathogenesis.

For enrichment analysis, to detect which pathways the FIRGs is mainly involved in the pathogenic process of ALS, we clustered all ALS samples to 3 groups based on the correlation with 15 FIRGs. The group 3 has the most significant correlation with 15 FIRGs. We performed KEGG pathway analysis on all upregulated genes and all downregulated genes in group 3. The result revealed that functional enrichment of downregulated DEGs in ALS 3 is in synaptically important pathways, calcium signaling pathway and cAMP signaling pathway. Progressive synapse loss and dysfunction is known to occur in the early stage of neurodegenerative disease, including Alzheimer's disease (AD) (Selkoe, 2002), Parkinson's disease (PD) (Villalba et al., 2015), and ALS (Belzil et al., 2016). Glutamate excitotoxicity, driven by the hyperactivity of excitatory neurons, plays an important role in ALS pathology. One possible reason is the inherent variations in the firing properties of neurons or a reduction in the inhibitory control of GABAergic cells. Interestingly, in KEGG analysis of this study, GABAergic synapse pathway was also enriched of downregulated DEGs in the ALS3 subgroup, suggesting that the inhibitory networks belonged to vulnerability in ALS, consistent with reports in ALS animal models and human cadavers (Maekawa et al., 2004; Allodi et al., 2021; Lin et al., 2021). On the other hand, a recent study revealed that cAMP/PKA activation and neuronal firing were beneficial for synaptic recovery and ameliorated the ALS-related pathobiochemistry (Bączyk et al., 2020). Their hypothesis is that dysfunction of excitatory synapses is an important factor affecting the excitatory drive of motor neurons and the degeneration of motor neurons. Our analysis also found the inactivation of the PKA signaling pathway in ALS3 cases. In addition, the calcium signaling pathway is downregulated in our analysis. Dysregulation of calcium homeostasis participates in the pathogenesis of ALS by affecting some major and interrelated toxicity pathways like oxidative stress, mitochondrial dysfunction and neuroinflammation (Jaiswal, 2013). In the pathways of upregulated DEGs enriched, phagosome plays an important role both in ALS and ferroptosis. Autophagosomes are double-membrane vesicles that participate in the process of autophagy. The main role of autophagy in ALS commonly includes affecting the accumulation of protein aggregates and the function of mitochondria in motor neurons (Taylor et al., 2016). Excessive autophagy, especially selective types of autophagy, and impaired lysosomal activity may drive cells toward ferroptosis. The key types include ferritinophagy, lipophagy, clockophagy, and chaperone-mediated autophagy (CMA) (Liu et al., 2020).

The primary motor cortex is essential for voluntary motor control, sending layer 5 intratelencephalic tract and pyramidal tract output projections to modulate the execution of movement (McColgan et al., 2020). ALS is the most common motor neuron disorder, and show selective vulnerability of motor neurons in cortex (Hammer et al., 1979; Cronin et al., 2007). To further investigate the role of FIRGs in motor cortex neurons in ALS, we further extracted primary motor cortex neurons' single-nucleus RNA-seq data from GSE174332, which generated the first high-resolution single-cell molecular atlas of the human primary motor cortex. Here we analyzed the 15 FIRGs' expression in primary motor cortex neurons between 17 sporadic ALS and 17 PN. More interestingly, by analyzing single-nucleus RNA-seq data, we found that in CHMP5, one of the 15 FIRGs, is dysregulated in ExL2_L3 and ExL3_L5, indicating that in ALS patient, excitatory neurons located in motor cortex layer 2_3 and layer 3_5 have higher CHMP5 expression and may be more vulnerable to ferroptosis and iron metabolism dysfunction.

In summary, our results demonstrate that FIRGs are significant factors in the ALS pathogenesis. These pinpointed 15 FIRGs are considered as potential biomarkers for ALS diagnosis. The KEGG analysis shows these FIRGs may involve the ALS pathogenesis by synapse pathways, calcium signaling pathway and cAMP signaling pathway. Finally, single-nucleus analysis reveals higher

expression of CHMP5 in L2_3 and L3_5 excitatory neurons in ALS, providing a target gene for further exploration of the pathogenesis and a potential treatment for ALS.

Conclusion

Taken together, those data indicate that there is a positive correlation between ferroptosis, iron metabolism dysfunction and ALS severity. Thus, these 15 FIRGs are protentional markers of ALS diagnosis and worth further investigation, especially the CHMP5 function in excitatory neurons.

Data availability statement

The original contributions presented in this study are included in this article/**Supplementary material**, further inquiries can be directed to the corresponding authors.

Author contributions

XF analyzed the data and wrote the initial version of the manuscript. YH analyzed a part of the data. ZL and YX designed the study and revised the manuscript. All authors reviewed and approved the final manuscript.

Funding

This work was supported by the Hunan Provincial Natural Science Foundation of China (No. 2021JJ40320) and the National Natural Science Foundation of China (No. 82000200).

Acknowledgments

We are grateful for the establishment and sharing of the GEO database.

Conflict of interest

The authors declare that the research was conducted in the absence of any commercial or financial relationships that could be construed as a potential conflict of interest.

Publisher's note

All claims expressed in this article are solely those of the authors and do not necessarily represent those of their affiliated organizations, or those of the publisher, the editors and the reviewers. Any product that may be evaluated in this article, or claim that may be made by its manufacturer, is not guaranteed or endorsed by the publisher.

Supplementary material

The Supplementary Material for this article can be found online at: https://www.frontiersin.org/articles/10.3389/fnins.2023.1113216/full#supplementary-material

SUPPLEMENTARY FIGURE 1
Module preservation analysis. **(A)** Modules preserved in primary dataset training set vs. test set; **(B)** modules preserved in primary dataset vs. secondary dataset. Each module was represented by its color-code and name. The dashed blue and red lines indicated the thresholds $Z = 2$ and $Z = 10$, respectively. Zsummary < 2 implied no evidence for module preservation, $2 <$ Zsummary < 10 implies weak to moderate evidence, and Zsummary > 10 implies strong evidence for module preservation.

SUPPLEMENTARY TABLE 1
The total of 763 FIRGs screened out from the FerrDb database and MsigDB database.

References

Allodi, I., Montañana-Rosell, R., Selvan, R., Löw, P., and Kiehn, O.J.N.c (2021). Locomotor deficits in a mouse model of ALS are paralleled by loss of V1-interneuron connections onto fast motor neurons. *Nat. Commun.* 12:3251. doi: 10.1038/s41467-021-23224-7

Baciu, C., Thompson, K. J., Mougeot, J.-L., Brooks, B. R., and Weller, J.W.J.B.b (2012). The LO-BaFL method and ALS microarray expression analysis. *BMC Bioinformatics* 13:244. doi: 10.1186/1471-2105-13-244

Bączyk, M., Alami, N. O., Delestrée, N., Martinot, C., Tang, L., Commisso, B., et al. (2020). Synaptic restoration by cAMP/PKA drives activity-dependent neuroprotection to motoneurons in ALS. *J. Exp. Med.* 217:e20191734. doi: 10.1084/jem.20191734

Bedard, K., and Krause, K.-H.J.P.r (2007). The NOX family of ROS-generating NADPH oxidases: Physiology and pathophysiology. *Physiol. Rev.* 87, 245–313.

Belzil, V. V., Katzman, R. B., and Petrucelli, L.J.A.n (2016). ALS and FTD: An epigenetic perspective. *Acta Neuropathol.* 132, 487–502. doi: 10.1007/s00401-016-1587-4

Chen, E. Y., Tan, C. M., Kou, Y., Duan, Q., Wang, Z., Meirelles, G. V., et al. (2013). Enrichr: Interactive and collaborative HTML5 gene list enrichment analysis tool. *BMC Bioinformatics* 14:128. doi: 10.1186/1471-2105-14-128

Cronin, S., Hardiman, O., and Traynor, B. J. (2007). Ethnic variation in the incidence of ALS: A systematic review. *Neurology* 68, 1002–1007. doi: 10.1212/01.wnl.0000258551.96893.6f

Dai, E., Meng, L., Kang, R., Wang, X., and Tang, D. J. B. (2020). ESCRT-III–dependent membrane repair blocks ferroptosis. *Biochem. Biophys. Res. Commun.* 522, 415–421. doi: 10.1016/j.bbrc.2019.11.110

Devos, D., Moreau, C., Kyheng, M., Garçon, G., Rolland, A. S., Blasco, H., et al. (2019). A ferroptosis–based panel of prognostic biomarkers for amyotrophic lateral sclerosis. *Sci. Rep.* 9:2918.

Doll, S., Proneth, B., Tyurina, Y. Y., Panzilius, E., Kobayashi, S., Ingold, I., et al. (2017). ACSL4 dictates ferroptosis sensitivity by shaping cellular lipid composition. *Nat. Chem. Biol.* 13, 91–98. doi: 10.1038/nchembio.2239

Goodwin, J. M., Dowdle, W. E., DeJesus, R., Wang, Z., Bergman, P., Kobylarz, M., et al. (2017). Autophagy-independent lysosomal targeting regulated by ULK1/2-FIP200 and ATG9. *Cell Rep.* 20, 2341–2356. doi: 10.1016/j.celrep.2017.08.034

Gupta, V. B., Hone, E., Pedrini, S., Doecke, J., O'Bryant, S., James, I., et al. (2017). Altered levels of blood proteins in Alzheimer's disease longitudinal study: Results from Australian imaging biomarkers lifestyle study of ageing cohort. *Alzheimers Dement.* 8, 60–72. doi: 10.1016/j.dadm.2017.04.003

Hammer, R. P. Jr., Tomiyasu, U., and Scheibel, A. B. (1979). Degeneration of the human Betz cell due to amyotrophic lateral sclerosis. *Exp. Neurol.* 63, 336–346. doi: 10.1016/0014-4886(79)90129-8

Hao, Y., Hao, S., Andersen-Nissen, E., Mauck, W. M. III, Zheng, S., Butler, A., et al. (2021). Integrated analysis of multimodal single-cell data. *Cell* 184, 3573.e–3587.e.

Harding, C. R., Sidik, S. M., Petrova, B., Gnädig, N. F., Okombo, J., Herneisen, A. L., et al. (2020). Genetic screens reveal a central role for heme metabolism in artemisinin susceptibility. *Nat. Commun.* 11:4813. doi: 10.1038/s41467-020-18624-0

Hayashi, G., and Cortopassi, G. J. P. O. (2016). Lymphoblast oxidative stress genes as potential biomarkers of disease severity and drug effect in Friedreich's ataxia. *PLoS One* 11:e0153574. doi: 10.1371/journal.pone.0153574

Higginbottom, A. J. E. J. (2016). The C9orf72 protein interacts with Rab1a and the ULK1 complex to regulate initiation of autophagy. *EMBO J.* 35, 1656–1676.

Jaiswal, M.K.J.F.i.c.n (2013). Calcium, mitochondria, and the pathogenesis of ALS: The good, the bad, and the ugly. *Front. Cell Neurosci.* 7:199. doi: 10.3389/fncel.2013.00199

Ji, C., and Kosman, D.J.J.J.o.n (2015). Molecular mechanisms of non-transferrin-bound and transferring-bound iron uptake in primary hippocampal neurons. *J. Neurochem.* 133, 668–683. doi: 10.1111/jnc.13040

Kleven, M. D., Dlakić, M., and Lawrence, C.M.J.J.o.B.C (2015). Characterization of a single b-type heme, FAD, and metal binding sites in the transmembrane domain of six-transmembrane epithelial antigen of the prostate (STEAP) family proteins. *J. Biol. Chem.* 290, 22558–22569. doi: 10.1074/jbc.M115.664565

Kwan, J. Y., Jeong, S. Y., Van Gelderen, P., Deng, H.-X., Quezado, M. M., Danielian, L. E., et al. (2012). Iron accumulation in deep cortical layers accounts for MRI signal abnormalities in ALS: Correlating 7 tesla MRI and pathology. *PLoS One* 7:e35241. doi: 10.1371/journal.pone.0035241

Langfelder, P., Luo, R., Oldham, M. C., and Horvath, S.J.P.c.b (2011). Is my network module preserved and reproducible? *PLoS Comput. Biol.* 7:e1001057. doi: 10.1371/journal.pcbi.1001057

Lark, D. S., and LaRocca, T.J.J.T.J.o.G.S.A (2022). Expression of exosome biogenesis genes is differentially altered by aging in the mouse and in the human brain during Alzheimer's disease. *J Gerontol. A Biol. Sci. Med. Sci.* 77, 659–663. doi: 10.1093/gerona/glab322

Li, W., Liu, J., and Zhao, H. J. A. (2020). Identification of a nomogram based on long non-coding RNA to improve prognosis prediction of esophageal squamous cell carcinoma. *Aging* 12:1512.

Lin, Z., Kim, E., Ahmed, M., Han, G., Simmons, C., Redhead, Y., et al. (2021). MRI-guided histology of TDP-43 knock-in mice implicates parvalbumin interneuron loss, impaired neurogenesis and aberrant neurodevelopment in amyotrophic lateral sclerosis-frontotemporal dementia. *Brain Commun.* 3:fcab114. doi: 10.1093/braincomms/fcab114

Liu, J., Kuang, F., Kroemer, G., Klionsky, D. J., Kang, R., and Tang, D. (2020). Autophagy-dependent ferroptosis: Machinery and regulation. *Cell Chem. Biol.* 27, 420–435. doi: 10.1016/j.chembiol.2020.02.005

Liu, T., Jiang, L., Tavana, O., and Gu, W.J.C.r (2019). The deubiquitylase OTUB1 mediates ferroptosis via stabilization of SLC7A11. *Cancer Res.* 79, 1913–1924. doi: 10.1158/0008-5472.CAN-18-3037

Love, M. I, Huber, W., and Anders, S.J.G.b (2014). Moderated estimation of fold change and dispersion for RNA-seq data with DESeq2. *Genome Biol.* 15:550. doi: 10.1186/s13059-014-0550-8

Maekawa, S., Al-Sarraj, S., Kibble, M., Landau, S., Parnavelas, J., Cotter, D., et al. (2004). Cortical selective vulnerability in motor neuron disease: A morphometric study. *Brain* 127, 1237–1251.

Matsumoto, T., Imagama, S., Hirano, K., Ohgomori, T., Natori, T., Kobayashi, K., et al. (2012). CD44 expression in astrocytes and microglia is associated with ALS progression in a mouse model. *Neurosci. Lett.* 520, 115–120. doi: 10.1016/j.neulet.2012.05.048

Matsuo, T., Adachi-Tominari, K., Sano, O., Kamei, T., Nogami, M., Ogi, K., et al. (2021). Involvement of ferroptosis in human motor neuron cell death. *Biochem. Biophys. Res .Commun.* 566, 24–29.

McColgan, P., Joubert, J., Tabrizi, S. J., and Rees, G. (2020). The human motor cortex microcircuit: Insights for neurodegenerative disease. *Nat. Rev. Neurosci.* 21, 401–415. doi: 10.1038/s41583-020-0315-1

Mejzini, R., Flynn, L. L., Pitout, I. L., Fletcher, S., Wilton, S. D., and Akkari, P.A.J.F.i.n (2019). ALS genetics, mechanisms, and therapeutics: Where are we now? *Front. Neurosci.* 13:1310. doi: 10.3389/fnins.2019.01310

Moreau, C., Danel, V., Devedjian, J. C., Grolez, G., Timmerman, K., Laloux, C., et al. (2018). *Could conservative iron chelation lead to neuroprotection in amyotrophic lateral sclerosis?*. New Rochelle, NY: Mary Ann Liebert, Inc.

Moreau, C., Gosset, P., Kluza, J., Brunaud-Danel, V., Lassalle, P., Marchetti, P., et al. (2011). Deregulation of the hypoxia inducible factor-1α pathway in monocytes from sporadic amyotrophic lateral sclerosis patients. *Neuroscience* 172, 110–117. doi: 10.1016/j.neuroscience.2010.10.040

Ousingsawat, J., Schreiber, R., and Kunzelmann, K. J. C. (2019). TMEM16F/anoctamin 6 in ferroptotic cell death. *Cancers* 11:625. doi: 10.3390/cancers11050625

Paydarnia, P., Mayeli, M., Shafie, M., Agah, E., Hasani, S. A., Jazani, M. R., et al. (2021). Alterations of the serum and CSF ferritin levels and the diagnosis and prognosis of amyotrophic lateral sclerosis. *eNeurologicalSci* 25:100379. doi: 10.1016/j.ensci.2021.100379

Pineda, S. S., Lee, H., Fitzwalter, B. E., Mohammadi, S., Pregent, L. J., Gardashli, M. E., et al. (2021). Single-cell profiling of the human primary motor cortex in ALS and FTLD. *bioRxiv* [Preprint]. doi: 10.1101/2021.07.07.451374

Pradhan, A. K., Maji, S., Das, S. K., Emdad, L., Sarkar, D., Fisher, P. B. J. C., et al. (2020). MDA-9/Syntenin/SDCBP: New insights into a unique multifunctional scaffold protein. *Cancer Metastasis Rev.* 39, 769–781. doi: 10.1007/s10555-020-09886-7

Prudencio, M., Humphrey, J., Pickles, S., Brown, A.-L., Hill, S. E., Kachergus, J. M., et al. (2020). Truncated stathmin-2 is a marker of TDP-43 pathology in frontotemporal dementia. *J. Clin. Invest.* 130, 6080–6092. doi: 10.1172/JCI139741

Robin, X., Turck, N., Hainard, A., Tiberti, N., Lisacek, F., Sanchez, J.-C., et al. (2011). pROC: An open-source package for R and S+ to analyze and compare ROC curves. *BMC Bioinformatics* 12:77. doi: 10.1186/147121051277

Selkoe, D. J. J. S. (2002). Alzheimer's disease is a synaptic failure. *Science* 298, 789–791.

Shabalin, A. A. J. B. (2012). Matrix eQTL: Ultra fast eQTL analysis via large matrix operations. *Bioinformatics* 28, 1353–1358. doi: 10.1093/bioinformatics/bts163

Sirabella, R., Valsecchi, V., Anzilotti, S., Cuomo, O., Vinciguerra, A., Cepparulo, P., et al. (2018). Ionic homeostasis maintenance in ALS: Focus on new therapeutic targets. *Front. Neurosci.* 12:510. doi: 10.3389/fnins.2018.00510

Sorce, S., Stocker, R., Seredenina, T., Holmdahl, R., Aguzzi, A., Chio, A., et al. (2017). NADPH oxidases as drug targets and biomarkers in neurodegenerative diseases: What is the evidence? *Free Radic. Biol. Med.* 112, 387–396. doi: 10.1016/j.freeradbiomed.2017.08.006

Soulard, C., Salsac, C., Mouzat, K., Hilaire, C., Roussel, J., Mezghrani, A., et al. (2020). Spinal motoneuron TMEM16F Acts at C-boutons to modulate motor resistance and contributes to ALS pathogenesis. *Cell Rep.* 30, 2581–2593e2587. doi: 10.1016/j.celrep.2020.02.001

Stockwell, B. R., Angeli, J. P. F., Bayir, H., Bush, A. I., Conrad, M., Dixon, S. J., et al. (2017). Ferroptosis: A regulated cell death nexus linking metabolism, redox biology, and disease. *Cell* 171, 273–285.

Tang, M., Chen, Z., Wu, D., and Chen, L.J.J.o.C.P (2018). Ferritinophagy/ferroptosis: Iron-related newcomers in human diseases. *J. Cell Physiol.* 233, 9179–9190. doi: 10.1002/jcp.26954

Taylor, J. P., Brown, R. H. Jr., and Cleveland, D. W. (2016). Decoding ALS: From genes to mechanism. *Nature* 539, 197–206. doi: 10.1038/nature20413

Tibshirani, R.J.J.o.t.R.S.S.S.B (1996). Regression shrinkage and selection via the lasso. *J. R. Statist. Soc. B* 58, 267–288.

Villalba, R. M., Mathai, A., and Smith, Y.J.F.i.n (2015). Morphological changes of glutamatergic synapses in animal models of Parkinson's disease. *Front. Neuroanat.* 9:117. doi: 10.3389/fnana.2015.00117

Wang, Q., Zhang, X., Chen, S., Zhang, X., Zhang, S., Youdium, M., et al. (2011). Prevention of motor neuron degeneration by novel iron chelators in SOD1G93A transgenic mice of amyotrophic lateral sclerosis. *Neurodegener. Dis.* 8, 310–321. doi: 10.1159/000323469

Wang, T., Tomas, D., Perera, N. D., Cuic, B., Luikinga, S., Viden, A., et al. (2022). Ferroptosis mediates selective motor neuron death in amyotrophic lateral sclerosis. *Cell Death Differ.* 29, 1187–1198. doi: 10.1038/s41418-021-00910-z

Yang, M., Chen, P., Liu, J., Zhu, S., Kroemer, G., Klionsky, D. J., et al. (2019). Clockophagy is a novel selective autophagy process favoring ferroptosis. *Sci. Adv.* 5:eaaw2238. doi: 10.1126/sciadv.aaw2238

Zhang, B., and Horvath, S.J.S.a.i.g (2005). A general framework for weighted gene co-expression network analysis. *Stat. Appl. Genet. Mol. Biol.* 4:17. doi: 10.2202/1544-6115.1128

Zhang, Q., Zhao, H., Luo, M., Cheng, X., Li, Y., Li, Q., et al. (2022). The classification and prediction of ferroptosis-related genes in ALS: A pilot study. *Front. Genet.* 13:919188. doi: 10.3389/fgene.2022.919188

Zhou, N., and Bao, J. J. D. (2020). FerrDb: A manually curated resource for regulators and markers of ferroptosis and ferroptosis-disease associations. *Database* 2020:baaa021. doi: 10.1093/database/baaa021

Zhou, N., Yuan, X., Du, Q., Zhang, Z., Shi, X., Bao, J., et al. (2022). FerrDb V2: Update of the manually curated database of ferroptosis regulators and ferroptosis-disease associations. *Nucleic Acids Res.* 51, D571–D582. doi: 10.1093/nar/gkac935

Zhu, Z.-y, Liu, Y.-d, Gong, Y., Jin, W., Topchiy, E., Turdi, S., et al. (2022). Mitochondrial aldehyde dehydrogenase (ALDH2) rescues cardiac contractile dysfunction in an APP/PS1 murine model of Alzheimer's disease via inhibition of ACSL4-dependent ferroptosis. *Acta Pharmacol. Sin.* 43, 39–49.

frontiers | Frontiers in Cellular Neuroscience

TYPE Original Research
PUBLISHED 09 May 2023
DOI 10.3389/fncel.2023.1132015

OPEN ACCESS

EDITED BY
Anwen Shao,
Zhejiang University, China

REVIEWED BY
Lufeng Zheng,
China Pharmaceutical University, China
Hang Song,
Anhui University of Chinese Medicine, China

*CORRESPONDENCE
Zhiming Cui
✉ zhimingcuispine@163.com

†These authors have contributed equally to this work

RECEIVED 26 December 2022
ACCEPTED 18 April 2023
PUBLISHED 09 May 2023

CITATION
Li C, Wu C, Ji C, Xu G, Chen J, Zhang J, Hong H, Liu Y and Cui Z (2023) The pathogenesis of DLD-mediated cuproptosis induced spinal cord injury and its regulation on immune microenvironment.
Front. Cell. Neurosci. 17:1132015.
doi: 10.3389/fncel.2023.1132015

The pathogenesis of DLD-mediated cuproptosis induced spinal cord injury and its regulation on immune microenvironment

Chaochen Li[1,2,3†], Chunshuai Wu[1,2,3†], Chunyan Ji[1,2,3†], Guanhua Xu[1], Jiajia Chen[1], Jinlong Zhang[1], Hongxiang Hong[1], Yang Liu[1] and Zhiming Cui[1,2,3*]

[1]The Affiliated Hospital 2 of Nantong University, Nantong University, The First People's Hospital of Nantong, Nantong, China, [2]Key Laboratory for Restoration Mechanism and Clinical Translation of Spinal Cord Injury, Nantong, China, [3]Research Institute for Spine and Spinal Cord Disease of Nantong University, Nantong, China

Introduction: Spinal cord injury (SCI) is a severe central nervous system injury that leads to significant sensory and motor impairment. Copper, an essential trace element in the human body, plays a vital role in various biological functions and is strictly regulated by copper chaperones and transporters. Cuproptosis, a novel type of metal ion-induced cell death, is distinct from iron deprivation. Copper deprivation is closely associated with mitochondrial metabolism and mediated by protein fatty acid acylation.

Methods: In this study, we investigated the effects of cuproptosis-related genes (CRGs) on disease progression and the immune microenvironment in acute spinal cord injury (ASCI) patients. We obtained the gene expression profiles of peripheral blood leukocytes from ASCI patients using the Gene Expression Omnibus (GEO) database. We performed differential gene analysis, constructed protein-protein interaction networks, conducted weighted gene co-expression network analysis (WGCNA), and built a risk model.

Results: Our analysis revealed that dihydrolipoamide dehydrogenase (DLD), a regulator of copper toxicity, was significantly associated with ASCI, and DLD expression was significantly upregulated after ASCI. Furthermore, gene ontology (GO) enrichment analysis and gene set variation analysis (GSVA) showed abnormal activation of metabolism-related processes. Immune infiltration analysis indicated a significant decrease in T cell numbers in ASCI patients, while M2 macrophage numbers were significantly increased and positively correlated with DLD expression.

Discussion: In summary, our study demonstrated that DLD affects the ASCI immune microenvironment by promoting copper toxicity, leading to increased peripheral M2 macrophage polarization and systemic immunosuppression. Thus, DLD has potential as a promising biomarker for ASCI, providing a foundation for future clinical interventions.

KEYWORDS

spinal cord injury (SCI), cuproptosis, immune microenvironment, DLD, machine learning

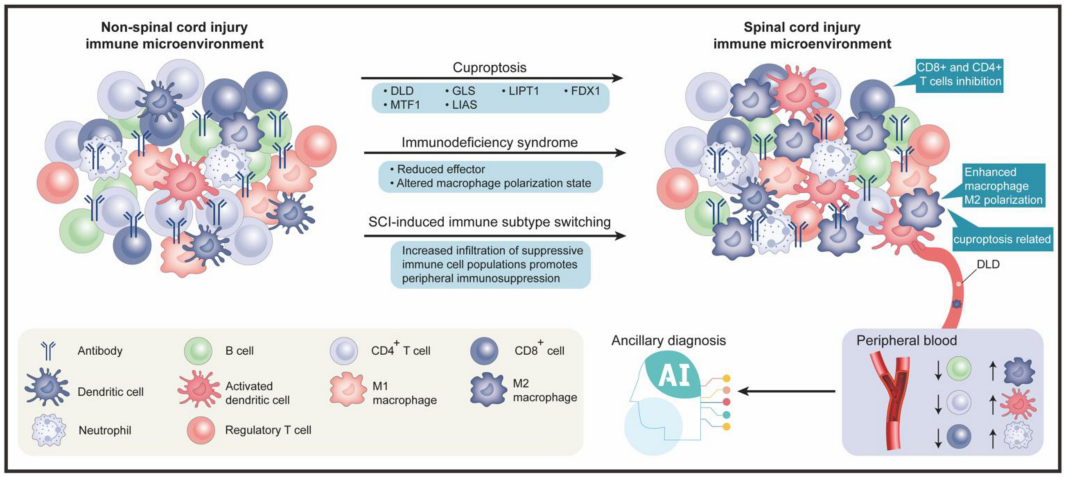

GRAPHICAL ABSTRACT

The graphical abstract is divided into two main sections, upper and lower. The upper section comprises three subsections, from left to right, which respectively represent the peripheral blood immune microenvironment in non-spinal cord injury, the involved biological processes and genes, and the peripheral blood immune microenvironment after spinal cord injury. The lower section also contains three subsections, from left to right, which respectively represent the legend for immune cells, the application of artificial intelligence in the field of spinal cord injury, and the specific trends of changes in the peripheral blood immune microenvironment after spinal cord injury.

1. Introduction

Spinal cord injury (SCI) is commonly caused by external trauma and is considered as one of the most serious injuries in traumatology, requiring advanced experience, practice, and knowledge to ensure the best outcomes for patients (Fehlings and Nguyen, 2010; Huang et al., 2020). SCI affects 1.3 million people in North America alone, and the direct lifetime cost per patient ranges from $1.1 to $4.6 million (Wilson et al., 2013; Ahuja et al., 2016; J Spinal Cord Med, 2016). Furthermore, SCI-related disability and death rates have been increasing in recent years (Byra, 2016; Casper et al., 2018).

The severity of spinal cord injuries can be divided into two stages: primary and secondary. Primary-stage injury is defined as direct mechanical damage to tissue, typically due to shearing, tearing, acute stretching, or sudden acceleration and deceleration (Wilkerson and Hayes, 2010; Van Gassen et al., 2015). Secondary injuries can be categorized as acute (within 48 h), subacute (2–14 days), intermediate (14 days to 6 months), or chronic (over 6 months) (Badhiwala et al., 2019). Hemorrhage and disruption of the blood-spinal cord barrier (BSCB) expose the spinal cord to inflammatory cells, such as neutrophils, macrophages, and cytokines, accompanied by the release of cytotoxic byproducts (Kim et al., 2017). Edema progresses during the subacute phase, causing further vascular damage, calcium dysregulation, inflammation, and persistent ischemia, which cyclically promote the cytotoxic microenvironment (Singh et al., 2012; Wang et al., 2014; Liu et al., 2015; Khan et al., 2018). The intermediate and chronic phases of SCI are characterized by dynamic vascular remodeling, alterations in extracellular matrix composition, and reorganization of local and distal neural circuits (Bradbury and Burnside, 2019). Additionally, after SCI, peripheral lymphoid organs (e.g., the spleen) lose sympathetic innervation, resulting in SCI-induced immune deficiency syndrome (SCI-IDS), which substantially increases the risk of peripheral infection (Brommer et al., 2016). Peripheral infections are the leading cause of death in patients with spinal cord injury (Savic et al., 2017; Kriz et al., 2021). Moreover, infections and associated hyperthermia can further impair the function of the central nervous system (CNS) after an SCI (Carpenter et al., 2020). Unfortunately, no curative treatment options are available for improving neurological outcomes after SCI (Burns et al., 2017; Badhiwala et al., 2018).

Unlike treatments for primary injuries, those for traumatic SCI focus on minimizing secondary injuries (Lee et al., 2018), achieved through the use of methylprednisolone (MP) and early surgical decompression (Badhiwala et al., 2018). However, studies have shown that high-dose MP treatment in the early stages of ASCI does not result in better sensory recovery (p-value = 0.07), but instead causes gastrointestinal bleeding (p-value = 0.04) and respiratory infections (p-value = 0.04) (Liu et al., 2019). Therefore, high doses of MP should be used with caution as routine treatment for ASCI in the early stages. As the global population ages, cervical spine injuries account for an increasing proportion of traumatic spinal cord injury (Devivo, 2012). Researchers have found that patients with cervical acute spinal cord injury (ASIA) who undergo early surgery (within 24 h) show better functional recovery after six months than those who undergo late surgery (more than 24 h) (Fehlings et al., 2012). Nevertheless, early surgical intervention for ASCI may encounter numerous obstacles, including a lack of operating room availability, transporting patients from injury sites or other centers, a lack of specialized operating room teams, and a lack of on-call surgeons (Glennie et al., 2017). This means a large proportion of patients are likely to miss the optimal time to undergo surgery, depriving them of timely treatment and compromising their clinical outcomes. Due to limited sensitivity and specificity, the application of therapeutic strategies, such as pharmacotherapy (Kjell et al., 2015), cell therapy (Cofano et al., 2019), biomaterials (Zuidema et al., 2014), and functional electrical stimulation (Kapadia et al., 2014; Bonizzato et al., 2018), on a large clinical scale has been difficult. Recent studies suggest that

the pathogenesis of SCI is closely related to the characteristics and dynamics of the infiltrating monocyte-derived macrophages (MDM) (Milich et al., 2019). As the field of SCI research grows, bioinformatics research based on next-generation sequencing attracts increasing attention. Gene expression analysis of three datasets (GSE92657, GSE93561, and GSE189070) in the GEO database identified a gene with high auxiliary value in SCI (Tong et al., 2022). Lai et al. (2013) investigated gene expression in thoracic intrinsic spinal cord neurons of 12 SCI rat models and 12 healthy control rats, identifying three genes of potential interest for future research (Lai et al., 2013). SCI-IDS can exacerbate peripheral infections after SCI, further impairing central nervous system function and resulting in increased mortality and complications. Therefore, studying changes in the immune microenvironment following SCI is necessary to further aid in the diagnosis of SCI and its adjuvant treatment.

Among essential trace elements, copper (Cu) plays an important role in growth, metabolism, and regulatory functions related to oxidative stress. It also potentially contributes to the pathophysiology of SCI and neural regeneration following injury (Che et al., 2016; Inesi, 2017; Guengerich, 2018; Timon-Gomez et al., 2018). Despite its usefulness as a cofactor for enzymes across the animal kingdom, copper can be toxic, resulting in cell death even at modest intracellular concentrations (Ge et al., 2022). The role of metal ions in SCI is diverse and important. A recent study shows that SCI patients exhibit a significant increase in iron deposits in their motor cortex, ultimately resulting in ferroptosis in motor neurons and impaired recovery of motor function (Feng et al., 2021). In a different study, zinc inhibited neuronal ferroptosis through the NRF2/HO-1 and GPX4 signaling pathways, exerting a neuroprotective effect (Ge et al., 2021). Following ferroptosis, a new metal ionic cell death pathway called cuproptosis has recently gained attention. It is associated with aggregation of fatty acylated proteins and proteotoxic stress resulting from excessive copper accumulation (Tsvetkov et al., 2022). Ten genes are implicated in the process of cuproptosis: FDX1, DLAT, LIPT1, PDHB, LIAS, DLD, and PDHA1 are positively regulated, while MTF1, GLS, and CDKN2A are negatively regulated (Tsvetkov et al., 2022). Cuproptosis has been shown to play a role in a variety of diseases. Wilson disease (WD) is associated with cuproptosis and is characterized by copper accumulation in cells and organs. Thus, copper chelators may be effective in treating WD (Aggarwal and Bhatt, 2018). A recent study evaluated the role of cuproptosis in hepatocellular carcinoma and identified a prognostic long non-coding (lnc) RNA profile associated with cuproptosis to predict response to immunotherapy (Zhang et al., 2022). Despite this, it remains unclear whether cuproptosis can be applicable as a therapeutic option for patients with spinal cord injuries. Serum copper levels have been found to be significantly higher in patients with spinal cord injuries than in healthy subjects (p-value = 0.002) (Salsabili et al., 2009). Abnormalities in serum copper levels after SCI could provide new insights into the pathogenesis of SCI.

Dihydrolipoamide dehydrogenase (DLD), a multifunctional oxidoreductase, is an essential component of multiple mitochondrial multienzyme complexes, and it is known to induce cuproptosis (Fan et al., 2014; Tsvetkov et al., 2022). Numerous studies have highlighted the importance of DLD in cell death. For example, DLD induced hyperphosphorylation of microtubule-associated tau protein, which led to neurodegeneration in Alzheimer's disease (Ahmad, 2018). Moreover, DLD has been shown to produce a significant amount of reactive oxygen species (ROS) in melanoma cells, inducing apoptosis (Dayan et al., 2019). In addition, DLD is known to promote ferroptosis in head and neck cancers (Shin et al., 2020). Although cell death is inevitable during the acute phase of spinal cord injury, it is unknown whether DLD influences this process.

Our study aimed to evaluate the effects of cuproptosis-related genes (CRGs) on ASCI progression and the immune microenvironment using a multi-omics and multi-dimensional approach, in addition to identifying peripheral blood biomarkers for acute (A) SCI. Therefore, an exploratory examination of the relationship between DLD, ASCI disease progression, and changes in the immune microenvironment was performed using bioinformatics analysis, including differential expression analysis, protein–protein interaction (PPI) network analysis, centrality analysis, weighted gene co-expression network analysis (WGCNA), risk model construction, deep learning-based clinical prediction model construction, functional enrichment analysis, molecular subtype analysis, and immune infiltration analysis. Our findings suggested that DLD affects the peripheral immune microenvironment in ASCI and induces M2 polarization of macrophages, which exacerbates SCI-IDS and adversely impacts ASCI outcome. Moreover, DLD shows potential as a peripheral blood biomarker for ASCI. As a result of our analysis, it becomes clear that CRGs play an important role in ASCI development, as well as providing a basis for therapeutic applications of cuproptosis regulators in ASCI.

2. Materials and methods

2.1. Data sources and preprocessing

We downloaded single-array ASCI patients' RNA-seqencing (seq) data from the GEO database[1] to eliminate the possibility of multi-array batch effects interfering with our results. The criteria for gene chip selection were as follows: (1) Complete raw RNA-sequencing data were available, (2) RNA-sequencing of peripheral blood leukocytes from patients with spinal cord injuries, (3) Within 48 h after the injury, peripheral blood samples were collected from the patient, and (4) Complete clinical baseline information was available for the patients. The selected gene microarray dataset was GSE151371 (Kyritsis et al., 2021), with *Homo sapiens* as the selected species and peripheral blood leukocytes as the selected tissue type. The dataset included data from 20 control patients without spinal cord injuries (Control group) and 38 ASCI patients (ASCI group). Data from microarray experiments were normalized using the Bioconductor package limma (Phipson et al., 2016). Clinical data for ASCI patients were obtained from the GSE151371 dataset (**Table 1**). Missing values and outlier samples were removed before training neural networks.

2.2. Expression profiling of CRGs

To determine the expression of CRGs in ASCI, we identified the chromosomal locations using the R software package RCircos

1 https://www.ncbi.nlm.nih.gov/geo/

(Zhang et al., 2013). Next, we analyzed the expression of CRGs in the ASCI and control groups using the Wilcoxon test and visualized the results using the ggplot2 (Ito and Murphy, 2013) package. The differential expression of CRGs was analyzed using the R package limma and visualized using the ggplot2 package. Since small changes in the nervous system can have a substantial impact, we set a cutoff at a p-value of <0.05 to ensure the comprehensiveness of the differential expression analysis.

Next, to analyze the correlation and interaction between positive (FDX1, DLAT, LIPT1, PDHB, LIAS, DLD, and PDHA1) and negative (MTF1, GLS, and CDKN2A) cuproptosis regulators, we performed Spearman correlation analysis on CRGs and visualized the results using the R package ggcorrplot.

2.3. Risk model and clinical prediction model construction

We first identified key genes associated with ASCI using univariate logistic regression analysis, and then used the least absolute shrinkage and selection operator (LASSO) algorithm to confirm the correlation between key genes and ASCI. Furthermore, a variance inflation factor cutoff of four was used to exclude multicollinearity in multivariate logistic regression analysis of ASCI. To validate the results of the multivariate logistic regression and assist in the diagnosis of ASCI, we developed a nomogram prediction model based on these results. A calibration curve was used to evaluate the performance of the nomogram model in identifying patients with ASCI.

After considering the ASIA score as the dependent variable, we incorporated the ASCI-related potential biomarker (DLD) and eight clinical features into the model. The clinical features included sex, age, race, prior central nervous system pathology, injury severe score, concurrent traumatic brain injury, blood draw time, and damaged spinal cord stage. We used the R package keras to model the classifier architecture using neural networks. The ASIA scores were compressed according to grades with the A, B, and C levels designated as level 2, whereas the D and E levels were designated as level 1. This neural network consisted of two layers, in which the input layer activation function was "relu" and the output layer activation function was "sigmoid," combined with a rmsprop optimizer and a custom penalty function. The ASCI patients were randomly assigned to training and validation sets in a 3:7 ratio. To measure the performance of the clinical prediction model, receiver operating characteristic (ROC) curves were calculated by comparing predicted and observed values from the neural network.

2.4. CRGs functional enrichment analysis and gene set variation analysis

CRG annotation using GO and KEGG pathway enrichment analysis was performed using the clusterProfiler package (Yu et al., 2012) in R. Statistical significance was determined using a false discovery rate of 0.05.

To determine whether there were differences between different groups regarding biological processes, we performed gene set variation analysis (GSVA) using the gene expression profiling dataset of ASCI patients. Gene set enrichment analysis (GSEA) evaluates whether two biological states are significantly different from each other by comparing a gene set (Subramanian et al., 2005). GSVA is a sub-algorithm of GSEA that estimates changes in pathway and biological process activity in samples of expression datasets. Using the annotation catalog (msigdb.v7.4.symbols.gmt) from the MSigDB database (Liberzon et al., 2015), we performed GSVA using the R package GSVA (Hanzelmann et al., 2013), and employed linear fitting and Bayesian network algorithms to determine the differences between the ASCI and control groups in the relevant GSVA pathways. A p-value threshold of 0.05 was used to determine statistical significance.

TABLE 1 Baseline information.

Characteristic	Levels	Overall
n		58
Group, *n* (%)	SCI	38 (65.5%)
	Control	20 (34.5%)
Sex, *n* (%)	F	19 (32.8%)
	M	39 (67.2%)
Race, *n* (%)	Asian	4 (6.9%)
	Black or African-American	5 (8.6%)
	Hispanic	25 (43.1%)
	Other	3 (5.2%)
	Unknown	16 (27.6%)
	White	5 (8.6%)
Prior CNS pathology, *n* (%)	No	41 (70.7%)
	Yes	12 (20.7%)
	Unknown	5 (8.6%)
Concurrent TBI, *n* (%)	No	48 (82.8%)
	Yes	8 (13.8%)
	Unknown	2 (3.4%)
NLI grouped, *n* (%)	Cervical	18 (47.4%)
	Lumbar	2 (5.3%)
	Thoracic	10 (26.3%)
	Unknown	8 (21.1%)
ASIA impairment scale, *n* (%)	A	12 (31.6%)
	B	4 (10.5%)
	C	6 (15.8%)
	D	11 (28.9%)
	Unknown	5 (13.2%)
Age, median (IQR)		51 (39, 66)
ISS, median (IQR)		21 (17, 32.5)
Blood draw time, median (IQR)		22.5 (17, 40)

2.5. Weighted gene co-expression network analysis (WGCNA)

Using the R package WGCNA (Langfelder and Horvath, 2008), we performed a WGCNA analysis of the eigengene set in ASCI. First, to eliminate outliers from the standardized gene

10.3389/fncel.2023.1132015

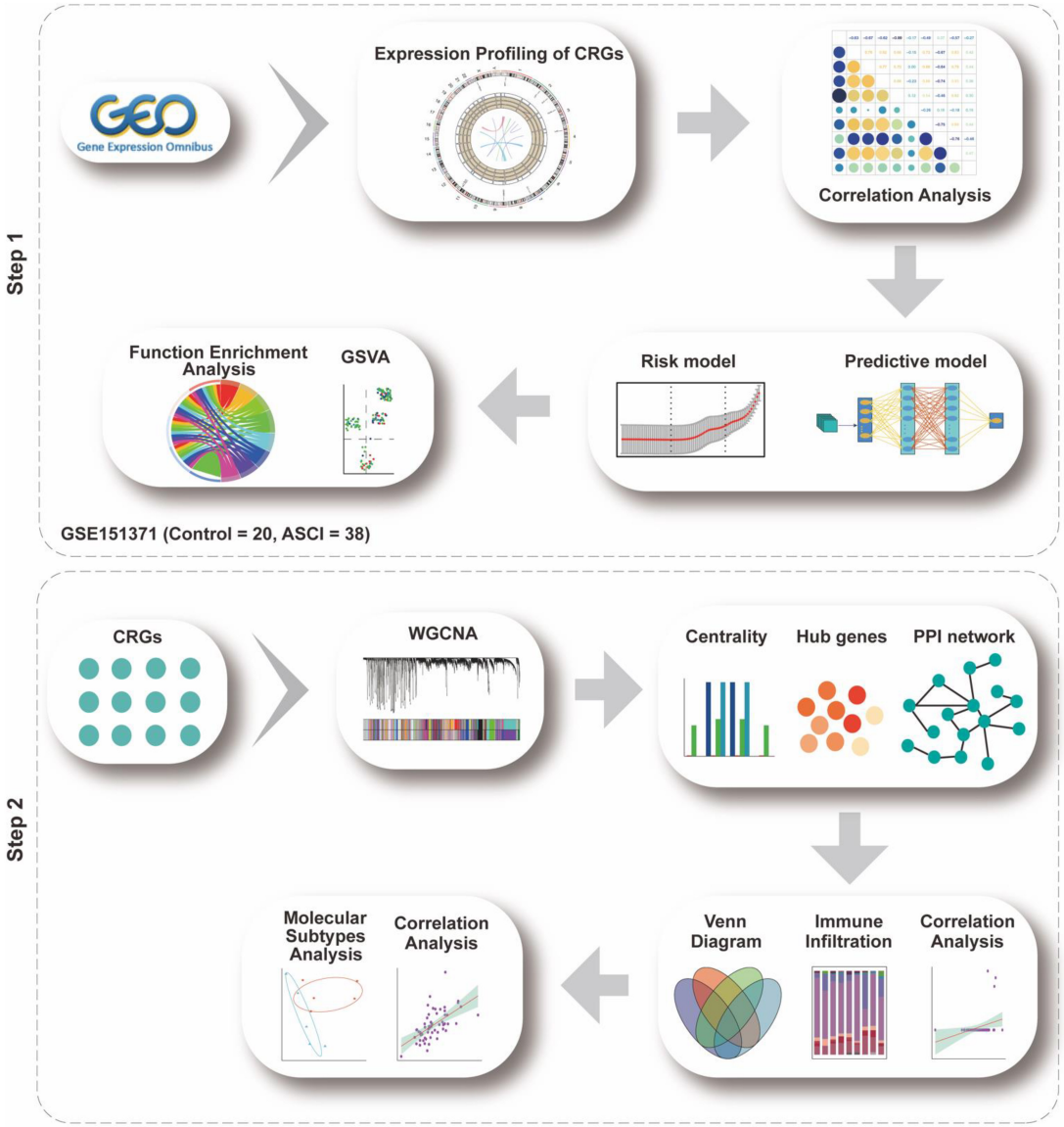

FIGURE 1
Analysis flow chart. The study flow chart is divided into two main sections according to the study sequence. Each icon represents schematically an analysis or a collection of data to be analyzed.

expression data, we performed hierarchical clustering. In the next step, we adopted the R^2 and slope values to determine the optimal soft threshold, as well as to validate the scale-free network. A dissimilarity analysis, with a threshold of 0.25, was used to determine the adjacency matrix and topology matrix, and dynamic shear trees were analyzed to identify network modules (deepSplit = 2, miniClusterSize = 30). Finally, we performed the correlation analysis in conjunction with the ASCI phenotype data.

2.6. Construction of protein–protein interaction (PPI) network

The PPI network of CRGs was constructed using the STRING database, and the sub-networks were extracted using the MCODE plugin of Cytoscape software (version: 3.9.1) (Shannon et al., 2003). Next, we examined the centrality of the PPI network of CRGs in four dimensions including betweenness centrality, closeness centrality, degree centrality, and stress centrality. Moreover, we analyzed the co-expression of ASCI-related WGCNA module genes, differentially expressed CRGs, PPI sub-network genes of CRGs, and the results of multivariate logistic regression.

2.7. Identification and correlation analysis of immune infiltration in ASCI

The extent of immune cell infiltration in the control and ASCI groups was calculated using the single-sample Gene Set Enrichment Analysis (ssGSEA) algorithm. According to gene expression data, ssGSEA can be used to determine the population of immune cells within a sample (Subramanian et al., 2005).

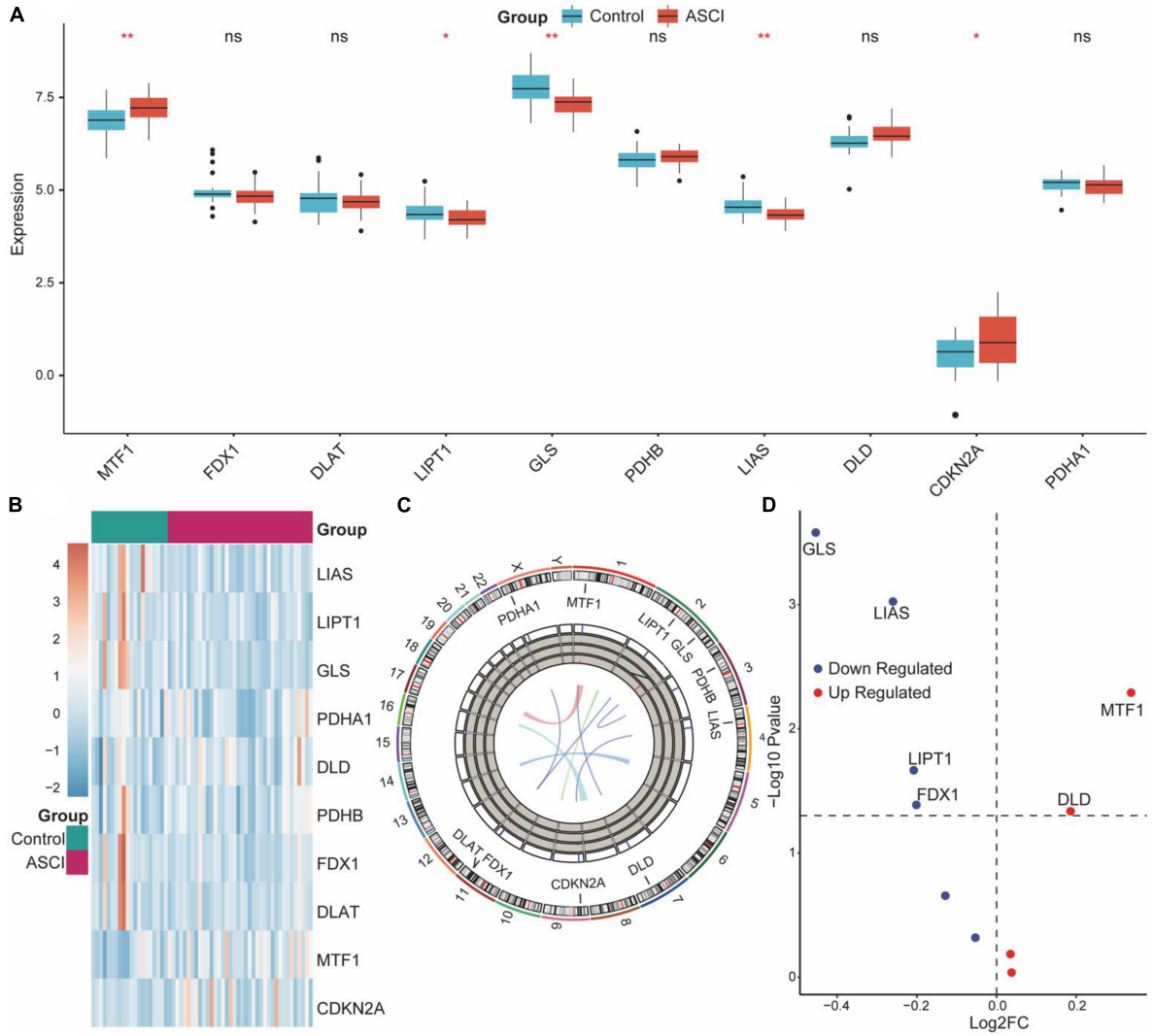

FIGURE 2
Overall expression of cuproptosis-related genes (CRGs) in acute spinal cord injury (ASCI) patients. **(A)** Differences in the expression of CRGs between the ASCI and control groups; ns indicates p-value = 0.05, * indicates p-value < 0.05, and ** indicates p-value < 0.01. **(B)** Expression heat map of CRGs. **(C)** Chromosome localization map of CRGs. **(D)** Volcano plot of the results of the differential genetic analysis of CRGs.

CIBERSORT is an analytical tool developed by Newman et al. to estimate the abundance of different cell types in mixed cell populations by using gene expression data (Newman et al., 2019). We validated immune infiltration results using the CIBERSORT algorithm in R. Statistically significant differences in immune cell proportions between normal and diseased sample groups were calculated using the Wilcoxon test, with a *p-value* of 0.05 being considered statistically significant. To determine the stability of the immune infiltration analysis results, based on the R package immunedeconv and ImmuCellAI, we also used different algorithms for validation, including: quanTIseq, Xcell, MCP-counter, and ImmuCellAI (Sturm et al., 2019; Miao et al., 2020).

Our analysis of ASCI key genes and immune characteristics was conducted using the R package corrr to quantify the correlation between ASCI key genes and immune characteristics. Based on the ASIA score, we divided the ASCI patients into two groups: the ASIA-high group, which included levels A, B, and C, and the ASIA-low group, which included levels D and E. Next, we further explored the effect of an altered immune microenvironment on ASCI disease progression through differential expression and correlation analysis.

2.8. Construction of the ASCI-related molecular subtype

To analyze the potential subtypes among the CRGs of ASCI patients, we first organized the expression matrix of CRGs, then compressed the data distribution using normalization, and finally performed consensus clustering analysis using the hclust algorithm (sample resampling ratio: 80%, number of resamplings: 1,000, maximum number of clusters: 7). The R package pheatmap was used to visualize molecular typing results. To evaluate ASCI molecular typing, we used the T-distributed Stochastic Neighbor Embedding (tSNE) algorithm. According to the results of the

10.3389/fncel.2023.1132015

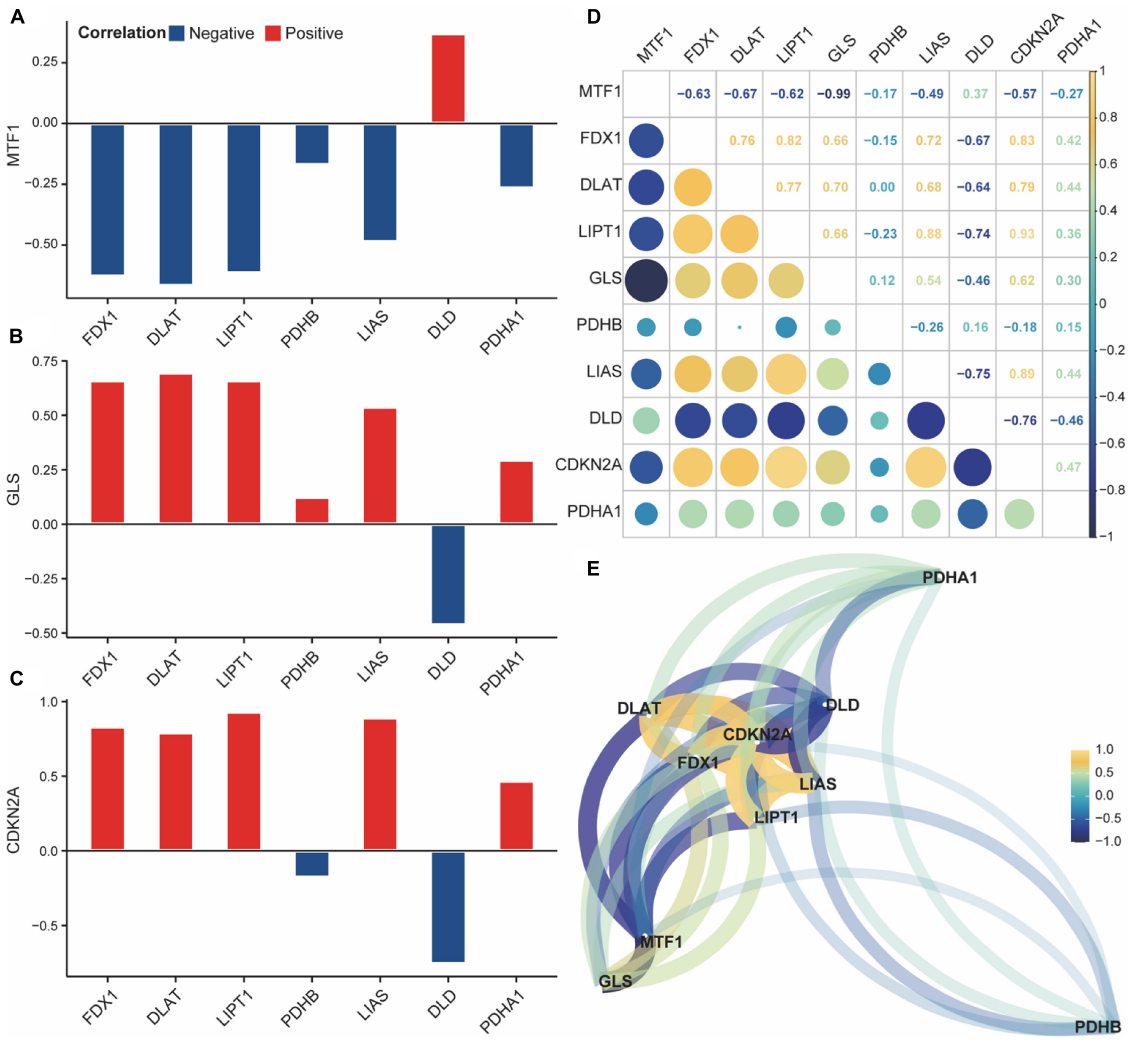

FIGURE 3
Correlation of cuproptosis-related genes (CRGs) in acute spinal cord injury (ASCI) patients. **(A–C)** Correlation histogram plot of CRGs; the abscissa represents positive cuproptosis regulators, and the ordinate represents negative cuproptosis regulators; Colour code indicates correlation. **(D)** Correlation heat map of CRGs; numbers represent correlation coefficients. **(E)** Correlation network diagram of CRGs; numbers represent correlation coefficients.

analysis of ASCI-related molecular subtypes, Spearman's coefficient was used to determine the relationships between key genes and ASCI-related molecular subtypes.

2.9. qRT-PCR and ELISA experiment

White cells were extracted from peripheral blood through Peripheral Blood Leukocyte Isolation Kit (TBD, WBC1077K), strictly following the manufacturer's instructions. We collected peripheral blood (5 ml) from patients in the ASCI group (n = 3) and control group (n = 3) using anticoagulant tubes. Carefully suck the blood sample with a straw and add it to the liquid level of the separation solution (5 ml), then centrifuge (500–800 g, 30 min). After centrifugation, carefully aspirate all circular milky white cell layers (one or two layers) using a pipette, add them to 10 ml of cleaning solution, and mix the cells evenly. Then centrifuge at low speed (250 g, 10 min). Repeat washing 2–3 times to obtain the required white blood cells. qRT-PCR and ELISA experimental processes are similar to our previous studies (Wu et al., 2022). The primers in qRT-PCR are LDHD-F sequence (5'–3' agc ctg agc acc gtg tta cc), LDHD-R Sequence (5'–3' gcc agg aca gga tgc gta gg), which purchased from Sangon Biotech (Shanghai, 007177). The Human DLD ELISA Kit was purchased from ZCi Biotech (Shanghai, ZC-56138). Measure the absorbance (OD value) using an enzyme-linked immunosorbent assay at a wavelength of 450 nm. Both qRT-PCR and ELISA experiments were repeated three times.

2.10. Statistical analysis

Data processing and analysis were conducted using the R software (version 4.2.0). When comparing two continuous variable groups, an independent Student's t-test was used to estimate the statistical significance of normally distributed variables, and Mann–Whitney U tests were used to examine differences between

10.3389/fncel.2023.1132015

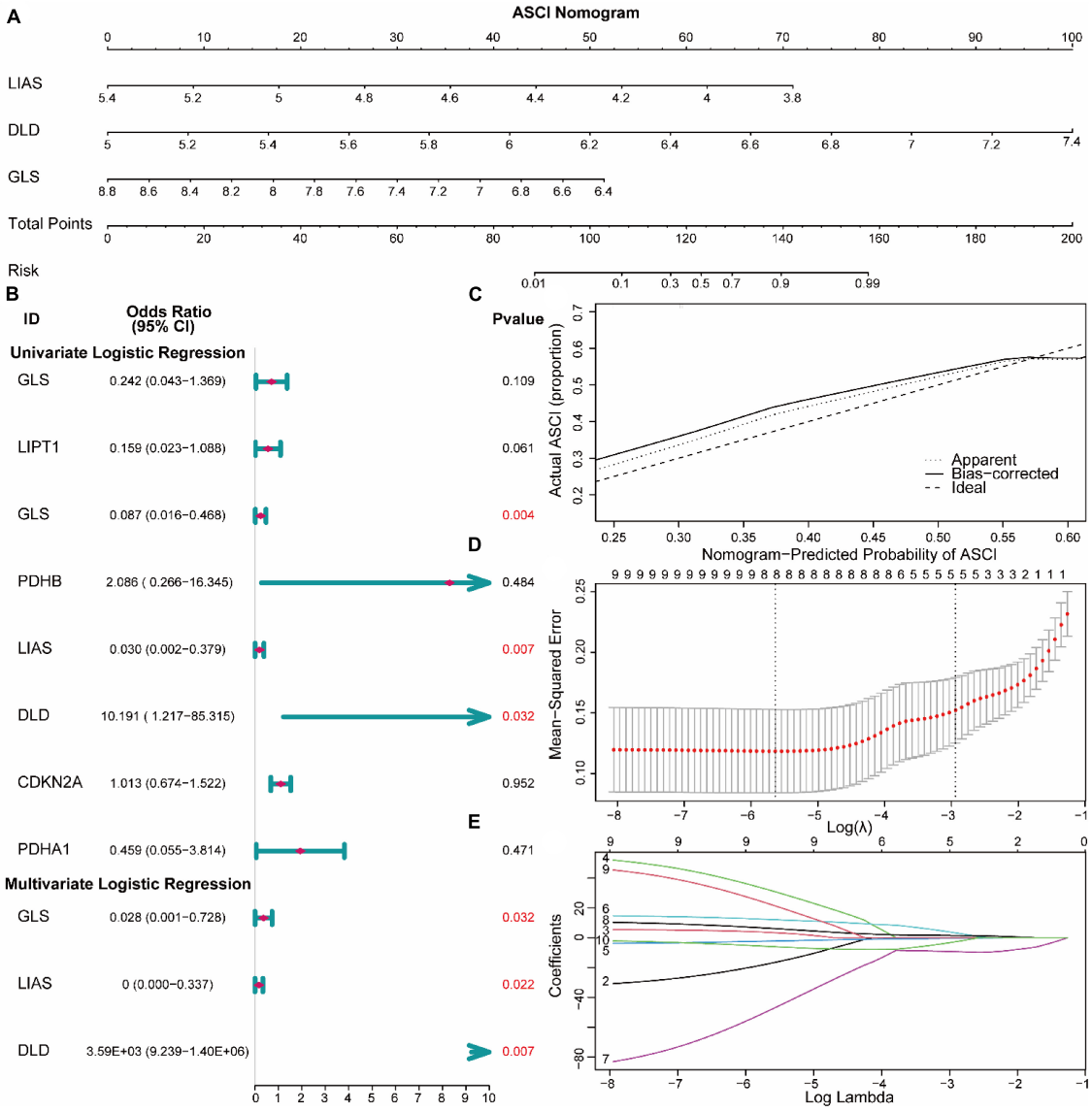

FIGURE 4
Construction of risk models for acute spinal cord injury (ASCI). **(A)** Nomogram prediction model for ASCI. **(B)** Forest plot base on logistic regression. **(C)** Calibration curves for the Nomogram prediction model. **(D,E)** LASSO regression recognized essential genes of ASCI.

non-normally distributed variables. Statistical significance of the two categorical variable groups was determined using the chi-square or Fisher's exact test. Spearman correlation analysis was used to measure the correlation coefficients of different genes. The statistical p-values were two-tailed, and statistical significance was set at $p < 0.05$.

3. Results

3.1. Gene chip quality control

The flow chart for this study can be found in Figure 1.

We analyzed the expression levels in ASCI and control groups from the GEO dataset using background calibration to evaluate how ASCI patients express CRGs overall (Supplementary Figure 1).

3.2. Expression profile of CRGs in ASCI

CRG expression distribution and chromosomal localization were analyzed to determine the overall expression of CRGs in ASCI patients (Figures 2B, C). Next, we determined whether the expression of CRGs in the ASCI group differed from that in the control group using the Wilcoxon test. The results demonstrated that MTF1, LIPT1, GLS, LIAS, and CDKN2A were significantly differentially expressed (Figure 2A). Subsequently, we performed differential gene expression analysis for CRGs in ASCI patients. We found that DLD and MTF1 were significantly upregulated in ASCI patients, whereas GLS, LIAS, LIPT1, and FDX1 were significantly

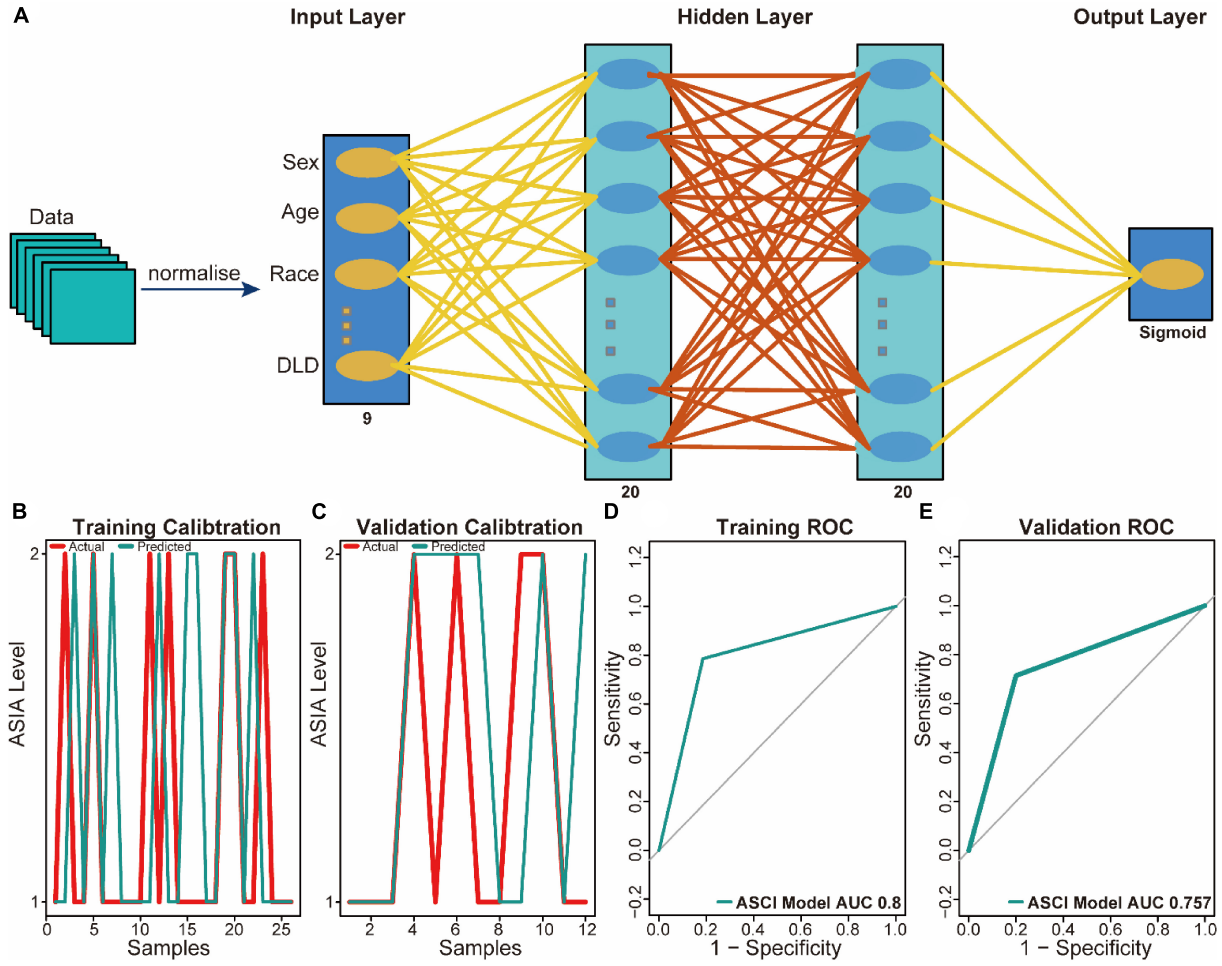

FIGURE 5
Predictive power analysis of neural network model for acute spinal cord injury (ASCI). **(A)** Architecture diagram of neural network model. **(B)** Calibration curve for the neural network model in the training set; the abscissa represents patients, and the ordinate represents the levels of ASIA. **(C)** Calibration curve for the neural network model in the validation set; the abscissa represents patients and ordinate represents the levels of ASIA. **(D)** Receiver operating characteristic (ROC) curve of the training set of the neural network model; the abscissa represents the specificity and ordinate represents the sensitivity. **(E)** ROC curve of the validation set of the neural network model; the abscissa represents the specificity and ordinate represents the sensitivity.

downregulated in ASCI patients (p-value < 0.05) (Figure 2D). To ensure the comprehensiveness of the study, we combined the results from Wilcoxon's test and differential gene expression analysis.

Next, we analyzed the correlation and interaction between positive and negative regulators within CRGs using the Spearman algorithm (Figure 3E). There was a positive correlation between DLD and MTF1, and a negative correlation between DLD, GLS, and CDKN2A (Figures 3A–C). Genes with a correlation coefficient greater than 0.7 were considered significantly correlated, and a significant negative correlation was observed between DLD and CDKN2A (Figure 3D).

3.3. Construction of risk models

To analyze the expression of CRGs in ASCI, we first performed a univariate logistic regression analysis to identify key genes associated with ASCI. We employed the LASSO algorithm to narrow down the analysis and validate the key genes associated with ASCI (Figures 4B, D, E). In a multivariate logistic regression model, ASCI-related eigengenes were incorporated, and GLS, LIAS, and DLD were identified as independent risk factors for ASCI (p-value < 0.05) (Figure 4B). Based on the multivariate logistic regression results, a predictive nomogram was constructed to predict the risk of ASCI (Figure 4A). The calibration curve demonstrated that the nomogram prediction model, based on the independent risk factors of ASCI, could identify patients with ASCI with excellent accuracy (Figure 4C).

3.4. Construction of clinical prediction models

To aid clinical diagnosis and treatment, we integrated DLD expression levels and clinical characteristics into our model, constructing an architecture of back-propagation neural networks with classifiers (Figure 5A). Based on the calibration curve, the

TABLE 2 Function enrichment analysis.

Category	ID	Description	*p*-value
BP	GO:0006086	Acetyl-CoA biosynthetic process from pyruvate	9.66E-13
BP	GO:0006085	Acetyl-CoA biosynthetic process	8.96E-12
BP	GO:0006084	Acetyl-CoA metabolic process	1.53E-10
BP	GO:0044272	Sulfur compound biosynthetic process	1.72E-10
BP	GO:0035384	Thioester biosynthetic process	4.35E-10
MP	GO:0016620	Oxidoreductase activity, acting on the aldehyde or oxo group of donors, NAD or NADP as acceptor	2.08E-10
MP	GO:0016903	Oxidoreductase activity, acting on the aldehyde or oxo group of donors	4.28E-10
MP	GO:0016747	Acyltransferase activity, transferring groups other than amino-acyl groups	2.11E-03
MP	GO:0016746	Acyltransferase activity	2.67E-03
MP	GO:0016783	Sulfurtransferase activity	3.26E-03
CC	GO:0005759	Mitochondrial matrix	2.12E-10
CC	GO:1990204	Oxidoreductase complex	1.52E-08
CC	GO:0098798	Mitochondrial protein-containing complex	2.71E-03
CC	GO:0045239	Tricarboxylic acid cycle enzyme complex	3.98E-03
CC	GO:0001669	Acrosomal vesicle	3.66E-02
KEGG	hsa00020	Citrate cycle (TCA cycle)	2.23E-09
KEGG	hsa00620	Pyruvate metabolism	1.45E-08
KEGG	hsa00010	Glycolysis/Gluconeogenesis	6.20E-08
KEGG	hsa01200	Carbon metabolism	5.54E-07
KEGG	hsa01240	Biosynthesis of cofactors	1.25E-04

model demonstrated excellent classification performance in both training and validation datasets (Figures 5B, C). A comparison between predicted and actual ASCI values was conducted to evaluate the performance of the neural network, resulting in ROC curves with area under the curve (AUC) of 0.8 and 0.757 in the training set and validation set, respectively (Figures 5D, E). These results confirm the outstanding ability of the neural network clinical prediction model to predict neurological function in ASCI patients. Moreover, by using the custom penalty function, we enhanced the goodness of fit of the neural network model for small datasets, thereby preventing the occurrence of overfitting.

3.5. Functional enrichment analysis

Comparing ASCI and control patients, we analyzed the effects of CRGs on biologically relevant functions (Table 2). The GO functional annotation results of CRGs revealed that biological processes were dominated by differentially expressed genes, such as the biosynthesis of acetyl-CoA from pyruvate, acetyl-CoA metabolic process, and acetyl-CoA biosynthetic process (Figure 6A); molecular functions such as antioxidant activity, acting on the aldehyde or oxo group of donors, NAD or NADP as acceptor, acyltransferase activity, and sulfurtransferase activity (Figure 6B); and cellular components such as mitochondria matrix, oxidoreductase complex, and mitochondrial protein-containing complex (Figure 6C). The first eight enrichment results of the GO biological process examined the regulation of CRGs (Figures 6D, E). The next step was to conduct an interactive study of enrichment of CRGs in KEGG pathways, and the results indicated that these CRGs were enriched in pathways such as the citrate cycle (TCA cycle), pyruvate metabolism, and glycolysis/gluconeogenesis (Figure 6F).

We performed GSVA analysis with CRGs to verify the accuracy of GO and KEGG enrichment analyses. Biological processes were found to differ significantly from one another: biosynthetic process, metabolic process, and oxidation process were significantly upregulated after ASCI (Figure 6G). Based on these findings, CRGs may play a role in metabolic processes associated with SCI.

3.6. Weighted gene co-expression network analysis (WGCNA)

To analyze the eigengene set of ASCI, we performed a WGCNA using all genes from the GSE151371 chip. First, we performed a hierarchical clustering analysis on the samples; then, outlier samples were removed, and a dynamic clipping tree was used to identify the network modules (Figure 7D). The scale-free network was verified upon selecting the best soft threshold. The results showed that R = 0.87 and slope = −1.97, and the scale-free network had been successfully established (Figures 7A–C). After excluding the gray module, we performed a correlation analysis using the scale-free network module and the external module (ASCI), revealing a significant relationship between the ivory, blue, darkgray, saddlebrown, brown, darkred, green, and black modules and ASCI (p-value < 0.05) (Figure 7E).

10.3389/fncel.2023.1132015

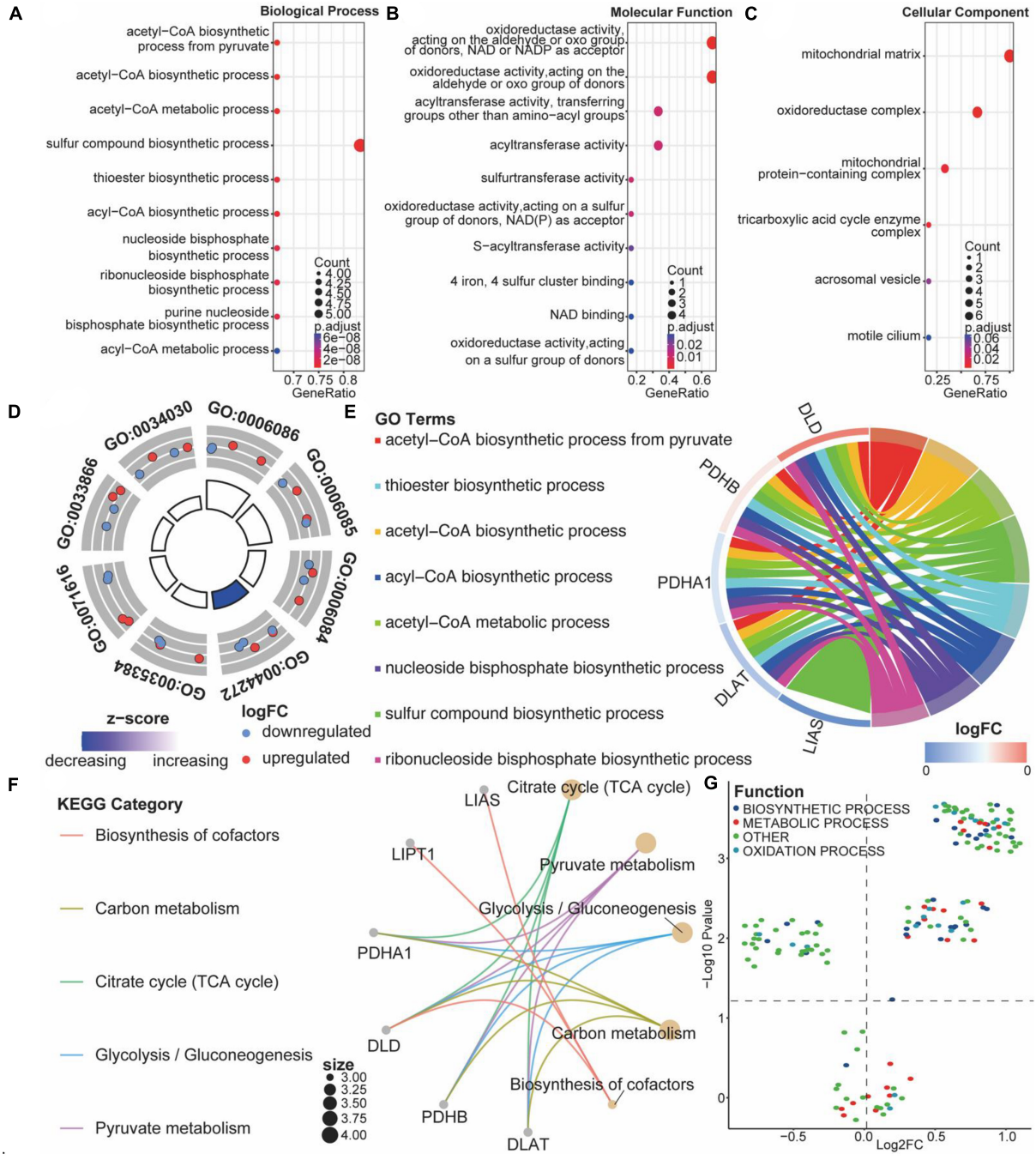

FIGURE 6
Functional enrichment analysis of cuproptosis-related genes (CRGs). **(A–C)** Bubble diagram of the first 10 biological processes, molecular functions, and cellular components items, with horizontal coordinates indicating GeneRatio, vertical coordinates indicating gene ontology (GO) terms, dot size indicating the number of genes, and dot color indicating adjust *p-value*. **(D)** Circle diagram of the first eight biological processes items, with the outer circle dot color representing upregulated and downregulated genes and the inner circle color representing activation or repression of GO terms. **(E)** String diagram of the first eight biological processes, the left outer half-circle represents genes within the pathways, the color indicates log fold change (FC), the right outer half-circle color indicates GO terms, and the inner connecting line indicates the association of GO terms with genes. **(F)** Interaction network diagram of the Kyoto encyclopedia of genes and genomes (KEGG) pathways. **(G)** Volcano plot of differential expression of gene set variation analysis (GSVA); colors represent different biological process.

3.7. PPI network of CRGs between ASCI and control groups

We explored differences in PPI networks by extracting protein interaction networks of CRGs from ASCI and control groups. The PPI network of CRGs was constructed using the STRING database, containing 17 interaction relationships and ten CRGs, with a confidence index of 0.7, an average local clustering coefficient of 0.733, and an enrichment *p*-value of 1.11e-16 (Figure 8B). Next, we used the Cytoscape software to extract the functional

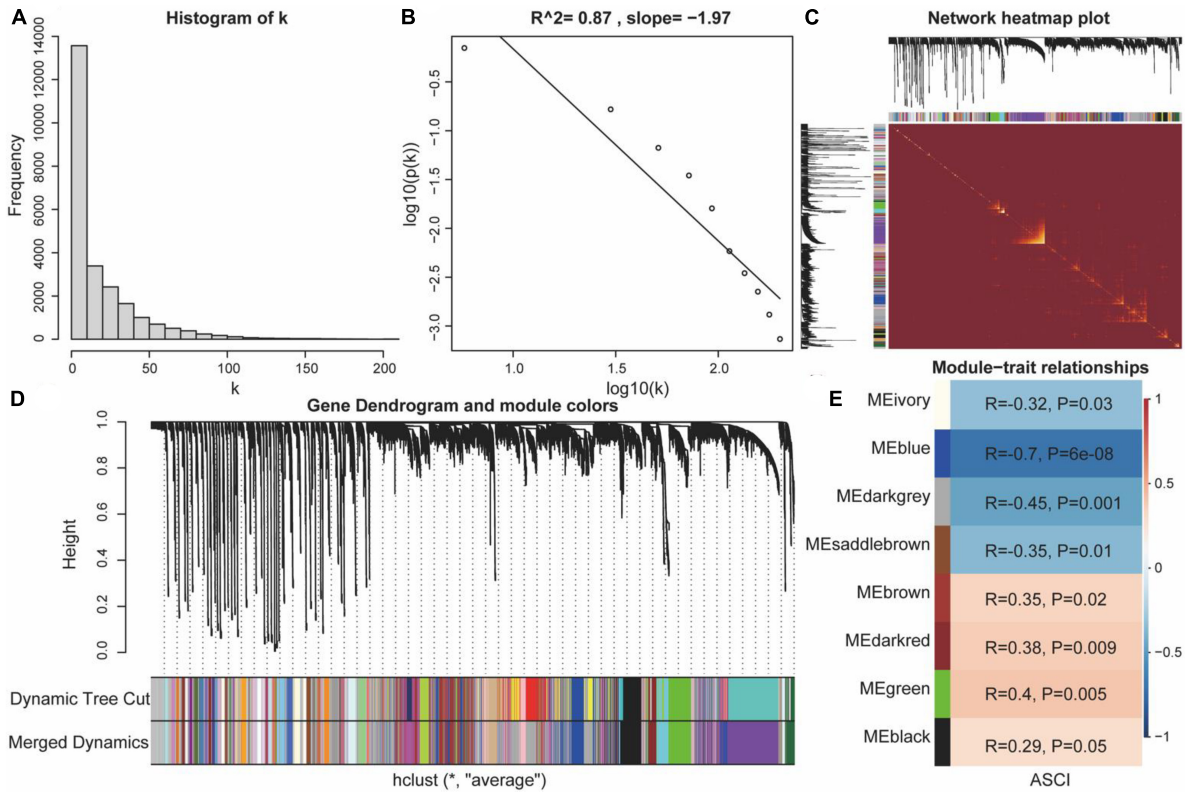

FIGURE 7
Weighted gene co-expression network analysis (WGCNA). **(A,B)** Scale-free network verification graph ($R^2 > 0.8$, slope < 0), conforming to the scale-free network standard. **(C)** TOM network clustering heatmap. **(D)** Dynamic clipping tree clustering diagram; the abscissa is the clustering module and ordinate is the tree height. **(E)** Heat map of correlations between WGCNA network modules and acute spinal cord injury (ASCI).

interaction subnets of the PPI network (Figure 8C). We also analyzed the centrality of PPI network nodes in four dimensions: betweenness centrality, closeness centrality, degree centrality, and stress centrality. The results indicated that DLD and LIAS occupy critical positions within the PPI network (Figure 8A). After conducting co-expression analyses of all CRGs, ASCI-related WGCNA modules, differentially expressed CRGs, and multivariate logistic regression, we found that DLD was not only highly correlated with ASCI but also exhibited significant changes in expression levels after ASCI (Figure 8D). Thus, cuproptosis regulator DLD may play an important role in ASCI, which was the focus of our next analysis.

3.8. Immune infiltration and correlation in ASCI and control groups

ASCI patients were assessed using the CIBERSORT algorithm for their immune profile and level of immune cell infiltration (Figure 9A). To further elucidate changes in the immune microenvironment of ASCI patients, we estimated the extent of immune cell infiltration using ssGSEA (Figure 9B). After ASCI, the number of activated B cells and activated CD8 T cells significantly decreased, while the number of macrophages significantly increased (p-value < 0.05). To evaluate the stability of the immune infiltration analysis, we used several immune infiltration algorithms for validation and obtained similar conclusions (Supplementary Figures 2A–D).

To determine whether CRGs play a role in the altered immune environment after ASCI, we analyzed the correlation between DLD and differentially expressed T cells, B cells, plasma cells, and macrophages. Correlations were considered significant when the p-value was less than 0.05. The results indicated that DLD and CD8 T cells were significantly negatively correlated ($R = -0.44$, $p = 5.6e\text{-}04$) (Figure 10C), DLD and CD4 naive T cells were significantly negatively correlated ($R = -0.39$, $p = 2.8e\text{-}0.3$) (Figure 10D), and DLD and M2 macrophages were significantly positively correlated ($R = 0.35$, $p = 7.9e\text{-}03$) (Figure 10G). There was no significant correlation between DLD and the remaining immune infiltrating cell population (p-value > 0.05) (Figures 10A, B, E, F). A significant positive correlation was also found between DLD and ASIA grades ($R = 0.37$, $p = 0.038$) (Figure 10H). We analyzed M2 macrophage levels in ASCI-high and ASCI-low patients to understand the role of immune cell abnormalities in ASCI disease progression. The results showed that the ASIA-high group had a significantly higher content of macrophage M2 (p-value < 0.05) (Supplementary Figure 2F). Moreover, M2 macrophage numbers and ASIA levels showed a significant positive correlation ($R = 0.12$, $p = 0.046$) (Supplementary Figure 2E). This suggests that peripheral blood macrophages M2 play an important role in the ASCI process.

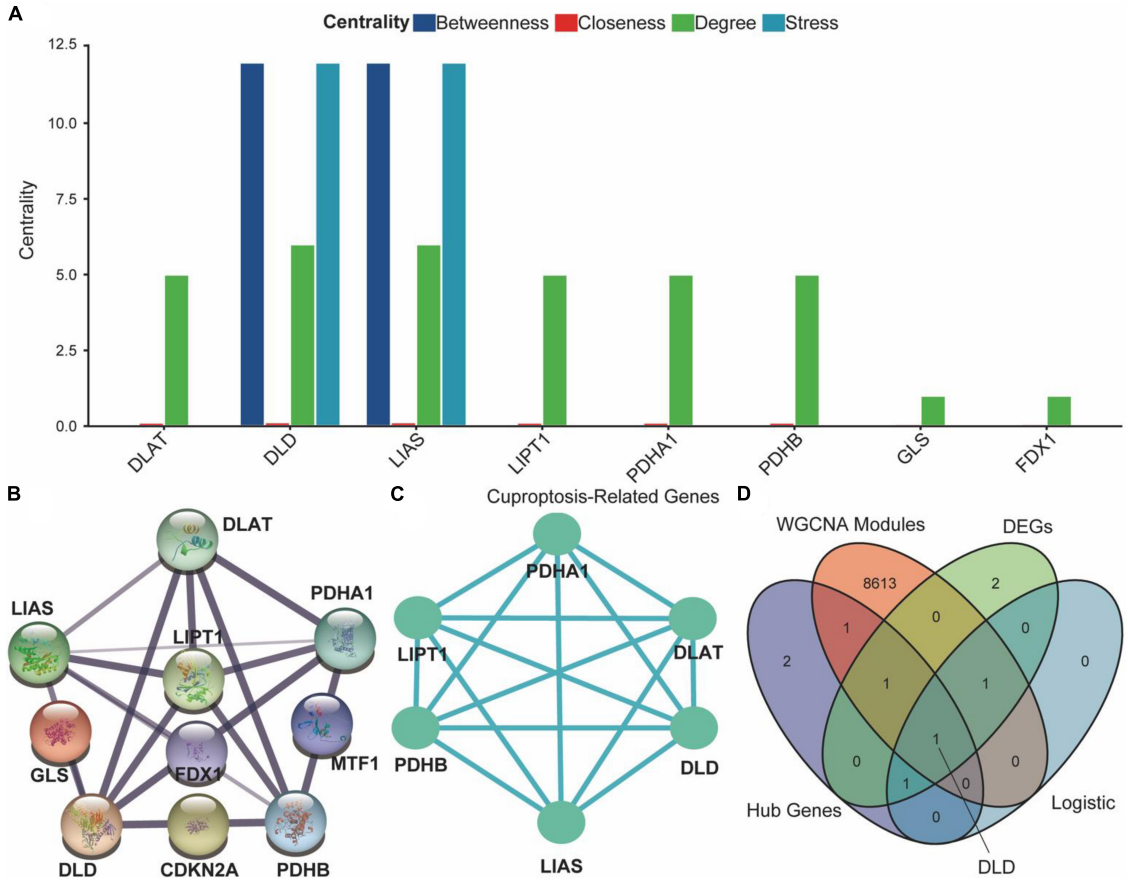

FIGURE 8
Protein–protein interaction (PPI) network of cuproptosis-related genes (CRGs). **(A)** Analysis of degree centrality, betweenness centrality, closeness centrality and stress centrality in PPI network. **(B)** PPI network of the CRGs; the width and colors of edges indicate the credibility of the evidence. **(C)** Network diagram of hub genes. **(D)** Venn diagram of hub genes, differential expression CRGs, acute spinal cord injury (ASCI)-related weighted gene co-expression network analysis (WGCNA) modules, and results of the multivariate logistic regression.

3.9. Construction and correlation analysis of relevant molecular subtypes of ASCI

We then constructed ASCI subtypes based on their molecular characteristics. Based on the cumulative distribution function (CDF), it was optimal to have two subtypes, named Cluster1 and Cluster2 (Figures 11A–C). To verify the effect of ASCI molecular typing, tSNE analysis was performed. The results indicated that Cluster1 and Cluster2 have excellent resolution (Figure 11D). Finally, we calculated the association between the ASCI key gene DLD and the two ASCI molecular subtypes, finding that both Cluster1 (R = 0.25, p = 0.005) and Cluster2 (R = 0.46, p = 4.1e-07) were significantly positively correlated with DLD (Figures 11E, F).

3.10. qRT-PCR and ELISA experiment confirmed the increase expression of DLD in white cells after ASCI

To verify the expression changes of DLD after ASCI, we extracted peripheral white blood cells from patients in the experimental group and control group. qRT-PCR and ELISA experiment indicated that DLD was significantly increased in mRNA and protein level in white blood cells after ASCI (Figures 12A, B). These results suggested that DLD might be related to immune infiltration in peripheral white blood cells after ASCI.

4. Discussion

An unintentional spinal cord injury is an extremely serious condition, with dire consequences for the patient's health and a significant financial burden (Wu et al., 2021). ASCI has been extensively studied, but no effective molecular targeted therapies have been validated. A new cell death pathway, cuproptosis, has recently gained increased attention (Tsvetkov et al., 2022). In the current study, we utilized human peripheral blood leukocyte data obtained from the GEO database to analyze the effects of CRGs on the ASCI immune microenvironment at a multi-omics level and their clinical significance. Using differential gene analysis, WGCNA, risk model construction, and PPI network centrality analysis, we identified potential ASCI peripheral blood diagnostic markers and the potential therapeutic target DLD. We integrated

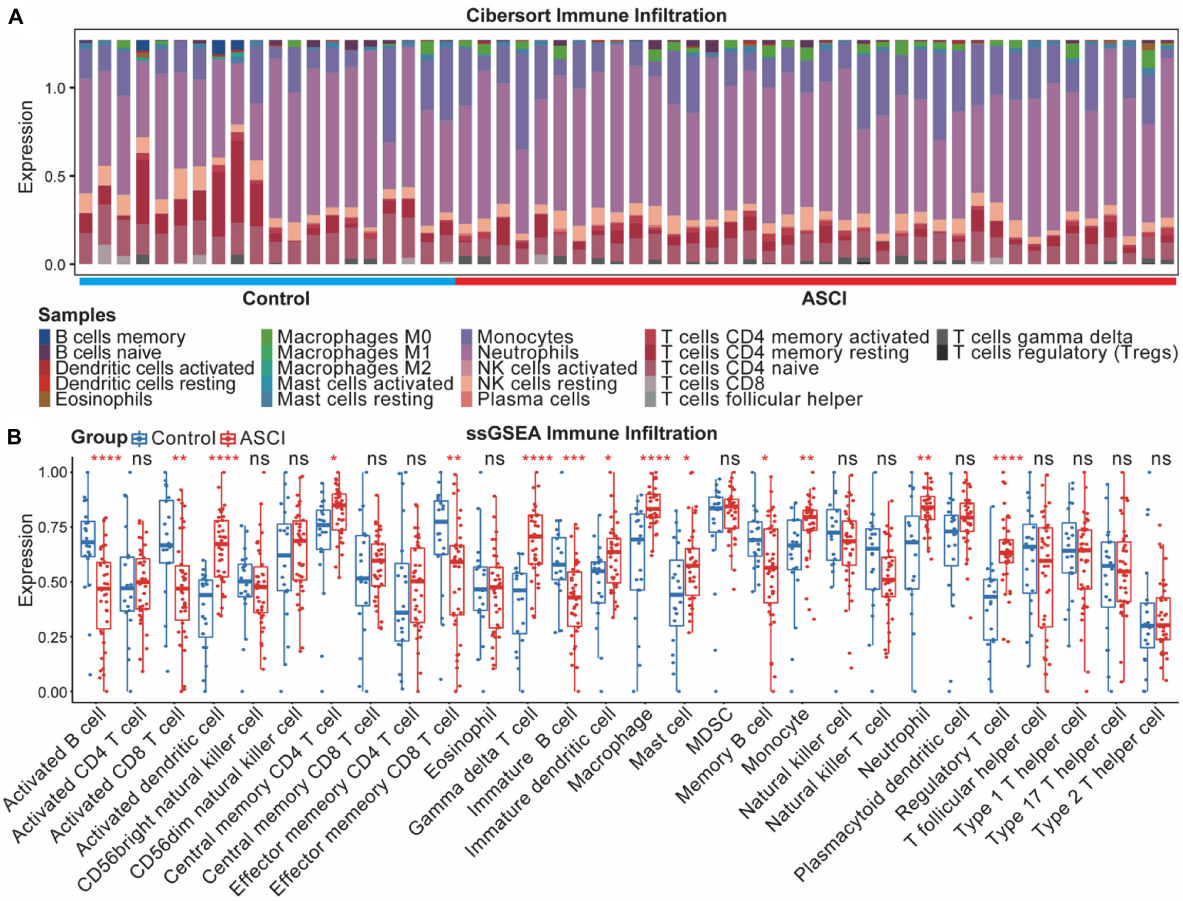

FIGURE 9
Acute spinal cord injury (ASCI) immune infiltration analysis. **(A)** Differential expression of infiltrating immune cells between ASCI and control groups determined using CIBERSORT immune infiltration analysis. **(B)** Differential expression of immune infiltrating cells in the ASCI and control groups based on single-sample gene set enrichment analysis (ssGSEA). ns indicates p-value = 0.05, * indicates p-value < 0.05, ** indicates p-value < 0.01, *** indicates p-value < 0.001, and **** indicates p-value < 0.0001.

these results with clinical information from ASCI patients to construct a predictive model for ASCI. Based on our findings, the enriched biological processes and pathways in ASCI are closely related to metabolic and oxidative processes. The immune infiltration results indicated that systemic immune function was suppressed following ASCI. We constructed two molecular subtypes of ASCI and elucidated the role of CRGs in both subtypes. In the ASCI subtypes Cluster1 and Cluster2, the cuproptosis process, positively regulated by DLD, affected the peripheral immune microenvironment and induced the polarization of M2 macrophages, further exacerbating systemic immunosuppression following ASCI and affected the prognosis.

Numerous studies have highlighted the importance of immune cells in ASCI. For example, a high-segment spinal cord injury can be treated by targeting the spleen in order to regain immune homeostasis (Noble et al., 2018). The function of natural killer (NK) cells is affected following SCI, and thus, NK cells are considered potential therapeutic targets for SCI (Laginha et al., 2016). Consequently, in this study, we selected human peripheral blood leukocyte sequencing data and used only one chip to eliminate batch effects. Initially, we normalized the GSE151371 microarray data to identify the chromosomal location of CRGs. Among the six CRGs identified by differential gene analysis, DLD and MTF1 were significantly upregulated in ASCI patients. Accordingly, DLD and MTF1 are likely key genes involved in cuproptosis affecting ASCI. Next, to investigate whether dynamic regulation of the cuproptosis process occurs after ASCI, we analyzed the interaction between positive and negative cuproptosis regulators, and the results indicated that DLD was significantly negatively correlated with CDKN2A. However, univariate logistic regression indicated no correlation between CDKN2A and ASCI; thus, DLD may represent an independent risk factor for ASCI. Due to its role as a multifunctional oxidoreductase, DLD is involved in various processes, such as DNA binding, apoptosis mediation, and reactive oxygen species generation (Fernandez and Bolanos, 2016; Ambrus and dam-Vizi, 2018; Lin et al., 2019). It has been reported that inhibition of DLD counteracts oxidative stress in type 2 diabetes (Yang et al., 2019). Furthermore, another study showed that DLD inhibition reduces ischemic stroke damage through reduced oxidative stress, reduced cell death, increased Nrf2 signaling, and increased NQO1 activity (Wu et al., 2017a). Our results reveal similar evidence for the important role played by DLD in the metabolic and oxidative processes of ASCI.

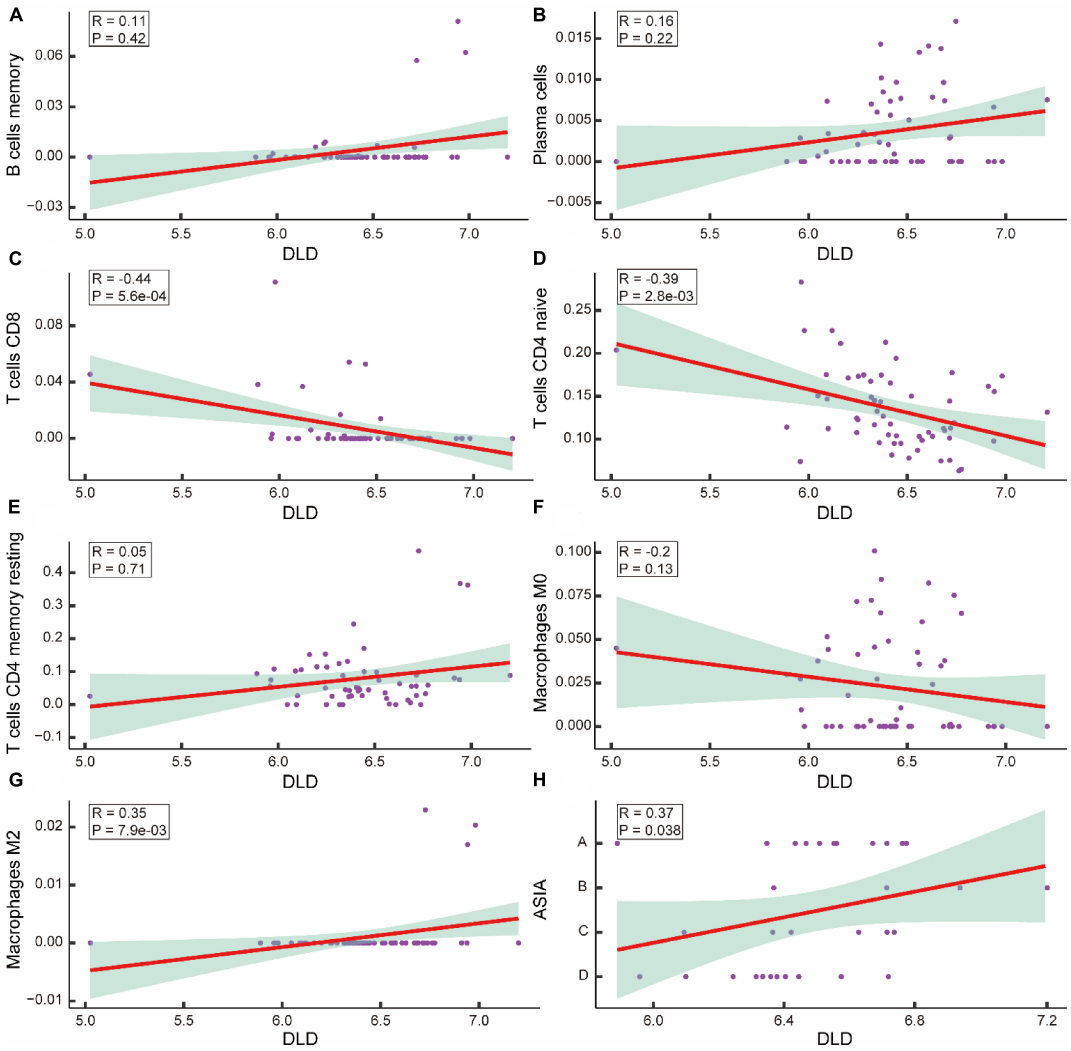

FIGURE 10
Correlation analysis of acute spinal cord injury (ASCI) key genes and immune infiltrating cells. **(A–G)** Scatter plot of the correlation between DLD and immune infiltrating cells, including B cells memory, Plasma cells, T cells CD8, T cells CD4 naive, T cells CD4 memory resting, macrophage M0, and macrophage M2; R represents correlation coefficient, and *P* represents *p*-value. **(H)** Scatter plot of the correlation between DLD and ASIA levels; R represents correlation coefficient, and *P* represents *p*-value.

Using the PPI network identified in this study, we discovered genes that play an important role in ASCI, specifically DLD and LIAS. Both univariate and multivariate logistic regressions analyses indicated that DLD, LIAS, and GLS were independent risk factors for ASCI. Based on the logistic regression results, we constructed a clinical prediction nomogram model. Using DLD, LIAS, and GLS expression levels, the model can accurately diagnose ASCI. A scale-free network using WGCNA was constructed to ensure the study was as comprehensive and stable as possible. Eight gene modules associated with ASCI were identified using this network. Next, we identified potential ASCI biomarkers from four aspects, including: linear relationships (logistic regression), scale-free networks (WGCNA), protein interaction relationships (PPI networks), and differential genes. Across all four latitudes, DLD showed significant importance. Therefore, DLD was confirmed to play an important role as an independent risk factor in the development of ASCI. After combining the clinical data of ASCI patients with the expression levels of DLD, we built a back-propagation neural network model that can be used to predict the neurological function of ASCI patients and assist with diagnosis and treatment. Using a custom penalty function, we optimized the fit of a neural network for a small training set, which not only achieved a higher recall rate, but also prevented under- or over-fitting. The clinical application value of DLD as a biomarker in the diagnosis and treatment of ASCI was further elucidated by the neural network clinical prediction model. In the enrichment analysis, the metabolism-related pathways such as pyruvate metabolism and citrate cycle (TCA cycle) were significantly enriched, suggesting that DLD played a critical role in the metabolic process of various diseases (Landgraf et al., 2017; Wu et al., 2017b; Purroy et al., 2020). After ASCI, metabolic and oxidative processes were active, as indicated by the results of the GO and GSVA analyses. Metabolism plays a significant role in ASCI, as dysregulated metabolic pathways are involved in pathological

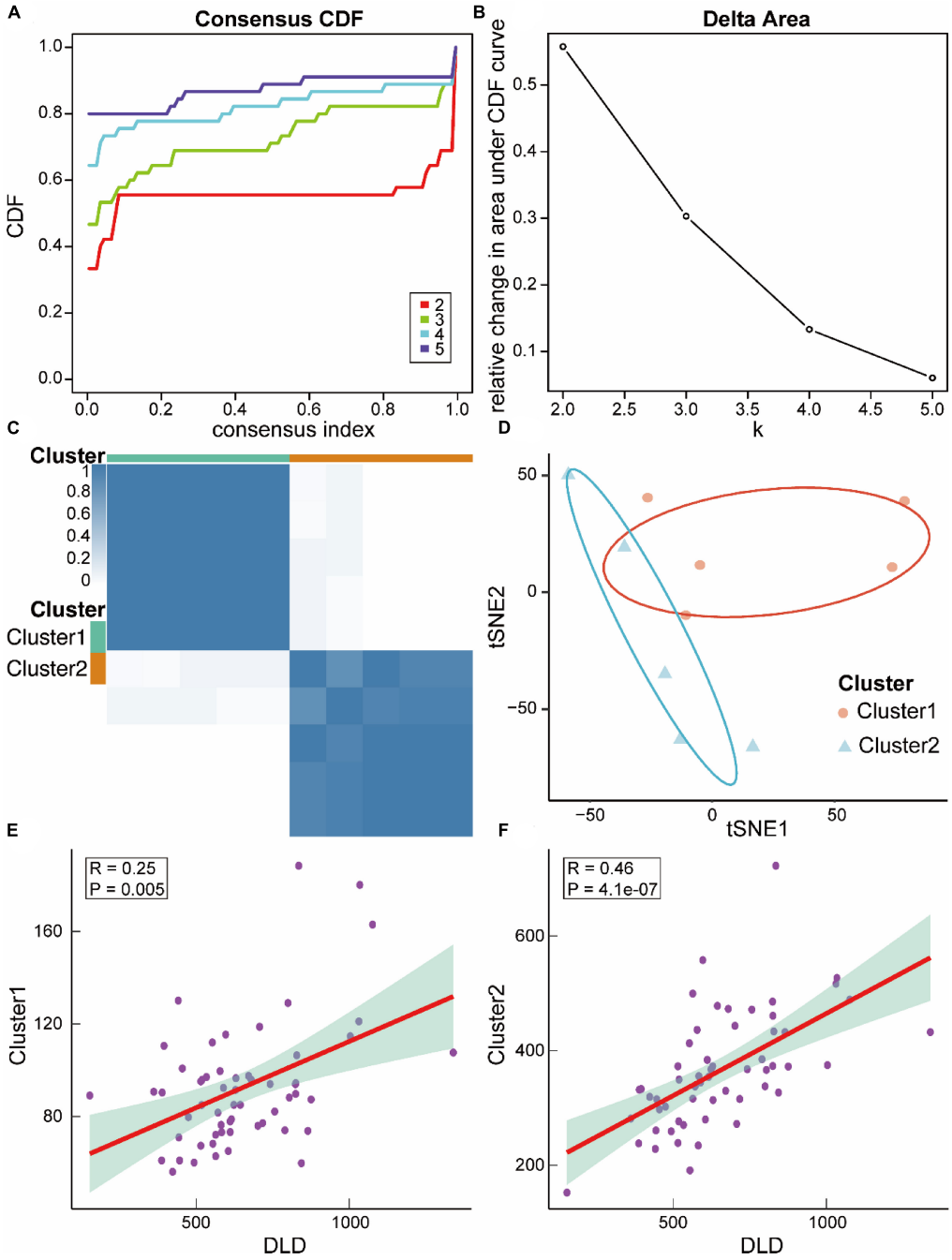

FIGURE 11
Relevant molecular subtypes and correlations of acute spinal cord injury (ASCI). **(A)** Cumulative distribution function (CDF) curve of consensus clustering of ASCI-related molecules; the abscissa represents the consensus index, and the ordinate represents the CDF index. **(B)** Relative change in the area under the CDF curve; the results show that it is divided into two types, and the change in trend is the most stable. **(C)** Cluster heat map of ASCI-associated molecular subtypes. **(D)** T-distributed Stochastic Neighbor Embedding (tSNE) analysis plot of ASCI-related molecular subtypes. **(E)** Scatter plot of the correlation between DLD and ASCI-related molecular subtype Cluster1; R represents correlation coefficient, and P represents *p*-value. **(F)** Scatter plot of the correlation between DLD and ASCI-related molecular subtype Cluster2; R represents correlation coefficient, and P represents *p*-value.

processes leading to tissue damage and functional impairment (Lepoutre et al., 2017; Neural Regen Res, 2021). Targeting metabolic pathways is a promising strategy for ASCI treatment, improving neuronal survival, promoting axonal regeneration, and reducing pathological processes (Meesters et al., 2017; Meier et al., 2017). Enriched metabolic pathways in ASCI include the TCA cycle, glycolysis, and ketone body metabolism. Their dysregulation leads to oxidative stress, cell death, and tissue damage, suggesting therapeutic potential for metabolic interventions (Lepoutre et al., 2017; Meier et al., 2017). Metabolic reprogramming may serve as a hallmark of ASCI progression and a potential target for therapy (Meier et al., 2017). Targeting metabolic pathways may offer new

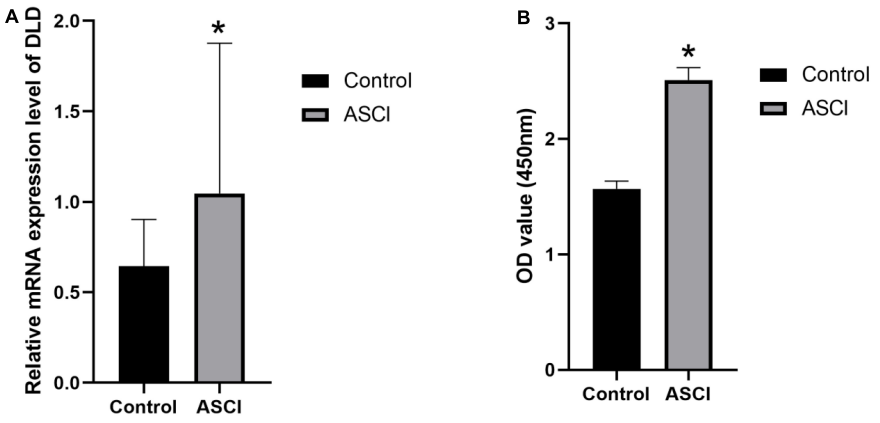

FIGURE 12
DLD expression in white cells from peripheral blood. **(A)** The mRNA (DLD) expression significantly increased in ASCI group in qRT-PCR experiment. **(B)** ELISA experiment detected a significant increase in DLD expression of ASCI group. (*$p < 0.05$).

avenues for treating ASCI. Further research is needed to elucidate the underlying mechanisms and potential therapeutic benefits of metabolic interventions.

Compared to the control group, the proportions of mature B cells and mature CD8 T cells in the ASCI group decreased, indicating suppressed peripheral immune function. On the other hand, M2 macrophage levels were elevated in ASCI patients, indicating altered polarization tendencies among peripheral macrophages. Macrophage polarization is unstable and may be affected by various factors (Boutilier and Elsawa, 2021). The cuproptosis-related gene DLD has been implicated in immunity by several studies. Pseudomonas aeruginosa virulence may be influenced by DLD, which is a complement-regulatory protein-binding protein (Hallstrom et al., 2015). Another study indicated that DLD was an autoantibody target in patients with endometrial cancer (Yoneyama et al., 2014). Consequently, we propose a hypothesis that DLD following ASCI facilitates copper binding to lipidated components of the TCA cycle in peripheral blood, promoting copper-induced cell death. As a result, the immune microenvironment is disrupted, and macrophage polarization is altered, exacerbating SCI-IDS and ultimately worsening ASCI. Further analysis revealed that M2 macrophage was highly expressed in ASCI-high patients, adversely affecting their prognosis. ASIA grading and M2 macrophage levels were significantly positively correlated with DLD expression levels in ASCI patients. Consequently, high levels of DLD after ASCI likely contribute to macrophage polarization and a poor prognosis for ASCI patients. Several studies have demonstrated that M2 macrophage secretes suppressive cytokines to downregulate the immune response, a process that further exacerbates SCI-IDS (Ivashkiv, 2013; Murray et al., 2014). Thus, we can conclude that our hypothesis is correct. In addition, we found that DLD has potential as a therapeutic target for ASCI. A previous study identified three clinical phenotypes with different risks of death among hyperchloremia patients, allowing for precise treatment based on the patient's clinical characteristics (Thongprayoon et al., 2021a). Thongprayoon et al. (2021b) divided hospitalized patients with acute kidney injury into four groups with different mortality risks, based on which adjuvant therapies were available (Thongprayoon et al., 2021b). To determine the applicability of DLD as a potential therapeutic target for ASCI, we identified two molecular subtypes associated with cuproptosis in ASCI patients and calculated the correlation between DLD expression levels and the two ASCI subtypes (Cluster1 and Cluster2). We found that DLD was significantly positively correlated with both ASCI subtypes Cluster1 and Cluster2, indicating that DLD may be a therapeutic target for ASCI in general.

Our study has multiple strengths. This is the first study to describe the effects of CRGs on the immune microenvironment of ASCI patients. Research on the immune microenvironment and cell death is an important component of SCI research, and programmed cell death is considered a key process in post-SCI recovery (Chavan et al., 2017; Prüss et al., 2017; Shi et al., 2021). Cuproptosis is a novel type of mitochondrial respiration-dependent metal ion cell death that differs from ferroptosis (Tsvetkov et al., 2022). It may be possible to develop new treatments for spinal cord injury due to this unusual mechanism. Furthermore, in contrast to most diagnostic models that focus primarily on ASCI disease states, our work also considers neurological function. The majority of current clinical prediction models use linear architecture but do not take the interference of multicollinearity into consideration. We used the variance inflation factor to eliminate the problem of multicollinearity in logistic regressions. Additionally, we used a more flexible neural network model to predict neurological function in ASCI patients, which not only had a high recall rate and a high goodness of fit but also could be continually evolved.

However, our study also has some limitations. First, this research relies heavily on bioinformatics analysis, and it needs more validation through both animal experiments and clinical trials. Second, in the case of human peripheral blood leukocyte gene chips, the volume of collected tissue samples is relatively small. Third, the generalizability of the clinical diagnostic model lacks external validation from patients at other medical centers. Although the clinical prediction model constructed in this study showed reasonable robustness (AUC of 0.757 for the validation set ROC curve), the detection ability of the deep learning model must be improved through the integration of a large amount

of data. Finally, due to the heterogeneity of ASCI, not all ASCI patients exhibit significant peripheral immunosuppression, and further subgroup analyses should consider additional immune profiles of ASCI patients.

5. Conclusion

In conclusion, our study highlights DLD's potential as a biomarker and therapeutic target for ASCI, and its association with M2 macrophage levels affecting patient prognosis. We developed a clinical prediction model and a neural network model for better diagnosis and treatment. Despite limitations, our findings emphasize the significance of metabolic pathways and the immune microenvironment in ASCI, encouraging further research on this topic.

Data availability statement

The original contributions presented in this study are included in the article/**Supplementary material**, further inquiries can be directed to the corresponding author.

Author contributions

CL, CW, and JC helped in the conception and design, data acquisition, analysis and interpretation, and critical revision of the article and final approval. GX, JC, JZ, HH, and YL helped in the data acquisition and final approval. ZC helped in the data acquisition, analysis, and drafting and critical revision of the article and obtained final approval. All authors have approved the submitted version of the manuscript.

Funding

This study was supported by National Natural Science Foundation of China (grant numbers: 81771319 and 82002394), Nantong Health Commission Research Project (grant number: MA2021016), and Medical Research Project of Jiangsu Commission of Health (grant number: ZDB2020004).

Acknowledgments

We would like to thank Editage (www.editage.cn) for English language editing.

Conflict of interest

The authors declare that the research was conducted in the absence of any commercial or financial relationships that could be construed as a potential conflict of interest.

Publisher's note

All claims expressed in this article are solely those of the authors and do not necessarily represent those of their affiliated organizations, or those of the publisher, the editors and the reviewers. Any product that may be evaluated in this article, or claim that may be made by its manufacturer, is not guaranteed or endorsed by the publisher.

Supplementary material

The Supplementary Material for this article can be found online at: https://www.frontiersin.org/articles/10.3389/fncel.2023.1132015/full#supplementary-material

References

Aggarwal, A., and Bhatt, M. (2018). Advances in treatment of Wilson disease. *Tremor. Other Hyperkinet. Mov. (N. Y.).* 8:525.

Ahmad, W. (2018). Dihydrolipoamide dehydrogenase suppression induces human tau phosphorylation by increasing whole body glucose levels in a C. elegans model of Alzheimer's Disease. *Exp. Brain Res.* 236, 2857–2866. doi: 10.1007/s00221-018-5341-0

Ahuja, C. S., Martin, A. R., and Fehlings, M. (2016). Recent advances in managing a spinal cord injury secondary to trauma. *F1000Res* 5, F1000 Faculty Rev-1017.

Ambrus, A., and dam-Vizi, V. A. (2018). Human dihydrolipoamide dehydrogenase (E3) deficiency: novel insights into the structural basis and molecular pathomechanism. *Neurochem. Int.* 117, 5–14. doi: 10.1016/j.neuint.2017.05.018

Badhiwala, J. H., Ahuja, C. S., and Fehlings, M. G. (2018). Time is spine: a review of translational advances in spinal cord injury. *J. Neurosurg. Spine* 30, 1–18.

Badhiwala, J. H., Ahuja, C. S., and Fehlings, M. G. (2019). Time is spine: a review of translational advances in spinal cord injury. *J. Neurosurg. Spine* 30, 1–18.

Bonizzato, M., Pidpruzhnykova, G., DiGiovanna, J., Shkorbatova, P., Pavlova, N., Micera, S., et al. (2018). Brain-controlled modulation of spinal circuits improves recovery from spinal cord injury. *Nat. Commun.* 9:3015. doi: 10.1038/s41467-018-05282-6

Boutilier, A. J., and Elsawa, S. F. (2021). Macrophage polarization states in the tumor microenvironment. *Int. J. Mol. Sci.* 22:6995.

Bradbury, E. J., and Burnside, E. R. (2019). Moving beyond the glial scar for spinal cord repair. *Nat. Commun.* 10:3879.

Brommer, B., Engel, O., Kopp, M. A., Watzlawick, R., Muller, S., Pruss, H., et al. (2016). Spinal cord injury-induced immune deficiency syndrome enhances infection susceptibility dependent on lesion level. *Brain* 139, 692–707. doi: 10.1093/brain/aww375

Burns, A. S., Marino, R. J., Kalsi-Ryan, S., Middleton, J. W., Tetreault, L. A., Dettori, J. R., et al. (2017). Type and timing of rehabilitation following acute and subacute spinal cord injury: a systematic review. *Glob. Spine J.* 7, 175S–194S. doi: 10.1177/2192568217703084

Byra, S. (2016). Posttraumatic growth in people with traumatic long-term spinal cord injury: predictive role of basic hope and coping. *Spinal. Cord* 54, 478–482. doi: 10.1038/sc.2015.177

Carpenter, R. S., Marbourg, J. M., Brennan, F. H., Mifflin, K. A., Hall, J. C. E., Jiang, R. R., et al. (2020). Spinal cord injury causes chronic bone marrow failure. *Nat. Commun.* 11:3702.

Casper, D. S., Zmistowski, B., Schroeder, G. D., McKenzie, J. C., Mangan, J., Vatson, J., et al. (2018). Preinjury patient characteristics and postinjury neurological status are associated with mortality following spinal cord injury. *Spine* 43, 895–899. doi: 10.1097/BRS.0000000000002533

Chavan, S. S., Pavlov, V. A., and Tracey, K. J. (2017). Mechanisms and therapeutic relevance of neuro-immune communication. *Immunity* 46, 927–942.

Che, M., Wang, R., Li, X., Wang, H. Y., and Zheng, X. F. S. (2016). Expanding roles of superoxide dismutases in cell regulation and cancer. *Drug Discov. Today* 21, 143–149.

Cofano, F., Boido, M., Monticelli, M., Zenga, F., Ducati, A., Vercelli, A., et al. (2019). Mesenchymal stem cells for spinal cord injury: current options, limitations, and future of cell therapy. *Int. J. Mol. Sci.* 20, 2698. doi: 10.3390/ijms20112698

Dayan, A., Fleminger, G., and Ashur-Fabian, O. (2019). Targeting the Achilles' heel of cancer cells via integrin-mediated delivery of ROS-generating dihydrolipoamide dehydrogenase. *Oncogene* 38, 5050–5061. doi: 10.1038/s41388-019-0775-9

Devivo, M. J. (2012). Epidemiology of traumatic spinal cord injury: trends and future implications. *Spinal Cord* 50, 365–372.

Fan, J., Shan, C., Kang, H. B., Elf, S., Xie, J., Tucker, M., et al. (2014). Tyr phosphorylation of PDP1 toggles recruitment between ACAT1 and SIRT3 to regulate the pyruvate dehydrogenase complex. *Mol. Cell* 53, 534–548. doi: 10.1016/j.molcel.2013.12.026

Fehlings, M. G., and Nguyen, D. H. (2010). Immunoglobulin G: a potential treatment to attenuate neuroinflammation following spinal cord injury. *J. Clin. Immunol.* 30(Suppl. 1), S109–S112.

Fehlings, M. G., Vaccaro, A., Wilson, J. R., Singh, A., W Cadotte, D., Harrop, J. S., et al. (2012). Early versus delayed decompression for traumatic cervical spinal cord injury: results of the Surgical Timing in Acute Spinal Cord Injury Study (STASCIS). *PLoS One* 7:e32037. doi: 10.1371/journal.pone.0032037

Feng, Z., Min, L., Chen, H., Deng, W., Tan, M., Liu, H., et al. (2021). Iron overload in the motor cortex induces neuronal ferroptosis following spinal cord injury. *Redox Biol.* 43:101984. doi: 10.1016/j.redox.2021.101984

Fernandez, E., and Bolanos, J. P. (2016). alpha-Ketoglutarate dehydrogenase complex moonlighting: ROS signalling added to the list: an editorial highlight for 'Reductions in the mitochondrial enzyme alpha-ketoglutarate dehydrogenase complex in neurodegenerative disease – beneficial or detrimental?'. *J. Neurochem.* 139, 689–690.

Ge, E. J., Bush, A. I., Casini, A., Cobine, P. A., Cross, J. R., DeNicola, G. M., et al. (2022). Connecting copper and cancer: from transition metal signalling to metalloplasia. *Nat. Rev. Cancer* 22, 102–113. doi: 10.1038/s41568-021-00417-2

Ge, M. H., Tian, H., Mao, L., Li, D. Y., Lin, J. Q., Hu, H. S., et al. (2021). Zinc attenuates ferroptosis and promotes functional recovery in contusion spinal cord injury by activating Nrf2/GPX4 defense pathway. *CNS Neurosci. Ther.* 27, 1023–1040. doi: 10.1111/cns.13657

Glennie, R. A., Bailey, C. S., Tsai, E. C., Noonan, V. K., Rivers, C. S., Fourney, D. R., et al. (2017). An analysis of ideal and actual time to surgery after traumatic spinal cord injury in Canada. *Spinal Cord* 55, 618–623. doi: 10.1038/sc.2016.177

Guengerich, F. P. (2018). Introduction to Metals in Biology 2018: copper homeostasis and utilization in redox enzymes. *J. Biol. Chem.* 293, 4603–4605. doi: 10.1074/jbc.TM118.002255

Hallstrom, T., Uhde, M., Singh, B., Skerka, C., Riesbeck, K., and Zipfel, P. F. (2015). *Pseudomonas aeruginosa* uses dihydrolipoamide dehydrogenase (Lpd) to bind to the human terminal pathway regulators vitronectin and clusterin to inhibit terminal pathway complement attack. *PLoS One* 10:e0137630. doi: 10.1371/journal.pone.0137630

Hanzelmann, S., Castelo, R., and Guinney, J. (2013). GSVA: gene set variation analysis for microarray and RNA-seq data. *BMC Bioinformatics* 14:7. doi: 10.1186/1471-2105-14-7

Huang, R., Meng, T., Zhu, R., Zhao, L., Song, D., Yin, H., et al. (2020). The integrated transcriptome bioinformatics analysis identifies key genes and cellular components for spinal cord injury-related neuropathic pain. *Front. Bioeng. Biotechnol.* 8:101. doi: 10.3389/fbioe.2020.00101

Inesi, G. (2017). Molecular features of copper binding proteins involved in copper homeostasis. *IUBMB Life* 69, 211–217.

Ito, K., and Murphy, D. (2013). Application of ggplot2 to pharmacometric graphics. *CPT Pharm. Syst. Pharmacol.* 2:e79. doi: 10.1038/psp.2013.56

Ivashkiv, L. B. (2013). Epigenetic regulation of macrophage polarization and function. *Trends Immunol.* 34, 216–223.

J Spinal Cord Med, (2016). Spinal Cord Injury (SCI) 2016 facts and figures at a glance. *J. Spinal Cord Med.* 39, 493–494. doi: 10.1080/10790268.2016.1210925

Kapadia, N., Masani, K., Catharine Craven, B., Giangregorio, L. M., Hitzig, S. L., Richards, K., et al. (2014). A randomized trial of functional electrical stimulation for walking in incomplete spinal cord injury: effects on walking competency. *J. Spinal Cord Med.* 37, 511–524. doi: 10.1179/2045772314Y.0000000263

Khan, I. U., Yoon, Y., Kim, A., Jo, K. R., Choi, K. U., Jung, T., et al. (2018). Improved healing after the Co-transplantation of HO-1 and BDNF overexpressed mesenchymal stem cells in the subacute spinal cord injury of dogs. *Cell Transplant.* 27, 1140–1153. doi: 10.1177/0963689718779766

Kim, Y.-H., Ha, K.-Y., and Kim, S.-I. (2017). Spinal cord injury and related clinical trials. *Clin. Orthoped. Surg.* 9, 1–9.

Kjell, J., Finn, A., Hao, J., Wellfelt, K., Josephson, A., Svensson, C. I., et al. (2015). Delayed imatinib treatment for acute spinal cord injury: functional recovery and serum biomarkers. *J. Neurotrauma* 32, 1645–1657. doi: 10.1089/neu.2014.3863

Kriz, J., Sediva, K., and Maly, M. (2021). Causes of death after spinal cord injury in the Czech Republic. *Spinal Cord* 59, 814–820. doi: 10.1038/s41393-020-00593-2

Kyritsis, N., Torres-Espín, A., Schupp, P. G., Huie, J. R., Chou, A., Duong-Fernandez, X., et al. (2021). Diagnostic blood RNA profiles for human acute spinal cord injury. *J. Exp. Med.* 218:e20201795.

Laginha, I., Kopp, M. A., Druschel, C., Schaser, K.-D., Brommer, B., Hellmann, R. C., et al. (2016). Natural Killer (NK) cell functionality after human Spinal Cord Injury (SCI): protocol of a prospective, longitudinal study. *BMC Neurol.* 16:170. doi: 10.1186/s12883-016-0681-5

Lai, J., He, X., Wang, F., Tan, J. M., Wang, J. X., Xing, S. M., et al. (2013). Gene expression signature analysis and protein-protein interaction network construction of spinal cord injury. *Eur. Rev. Med. Pharmacol. Sci.* 17, 2941–2948.

Landgraf, T. N., Costa, M. V., Oliveira, A. F., Ribeiro, W. C., Panunto-Castelo, A., and Fernandes, F. F. (2017). Involvement of dihydrolipoyl dehydrogenase in the phagocytosis and killing of *Paracoccidioides brasiliensis* by macrophages. *Front. Microbiol.* 8:1803. doi: 10.3389/fmicb.2017.01803

Langfelder, P., and Horvath, S. (2008). WGCNA: an R package for weighted correlation network analysis. *BMC Bioinformatics* 9:559. doi: 10.1186/1471-2105-9-559

Lee, D. Y., Park, Y. J., Song, S. Y., Hwang, S. C., Kim, K. T., and Kim, D. H. (2018). The importance of early surgical decompression for acute traumatic spinal cord injury. *Clin. Orthop. Surg.* 10, 448–454.

Lepoutre, T., Madeira, M. L., and Guerin, N. (2017). The Lacanian concept of paranoia: an historical perspective. *Front. Psychol.* 8:1564. doi: 10.3389/fpsyg.2017.01564

Liberzon, A., Birger, C., Thorvaldsdóttir, H., Ghandi, M., Mesirov, J. P., and Tamayo, P. (2015). The molecular signatures database hallmark gene set collection. *Cell Syst.* 1, 417–425.

Lin, K. H., Xie, A., Rutter, J. C., Ahn, Y. R., Lloyd-Cowden, J. M., Nichols, A. G., et al. (2019). Systematic dissection of the metabolic-apoptotic interface in AML reveals heme biosynthesis to be a regulator of drug sensitivity. *Cell Metab.* 29, 1217–1231.e7. doi: 10.1016/j.cmet.2019.01.011

Liu, M., Wu, W., Li, H., Li, S., Huang, L. T., Yang, Y. Q., et al. (2015). Necroptosis, a novel type of programmed cell death, contributes to early neural cells damage after spinal cord injury in adult mice. *J. Spinal Cord Med.* 38, 745–753. doi: 10.1179/2045772314Y.0000000224

Liu, Z., Yang, Y., He, L., Pang, M., Luo, C., Liu, B., et al. (2019). High-dose methylprednisolone for acute traumatic spinal cord injury: a meta-analysis. *Neurology* 93, e841–e850.

Meesters, C., Muris, P., Dibbets, P., Cima, M., and Lemmens, L. (2017). On the link between perceived parental rearing behaviors and self-conscious emotions in adolescents. *J. Child Fam. Stud.* 26, 1536–1545. doi: 10.1007/s10826-017-0695-7

Meier, A. K., Worch, S., Boer, E., Hartmann, A., Mascher, M., Marzec, M., et al. (2017). Agdc1p – a gallic acid decarboxylase involved in the degradation of tannic acid in the yeast Blastobotrys (Arxula) adeninivorans. *Front. Microbiol.* 8:1777. doi: 10.3389/fmicb.2017.01777

Miao, Y. R., Zhang, Q., Lei, Q., Luo, M., Xie, G. Y., Wang, H., et al. (2020). ImmuCellAI: a unique method for comprehensive T-cell subsets abundance prediction and its application in cancer immunotherapy. *Adv. Sci. (Weinh)* 7:1902880. doi: 10.1002/advs.201902880

Milich, L. M., Ryan, C. B., and Lee, J. K. (2019). The origin, fate, and contribution of macrophages to spinal cord injury pathology. *Acta Neuropathol.* 137, 785–797.

Murray, P., Allen, J., Biswas, S., Fisher, E., Gilroy, D., Goerdt, S., et al. (2014). Macrophage activation and polarization: nomenclature and experimental guidelines. *Immunity* 41, 14–20. doi: 10.1016/j.immuni.2014.06.008

Neural Regen Res (2021). Retraction: brain-derived neurotrophic factor expression in dorsal root ganglion neurons in response to reanastomosis of the distal stoma after nerve grafting. *Neural. Regen. Res.* 16:1927.

Newman, A. M., Steen, C. B., Liu, C. L., Gentles, A. J., Chaudhuri, A. A., Scherer, F., et al. (2019). Determining cell type abundance and expression from bulk tissues with digital cytometry. *Nat. Biotechnol.* 37, 773–782.

Noble, B. T., Brennan, F. H., and Popovich, P. G. (2018). The spleen as a neuroimmune interface after spinal cord injury. *J. Neuroimmunol.* 321, 1–11. doi: 10.1016/j.jneuroim.2018.05.007

Phipson, B., Lee, S., Majewski, I. J., Alexander, W. S., and Smyth, G. K. (2016). Robust hyperparameter estimation protects against hypervariable genes and improves

power to detect differential expression. *Ann. Appl. Stat.* 10, 946–963. doi: 10.1214/16-AOAS920

Prüss, H., Tedeschi, A., Thiriot, A., Lynch, L., Loughhead, S. M., Stutte, S., et al. (2017). Spinal cord injury-induced immunodeficiency is mediated by a sympathetic-neuroendocrine adrenal reflex. *Nat. Neurosci.* 20, 1549–1559. doi: 10.1038/nn.4643

Purroy, R., Medina-Carbonero, M., Ros, J., and Tamarit, J. (2020). Frataxin-deficient cardiomyocytes present an altered thiol-redox state which targets actin and pyruvate dehydrogenase. *Redox Biol.* 32:101520. doi: 10.1016/j.redox.2020.101520

Salsabili, N., Mehrsai, A. R., and Jalaie, S. (2009). Concentration of blood and seminal plasma elements and their relationships with semen parameters in men with spinal cord injury. *Andrologia* 41, 24–28. doi: 10.1111/j.1439-0272.2008.00885.x

Savic, G., DeVivo, M. J., Frankel, H. L., Jamous, M. A., Soni, B. M., and Charlifue, S. (2017). Causes of death after traumatic spinal cord injury—a 70-year British study. *Spinal Cord* 55, 891–897. doi: 10.1038/sc.2017.64

Shannon, P., Markiel, A., Ozier, O., Baliga, N. S., Wang, J. T., Ramage, D., et al. (2003). Cytoscape: a software environment for integrated models of biomolecular interaction networks. *Genome Res.* 13, 2498–2504. doi: 10.1101/gr.1239303

Shi, Z., Yuan, S., Shi, L., Li, J., Ning, G., Kong, X., et al. (2021). Programmed cell death in spinal cord injury pathogenesis and therapy. *Cell Prolif.* 54:e12992.

Shin, D., Lee, J., You, J. H., Kim, D., and Roh, J. L. (2020). Dihydrolipoamide dehydrogenase regulates cystine deprivation-induced ferroptosis in head and neck cancer. *Redox Biol.* 30:101418. doi: 10.1016/j.redox.2019.101418

Singh, P. L., Agarwal, N., Barrese, J. C., and Heary, R. F. (2012). Current therapeutic strategies for inflammation following traumatic spinal cord injury. *Neural Regen. Res.* 7, 1812–1821.

Sturm, G., Finotello, F., Petitprez, F., Zhang, J. D., Baumbach, J., Fridman, W. H., et al. (2019). Comprehensive evaluation of transcriptome-based cell-type quantification methods for immuno-oncology. *Bioinformatics* 35, i436–i445. doi: 10.1093/bioinformatics/btz363

Subramanian, A., Tamayo, P., Mootha, V. K., Mukherjee, S., Ebert, B. L., Gillette, M. A., et al. (2005). Gene set enrichment analysis: a knowledge-based approach for interpreting genome-wide expression profiles. *Proc. Natl. Acad. Sci. U.S.A.* 102, 15545–15550.

Thongprayoon, C., Nissaisorakarn, V., Pattharanitima, P., Mao, M. A., Kattah, A. G., Keddis, M. T., et al. (2021a). Subtyping hyperchloremia among hospitalized patients by machine learning consensus clustering. *Medicina (Kaunas)* 57:903. doi: 10.3390/medicina57090903

Thongprayoon, C., Vaitla, P., Nissaisorakarn, V., Mao, M. A., Genovez, J. L. Z., Kattah, A. G., et al. (2021b). Clinically distinct subtypes of acute kidney injury on hospital admission identified by machine learning consensus clustering. *Med. Sci. (Basel)* 9:60.

Timon-Gomez, A., Nyvltova, E., Abriata, L. A., Vila, A. J., Hosler, J., and Barrientos, A. (2018). Mitochondrial cytochrome c oxidase biogenesis: recent developments. *Semin. Cell Dev. Biol.* 76, 163–178.

Tong, D., Zhao, Y., Tang, Y., Ma, J., Wang, M., Li, B., et al. (2022). MiR-487b suppressed inflammation and neuronal apoptosis in spinal cord injury by targeted Ifitm3. *Metab. Brain Dis.* 37, 2405–2415. doi: 10.1007/s11011-022-01015-3

Tsvetkov, P., Coy, S., Petrova, B., Dreishpoon, M., Verma, A., Abdusamad, M., et al. (2022). Copper induces cell death by targeting lipoylated TCA cycle proteins. *Science* 375, 1254–1261.

Van Gassen, S., Callebaut, B., Van Helden, M. J., Lambrecht, B. N., Demeester, P., Dhaene, T., et al. (2015). FlowSOM: using self-organizing maps for visualization and interpretation of cytometry data. *Cytometry A* 87, 636–645.

Wang, Y., Wang, H., Tao, Y., Zhang, S., Wang, J., and Feng, X. (2014). Necroptosis inhibitor necrostatin-1 promotes cell protection and physiological function in traumatic spinal cord injury. *Neuroscience* 266, 91–101. doi: 10.1016/j.neuroscience.2014.02.007

Wilkerson, M. D., and Hayes, D. N. (2010). ConsensusClusterPlus: a class discovery tool with confidence assessments and item tracking. *Bioinformatics* 26, 1572–1573. doi: 10.1093/bioinformatics/btq170

Wilson, J. R., Forgione, N., and Fehlings, M. G. (2013). Emerging therapies for acute traumatic spinal cord injury. *Can. Med. Assoc. J.* 185, 485–492.

Wu, C., Xu, G., Bao, G., Gao, H., Chen, J., Zhang, J., et al. (2022). Ubiquitin ligase triad1 promotes neurite outgrowth by inhibiting MDM2-mediated ubiquitination of the neuroprotective factor pleiotrophin. *J. Biol. Chem.* 298:102443. doi: 10.1016/j.jbc.2022.102443

Wu, C., Yu, J., Xu, G., Gao, H., Sun, Y., Huang, J., et al. (2021). Bioinformatic analysis of the proteome in exosomes derived from plasma: exosomes involved in cholesterol metabolism process of patients with spinal cord injury in the acute phase. *Front. Neuroinf.* 15:662967. doi: 10.3389/fninf.2021.662967

Wu, J., Jin, Z., and Yan, L. J. (2017b). Redox imbalance and mitochondrial abnormalities in the diabetic lung. *Redox Biol.* 11, 51–59. doi: 10.1016/j.redox.2016.11.003

Wu, J., Li, R., Li, W., Ren, M., Thangthaeng, N., Sumien, N., et al. (2017a). Administration of 5-methoxyindole-2-carboxylic acid that potentially targets mitochondrial dihydrolipoamide dehydrogenase confers cerebral preconditioning against ischemic stroke injury. *Free Radic. Biol. Med.* 113, 244–254. doi: 10.1016/j.freeradbiomed.2017.10.008

Yang, X., Song, J., and Yan, L. J. (2019). Chronic inhibition of mitochondrial Dihydrolipoamide Dehydrogenase (DLDH) as an approach to managing diabetic oxidative stress. *Antioxidants (Basel)* 8:32. doi: 10.3390/antiox8020032

Yoneyama, K., Shibata, R., Igarashi, A., Kojima, S., Kodani, Y., Nagata, K., et al. (2014). Proteomic identification of dihydrolipoamide dehydrogenase as a target of autoantibodies in patients with endometrial cancer. *Anticancer Res.* 34, 5021–5027.

Yu, G., Wang, L. G., Han, Y., and He, Q. Y. (2012). clusterProfiler: an R package for comparing biological themes among gene clusters. *OMICS* 16, 284–287. doi: 10.1089/omi.2011.0118

Zhang, G., Sun, J., and Zhang, X. (2022). A novel cuproptosis-related LncRNA signature to predict prognosis in hepatocellular carcinoma. *Sci. Rep.* 12:11325.

Zhang, H., Meltzer, P., and Davis, S. (2013). RCircos: an R package for Circos 2D track plots. *BMC Bioinformatics* 14:244. doi: 10.1186/1471-2105-14-244

Zuidema, J. M., Hyzinski-Garcia, M. C., Van Vlasselaer, K., Zaccor, N. W., Plopper, G. E., Mongin, A. A., et al. (2014). Enhanced GLT-1 mediated glutamate uptake and migration of primary astrocytes directed by fibronectin-coated electrospun poly-L-lactic acid fibers. *Biomaterials* 35, 1439–1449. doi: 10.1016/j.biomaterials.2013.10.079

Frontiers in
Cellular Neuroscience

Leading research in cellular mechanisms underlying brain function and development

Part of the world's most cited neuroscience journal series that advances our understanding of the cellular mechanisms underlying cell function in the nervous system across all species.

Discover the latest Research Topics

See more →

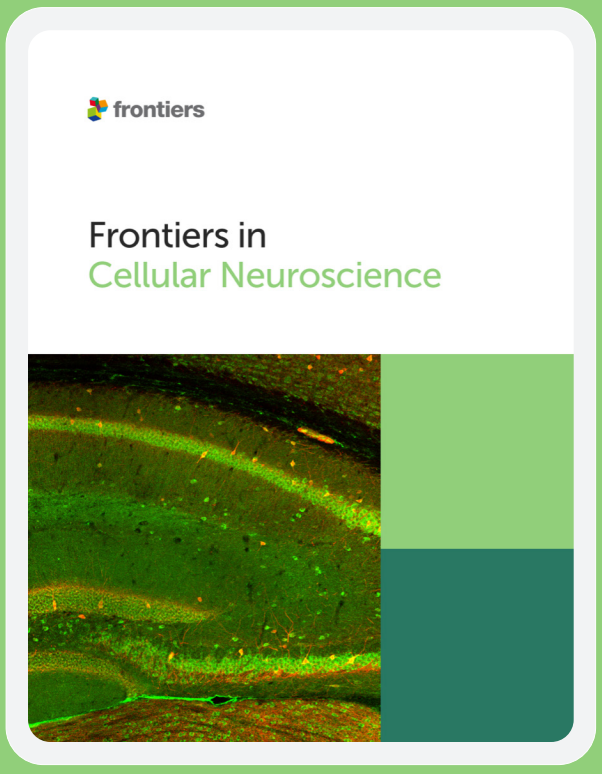

Frontiers

Avenue du Tribunal-Fédéral 34
1005 Lausanne, Switzerland
frontiersin.org

Contact us

+41 (0)21 510 17 00
frontiersin.org/about/contact